The Intermodal Freight Transportation Institute (IFTI)
Herff College of Engineering

Preliminary Evaluation of Geofoam for Support of Freight Rail Tracks

Principal Investigator

David Arellano, Ph.D., P.E.

Associate Professor, Dept. of Civil Engineering, University of Memphis, 104C Engr. Sc. Bldg., 3815 Central Avenue, Memphis, TN 38152, Tel: 901-678-3272, Fax: 901-678-3026, Email: darellan@memphis.edu

Co-Principal Investigators

Steven F. Bartlett, Ph.D., P.E.

Associate Professor, Dept. of Civil & Environmental Engineering, University of Utah, 110 Central Campus Dr., Salt Lake City, UT 84112, Tel: 801-587-7726, Fax: 801-585-5477, Email: bartlett@civil.utah.edu

Ramesh Neupane

Shun Li

Graduate Research Assistants, Dept. of Civil & Environmental Engineering, University of Utah, 110 Central Campus Dr., Salt Lake City, UT 84112, Tel: 801-587-7726, Fax: 801-585-5477

June 10, 2015

Left Blank Intentionally

Left Blank Intentionally

Technical Report Standard page

1. Report No.	2. Government Accession No.	3. Recipient's Catalog No.	
4. Title and Subtitle Preliminary Evaluation of Geofoam for Support of Freight Rail Tracks		**5. Report Date** **June, 2015** **6. Performing Organization Code**	
7. Author(s) David Arellano - University of Memphis Steven F. Bartlett - University of Utah Ramesh Neupane - University of Utah Shun Li - University of Utah		**8. Performing Organization Report No.**	
9. Performing Organization Name and Address Intermodal Freight Transportation Institute University of Memphis Herff College of Engineering 302 Engineering Administration Building Memphis, TN 38152-3107		**10. Work Unit No. (TRAIS)** **11. Contract or Grant No.**	
12. Sponsoring Organization Name and Address Office of the Assistant Secretary for Research and Technology U.S. Department of Transportation 1200 New Jersey Ave, SE Washington, D.C. 20590		**13. Type of Report and Period Covered** **14. Sponsoring Agency Code**	
15. Supplementary Notes Visit www.memphis.edu/ifti for color PDF files of this and other research reports.			
16. Abstract This report presents the results of a study performed to evaluate the use of geofoam to support freight rail tracks. The objectives of this project were (1) to develop preliminary design guidelines for the use of geofoam to support freight rail tracks and (2) to develop a design of a full-scale test embankment for freight rail. The research approach consisted of laboratory static and cyclic tests on railway ballast (Phase I), evaluation and numerical modeling of deflections and vertical displacements of rail systems supported by EPS embankments (Phase II), and field dynamic deflection monitoring of EPS embankments along the Utah Transit Authority's Front Runner South commuter rail line and the West Valley TRAX light rail extension line (Phase III). The study revealed that adequately designed EPS embankments can yield deflections of rail systems on EPS embankments that are relatively small and, therefore, can have similar or better performance than that of earthen embankments. The current successful performance of geofoam along the Front Runner South commuter line and West Valley TRAX light rail extension line suggests that these geofoam configurations can serve as the basis for preliminary design of other proposed rail systems supported on geofoam. The numerical models developed in this study can be used to develop preliminary designs of EPS embankments that support freight rail loads for the purpose of developing a design of a full-scale test embankment. The full-scale test embankment can be monitored with accelerometers to measure deflections under freight car loadings and the field deflection results can be used to develop a design procedure for EPS-block geofoam embankments to support freight rail loads.			
17. Key Words Geofoam, expanded polystyrene, EPS, lightweight fill, embankments		**18. Distribution Statement** No restrictions.	
19. Security Classification (of this report) Unclassified.	**20. Security Classification (of this page)** Unclassified.	**21. No. of Pages**	**22. Price** -0-

DISCLAIMER

This research was funded by the Intermodal Freight Transportation Institute at the University of Memphis. The contents of this report reflect the views of the authors, who are responsible for the facts and the accuracy of the information presented herein. This document is disseminated under the sponsorship of the Department of Transportation, University Transportation Centers Program, in the interest of information exchange. The U.S. Government assumes no liability for the contents or use thereof. The contents do not necessarily reflect the official views of the Intermodal Freight Transportation Institute, the University of Memphis, the University of Utah, or the USDOT.s RITA at the time of publication.

TABLE OF CONTENTS

AUTHOR ACKNOWLEDGMENTS

The research reported herein was conducted as a joint effort between the University of Memphis and University of Utah. Dr. David Arellano, P.E., Associate Professor of Civil Engineering at the University of Memphis and Dr. Steven F. Bartlett, P.E., Associate Professor of Civil Engineering at the University of Utah were the Co-Principal Investigators. Mr. Ramesh Neupane and Shun Li were the graduate research assistants at the University of Utah.

The authors would like to acknowledge the Department of Civil and Environmental Engineering at the University of Utah and Department of Civil Engineering at the University of Memphis for providing matching funding support, Mr. Sean Ellis of the Center for Intermodal Freight Transportation Studies for his contractual administrative assistance, Mr. Shaun Dustin of Campbell Scientific for assisting us with configuring the data acquisition system for the field accelerometers, and Mr. Jon Cluff and Mr. James Webb of the Utah Transit Authority for facilitating access to the Front Runner commuter rail south line in Draper City, Utah and the light rail line (Green Line) near Roper Yard in Salt Lake City, Utah.

EXECUTIVE SUMMARY

Expanded-polystyrene (EPS)-block geofoam has successfully been used in numerous projects predominately in Europe, Japan, and the U.S. as lightweight fill to support roadway embankments. However, geofoam has not been used extensively in light and commuter rail embankments and has not been used in the U.S. to support freight rail tracks. This report presents the results of a study performed to evaluate the use of geofoam to support freight rail tracks. The objectives of this project were (1) to develop preliminary design guidelines for the use of geofoam to support freight rail tracks and (2) to develop a design of a full-scale test embankment for freight rail. The research approach consisted of laboratory static and cyclic tests on railway ballast (Phase I), evaluation and numerical modeling of deflections and vertical displacements of rail systems supported by EPS embankments (Phase II), and field dynamic deflection monitoring of EPS embankments along the Utah Transit Authority's Front Runner South commuter rail line and the West Valley TRAX light rail extension line (Phase III).

Field deflection measurements of a section of the Front Runner commuter rail system showed that the maximum and average displacements for the rail ties positioned on the EPS embankment were about 6 mm and 2 mm, respectively. An adjacent earthen embankment underwent maximum and average displacements of 22 mm and 7.5 mm, respectively. Therefore, the average displacements occurring on the EPS embankment were about 25 percent of that incurred by the earthen embankment. This suggests that adequately designed EPS embankments can yield deflections of rail systems on EPS embankments that are relatively small and, therefore, can have similar or better performance than that of earthen embankments. The current successful performance of over 129,000 m^3 (168,000 yd^3) of EPS-block geofoam along the TRAX light rail and 10,900 m^3 (14,300 yd^3) of geofoam along the Front Runner South commuter line suggests that these geofoam configurations can serve as the basis for preliminary design of other proposed rail systems supported on geofoam.

Although the field monitoring program was limited to commuter and light rail loads, the field instrumentation data collected as part of this study suggests that the FLAC3D model developed as part of this project can be used to perform further numerical studies to evaluate displacements of freight rail systems supported by EPS embankments. The results of the numerical studies can be used to develop preliminary designs of EPS embankments that support freight rail loads for the purpose of developing a design of a full-scale test embankment. The full-scale test embankment can be monitored with accelerometers to measure deflections under freight car loadings and the field deflection results can be used to develop a design procedure for EPS-block geofoam embankments to support freight rail loads. The

selection of a specific site for the full-scale embankment study is required before the design of a full-scale test embankment for support of freight rail can be accomplished because site-specific information such as the properties of the EPS embankment foundation materials are needed. The results of the field instrumentation data collected as part of a full-scale freight railroad embankment study can then be used to develop design procedures for the use of EPS-block geofoam in freight railroad embankments.

CHAPTER 1: INTRODUCTION

INTRODUCTION

Geofoam has successfully been used in numerous projects predominately in Europe, Japan, and the U.S. as lightweight fill to support roadway embankments. However, geofoam has not been used extensively in light and commuter rail embankments and has not been used in the U.S. to support freight rail tracks. In an effort to extend the use of geofoam to these systems, the project team performed a research study to evaluate the use of geofoam to support freight rail tracks.

In the U.S., geofoam was recently incorporated in portions of the light and commuter rail systems in Salt Lake City, Utah by the Utah Transit Authority (UTA). Approximately, 60,350 m^3 (78,935 yd^3) of geofoam was used to construct approach embankments of four bridges along the 5.1 mile alignment of the West Valley TRAX light rail extension line. Also, approximately 68,810 m^3 (90,000 yd^3) of geofoam has been used for bridge embankments along the Salt Lake City Airport light rail extension. In addition to these light rail projects, 10,988 m^3 (14,360 yd^3) of geofoam embankments have also been used along the UTA Front Runner South commuter rail line that extends from Salt Lake City to Provo, Utah. These UTA light rail and commuter rail lines provide an excellent opportunity to obtain data of the field performance of geofoam embankments subjected to light and commuter rail loads.

Although loads from light and commuter rail systems are typically less than freight rail loads, the field instrumentation data collected as part of this study can be used to develop preliminary designs of freight rail. Additionally, the field data can also be used to improve current light and commuter rail designs. The availability of actual performance data will also make the use of geofoam more attractive to light and commuter rail agencies throughout the U.S. because it will remove current uncertainties and misconceptions that exist regarding the use of geofoam to support rail loads. For example, a transit agency in Texas has expressed concerned regarding the magnitude of the transient vibrations and deflections that occur in geofoam embankments subjected to rail loads. Because these evaluations were not available, the transit agency did not further consider geofoam. In summary, data from field instrumentation and evaluation of these and other issues will contribute to wider understanding and application of geofoam in light and commuter rail projects, as well as provide a pathway for wider acceptance of the technology for freight rail applications.

RESEARCH OBJECTIVES AND APPROACH

The objectives of this project are (1) to develop preliminary design guidelines for the use of geofoam to support freight rail tracks and (2) to develop a design of a full-scale test embankment for freight rail. The project initially consisted of three phases. Phase I consisted of performing field vibration and deflection measurements and evaluations of geofoam embankments located along the light and commuter rail systems in Salt Lake City, Utah. Phase II consisted of performing laboratory prototype track model load tests of various geofoam track systems. The results of Phases I and II were to be used to develop preliminary recommendations for the use of geofoam to support freight rail track systems and to develop a design of a full-scale test embankment as part of Phase III.

A major obstacle that significantly impacted the project progress and schedule involved the unexpected requirement by the Utah Transit Authority that both University of Memphis and University of Utah have Railroad Protective Liability Insurance in order to perform field vibration and deflection measurements of their light- and commuter-rail sections supported on geofoam. The University of Memphis insurance coverage does not contain this railroad protective liability insurance. Therefore, the project team had to purchase this insurance to perform the field testing and meet the project objectives. However, in order to purchase this insurance, the project team had to obtain approval from the State of Tennessee Treasury Department Division of Claims Administration. This approval took four months to obtain.

The four month Division of Claims Administration approval process significantly delayed the project. The initial project duration was from March 1, 2013 to February 28, 2014. This project schedule was based on performing the field testing during the summer 2013. However, because the project team did not obtain approval to purchase the railroad protective liability insurance from the state Division of Claims Administration until late September 2013 as indicated above and because the project team could not order and calibrate the field test equipment until insurance approval was obtained to ensure that the field testing could indeed be accomplished, the project team was not be able to perform the field testing in Salt Lake City until summer 2014. Therefore, a project extension until December 31, 2014 was requested and was obtained. The delivery of the field accelerometers was delayed several weeks because the manufacturer experienced a strike by employees. Additionally, the calibration of the accelerometers took longer than planned. Therefore, the field testing was not performed until fall 2014.

The field testing is a significant part of the project and the delay in the field testing significantly impacted the project progress. In order to minimize the impact of the field testing delay on the revised overall project

completion date of December 31, 2014, the project team revised the research approach. The revised research approach consisted of laboratory static and cyclic tests on railway ballast (Phase I), evaluation and numerical modeling of deflections and vertical displacement of rail systems supported by EPS embankment (Phase II), and field dynamic deflection monitoring of EPS embankments along the UTA Front Runner South commuter rail line and the West Valley TRAX light rail extension line (Phase III).

REPORT ORGANIZATION

This report is organized into six chapters. This chapter, Chapter 1, provides the research objectives and a summary of the research approach used for this study. Chapter 2 provides a summary of the literature search related to the use of geofoam to support railroad tracks. Chapter 3 provides a summary of the laboratory static and cyclic tests on railway ballast and Chapter 4 provides a summary of the evaluation and numerical modeling of deflections and vertical displacements of rail systems supported by EPS embankments. Chapter 5 presents the results of field dynamic deflection monitoring of EPS embankments along the UTA Front Runner South commuter rail line and the West Valley TRAX light rail extension line. Chapter 6 provides a summary of the conclusions and recommendations of the findings from this study.

CHAPTER 2: LITERATURE REVIEW

INTRODUCTION

This chapter presents a summary of the literature on general expanded polystyrene (EPS)-block geofoam usage for embankment systems that includes a general geofoam construction history in various countries, summary of long-term performance of EPS as well as a summary of rail systems in various countries that are supported by EPS geofoam embankments. Additionally, a brief summary of numerical modeling studies of deflections of rail systems supported by EPS geofoam embankments performed by others and a summary of key aspects of field dynamic deflection monitoring of railway systems is also provided.

GENERAL GEOFOAM USAGE FOR EMBANKMENT SYSTEMS

Construction History and Methods

Expanded polystyrene (EPS) geofoam has been used in embankment and roadway construction since 1972. The development initially began in Norway and nearby Scandinavian countries and soon spread to Japan and the U.S. The following is brief history of EPS as pertaining to embankment applications.

Norway

The first attempt at building a non-subsidence road with large EPS blocks instead of earth was successfully implemented in a marshland in Lillestrom, Norway in 1972 (Miki, 1996; Alfheim et al., 2011). The successful roadway repair and settlement mitigations was credited to Norwegian road construction engineers associated with what is now called the Norwegian Public Roads Administration (NPRA). This novel construction method was further improved and increasingly used in many construction sites in Norway and made its way steadily into Northern European countries and others.

Japan

The Expanded Poly–Styrol Construction Method Development Organization (EDO) was established in Japan in 1986. This organization sought technical exchange with NPRA and committed itself to the development and practice of the EPS method in Japan EDO quickly embraced this technology. The Japanese engineers use the EPS method as an alternative to earth

embankments in settlement prone area and areas with soft ground or slope stability concerns. For example, the EPS method is used in a soft ground application as a light fill method (Miki, 1996).

U.S.

Many states have used EPS geofoam in large and small highway projects since the mid 1990s. A few large and/or high-profile jobs are of particular note in the U.S.: (1) the Big Dig in Boston, Massachusetts (Riad et al., 2004), (2) the I-15 Reconstruction Project in Salt Lake City, Utah (Bartlett et al., 2012), (3) the Woodrow Wilson Bridge in Virginia (FHWA, 2013) and (4) the Utah Transit Authority (UTA) light rail system in Salt Lake City, Utah (Snow et al., 2010). EPS geofoam helped the projects maintain extremely tight construction schedules that did not have sufficient time for conventional embankment construction. These projects illustrated the ease and speed with which EPS geofoam can be constructed for embankments. (FHWA, 2011).

In addition to these project, engineers at the Minnesota Department of Transportation (DOT), the Maine DOT, and the Indiana DOT have realized significant time and cost savings for small and moderate-sized EPS roadway embankment projects constructed over deep, soft organic soil deposits prevalent in these state (FHWA, 2011).

EPS has also been used as light-weight embankment in slope stabilization project. Projects have been completed in Colorado, New York, Alabama and Arizona. After years of searching for permanent solutions to failing slope problems, the New York State DOT and the Alabama DOT turned to EPS geofoam. By replacing upper sections of the slide area, State engineers significantly reduced the driving forces that were causing the slide and successfully rehabilitated the roadway section (FHWA, 2011).

General guidance for slope stability projects have been developed by others found in report "Guidelines for Geofoam Applications in Slope Stability Projects" (Arellano et al., 2011).

Long-Term Performance of EPS

Physical Properties

The compressive resistance of EPS is an important design property and is somewhat correlated with the density of the EPS material. One major indicator of possible deterioration of blocks with time would be a decrease in the material compressive resistance or strength (Aabøe and Frydenlund,

2011). Unconfined compressive strength tests performed on retrieved samples from embankments constructed in Norway that have been in the ground for up to 24 years are shown in Figure 2.1 as a function of dry unit density and compressive strength.

From Figure 2.1 and Figure 2.2 it may also be observed that the majority of tests show values of compressive strength in relation to unit density above that of a "normal" quality material (i.e., the expected compressive resistance for that particular density of EPS). The results indicate clearly that there are no signs of significant material deterioration over the total time span of 24 years. Furthermore there is no indication of significant variation in the material strength whether the retrieved specimens are tested wet or dry. This indicates that water pickup over years in the ground from groundwater does not appear to affect the material strength in a significant manner.

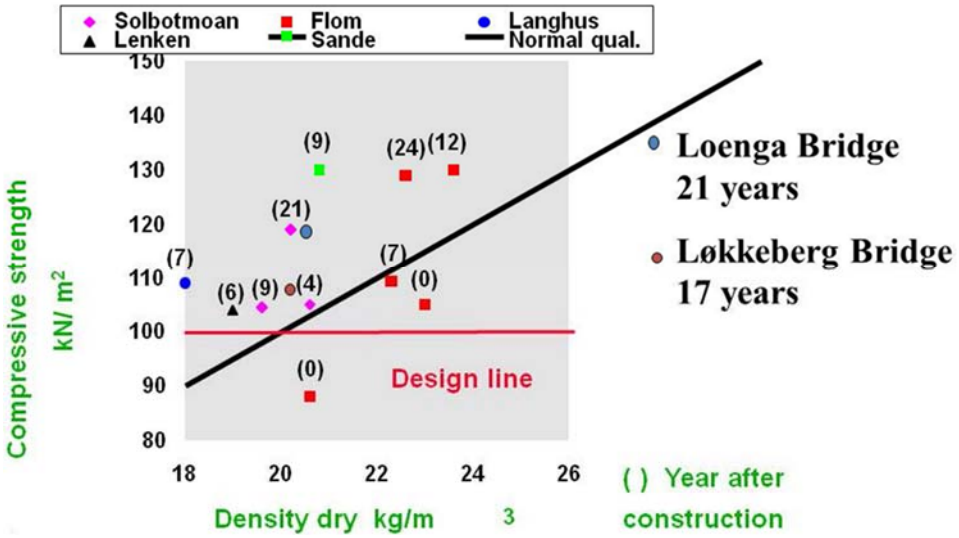

Figure 2.1. Compressive Strength on Retrieved Samples from EPS Embankments

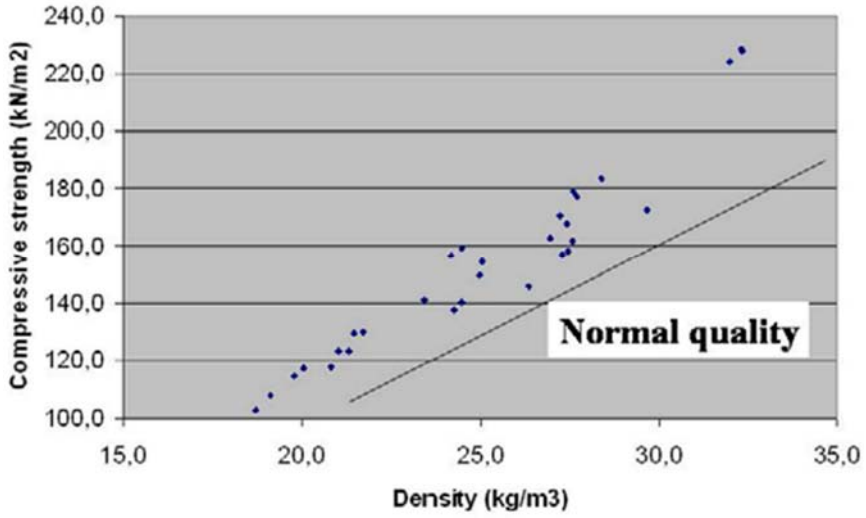

Figure 2.2. Loenga Bridge 1983 Compressive Strength after 21 Years of Burial

Creep

Creep strain can be significant in EPS geofoam, if it is overloaded beyond the elastic range. The design guidance for minimizing creep settlement can be found in report "Guideline and Recommended Standard for Geofoam Applications in Highway Embankments", (Stark et al., 2004) and "Geofoam Applications in the Design and Construction of Highway Embankments", (Stark et al., 2004) for U.S. Projects and in EPS Whitebook, 2011 for Europe (EUMEPS, 2011).

Laboratory and field creep measurements have been carried out to determine the allowable loading conditions in the EPS block to keep creep strain to tolerable limits. Some pertinent studies are summarized below.

To determine of the EPS creep range under representative loadings, a series of tests were carried out by Duskov (1997). In the first series of tests, only EPS20 cylinders exposed to a single stress level were tested. In a second series, creep of both EPS15 and EPS20 samples was measured under two different stress levels. For both test series only the EPS samples in dry conditions were used. The creep level of EPS20 caused by a static stress of 20 kPa was rather limited and seemed to be less than 0.2% after more than a year. Duskov concluded that creep seems to be semi-linear log linear for both EPS15 and EPS20 when loaded statically in its elastic range. About half of the expected maximum creep occurs already with in the first day. Duskov concluded that all in all, the additional settlement of a pavement structure due to creep in the EPS sub-base will be rather

limited, in order of a few tenths of a percent. Therefore, this creep deformation was considered to be of minor practical importance for pavement performance.

The I-15 Reconstruction Project in Salt Lake City, Utah was designed so that the combination of the dead load and live load did not exceed the compressive resistance of EPS19 at 10 percent strain, which was the guidance given at that time in the draft European code (Bartlett et al., 2012). This is approximately equivalent to maintaining the combination of dead and live loads to a compressive resistance of about 1 percent axial strain. To monitor the performance of the EPS embankments for this project, instrumentation was installed at several locations to monitor the long-term creep and settlement performance of EPS embankments (Bartlett and Farnsworth, 2004). The most extensive array was installed at 100 South Street and the results obtained will be discussed below.

The I-15 reconstruction at 100 South Street in Salt Lake City, Utah required raising and widening the existing embankment to the limits of the right-of-way. The geofoam fills in both the north and southbound directions were placed over a 406-mm high-pressure natural gas line and other buried utilities as shown in Figures 2.3 and 2.4 (Negussey and Stuedlein, 2003). The southbound portion of this embankment employed approximately 3,400 m^3 of EPS 20, and the height of the embankment decreased southward to conform to the roadway elevation. The embankment height (not including the pavement thickness) decreased from 8.1 to 6.9 meters, corresponding to 10 to 8.5 layers of geofoam blocks, respectively (Figure 2.3). The geofoam embankment transitions to two-stage MSE walls on both the north and south sides. In this area, the top part of the existing embankment was sub excavated and replaced with scoria fill to raise the roadway grade within the utility corridor without causing primary consolidation in the underlying, compressible, foundation soils.

The instrumentation installed at this location consisted of: (1) basal vibrating wire (VW) total earth pressure cells placed in sand underneath the EPS, (2) horizontal inclinometers (one placed near the base and one near the top of embankment) and (3) two magnet extensometer placed within the geofoam fill (Figures 2.3 and 2.4). The magnet plates for the extensometers were placed at EPS layers 0, 1.5, 3.5, 5.5, 7.5, 8.5 and 9.5 at the northern (i.e., left) location and at layers 0, 1.5, 3.5, 5.5, 7.5, 8.5, and 9 at the southern (i.e., right) location (Figure 2.3). All extensometer measurements were referenced to their respective base plate underlying the geofoam fill (and not the top of the riser pipe) hence, these data represent deformations of the geofoam fill with time and do not include any settlement of the foundation soils.

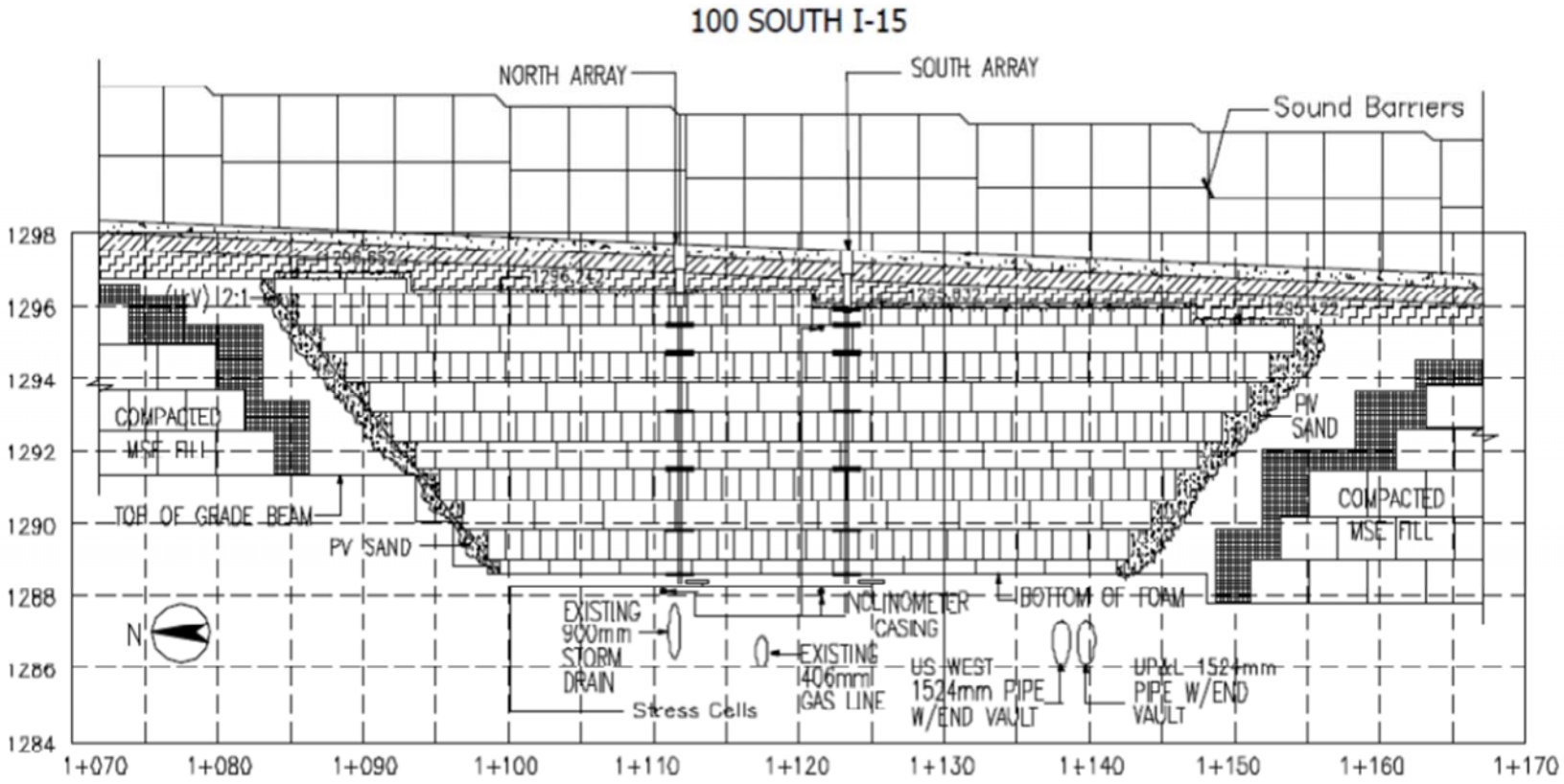

Figure 2.3. Profile View of the EPS Embankment and Instrumentation

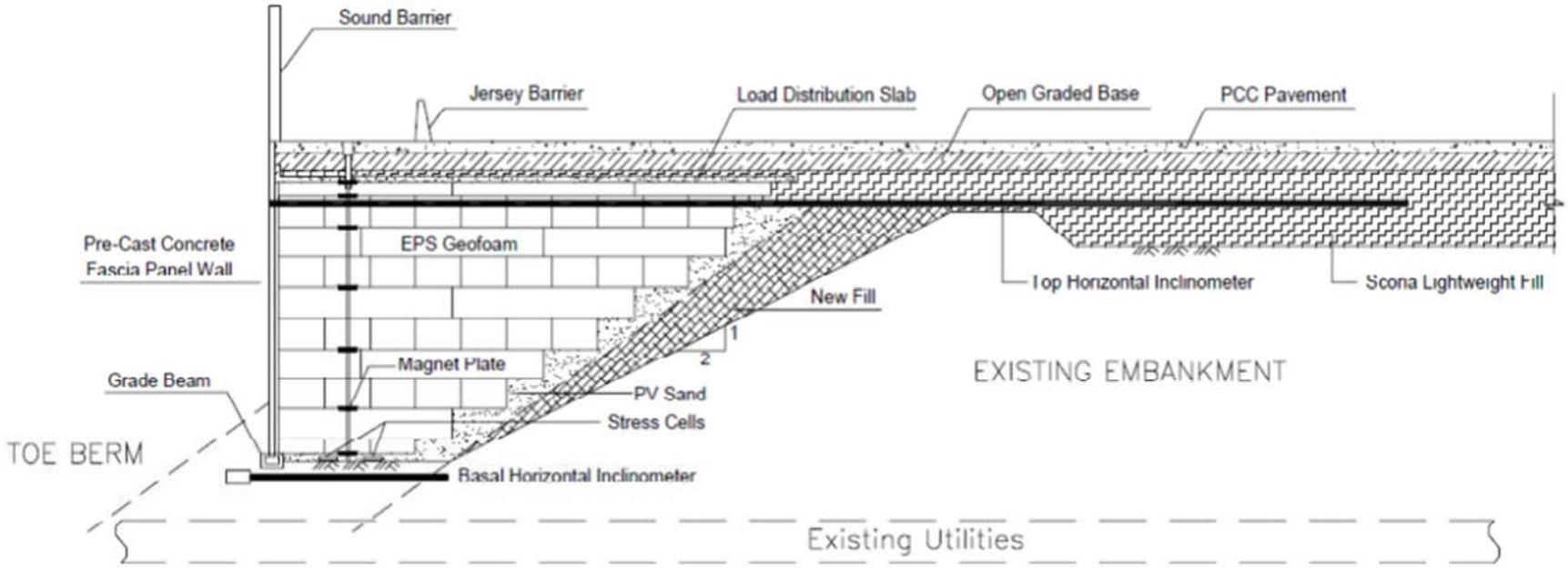

Figure 2.4. Cross-sectional View of the EPS Embankment and Instrumentation

Figure 2.5 (Negussey and Stuedlein, 2003) shows the construction and post construction strain time history of the southern location as calculated from the magnet extensometer observations. The basal layers (0 to 1.5 m) underwent 1.8 percent vertical strain by end of construction at approximately 300 days. The total strain of the EPS embankment (0 to 9 m) was about 1 percent at end of construction at this same location (Figure 2.5). Figure 2.6 (Farnsworth et al., 2008) shows the construction and post construction strain of the entire embankment (0 to 9 m). The vertical strain at the southern location is about 1.5 percent after 10 years of monitoring and is projected to be about 1.7 percent creep strain after 50 years.

The post construction settlement trend of Figure 2.6 is consistent with the limit 2 percent global strain in 50 years assumed in the I-15 design. Approximately 1 percent strain occurred during construction as materials were placed atop the EPS fill. The remaining strain is creep strain that has occurred post construction. Figure 2.5 shows that the lowest geofoam interval experienced more vertical strain when compared with the relatively uniform strain that occurred in the overlying layers. It should be noted that the foundation footing for the adjacent panel wall laterally restrains the lowest geofoam layer. As a result, the mean normal stress in the lower geofoam layers is probably somewhat higher than the corresponding states of stress in the overlying geofoam layers. This effect would produce more vertical strain and also suggests that the influence of confinement may need to be considered in future design evaluations, as appropriate.

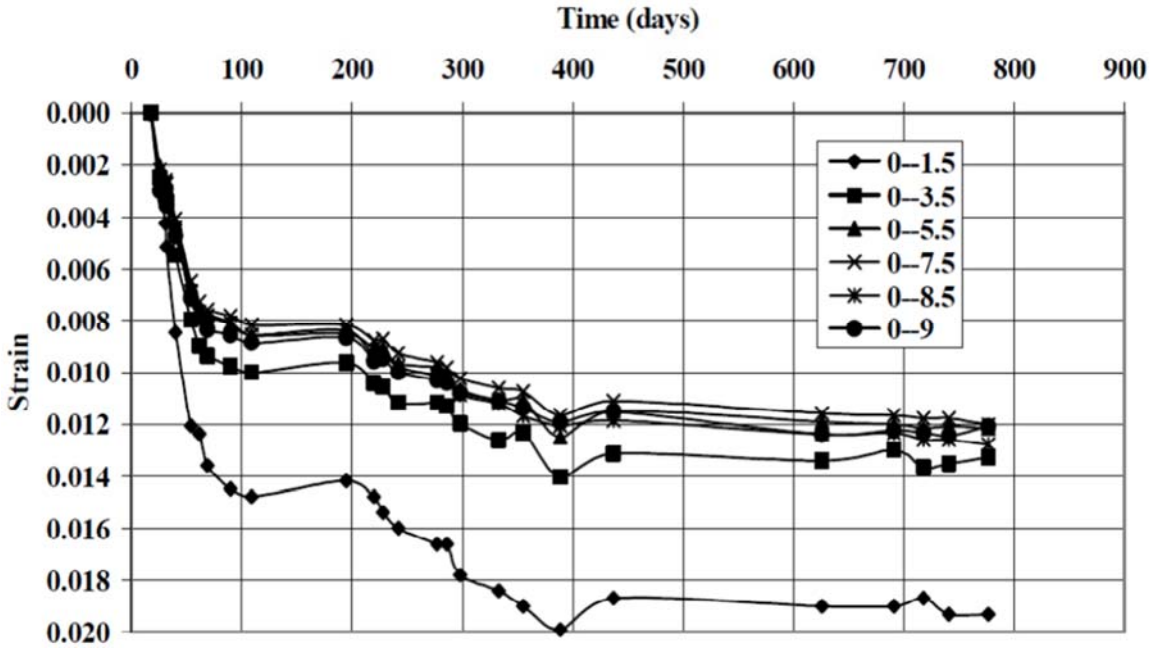

Figure 2.5. Construction and Post Construction Strain in EPS

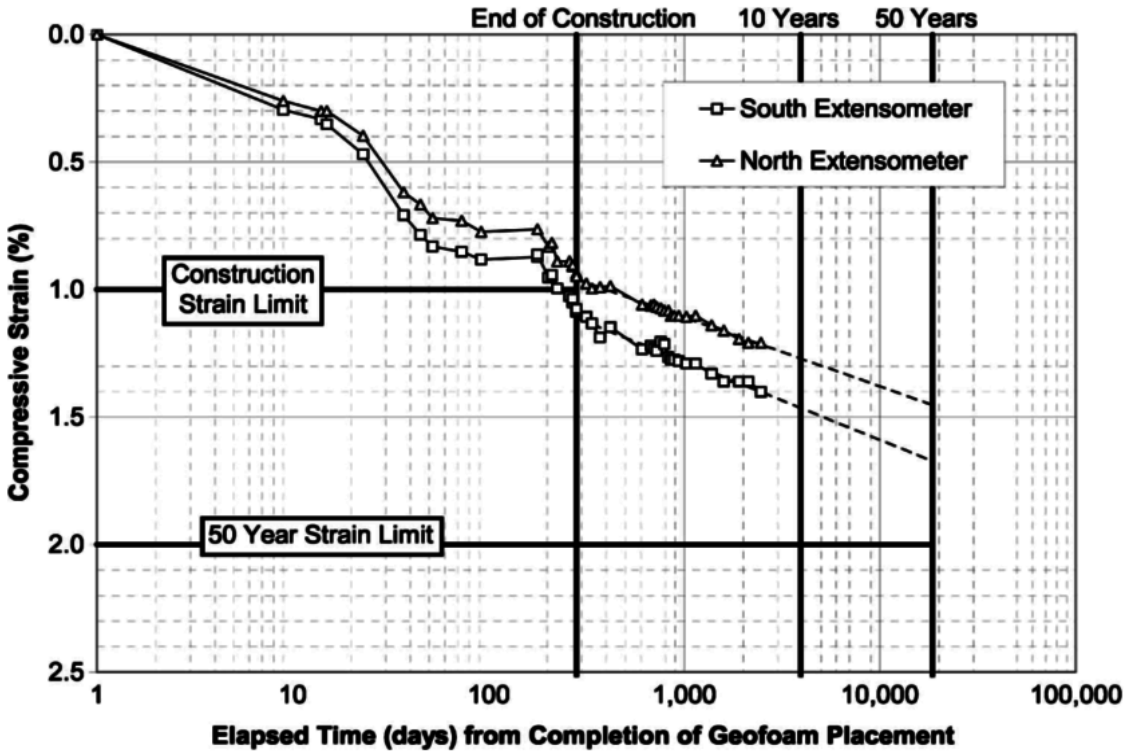

Figure 2.6. Construction and Post Construction Global Strain of Entire EPS Embankment

RAIL SYSTEMS SUPPORTED BY EPS GEOFOAM EMBANKMENTS

The primary focus of this report is on the use of EPS geofoam block for embankment support of rail systems. Unlike embankment support of roadway systems, this application is not widely used and is still in its development. The following section summarizes the known examples worldwide where EPS has been used for rail support.

Norwegian (NSB) Commuter Rail System

Plans to reconstruct national road 36 at Bole near the City of Skien in Telemark included building a new railway bridge at a road underpass (Frydenlund et al., 1987). In order to increase the free height at the underpass, the road level was lowered and the railway line elevated somewhat. The new bridge is constructed on footings in a sand layer.

With the wider road and lowered road level, the upper clayey soil caused potential stability problems and the use of Expanded Polystyrene (EPS) as a superlight fill material against the northern bridge abutment was suggested and adopted. One problem to consider was that the loads from trains on the EPS material

might create intolerable deflections close to the bridge, thus creating hammer effects on the bridge. In order to minimize such effects, it was decided to use EPS-blocks with unit density 30 kg/m^3. Furthermore the total layer thickness of EPS was reduced somewhat towards the abutment and an approximate 1-m thick slab of Leca-concrete (Light Expanded Clay Aggregate) was cast on top of the EPS to provide a supplemental lightweight fill material layer and provide a platform for further load distribution. A 15-cm thick reinforced concrete slab is cast on top of the EPS- blocks in the sections that did not include Leca-concrete. For fire safety, the outer blocks were specified as made of self-extinguishing EPS. The thickness of EPS-blocks used was 0.6 m.

After the new bridge was completed, load tests were carried out in order to measure deformations due to train live loads. Locations with various thicknesses of EPS along the railway track were selected and deformations measured with the 155 kN axle load at each location. Deflections were measured both on the sleepers and on bolts in the concrete slab above the EPS-blocks. The design adopted for the bridge is considered satisfactory, and trains are now passing the bridge daily. This case history will be modeled by this report, and details will be provided later in Chapter 4.

Utah Transit Authority (UTA)

Snow et al. (2010) and Arellano and Bartlett (2012) reported that geofoam was recently incorporated in portions of the light and commuter rail systems in Salt Lake City, Utah by the Utah Transit Authority (UTA). Approximately, 60,350 m^3 (78,935 yd^3) of geofoam was used to construct approach embankments of four bridges along the 5.1 mile alignment of the West Valley TRAX light rail extension line. Also, approximately 68,810 m^3 (90,000 yd^3) of geofoam has been used for bridge embankments along the Salt Lake City Airport light rail extension. In addition to these light rail project, 10,988 m^3 (14,360 yd^3) of geofoam embankment has also been used along the UTA FrontRunner South commuter rail line that extends from Salt Lake City to Provo, Utah. See Figure 2.7 and Figure 2.8 for examples of geofoam utilization by UTA. The FrontRunner embankment shown in Figure 2.8 is also be modeled in this report and details regarding its construction are given in Chapter 4.

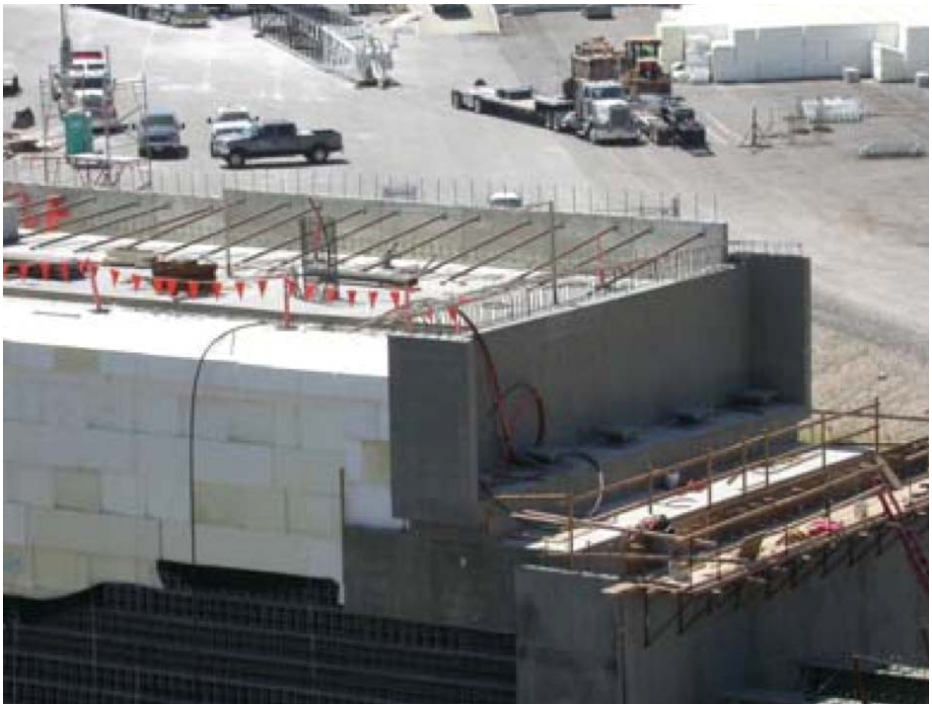

Figure 2.7. Geofoam at UTA TRAX Light Rail

Figure 2.8. Geofoam at UTA FrontRunner Commuter Rail

Netherlands

Esveld et al. (2001) reported that large areas of the densely-populated western and northern parts of The Netherlands consist of subsoil with geotechnical characteristics ranging from poor to very poor. Building of railway structures under these conditions would require a substantial improvement of the bearing capacity. The conventional approach consists of replacing a great deal of the poor soil by sand (sub-grade improvement). Even if pre-loading of a sub-grade layer is applied, relatively large settlements due to high weight of a track structure are likely to occur during the initial phase of the structure's life. With the application of ultra-light materials, such as EPS, a so-called “equilibrium” structure can be created, which would practically prevent the increase of stresses in the sub-grade. In other words, the weight of the track structure plus lightweight material should approximately compensate the weight of the excavated material. In the research performed by Esveld et al. (2001), an unconventional railway track, a so-called Embedded Rail Structure (ERS) is considered. Traditional ballast is replaced by a reinforced concrete slab in such a structure. To reduce the total weight of a structure and consequently stresses in the sub-grade an EPS layer is applied between the slab and sub-grade. The static and dynamic properties of such a track investigated by Esveld et al. (2001) demonstrated the feasibility and advantages of EPS usage in railway track design.

Figure 2.9 shows that the EPS geofoam bridge approaches constructed for the light rail system in Brederoweg, Schiedam, Netherlands. The picture was obtained in Google Earth.

Figure 2.9. EPS Embankment in Netherlands

United Kingdom

O'Brien (2001) described the innovative solution for the replacement of an old railway bridge by using EPS geofoam embankment in United Kingdom (UK).

Japan

EPS geofoam has been used in one of the several railway lines in Japan (Meitetsu Tsushima railway line) as described by Sagara et al. (2000). The project involved the construction of a new elevated track over the existing track. To construct the new elevated track, it was necessary to shift the current train service to the temporary track adjacent to the current track. An embankment structure was required on the temporary track section to connect the approach section of current elevated track to the ground level track. The ground was relatively soft and therefore EPS geofoam embankment was used for temporary embankment construction.

NUMERICAL MODELING OF DEFLECTIONS AND VERTICAL DISPLACEMENT OF RAIL SYSTEMS SUPPORTED BY EPS GEOFOAM EMBANKMENTS

One objective of this project is to develop a numerical method for modeling EPS embankments used to support rail systems. Important to its development is a brief summary of modeling studies performed by others.

Analytical Approaches

According to Zakeri and Sadeghi (2007), the most common analytical method of calculating railway sleeper, i.e., tie, deflection (deflection of the rail at the sleeper positions) is the Winkler equation. However, this model is of limited value in considering the behavior of the sub-structure beneath the rail. Since the EPS-supported embankment that is being studied in this report is a multi-layered system, this method cannot be used.

Numerical Approaches

Even though there are some numerical analysis on railway systems in the literature, these studies generally do not focus on the vertical displacement of the system.

Most relevant to this study is a modeling study performed by Powrie et al. (2007). These authors reported the results of finite element analyses (FEA) analyses carried out to investigate the ground surface

displacement and stress changes due to train loading. This study will be discussed in more detail and used to develop and validate the proposed modeling approach presented herein.

Track System Geometry

The typical track structure shown was modeled in the FEA, but without geotextile. Depths of 300 mm of ballast, 200 mm of sub-ballast, and 500 mm of prepared subgrade were adopted in the analysis. The rail cross-section was modeled as a rectangle of 153 mm high × 78 mm wide. With a Young's modulus $E = 210$ GPa, the bending stiffness $EI = 4889$ kN·m^2 corresponds to a 56.4 kg/m steel rail. Sleepers were modeled as cuboids of 200 mm high, 242 mm wide, and 2420 mm long, with a spacing of 650 mm between centers. Rail pads were not modeled explicitly, as they would have no effect on the transmission of loads to the ground in a static analysis. More discussion will be provided in Chapter 4.

Loading Condition

The analyses were based on a typical modern freight car as used by English Welsh & Scottish Railways (EWS) to convey heavy bulk materials such as coal, aggregates, and construction materials. These have an axle load of 25.4 tones (the maximum normally permitted on the UK rail network), corresponding to a static wheel load of 125 kN.

Adequacy of a Static Analysis

In reality, vertical loads exerted by a moving railway vehicle may be greater or less than the static value, depending on whether the vehicle is momentarily accelerating downward or upward. However, it is a common practice to carry out a static analysis, in which dynamic effects are taken into account by multiplying the static load by a dynamic amplification factor (DAF). The DAF depends on the train speed, the track quality, and confidence intervals required and may normally range from 1.1 to 2.8 (Esveld, 2001). DAFs have not been used in this analysis, but with the geomaterials assumed to behave as linear elastic materials, the calculated stress changes will be directly proportional to the loads. Dynamic finite element analyses carried out by Grabe (2002) indicated that for speeds up to 240 km/h, the impact of dynamic effects on the calculated maximum changes in stress in the ground below a railway line were small, whereas the ground response from moving train loads is essentially quasistatic for speeds up to 140 km/h (Kaynia et al., 2000). Thus, it was concluded that for the study described herein in Chapter 4, for the purpose of determining representative ground surface displacement and stress changes, a static analysis would suffice.

Model properties

The geotechnical properties of all the materials were modeled by Powrie et al. (2007) as linear elastic.

DYNAMIC DEFLECTION MONITORING OF EPS EMBANKMENT TO SUPPORT RAILWAY SYSTEM

The amount of deflection of the rail caused by the passing of a locomotive or rail car is a significant safety issue for rail system operations. Large deflections could pose the risk of possible derailment, especially at higher speeds of operation. Dynamic rail deflections can occur on all types of embankment support systems.

The amount of deflection can be measured by using direct or indirect methods. For direct methods, measurement is usually done by via survey equipment, lasers, or other optical equipment (e.g., high-speed cameras) deployed in the field. When optical techniques are used, optical equipment are used to obtain images, and those images are subsequently processed to determine relative displacement. For indirect methods, the amount of deflection is typically measured by instrumentation and numerical interpretation. The most common indirect method involves the installation of accelerometers or geophones at the site. These sensors can provide time history data of acceleration or velocity. This information can be integrated to provide estimates of displacement of the rail versus time.

The use of optical techniques to measure the dynamic deflection on rails and rail ties (i.e., sleepers) overlying embankments made from conventional materials have been carried out by several researchers (Ho et al., 2006; Bowness et al., 2007; Lu, 2008; Pinto et al., 2009; Psimoulis and Stiros, 2013). Videography and image processing techniques were used to monitor the vertical displacements of rail sleepers with the passage of trains by Ho et al. (2006). Bowness et al. (2007) monitored the dynamic displacement of railway track using remote video monitoring system. Lu (2008) developed a system to measure track deflection from a moving railcar. The system was comprised of a loaded hopper car fitted with a camera/lesser sensor system which detected the vertical deflection of the rail relative to the wheel/rail contact point. Pinto et al. (2009) used an optical system for monitoring the vertical displacements of the track in high speed railways. The system was based on a diode laser module mounted away from the track. Psimoulis and Stiros (2013) measured the deflection of a short-span railway bridge using robotic total station (RTS).

The use of indirect methods to measure the dynamic deflection in the field have been carried out by several researchers (Madshus and Kaynia, 2000; Bowness et al., 2007; Chebli et al., 2008; Priest and Powrie, 2009; Ling et al., 2010). Madshus and Kaynia (2000) studied the motions of the track and embankment by

installing accelerometers in the field. In this study the displacement was calculated and the results were compared with numerical simulation. Bowness et al. (2007) monitored the dynamic deflection of railway tracks by placing geophones on the sleepers. The field test results were then compared with the results obtained from an optical target method. Chebli et al. (2008) studied the dynamic response of high-speed ballasted railway tracks using a three dimensional (3D) periodic model and in-situ measurement. As an in-situ measurement, accelerometers were installed at various locations to measure the vertical acceleration and displacement. In this method, the accelerometers were placed on the sleepers. The in-situ measurement results were then compared with the results obtained from 3D periodic model. Priest and Powrie (2009) evaluated the dynamic track modulus by measuring track velocity during train passage. In this method, geophones were attached to the sleeper outside the rail. Dynamic displacement was calculated from the measured velocity. Ling et al. (2010) studied train induced vibration response characteristics and dynamic stability of track structures by installing accelerometers on sleepers, rail and embankment slopes.

The use of EPS geofoam for railway embankments has not been studied to any great extent. Frydenlund et al. (1987) reported the use of EPS block in the abutment to support a railway bridge in Norway. The deflection was measured on the sleepers. The maximum deflection was found to be around 7 mm. O'Brien (2001) described the innovative solution for the replacement of an old railway bridge by using EPS geofoam embankment in United Kingdom (UK). From this study, one can understand the potential of using EPS geofoam as a lightweight fill material for railway embankments for short term and long term purposes. However, there are very few studies focusing exclusively on vertical deflection monitoring of EPS embankments to support railway systems.

In the United States, EPS geofoam was recently incorporated in portions of the commuter and light rail systems in Salt Lake City, Utah by the Utah Transit Authority (UTA). The FrontRunner commuter rail south line extends from Salt Lake City to Provo, Utah. Along this line at Corner Canyon in Draper City, EPS has been used in the embankment in order to minimize the stress over a reinforced concrete box culvert. This location has both EPS geofoam and adjacent earthen embankment. Similarly, the light rail line (Green Line) extends from West Valley Central to Salt Lake City International Airport. In this line, EPS has been used in the embankment near Roper Yard, which is operated by the Union Pacific Railroad. These two sites were selected to monitor the field dynamic deflections of EPS geofoam embankment for this project that is described in this report.

The monitoring of the amount of vertical dynamic deflection of the rail (i.e., deflection due to passage of a train) is necessary in order to find the amount of deflection. The monitoring of deflection is important

because more than acceptable deflection could pose potential safety issues. There are no guidelines regarding the acceptable level of deflection occurring in EPS embankment to support railway system. This study would yield data on deflection occurring in both EPS and earthen embankment. The comparison of amount of deflection could provide an indication of how much deflection would occur in EPS embankments in comparison to earthen embankments. This study could provide a basis for understanding the typical levels of vertical deflection that develop in these somewhat unique systems.

SUMMARY

This chapter presents a summary of the literature on general expanded polystyrene (EPS)-block geofoam usage for embankment systems as well as a summary of rail systems in various countries that are supported by EPS geofoam embankments. The literature search summary provides the background information for the numerical modeling study of deflections of rail systems supported by EPS geofoam embankments that is presented in Chapter 4 and for the field dynamic deflection monitoring study of two geofoam embankments that is presented in Chapter 5. However, a summary of the laboratory static and cyclic tests on ballast performed to determine the Young's modulus of elasticity and resilient modulus of ballast material for use in the numerical modeling study is presented next in Chapter 3.

REFERENCES

Aabøe, R., and Frydenlund, T. E., (2011). "40 years of experience with the use of EPS geofoam blocks in road construction", *EPS 2011*, Lillestrom, Norway.

Alfhein, S., Flaate, K., Refsdal, G., Rygg, N., and Aarhus, K., (2011). "The first EPS geoblock road embankment – 1972", NRRL, Norwegian Public Roads Administration, Road Authority of Akershus County, Norwegian Public Roads Administration.

American Railway Engineering and Maintenance-of-Way Association, (2007). "Economics of railway engineering and operations - construction and maintenance operations", *Manual for Railway Engineering*, Volume 4, Chapter 16, Part 10.11.

Arellano, D., and Bartlett, S. F., (2012). "Evaluation of geofoam for support of freight rail tracks", Proposal of National Center for Freight and Infrastructure Research and Education (CFIRE)**,** University of Memphis**,** Herff College of Engineering.

Arellano, D., Stark, T. D., Horvath, J. S., and Leshchinsky, D., (2011). "Guidelines for geofoam applications in slope stability projects", final report prepared for National Cooperative Highway Research Program (NCHRP24-11), Transportation Research Board of the National Academies.

Bartlett, S.F. and Farnsworth, C.B. (2004). "Monitoring and modeling of innovative foundation treatment and embankment construction used on the I-15 reconstruction project, project management plan

and instrument installation report," *Utah Department of Transportation (UDOT)* research report No. UT-04.19, University of Utah, Department of Civil and Environmental Engineering, 202.

Bartlett, S. F., Lawton, E. C., Farnsworth, C. B. and Newman, M. P, (2012), "Design and evaluation of expanded polystyrene geofoam embankments for the I-15 reconstruction project, Salt Lake City, Utah", report prepared for *Utah Department of Transportation Research Division.* University of Utah, Department of Civil and Environmental Engineering

Bowness, D., Lock, A., Powrie, W., Priest, J., and Richards, D. "Monitoring the dynamic displacements of railway track." Proc., Institution of Mechanical Engineers, Part F: Journal of Rail and Rapid Transit, 13-22.

Chebli, H., Clouteau, D., and Schmitt, L. (2008). "Dynamic response of high-speed ballasted railway tracks: 3D periodic model and in situ measurements." Soil Dynamics and Earthquake Engineering, 28(2), 118-131.

Duskov, M., (1997), "EPS as a light-weight sub-base material in pavement structures," Thesis, Delft University of Technology, Delft, Netherlands, 91-95.

European Manufacturers of EPS (EUMEPS) (2011), "EPS white book, EUMEPS background information on standardisation of EPS", Version 31/03/11, Belgium.

Esveld, C., (2001). "Modern railway track," 2nd Ed., MRT-Productions, Zaltbommel, The Netherlands.

Esveld, C., Markine, V. and Duškov, M., (2001). "Feasibility of EPS as a lightweight sub-base material in railway track structures," *Proceedings of the third international conference on EPS Geofoam,* Salt Lake City, Utah, 10-12 December, 1-10.

Farnsworth C. F., Bartlett S. F., Negussey, D. and Stuedlein A., (2008). "Construction and post-construction settlement performance of innovative embankment systems, I-15 reconstruction project, Salt Lake City, Utah," *Journal of Geotechnical and Geoenvironmental Engineering*, 134, 289-301.

Frydenlund, T. E., Myhre, O., Refsdal, G., Aaboe, R., (1987). "Plastic foam in road embankments," Norwegian Road Research Laboratory, Norwegian Edition 61 (in English).

Grabe, P. J., (2002). "Resilient and permanent deformation of railway foundations under principal stress rotation," PhD Dissertation, University of Southampton, UK.

Ho, S., Tsang, W., Lee, K., Lee, K., Lai, W., Tam, H., and Ho, T., (2006). "Monitoring of the vertical movements of rail sleepers with the passage of trains." Proc., Institution of Engineering and Technology International Conference on Railway Condition Monitoring, IEEE, 108-114.

Kaynia, A. M., Madshus, C., and Zackrisson, P (2000). "Ground vibration from high-speed trains: prediction and countermeasure," *J. Geotech. Geoenviron. Eng*, 126(6), 531-537.

Ling, X.-Z., Chen, S.-J., Zhu, Z.-Y., Zhang, F., Wang, L.-N., and Zou, Z.-Y. (2010). "Field monitoring on the train-induced vibration response of track structure in the Beiluhe permafrost region along Qinghai–Tibet railway in China." Cold Regions Science and Technology, 60(1), 75-83.

Lu, S. (2008). "Real-time vertical track deflection measurement system." Ph.D. thesis, University of Nebraska, Lincoln, Nebraska, USA.

Madshus, C., and Kaynia, A. (2000). "High-speed railway lines on soft ground: dynamic behaviour at critical train speed." Journal of Sound and Vibration, 231(3), 689-701.

Miki, G. (1996). "Ten year history of EPS method in Japan and its future challenges," *Proceeding of International Symposium on EPS Construction Method*, Tokyo, 29-30 October, 394-411.

Negussey, D. and Stuedlein, A. (2003). "Geofoam fill performance monitoring." *Utah Department of Transportaion Research Division* Report No. UT-03.17.

O'Brian, A.S. (2001). "Design and Construction of the UK's first Polystyrene Embankment for Railway Use." ." *Proc., 3rd Int. Geofoam Conf.,* Salt Lake City, Utah.

Pinto, N., Ribeiro, C., Mendes, J., and Calçada, R. (2009). "An optical system for monitoring the vertical displacements of the track in high speed railways." Proc., 3rd International Integrity Reliability and Failure, Portugal, 1-9.

Powrie, W., Yang, L. A., and Clayton, C. R. I. (2007). "Stress changes in the ground below ballasted railway track during train passage," *Proceedings of the Institution of Mechanical Engineers, Part F, Journal of rail and rapid transit*, March, 221(2), 247-262.

Priest, J., and Powrie, W. (2009). "Determination of dynamic track modulus from measurement of track velocity during train passage." Journal of geotechnical and geoenvironmental engineering, 135(11), 1732-1740.

Psimoulis, P. A., and Stiros, S. C. (2013). "Measuring deflections of a short-span railway bridge using a robotic total station." Journal of Bridge Engineering, 18(2), 182-185.

Riad, H. L., Ricci, A. L., Osborn, P. W., D'Angelo, D. A. and Horvath, J. S. (2004). "Design of lightweight fills for road embankments on Boston's central artery/tunnel project," *Proceedings: Fifth international conference on case histories in geotechnical engineering*, New York, NY, 13-17 April.

Sagara et al 2000?

Snow, R., Webb J., Sander M., (2010). "Light rail on geofoam West Valley UTA TRAX project", *2010 AREMA Conference and Exposition*, Orlando, Florida.

Stark, T. D., Arellano, D., Horvath, J. S., and Leshchinsky, D., (2004a), "Guideline and recommended standard for geofoam applications in highway embankments", Report prepared for National Cooperative Highway Research Program (NCHRP 529), Transportation Research Board of the National Academies.

Stark, T. D., Arellano, D., Horvath, J. S., and Leshchinsky, D., (2004b). "Geofoam applications in the design and construction of highway embankments", Report prepared for National Cooperative Highway Research Program (NCHRP Web Document 65, Project 24-11), Transportation Research Board of the National Academies.

United States Department of Transportation - Federal Highway Administration (2011), "Expanded Polystyrene (EPS) Geofoam." <http://www.fhwa.dot.gov/research/deployment/geofoam.cfm> (5 April, 2014)

United States Department of Transportation - Federal Highway Administration (2013), "Case in point: the Woodrow Wilson Bridge." <http://www.fhwa.dot.gov/bridge/abc/epscasestudy.cfm> (5 April, 2014)

Zakeri, J. A., and Sadeghi, J. (2007). "Field investigation on load distribution and deflections of railway track sleepers," *Journal of Mechanical Science and Technology*, 21(12), 1948-1956.

CHAPTER 3: LABORATORY STATIC AND CYCLIC TESTS ON RAILWAY BALLAST

INTRODUCTION

Deflection in the railway system is a significant issue of safety. Static and dynamic are the two types of deflection that can occur in any type of embankment supporting the railway system. In the past, most of the embankments were made by using conventional fill materials like soil and rock. As indicated in Chapter 2, recently EPS geofoam has been in use for constructing embankments to support railway systems. Several studies have been carried out to monitor railway track deflections that occur in embankments made from conventional materials using various techniques (Ho et al., 2006; Bowness et al., 2007; Lu, 2008; Pinto et al., 2009; Psimoulis and Stiros, 2013). However, there are limited studies done to measure static and dynamic deflection on EPS embankments. A section of the FrontRunner commuter rail system in Corner Canyon in Draper City, Utah includes an EPS geofoam embankment. The embankment substructure consists of ballast, sub-ballast, and EPS geofoam overlying sand. This chapter presents a summary of the laboratory static and cyclic tests on ballast performed to determine the Young's modulus of elasticity and resilient modulus of ballast material for use in the numerical modeling study that is presented in Chapter 4.

Resilient Modulus is a measure of material stiffness and provides a mean to analyze stiffness of unbound pavement materials under different conditions, such as moisture, density and stress level (MnDOT, 2015). Resilient Modulus is the elastic modulus defined as the ratio of applied deviator stress and recoverable elastic strain. A material's resilient modulus is actually an estimate of its modulus of elasticity (Pavement Interactive, 2007). The primary difference between Young's modulus of elasticity and resilient modulus is that modulus of elasticity is stress divided by strain for a slowly applied load while resilient modulus is stress divided by strain for rapidly applied loads. Therefore, in general, the modulus typically used to represent materials subjected to static loads is Young's modulus of elasticity and the modulus typically used to represent materials subjected to cyclic loads is resilient modulus.

Deflectometer and plate bearing load tests are the most common field tests whereas triaxial tests are the common laboratory tests for determining the modulus of elasticity of geomaterials (Ping et al., 2002). The main objective of this laboratory study was to determine the Young's modulus of elasticity and resilient modulus of ballast material based on triaxial tests. A summary of the ballast material tested, the laboratory test procedures utilized, and the test results are presented subsequently.

MATERIAL DESCRIPTION

As described in the next section, tests were performed using a large scale triaxial test system and a large chamber test system. The ballast samples tested in the large scale triaxial system was supplied by Utah Transport Authority (UTA) and samples tested in the large chamber system was supplied by Geneva Rock, Inc. The materials were similar to the material used in the FrontRunner commuter rail system in Utah. The ballast material sizes ranged from 25.4 mm to 76.2 mm. The large scale triaxial set up had a capacity to prepare a sample of 152 mm diameter and 330 mm in height and the large chamber system had a sample capacity of 1.064 m diameter and 0.914 m in height. Therefore the ballast material was directly used for large chamber testing whereas the sample for large scale triaxial testing had to be crushed into sizes smaller than 25.4 mm because the ASTM test procedure (ASTM, 2004) indicates that the largest size of the material to be tested should be smaller than 1/6 of the specimen diameter.

EXPERIMENTAL SETUP AND PROCEDURE

The main objective of this laboratory study was to determine the Young's modulus of elasticity and resilient modulus of ballast material by using two different laboratory techniques, compare the results between the two test techniques, and suggest recommendations based on the laboratory test findings. The two different laboratory tests consisted of monotonic and cyclic testing conducted by using a large scale triaxial test system and a large chamber test system.

Large Scale Triaxial Test

The large scale triaxial test system consists of a triaxial cell, a pressure regulator console, a FlowTrac volume pressure controller, a de-aired water tank and a MTS system. The triaxial cell consists of a triaxial base, vertical metal bars, plexiglass chamber and top cap. The FlowTrac controller was used to supply the pressure on the sample. The de-aired water tank provides de-aired water to the sample. The MTS system measures the load and displacement according to the loading protocol. The test was divided into three stages: sample preparation, sample saturation and shearing. The sample preparation and sample saturation procedure was the same for both monotonic and cyclic triaxial tests.

Sample Preparation

The density of ballast material was measured by using a mold with the same dimensions as the triaxial cell, i.e., 152 mm in diameter and 330 mm in height. The material was compacted into four equal layers by using a tamping rod and the weight was measured. The density of ballast material was found to be 1410 kg/m^3.

Since the diameter and height of the sample to be prepared in the triaxial test chamber is the same as the mold used to measure the density of the ballast, the same weight of ballast used during density determination was used to fill the triaxial test chamber to acquire a similar density of 1410 kg/m^3 obtained in the mold used to obtain the ballast density.

A two part split metal mold was used to place the ballast sample into two double rubber membranes. Double membranes were used to prevent puncture. The two part split metal mold was attached to a base plate containing three vertical metal bars and two O-rings were placed on each side of the mold over the double membranes.as shown in Figure 3.1. A vacuum was attached (see Figure 3.1) and applied to the middle of the mold to evacuate the air between the membrane and the metal mold and to stretch the rubber membrane.

Figure 3.1. Mold attached to the vacuum

Two porous stones were boiled in water and one of the saturated stones was placed onto the triaxial base plate. Above the porous stone, the ballast was placed in four equal layers with each layer of height 82.5 mm. Then each layer was compacted slightly by a tamping rod. Special care was taken during compaction so that the membrane did not get punctured. Once all the layers were compacted, another saturated porous stone was placed over the sample and a triaxial cap was placed above the porous stone.

The vacuum was then disconnected from the middle of the mold and was connected to the bottom outlet valve in the triaxial base plate. Vacuum was then applied to the inside of the sample through the bottom valve to assist in separating the membrane from the split metal mold. The metal mold was removed from the sample and the O-rings were rearranged as shown in Figure 3.2.

Figure 3.2. Specimen once the mold is removed

Vacuum grease was applied on the top of all three metal rods coming out of the triaxial bottom plate. The O-rings were removed from both the triaxial base and top cap and vacuum grease was applied over the sections of membrane where the O-rings were previously located. The O-rings were then replaced. Vacuum grease was also applied to the ends of the triaxial plexiglass chamber wall, which was placed over the sample. The plexiglass chamber was pushed down into the triaxial bottom plate and was twisted back and forth until a good seal was obtained between the plexiglass chamber and bottom plate.

The middle valve on the triaxial base was connected with the de-aired water tank and the chamber was filled with de-aired water. Once the water reached the top of the chamber, it was allowed to spill out from the top port and the chamber was tipped in various directions to remove any air bubbles. The top of the plexiglass chamber was then sealed with the triaxial top cap. The completed sample set up is shown in Figure 3.3.

Figure 3.3. Specimen fully set up with de-aired water

Sample Saturation

The middle valve of the triaxial base was connected with a pressure regulator to apply confining pressure to the ballast, i.e., cell pressure. In the field, the ballast material is located at a shallow depth of around 600 mm. Consequently, the overburden pressure within the ballast is very low and is estimated to be on the order of 34.5 kPa. Therefore, a cell pressure of 34.5 kPa was applied to the sample.

The bottom valve of the triaxial base was connected with de-aired water and the sample was saturated. After the sample was saturated, the bottom valve was detached from the de-aired water line and was connected to the output line of FlowTrac controller. The cell pressure was increased to 41.4 kPa and a back pressure of 6.9 kPa was adjusted from the FlowTrac controller. The FlowTrac controller, pressure regulator console, and full triaxial set up within the MTS machine is shown in Figure 3.4.

Figure 3.4. Triaxial set up with console and FlowTrac controller in MTS Machine

Shearing under Monotonic Loading

The shearing was applied under the strain-controlled and drained conditions. The loading protocol was set with the strain rate of 1.65 mm/minute (0.5 % per minute) in the MTS system. The MTS system is shown in Figure 3.5.

Figure 3.5. System to control and measure load and displacement

Once the load was applied, the system provides data related to time, displacement and force. Then, area and membrane corrections were applied (ASTM, 2004). The area and membrane correction equations are Eqs. (3.1) and (3.2).

Correction of area is

$$A = A_c/(1 - \epsilon_1) \quad \textbf{(3.1)}$$

where A_c = average cross-sectional area and ϵ_1= axial strain for the given axial load.

Correction of rubber membrane is

$$\Delta(\sigma_1 - \sigma_3)_m = (4E_m t_m \epsilon)/D_c \quad \textbf{(3.2)}$$

where $\Delta(\sigma_1 - \sigma_3)_m$ = membrane correction to be subtracted from the measured principal stress difference (deviator stress), kN/m^2,

$D_c = (4A_c/\pi)^{0.5}$ = diameter of specimen after consolidation, mm or cm,

E_m = Young's modulus for the membrane material, kN/m^2,

t_m = thickness of the membrane, mm or cm, and

ϵ = axial strain (decimal form).

Shearing under Cyclic Triaxial Loading

The loading was applied under strain-controlled and drained conditions. The loading protocol was set to amplitude of 5 mm, frequency of 0.5 Hz and 10000 cycles in the MTS system. Similar to monotonic loading, area and membrane corrections were applied in the test.

Large Chamber Test

The large chamber test system consists of a large steel chamber, a loading ram and a MTS system. The test procedure was divided into two stages: sample preparation and shearing.

Sample Preparation

The inside of the large steel chamber was divided into five equal heights of 152.4 mm each and these five sections were marked on the inner circumference of the chamber. Ballast material was poured into the large chamber and each layer was compacted to obtain a height of 152.4 mm within each layer. Compaction was performed by using a hand-held tamper. Seventy five tamps were applied in each layer. The process of compaction using tamper is shown in Figure 3.6. The density of material was obtained by measuring the weight of the sample required to fill the steel chamber. The initial density of the sample was 1450 kg/m^3.

No ballast material was placed in the top 152.4 mm of the large steel chamber to allow space for the loading ram. The ballast sample with loading ram is shown in Figure 3.7 and the loading ram set in position for testing is shown in Figure 3.8.

Figure 3.6. Compaction with tamper

Figure 3.7. Specimen with loading arm

Figure 3.8. Specimen ready for testing

Shearing

The chamber was connected to the MTS system for shearing. Then, the chamber was subjected to a loading of 267 kN. The shearing was done in two stages in order to evaluate the behavior at low and higher level of strain. In the first stage, the cyclic loading was conducted under a maximum amplitude of 5 mm and in the second stage, a maximum amplitude of 30 mm was used. For the cyclic testing, the loading protocol consisted of a frequency of 0.5 Hz, 1000 cycles and 20 data points for each cycle. The protocol was set so that it yields time, displacement and force as output. At the end of each stage, the distance of top level of cover from top of the chamber was measured in order to find the volume of compacted specimen. The density at the end of each stage of test was then determined.

MONOTONIC AND CYCLIC TEST RESULTS

The data from both monotonic and cyclic tests were obtained in the form of time, displacement and force. Analysis was done by plotting stress versus strain to calculate the Young's modulus of elasticity and resilient modulus. The results of both the triaxial tests and the large chamber tests are initially presented and then the results of both tests are compared.

Monotonic Triaxial Test Results

Data related to time, displacement and force were obtained from the test. The axial strain was calculated from the ratio of displacement to the original height of the sample. Area was corrected accordingly Eq. 3.1. The deviator stress was then calculated by dividing force by the corrected area. The membrane correction was made by using Eq. 3.2. A latex membrane was used for testing and the Young's modulus of elasticity of latex membrane was estimated to be 1400 kPa (ASTM, 2004). Final deviator stress was calculated by subtracting the deviator stress with the stress obtained from Eq. 3.2.

The initial seating condition was observed in the test and a seating correction was made and a plot was made between adjusted deviator stress and axial strain as shown in Figure 3.9. The slope of the initial linear portion of the stress-strain curve is the Young's modulus of elasticity. The modulus of elasticity for the applied cell pressure was found to be 52,000 kPa and is in agreement with the results reported by Anderson and Fair (2008). Anderson and Fair (2008) reported modulus of elasticity values in the range of 30,000 to 60,000 kPa for tests on ballast materials.

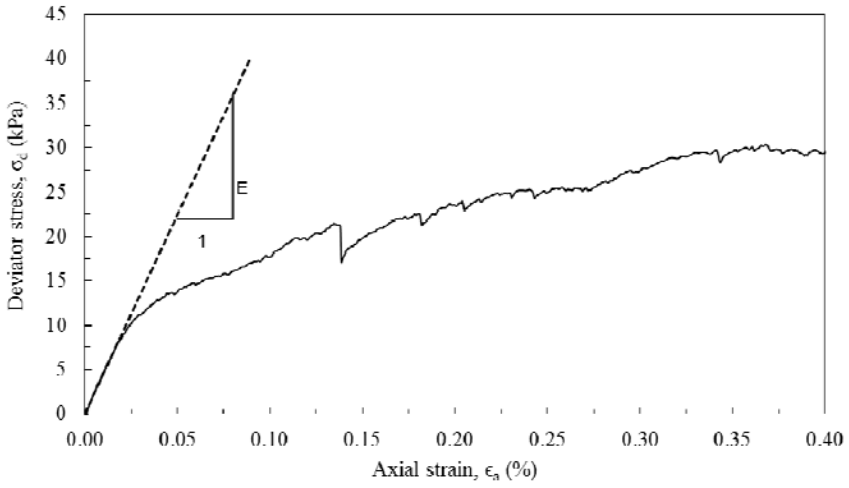

Figure 3.9. Stress-strain behavior of ballast under the monotonic loading in triaxial test

The cyclic deviator stress and cyclic axial strain was calculated from the displacement and force data. The triaxial test result for 10,000 cycles is shown in Figure 3.10. The data at the beginning of the test is not reliable because ballast particles take time to be in a stable condition under the applied load. Therefore, the third cycle was selected to determine the resilient modulus for the initial stage. The eight hundredth cycle was selected in order to compare the triaxial results with the large chamber test results. The cyclic deviator stress versus cyclic axial strain for the third cycle and eight hundredth cycle is shown in Figure 3.11. The resilient modulus (M_r) for both selected cycles was found to be almost equal and averaged 14,000 kPa.

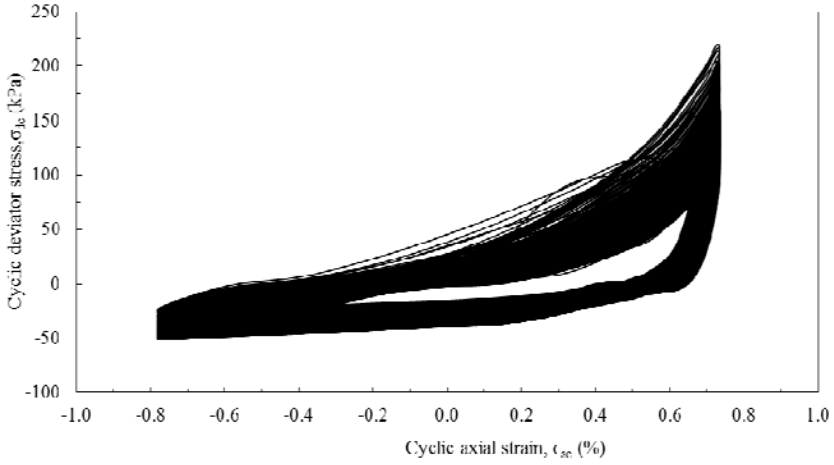

Figure 3.10. Cyclic triaxial test results on ballast at 10000 cycles

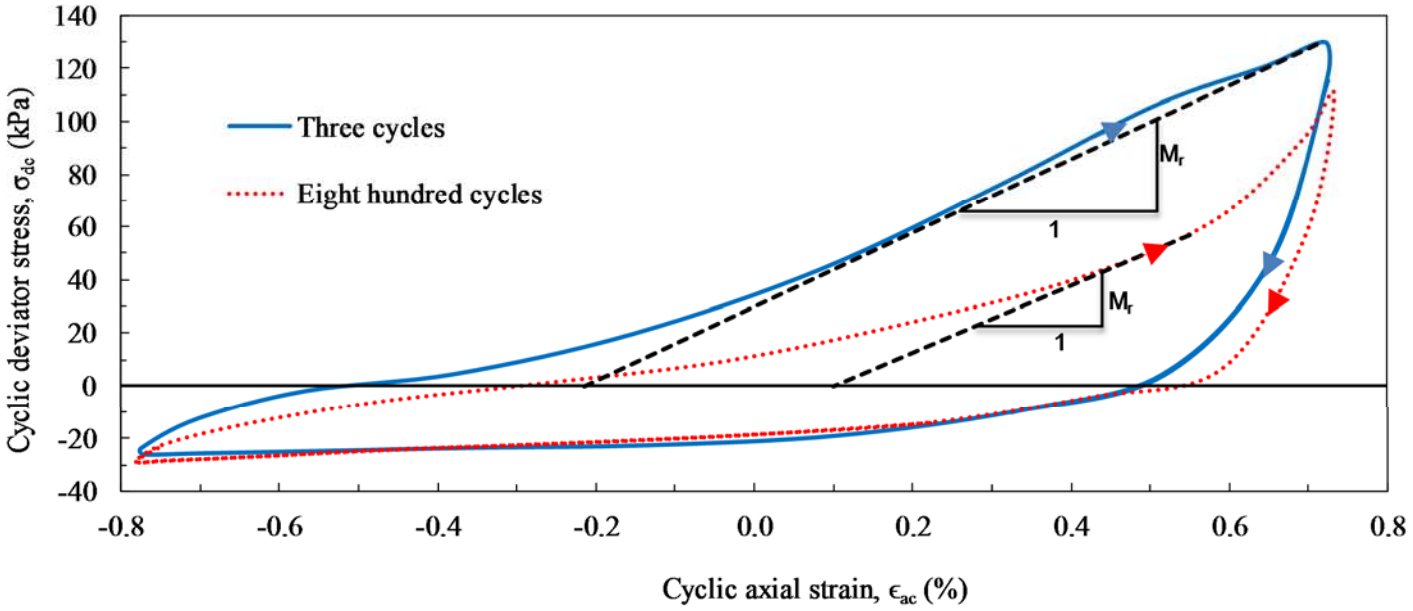

Figure 3.11. Resilient modulus determinations after cyclic triaxial tests

Large Chamber Test Results

Data related to time, displacement and force were obtained from the large chamber tests. The stress is the ratio of force to the cross-sectional area of the sample and strain is the ratio of displacement to the original height of sample. The results of the first and second stages of cyclic loading in the large chamber test is shown in Figure 3.12. The stress-strain behavior of the first and second stages of cyclic loading were evaluated to measure the Young's modulus but the monotonic test results from the large chamber were not included because the modulus at low amplitude cyclic test is more representative of Young's modulus.

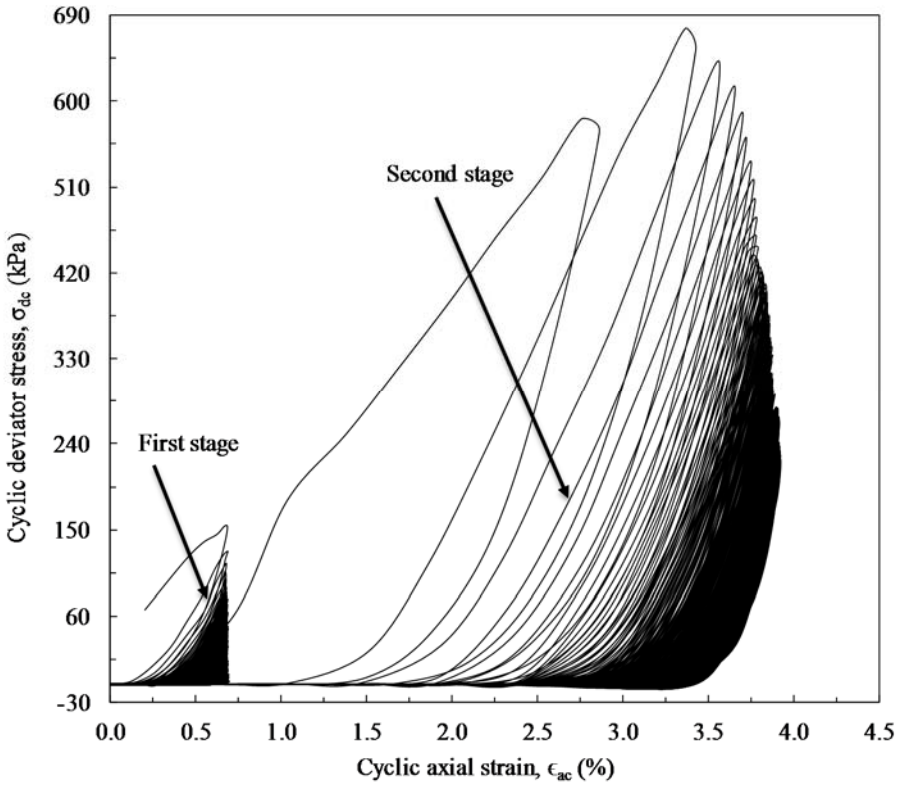

Figure 3.12. Cyclic tests on ballast in large chamber tests at two amplitudes

The modulus at the beginning and at the end of both stages of cyclic tests was calculated from stress-strain plots. This modulus is called constrained modulus. The resilient modulus was then determined using Eq. 3.3 (Fang, 1990).

$$M = \frac{E(1-\nu)}{(1+\nu)(1-2\nu)} \tag{3.1}$$

where M = Constrained modulus, E = Resilient modulus and ν = Poisson's ratio.

The stress-strain results for the start and end of the first stage cyclic loading test are shown in Figures 3.13 and 3.14, respectively, and the stress-strain results for the start and end of the second stage cyclic loading test are shown in Figures 3.15 and 3.16, respectively.

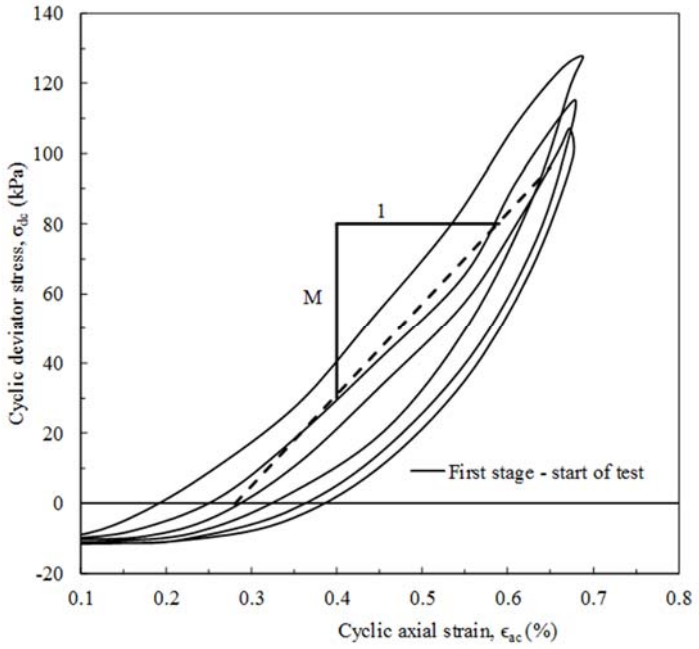

Figure 3.13. Resilient modulus at beginning of test for first stage

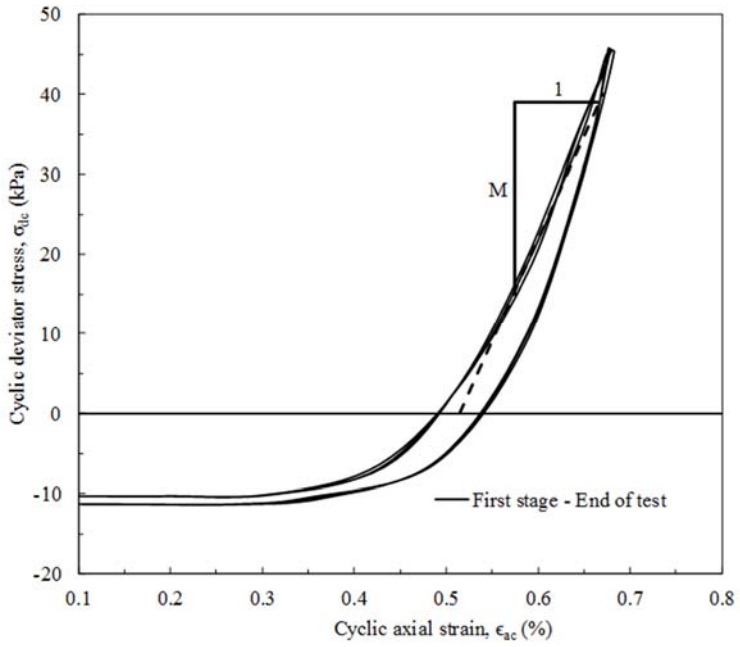

Figure 3.14. Resilient modulus at the end of test for first stage

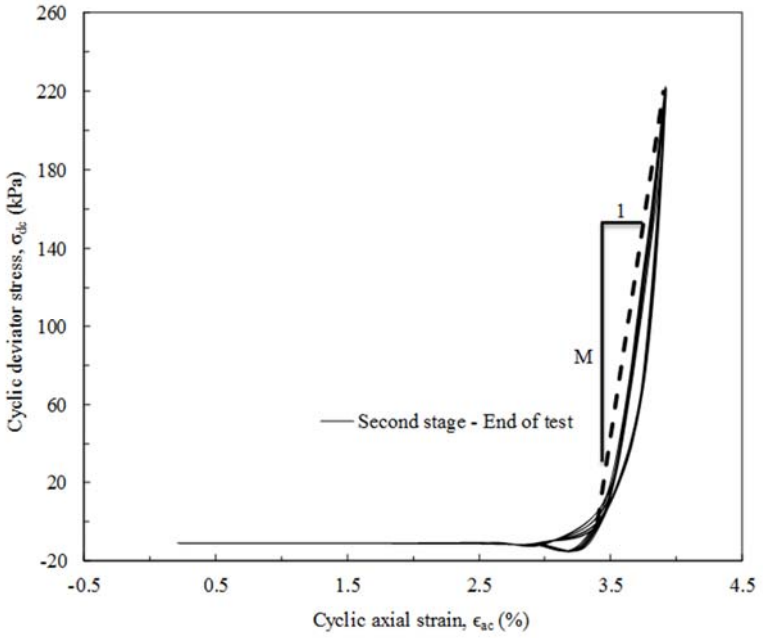

Figure 3.15. Resilient modulus at beginning of test for second stage

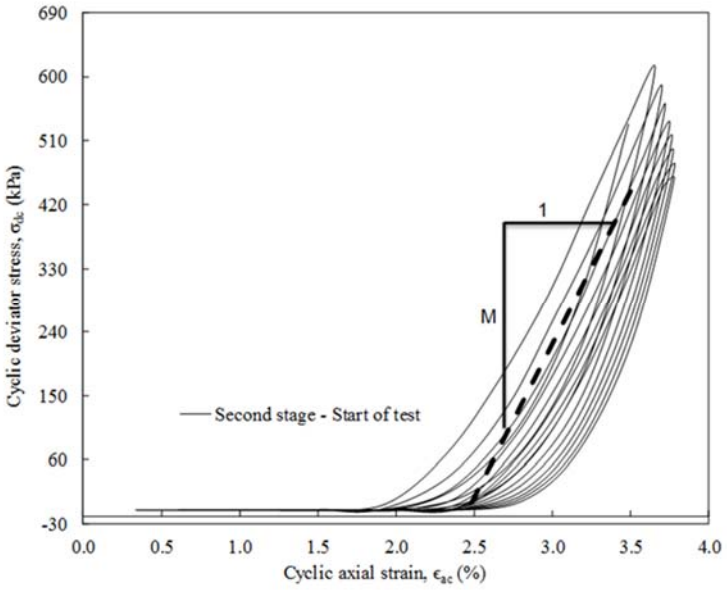

Figure 3.16. Resilient modulus at end of test for second stage

An average constrained modulus value of 25,000 kPa and 44,000 kPa was obtained for the first stage and second stage cyclic loading tests, respectively. A Poisson's ratio of 0.3 was assumed for the ballast material based on gravel (Li et al., 2008) and Eq. 2.3 was used to estimate the resilient modulus. An average resilient modulus value of 19,000 kPa and 33,000 kPa was obtained for the first stage and second stage cyclic loading tests, respectively. The densities for first and second stages were found to be 1500 kg/m^3 and 1600 kg/m^3. The resilient modulus in the second stage was higher due to the higher resulting density of the ballast material that may have occurred from the higher amplitude of the cyclic loading during the second stage compared to the first stage. The amplitude during the second stage loading was five time larger than the first stage.

Table 3.1 and Figure 3.17 provide the density and resilient modulus at different amplitude levels. Figure 3.17 indicates that density and resilient modulus both increased with increase in amplitude.

Table 3.1. Density and resilient modulus at different stages of loading

Stages	Amplitude (mm)	Density (ρ) (Kg/m^3)	Resilient modulus (M_r) (kPa)
First	5	1500	19000
Second	30	1600	33000

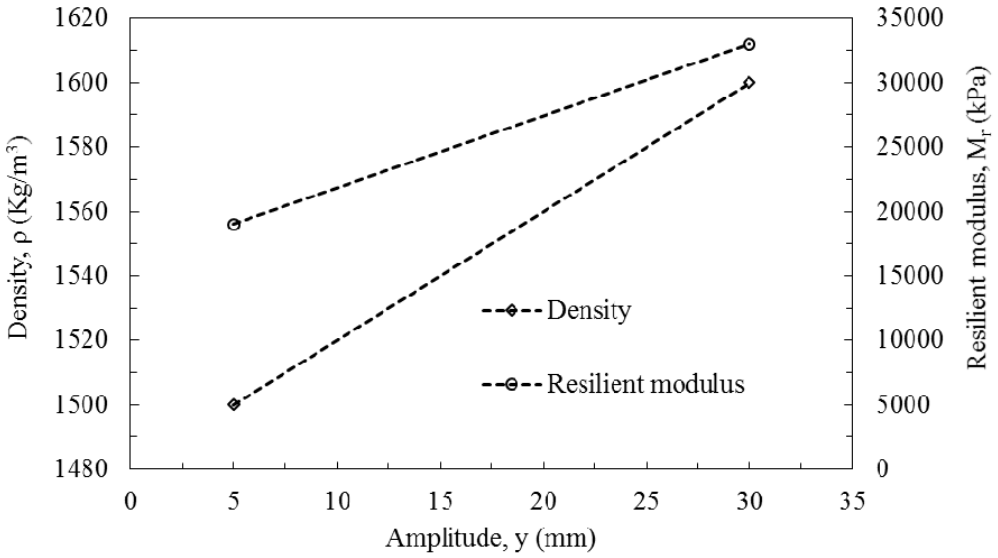

Figure 3.17. Density and resilient modulus at two levels of amplitude

Comparison of Resilient Moduli

The resilient modulus at three and 800 cycles obtained for the cyclic triaxial tests was found to be almost similar and averaged 14,000 kPa. The triaxial test was conducted at low level of amplitude because the average dynamic deflection was determined to be in the range of 1 mm to 5 mm in most of the cases under traffic loads (Bowness et al., 2007). An average resilient modulus value of 19,000 kPa was obtained for the large chamber first stage cyclic loading test that was conducted at a low level of 5 mm amplitude, which is similar to the amplitude that the triaxial test was performed. The density of the ballast material tested in the triaxial device was on the order of 1410 kg/m^3 and the density of the ballast tested in the large chamber device was 1500 kg/m^3.

The resilient modulus obtained from the cyclic triaxial test was approximately 25 percent less than large chamber test value. The lower resilient modulus obtained from the triaxial test can be partially attributed to the lower density of the ballast material tested in the triaxial test. Another potential reason for the difference in resilient modulus values obtained between the two tests is the need to assume a Poisson's ratio to obtain the resilient modulus based on the large chamber test results while an estimate of Poisson's ratio is not needed to obtain the resilient modulus from triaxial test results. Additionally, the boundary condition for cyclic triaxial test was flexible whereas the boundary condition for the large chamber test was constrained. Thus, the difference in boundary conditions between the two tests may have also contributed to variance between the resulting resilient modulus values obtained in the two tests.

The ballast material was directly used for large chamber testing whereas the sample for large scale triaxial testing had to be crushed into sizes smaller than 25.4 mm because the ASTM test procedure indicates that the largest size of the material to be tested should be smaller than 1/6 of the specimen diameter. The variance in particle diameters in the samples tested may have also contributed to the difference in resilient modulus values between the two test procedures.

Additional studies are needed to verify the differences between the two test procedures. Although the triaxial test is typically regarded as a more precise test, large chamber test results could be used to determine the resilient modulus of granular material for preliminary design.

SUMMARY AND CONCLUSIONS

Monotonic and cyclic triaxial tests at low amplitude and cyclic tests in a large chamber at low and high amplitudes were conducted in the laboratory to determine the Young's modulus of elasticity and resilient modulus of ballast material that has been used over an EPS geofoam embankment in a section of the FrontRunner commuter rail system in Corner Canyon in Draper City, Utah.

The monotonic triaxial test results revealed that the Young's modulus of elasticity was 52,000 kPa at very low confining pressure. The average resilient modulus at low amplitude (5 mm) was found to be 14,000 kPa based on cyclic triaxial tests. The resilient modulus obtained from the cyclic triaxial test was approximately 25 percent less than large chamber test value. The lower resilient modulus obtained from the triaxial test can be partially attributed to the lower density of the ballast material tested in the triaxial test, the need to assume a Poisson's ratio to obtain the resilient modulus based on the large chamber test results while an estimate of Poisson's ratio is not needed to obtain the resilient modulus from triaxial test results, the difference in boundary conditions, i.e., flexible in the cyclic triaxial test and constrained in the large chamber test, between the two tests, and the variance in particle diameters in the ballast samples tested between the traixial test, which had to be crushed into sizes smaller than 25.4 mm per the ASTM test procedure, and the full-size ballast used in the large chamber test.

Additional studies are needed to verify the differences between the two test procedures. Although the triaxial test is typically regarded as a more precise test, large chamber test results could be used to determine the resilient modulus of granular material for preliminary design.

The resilient modulus was almost double when the amplitude was increased by 6 times based on large chamber tests. The increase in resilient modulus with amplitude can be caused by the increase in density that occurs with increase in amplitude.

This chapter included a summary of the laboratory static and cyclic tests on ballast performed to determine the Young's modulus of elasticity and resilient modulus of ballast material for use in the numerical modeling study that is presented in Chapter 4.

REFERENCES

Anderson, W. F., and Fair, P. (2008). "Behavior of railroad ballast under monotonic and cyclic loading." *Journal of geotechnical and geoenvironmental engineering*, 134(3), 316-327.

ASTM D4767 (2004). *Standard test method for consolidated undrained triaxial compression test for cohesive soils*, American society for testing and materials, West Conshohocken, PA, USA.

Bowness, D., Lock, A., Powrie, W., Priest, J., and Richards, D. "Monitoring the dynamic displacements of railway track." *Proc., Institution of Mechanical Engineers, Part F: Journal of Rail and Rapid Transit*, 13-22.

Fang, H. Y. (1990). *Foundation engineering handbook*, Springer, New York, USA.

Ho, S., Tsang, W., Lee, K., Lee, K., Lai, W., Tam, H., and Ho, T. "Monitoring of the vertical movements of rail sleepers with the passage of trains." *Proc., Institution of Engineering and Technology International Conference on Railway Condition Monitoring, 2006*, IEEE, 108-114.

Li, G.-X., Chen, Y.-M., and Tang, X.-W. "Geosynthetics in Civil and Environmental Engineering." *Proc., Geosynthetics Asia 2008 Proceedings of the 4th Asian Regional Conference on Geosynthetics in Shanghai, China, Zhejiang University Press, Hangzhou and Springer-Verlag GmbH Berlin*.

Lu, S. (2008). "Real-time vertical track deflection measurement system." Ph.D. thesis, University of Nebraska, Lincoln, Nebraska, USA.

MnDOT (2015). "What is Resilient Modulus?"*Minnesota Department of Transportation Resilient Modulus Testing,* <http://www.dot.state.mn.us/materials/mr/> (June 5, 2015).

Pavement Interactive. (2007). "Resilient Modulus.*" Design, Design Parameters, Resilient Modulus."* <http://www.pavementinteractive.org/article/resilient-modulus/> (June 5, 2015).

Ping, W. V., Yang, Z., and Gao, Z. (2002). "Field and laboratory determination of granular subgrade moduli." *Journal of Performance of Constructed Facilities*, 16(4), 149-159.

Pinto, N., Ribeiro, C., Mendes, J., and Calçada, R. (2009). "An optical system for monitoring the vertical displacements of the track in high speed railways." *Proc., 3rd International Integrity Reliability and Failure,* Portugal, 1-9.

Psimoulis, P. A., and Stiros, S. C. (2013). "Measuring deflections of a short-span railway bridge using a robotic total station." *Journal of Bridge Engineering*, 18(2), 182-185.

CHAPTER 4: EVALUATION AND NUMERICAL MODELING OF DEFLECTIONS AND VERTICAL DISPLACMENT OF RAIL SYSTEMS SUPPORTED BY EPS GEOFOAM EMBANKMENTS

INTRODUCTION

The main purposes of the literature review were to: (1) explore potential methods to model EPS embankments and the deformations associated with train loadings, and (2) review models and embankment performance cases that could be potentially used in the development and validation of the proposed model of the section of the FrontRunner commuter rail system in Corner Canyon in Draper City, Utah that includes an EPS geofoam embankment.

OBJECTIVES OF THE NUMERICAL MODEL STUDY

This research seeks to develop a numerical method to evaluate the rail deflections for systems constructed atop EPS embankments. The objectives of the numerical model study are: (1) develop the numerical method, (2) validate the model through a series of modeling exercises, and (3) verify and calibrate the numerical approach for real rail systems using deflection measurements obtained from Norway, and from the UTA FrontRunner project in Draper, Utah. To accomplish these objectives, the following tasks/activities are required: (1) literature review of numerical modeling studies of deflections of rail systems, (2) laboratory testing of material properties, (3) model development, (4) model validation, (5) model calibration, (6) comparison with measurements obtained for real systems.

Chapter 2 includes a summary of the literature numerical modeling studies of deflections of rail systems supported by EPS geofoam embankments and Chapter 3 presents a summary of the laboratory static and cyclic tests on ballast performed to determine the Young's modulus of elasticity and resilient modulus of ballast material for use in this numerical modeling study. This chapter presents the numerical model studies performed to evaluate deflections and vertical displacements of the section of the FrontRunner commuter rail system that includes an EPS geofoam embankment.

DEVELOPMENT OF NUMERICAL APPROACH FOR DEFLECTION ESTIMATION

According to AREMA Manual for Railway Engineering, this type of analysis is conducted by considering the rail to be supported on an elastic foundation. Because the deformation caused by rail loads is very small compared to the size of the embankment system, the deformation can be assumed to be within the elastic range of the materials; hence elastic properties of the materials can be used in the constitutive model.

Therefore, the modeling done is this study will be elastic models using the finite difference method (FDM). Both 2D finite difference models, i.e., FLAC2D v. 5 (Fast Lagrangian Analysis of Continua) (Itasca, 2005) and 3D finite difference models, i.e., FLAC3D v. 3 (Itasca, 1993-2002) will be implemented. 2D models will be used as exploratory models to identify the appropriate mesh size and the associated level of discretization of 3D models.

VALIDATION OF NUMERICAL APPROACH

For validation purposes, the FDM modeling approach developed in this study will be checked against existing closed-form solutions, other FEM (finite element method) models from the literature and with measurements obtained from case histories from real railway systems. It is hoped that the results obtain herein should reasonably match these modeling and case history examples in order to validate of the FDM modeling approach for potential use in evaluating real systems.

To this end, the FDM model development will start from simple analytical cases and progress to modeling real rail systems supported on EPS embankments. The progressive modeling cases considered and compared will include: (1) point load on homogeneous elastic half-space using elastic theory (Appendix A), line load on homogeneous elastic half-space using FEM (Helwany, 2007) (Appendix B), and a circular load on layered soil systems using FEM (Appendix C),

VERIFICATION AND CALIBRATION OF THE NUMERICAL APPROACH

Chapter 3 presents a summary of the laboratory static and cyclic tests on ballast performed to determine the Young's modulus of elasticity and resilient modulus of ballast and sub-ballast material for use in this numerical modeling study. Other material properties, such as Poisson's ratio of the ballast and sub-ballast, the properties of other materials including EPS, rail, and sleeper are obtained from the literature.

The deflections of rail systems supported by regular earth embankments due to train load have been analyzed using the FEM for a real system (Powrie et al., 2007). This case will be initially modeled using the FDM to initiate the development of the modeling method for rail systems supported on EPS. Next. The FDM will be used to model of the measured deflections obtained by the Norwegian Railways (NSB) for a case history of EPS embankment in Central Norway. Finally, based on the results of the FDM studies of the Powrie et al. (2007) case history for regular rail earth embankment and the NSB case history for an EPS embankment, a FDM model for the UTA FrontRunner EPS embankment in Corner Canyon, Draper Utah is developed. The FDM model will then be used to make predictions of the deflections of the UTA

Frontrunner EPS embankment in Corner Canyon, Draper Utah. The deflections obtained from the FDM model will be compared with actual field measurements of deflections in Chapter 5. It is hoped that when validated, the FDM approach can be used in future projects for the design and evaluation of EPS supported rail systems.

FDM MODELING INTRODUCTION

As a main part of this study, three FDM models were developed and evaluated: (1) a hypothetical earthen rail embankment where the results were compared and verified with FEM modeling of the same embankment as presented in the literature by Powrie et al. (2007), (2) an actual EPS-supported, multilayered, Norwegian, commuter railway embankment system where the results were compared and verified with field deflection measurements from Norway for that same system (Frydenlund et al., 1987), and (3) an actual EPS-supported embankment for the Utah Transit Authority (UTA) Commuter Rail System (i.e., FrontRunner) in Corner Canyon, Draper City, Utah. The field deflection measurements of the FrontRunner commuter rail system that includes an EPS geofoam embankment are presented in Chapter 5.

This chapter contains problem statements for each case and the simplifications made for modeling purposes. In addition, the details of the FDM models including geometry, boundary and loading conditions and model properties are also described. The results are presented and compared with the FEM modeling by others, or with actual field measurements of railway deflections, when available.

In order to calculate the vertical deflections induced in the rail systems, both 2D finite difference models, i.e., FLAC2D v. 5 (Fast Lagrangian Analysis of Continua) (Itasca, 2005) and 3D finite difference models, i.e., FLAC3D v. 3 (Itasca, 1993-2002) were implemented. The 2D models are axisymmetrical or plane strain models that include structural elements. The 3D models are plane-symmetrical models. The FDM model for regular earth embankments based on the case history presented by Powrie et al. (2007) is initially presented followed by the FDM model for the Norway EPS embankment case history and the FrontRunner commuter rail EPS geofoam embankment.

RAIL SYSTEM SUPPORTED BY REGULAR EARTH EMBANKMENT

Problem Statement

Powrie et al. (2007) conducted a 2D FEM analysis on displacements caused by wheel load at the ground surface of a railway system supported by an embankment using the geometry shown in Figure 4.1 with a

static wheel load of 125 kN. A similar 2D FDM analysis was conducted in this current project for comparison and verification of the FDM modeling.

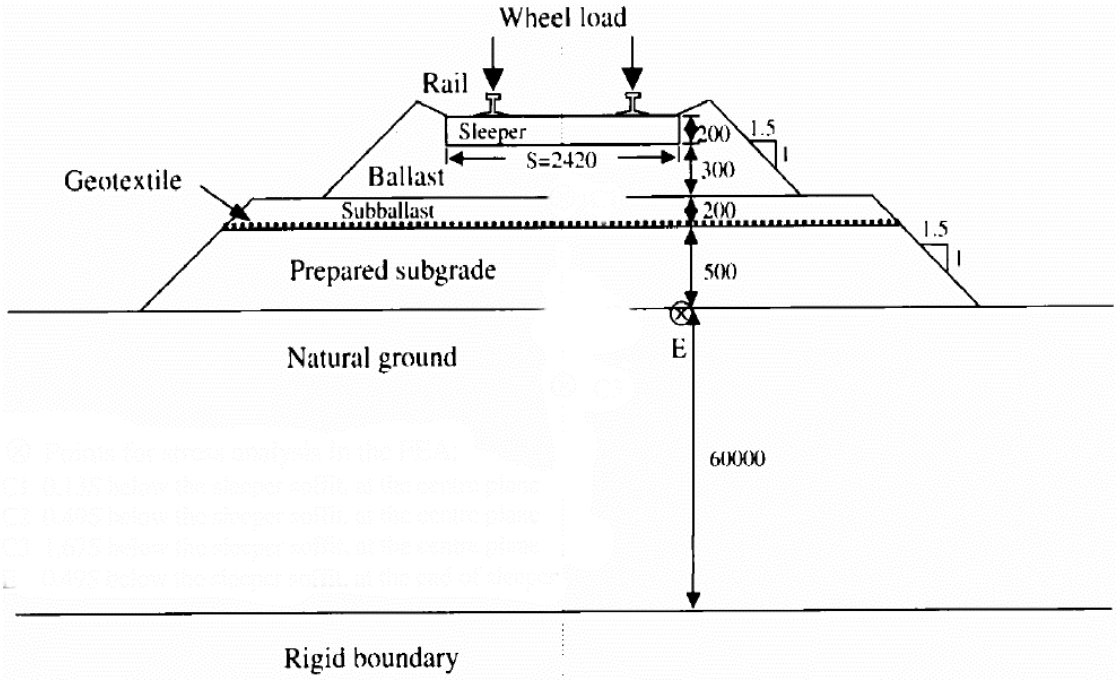

Figure 4.1. Schematic Cross-section of a Typical Track Structure (mm)

Assumption/Simplifications

To analyze the 3D railway system in a 2D model, Powrie et al. (2007) used the following simplification to convert the discrete sleeper spacing into an equivalent, continuous loading for the 2D plane strain model. Because in a 2D analysis the sleepers are inherently continuous, the Young's modulus (E) of the sleepers was scaled by the ratio of sleeper width (w, 242 mm) to spacing (a, 650 mm) to give the same value of lateral bending stiffness EI per meter length of the track as for the discrete sleepers.

FEM Solution

In order to determine the appropriate mesh spacing for the analyses, three mesh densities were investigated by Powrie et al. (2007): (1) an intermediate mesh (Figure 4.2), (2) a coarse mesh which had half the element density (i.e., approximately one-quarter of the number of elements) and (3) a fine mesh which had twice the element density (i.e., about four times the number of elements). In all cases, the bottom and right-hand boundaries were restrained in both the horizontal and vertical directions. The left-hand boundary was

prevented from moving in the horizontal direction, but allowed to move freely in the vertical direction, which is consistent for an axis of symmetry found along the left-hand margin of the model.

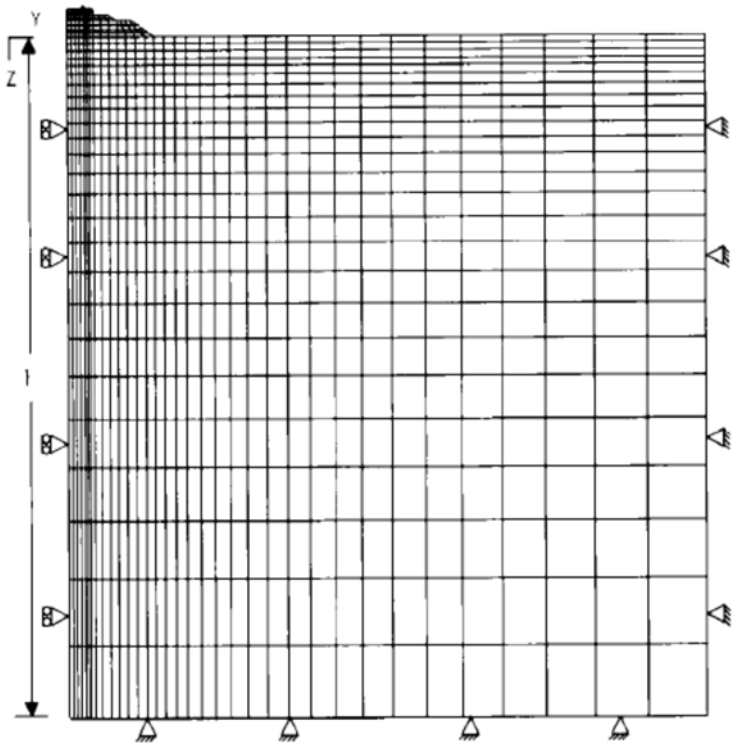

Figure 4.2. FEM Mesh

Powrie et al. (2007) found that all three meshes gave almost identical ground-surface displacements. However, differences in the stresses within the ballast layer were noted, particularly for the coarse mesh, so the intermediate mesh was used by Prowie et al. for subsequent analyses. The intermediate density mesh had dimension 60 m × 60 m for the depth and width of natural ground (Figure 4.2). A ground displacement of 1.14 cm was obtained by Powrie et al. (2007) for the 125 kN wheel load.

2D FDM FLAC Solution

The 2D FEM solution of Powrie et al. (2007) was modeled in FLAC 2D as a check of the 2D FDM approach. Figure 4.1 shows the geometry of the multilayer rail system that was used in the verification. In the FEM and FDM models, only half of the system was included because the system is symmetrical (Figure 4.2). Figure 4.3 shows the FDM mesh that was developed to represent the system. The FDM used approximately the same intermediate density mesh of Powrie et al. (2007) with dimensions of 60 m × 60 m (depth and width of natural ground).

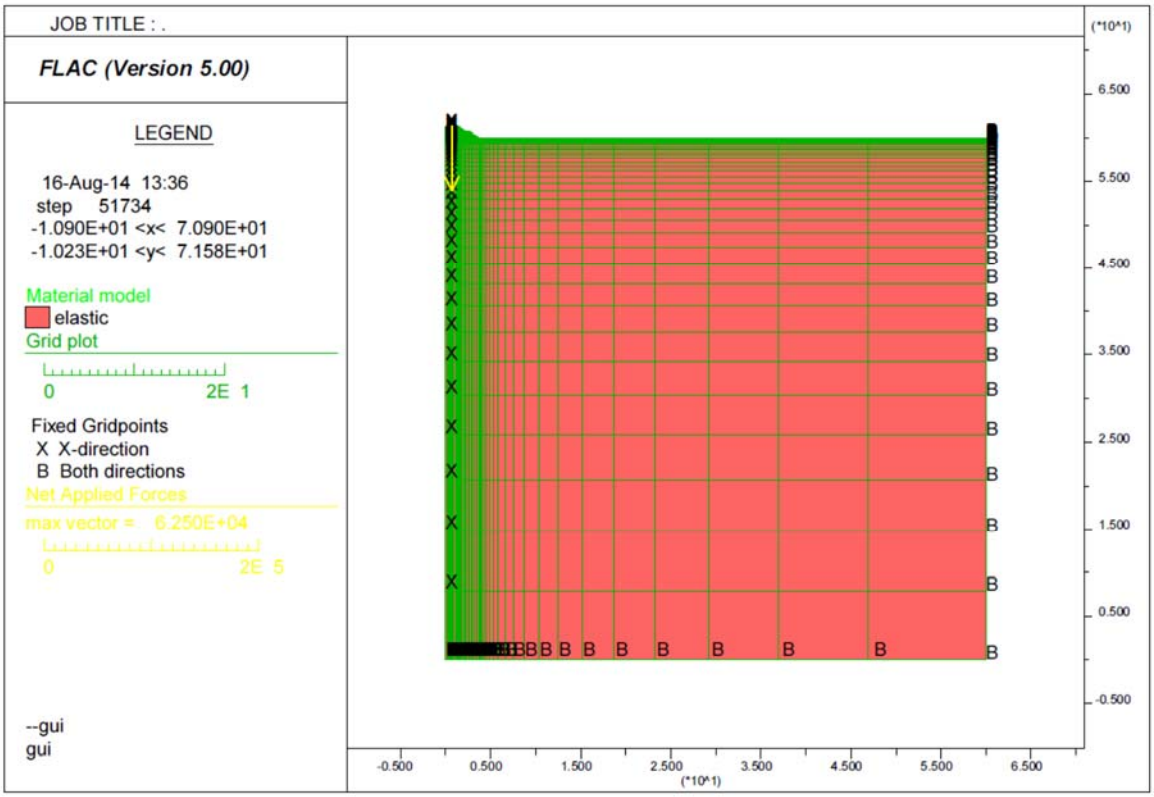

Figure 4.3. FDM Mesh (m)

The bottom and right-hand boundaries were restrained in both the horizontal and vertical directions. The left-hand boundary was prevented from moving in the horizontal direction, but was free to move vertically. A wheel load of 125 kN was applied on each rail. (In the FLAC modeling, because there are two nodes assigned to a single rail, a vertical force of 62.5 kN was applied to each node.) The properties of each material are shown in Table 4.1. These were used for both the FEM and FDM modeling and were taken from Powrie et al. (2007). Values of the shear modulus (G) and bulk modulus (K) required for the FLAC modeling were calculated using elastic theory based on the values of Young's modulus (E) and Poisson's ratio (v) given in Table 4.1.

Table 4.1. Material Properties Used in FEM and FDM Analysis

Description	E (MPa)	v	Note
Rail	210000	0.3	78 mm wide, 153 mm deep
Sleeper (2D)	13000	0.3	242 mm wide, 200 mm deep
Ballast	310	0.3	
Sub-ballast	130	0.49	
Prepared subgrade	100	0.49	
Natural Ground	30	0.49	

Comparison, Conclusion and Discussion

The FDM, as implemented in the FLAC model, gave results that were very similar to those reported in Powrie et al. (2007) using the FEM. The vertical displacement contours for the FDM are shown in Figure 4.4. Directly under the rail, the FDM FLAC model estimates a total ground surface displacement of 11.7 mm from the 125 kN wheel load; the FEM analysis of Powrie et al. (2007) resulted in a total ground surface displacement of 11.4 mm. The difference in these modeling results is about 3%. The similarity in the results demonstrates that both methods are capable of producing consistent results when used to estimate ground surface displacement of railway system under static loading. The FLAC code used for this modeled case is found in Appendix D.

RAIL SYSTEM SUPPORTED BY EPS EMBANKMENT IN NORWAY

Problem Statement

The next step in the modeling progression was to see if the FDM is capable of estimating total ground displacement for a real EPS embankment system. This will be done using an example of an EPS embankment constructed in Norway that was subjected to a commuter-rail loading. Survey measurements were made of the static rail deflections resulting from this loading and documented by the Norwegian Public Road Administration (Frydenlund et al., 1987).

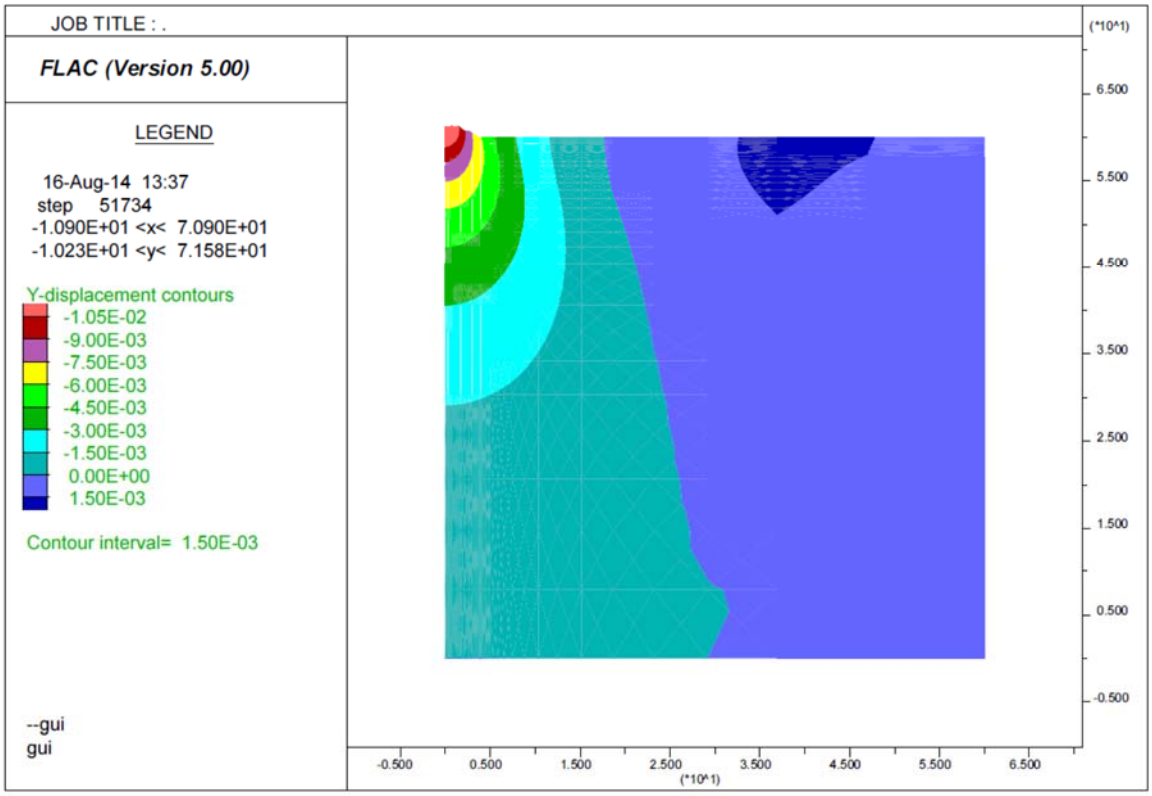

Figure 4.4. Vertical Displacement Contours (m)

Plans to reconstruct the National Road 36 at Bole near the City of Skien in Telemark, Norway included building a new railway overpass bridge at a road underpass (Frydenlund et al., 1987). In order to increase the headroom at the underpass for the highway, the road elevation was lowered and the railway line embankment was elevated somewhat. The new bridge was to be constructed on footings founded in a sand layer; however, associated with the wider road and lowered road level, the construction could potentially cause stability issues in the foundation soils which were soft and clayey in nature. To address this issue, Expanded Polystyrene (EPS) geofoam block was selected as a superlight fill material against the northern bridge abutment.

EPS with a unit density of 30 kg/m^3 (i.e., EPS30) was used at this location. A 15-cm thick reinforced concrete slab was cast atop the EPS geofoam blocks (Figures. 4.5 and 4.6). The height of the EPS embankment was 4 blocks high (Figure 4.5), and the corresponding height of each individual block was 0.6 m, making the total EPS embankment height equal to 2.4 m. The length of the sleepers supporting the rail was estimated to be 2.42 m. The material properties used in the FDM modeling are given in Table 4.2. (Note that the EPS was modeled in the FLAC model using published properties from ASTM D6817 for

EPS29 (density = 29 kg/m^3) instead of EPS30 (density = 30 kg/m^3) because material properties were not available from Frydenlund et al., 1987 for EPS30. Because EPS29 has nearly the same density as EPS30, only very minor differences in the material properties are expected, and these differences should not affect the modeling results in a significant manner.)

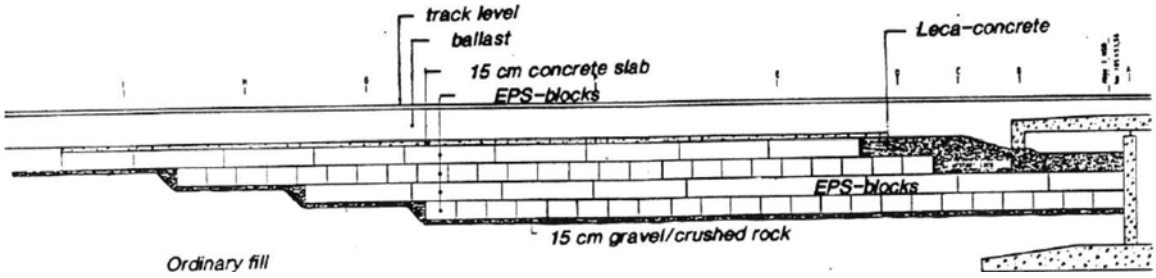

Figure 4.5. Longitudinal Section of the EPS Supported Embankment

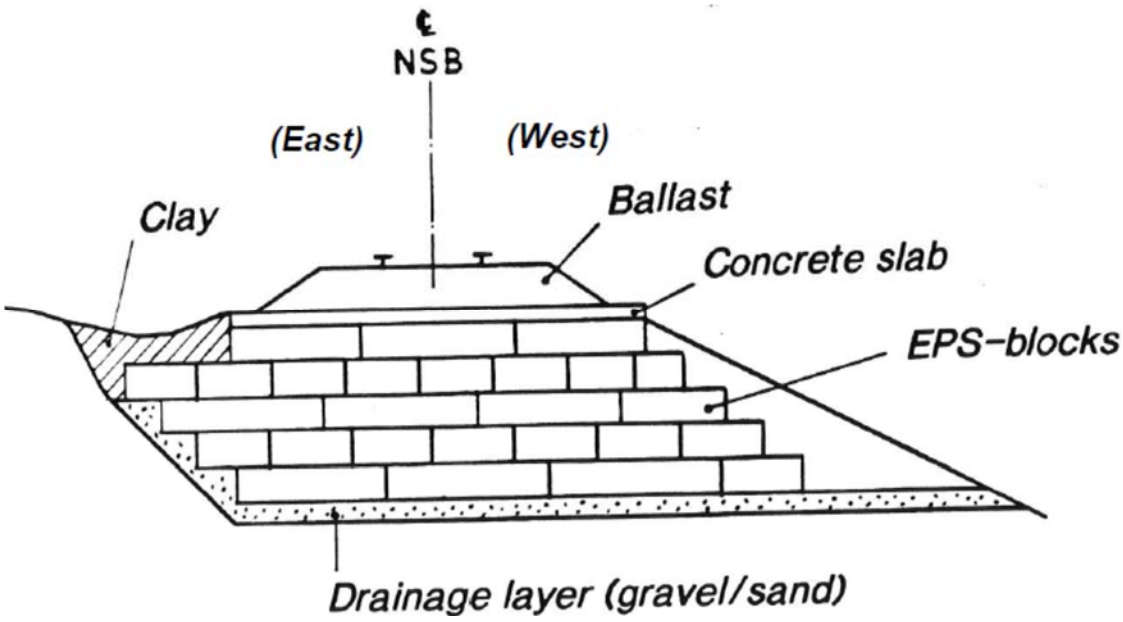

Figure 4.6. Cross-section of the EPS Supported Embankment

Table 4.2. Material Properties Used in FDM Analysis

Description	E MPa	v	Note
Rail	210000	0.3	78 mm wide, 153 mm deep
Sleeper (3D/2D)	31000/13000	0.3	242 mm wide, 200 mm deep
Ballast	130	0.3	
Concrete Slab	40000	0.2	
EPS29	7.5	0.103	
Drainage Layer	300	0.3	
Fill	300	0.3	
Sand (Natural Ground)	100	0.3	

2D Model Preparatory Study

To model the Bole embankment rigorously, a 3D model is required; however, a 2D model was developed beforehand to identify the appropriate mesh size and the associated level of discretization required to reasonably estimate the total surface displacement from the train loading. This exploratory use of a 2D model was preferable because it required significantly less computational time and computer memory.

Similar to Powrie et al. (2007), three mesh densities were investigated: (1) an intermediate mesh (Figure 4.7, see also FLAC code in Appendix E), (2) a coarse mesh and (3) a fine mesh. In all the cases, the bottom and right-hand boundaries were restrained in both the horizontal and vertical directions. The left-hand boundary was prevented from moving the horizontal direction, but free to move vertically. All three meshes produced nearly the same vertical displacement of the sleeper. Thus, within this range, the influence of mesh density was negligible on the prediction of vertical displacement, which was also found by Powrie et al. (2007) in their FEM. An intermediate or fine mesh was used in the subsequent 2D and 3D modeling.

Five mesh sizes were developed and investigated. For these, a line load of 155 kN/m was applied at the top of the rail in the FDM model. The vertical displacement of the sleeper as a function of mesh size is found in Figure 4.8. These results suggest that the predicted vertical displacement of the sleeper converged rapidly, and a mesh size of 60 m × 60 m (width × depth) was sufficient to produce stable results. Thus, this spacing was used in the 3D modeling described in the next section.

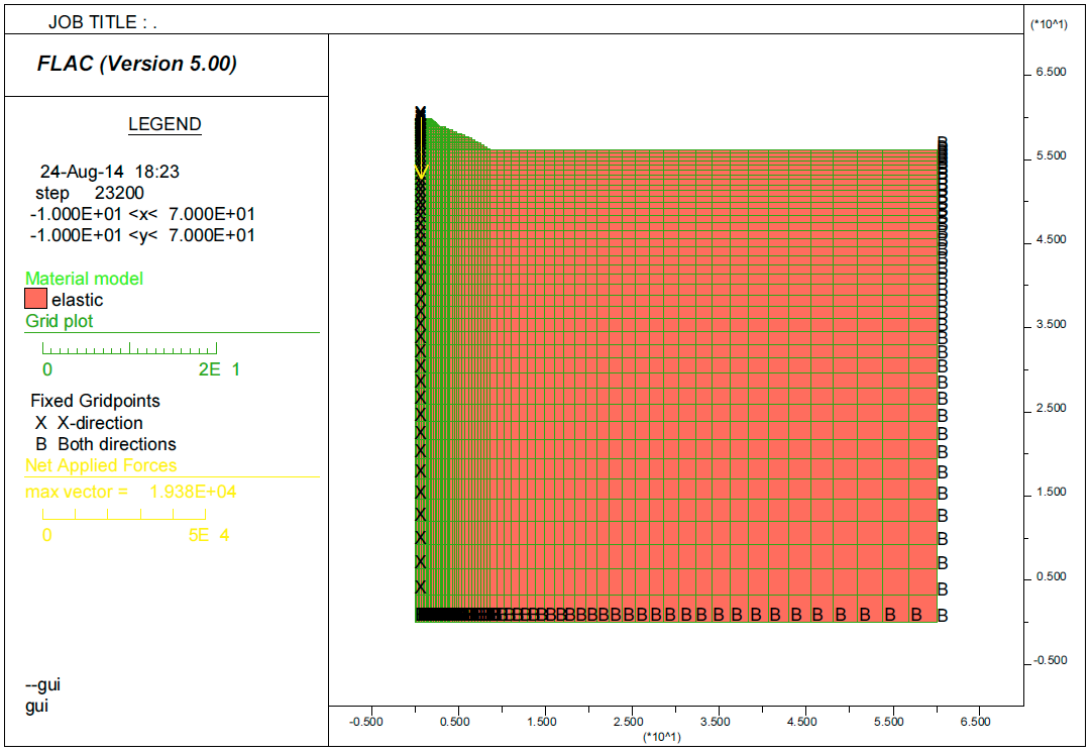

Figure 4.7. FDM Intermediate Mesh (m)

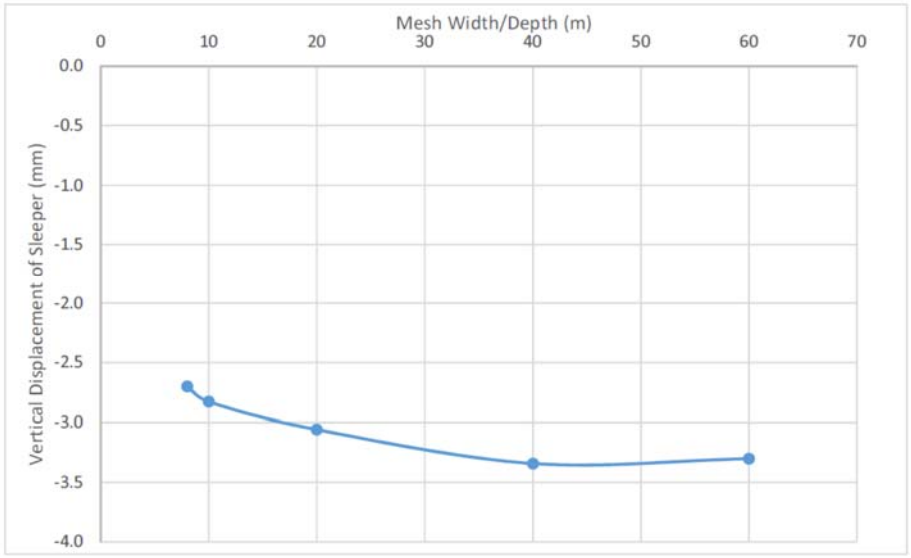

Figure 4.8. Mesh Size's Influence on Vertical Displacement of Sleeper

3D Solution

FIELD TEST RESULT

After the new bridge was completed, static load tests were carried out by the Norwegian Public Roads Administration (NPRA) in order to measure the vertical displacement of the rail and sleepers due to train loads using precision survey techniques (Frydenlund et al., 1987). For that purpose, a locomotive with wheel configurations as shown in Figure 4.9 was used. Deflections were measured (1988-08-31) on the bolts in the concrete slab above the EPS-blocks at different stations along the embankment (See Figure 4.10). The results are between 2 and 3 mm of vertical deflection for the west rail (i.e., right side of Figure 4.6)

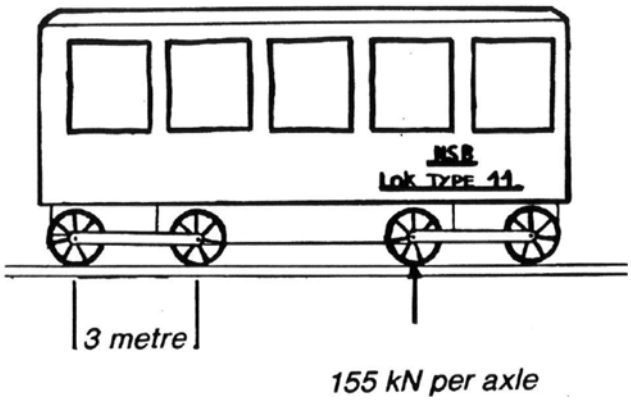

Figure 4.9. Load Configuration

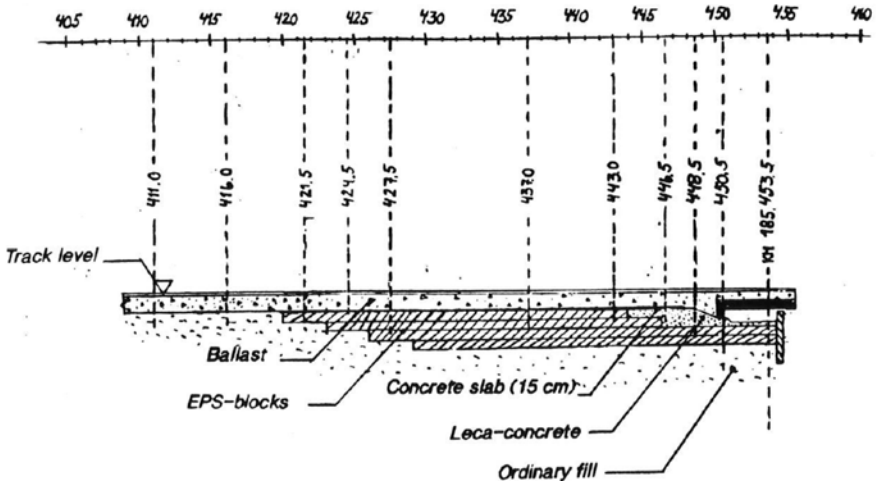

Figure 4.10. Stationings of the Embankment

FDM SOLUTION (FLAC)

Figures. 4.5 and 4.6 were used to create the geometry for the 3D FLAC model. Key measurements of the system have been previously stated in the Problem Statement Section of this Norway case history. The remaining dimensions used for this model were obtained based on scaling from these figures. In the 3D model, only the west half of the system was analyzed because the system is reasonably symmetrical. Figures. 4.11 and 4.12 show the mesh developed for the FLAC modeling.

The length of the mesh in the longitudinal (y) direction was taken as that of the locomotive. In the vertical (z) and lateral (x) directions, the dimensions of the mesh were set at 60 m because the results of the two-dimensional analyses indicated that this should be sufficient to eliminate the boundary effects. Smaller elements were used near the track where the changes of stresses and strains were expected to be the greatest. The bottom and far-lateral boundaries (Plane 2 and 3 in Figure 4.12) were prevented from movement in all three directions. The longitudinal boundaries (Plane 4 in Figure 4.12) were fixed in the x direction only. The center plane (Plane 1 in Figure 4.12) was fixed in the y direction only.

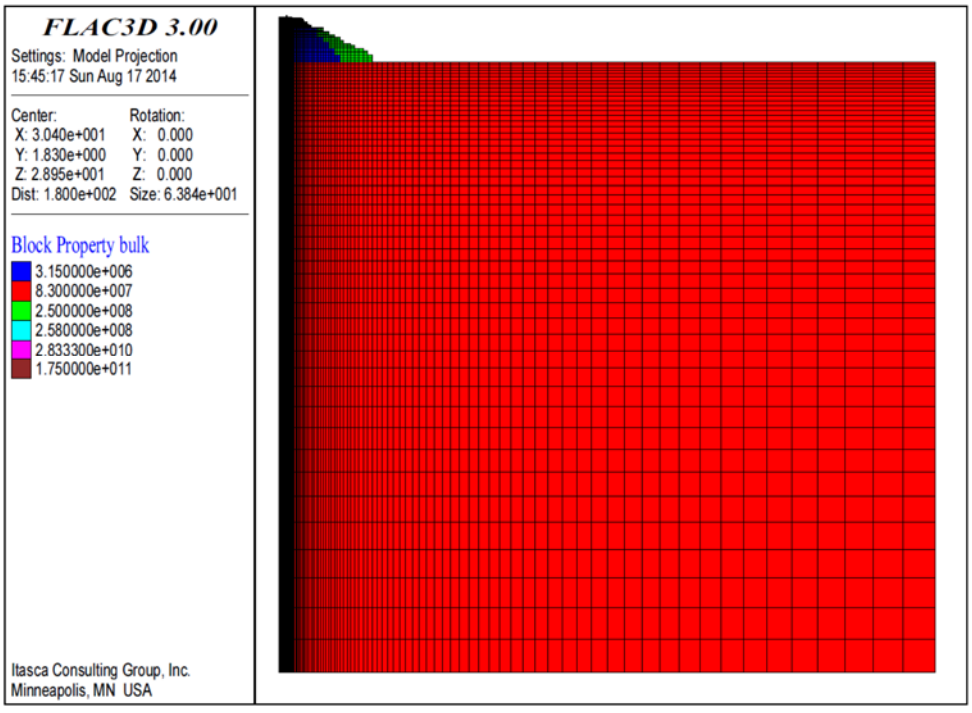

Figure 4.11. Cross-section View of Model Mesh

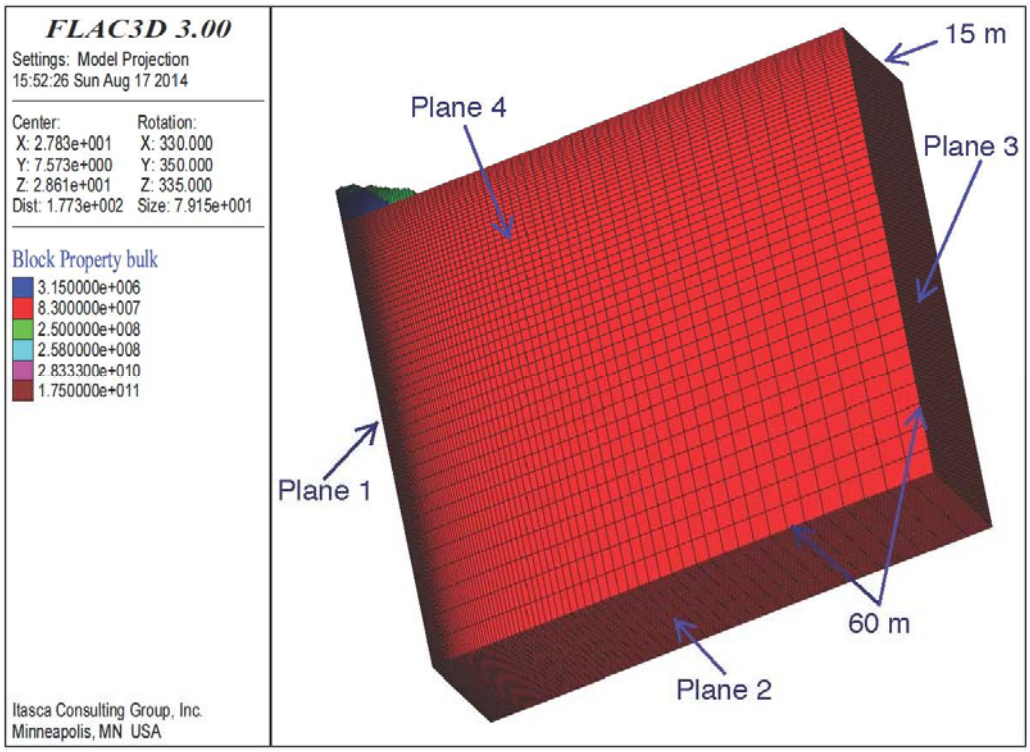

Figure 4.12. 3D view of Model Mesh

The loading conditions for this case are illustrated in Figure 4.13. The properties of each material are shown in Table 4.2. Estimates of the shear modulus (G) and bulk modulus (K) were calculated based on the E and v values in this table using elastic theory and input in the FLAC model for the respective materials. See Figure 4.11 and Figure 12 for plots of the properties used in the model.

The vertical displacement contours are shown in Figures. 4.14 through 4.17. The maximum vertical rail displacement calculated by FLAC is 2.3 mm which occurs directly under the wheels. In addition, FLAC3D indicates that the concrete slab has a vertical displacement ranging from 1.8 mm to 2.3 mm. (Compare Figures. 4.14 and 4.15 with Figures. 4.16 and 4.17.) Based on this, it is obvious that the railway embankment system settles much more uniformly in the longitudinal (y) direction than in the lateral (x) direction. In addition, even though the thickness of the EPS layer is only approximately 5% of the full depth of the embankment model, approximately 60% of the vertical deformation occurs in the EPS. This is due to the fact that the EPS has a much lower bulk and shear moduli than other materials (i.e., rail, sleeper, ballast, concrete slab, natural ground, etc.).

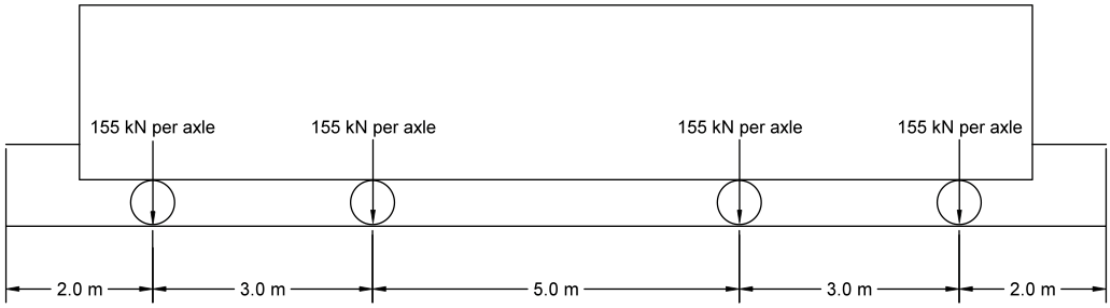

Figure 4.13. Loading Conditions

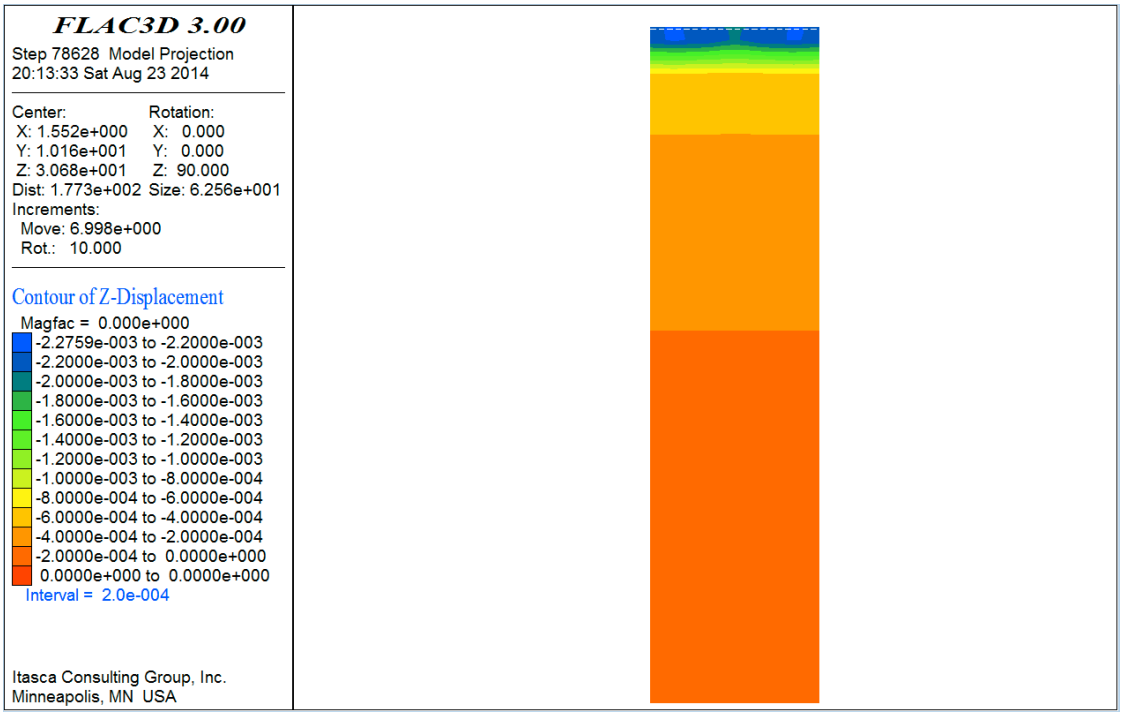

Figure 4.14. Full Model Profile View of Vertical Displacement Contours (m)

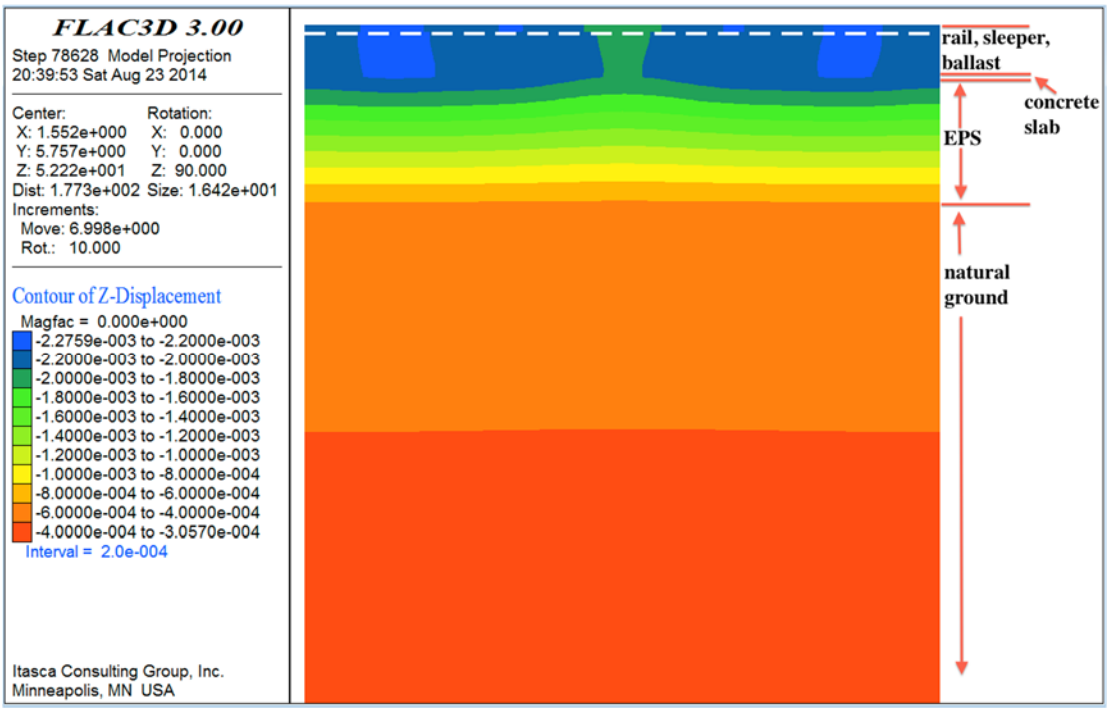

Figure 4.15. Zoomed-in Profile View of Vertical Displacement Contours (m)

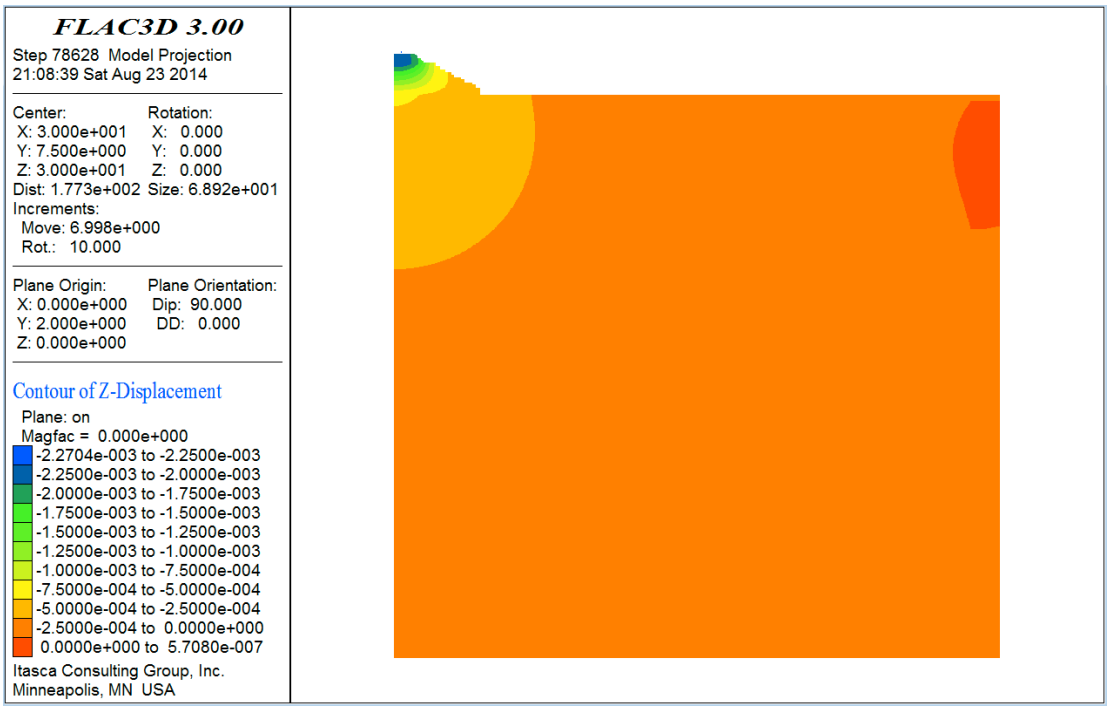

Figure 4.16. Full Model Cross-section View of Vertical Displacement Contours (m)

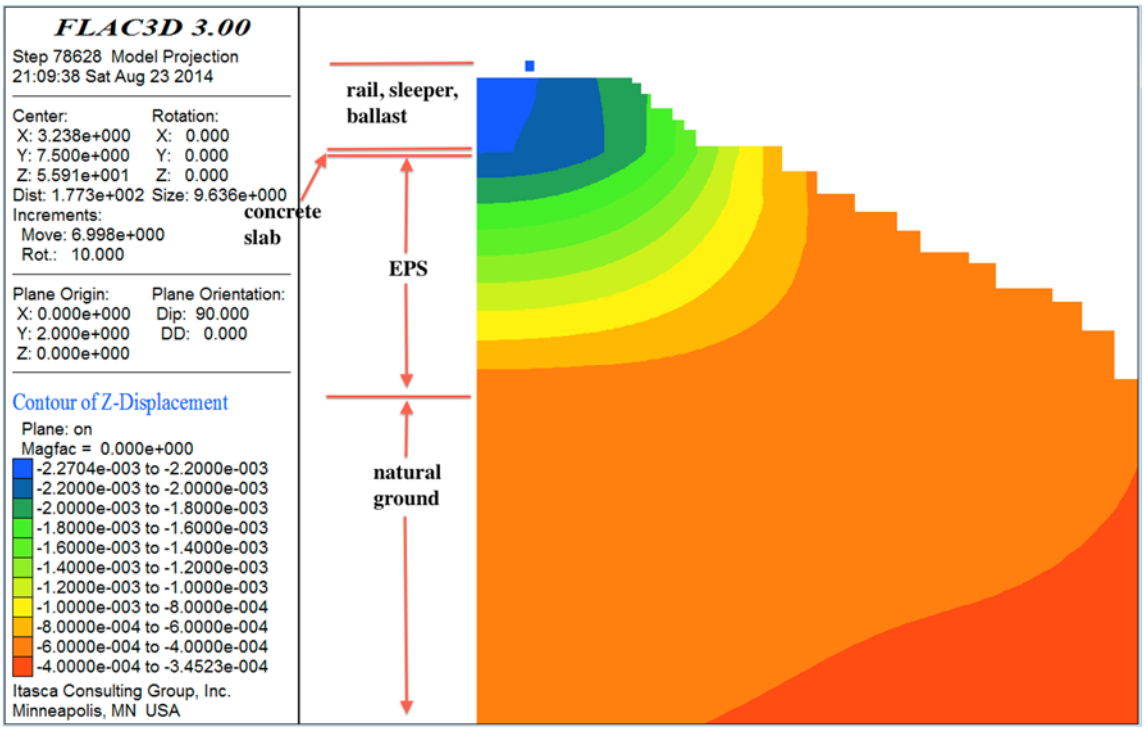

Figure 4.17. Zoomed-in Cross-section View of Vertical Displacement Contours (m)

Figures. 4.18 and 4.19 show the lateral (x direction) and longitudinal (y direction) displacement of the railway embankment system. The system has a maximum lateral displacement of 0.2 mm, and a maximum longitudinal displacement of 0.02 mm. Both of which are relatively insignificant compared with the magnitude of the predicted vertical displacement.

Figure 4.20 shows the vertical stress contours of the railway embankment system. Figures. 4.21 and 4.22 show the horizontal stress contours of the railway embankment system in lateral (x) direction and longitudinal (y) direction. Figures. 4.23 and 4.24 show the shear stress contours of the railway embankment system. Using the results of these plots, one can observe that the normal and shear stresses within the system are distributed relatively uniformly by the rail-sleeper-ballast-concrete slab system. This is due to the high stiffness (i.e., high bulk and shear moduli) of these materials in relation to the underlying EPS and soil materials.

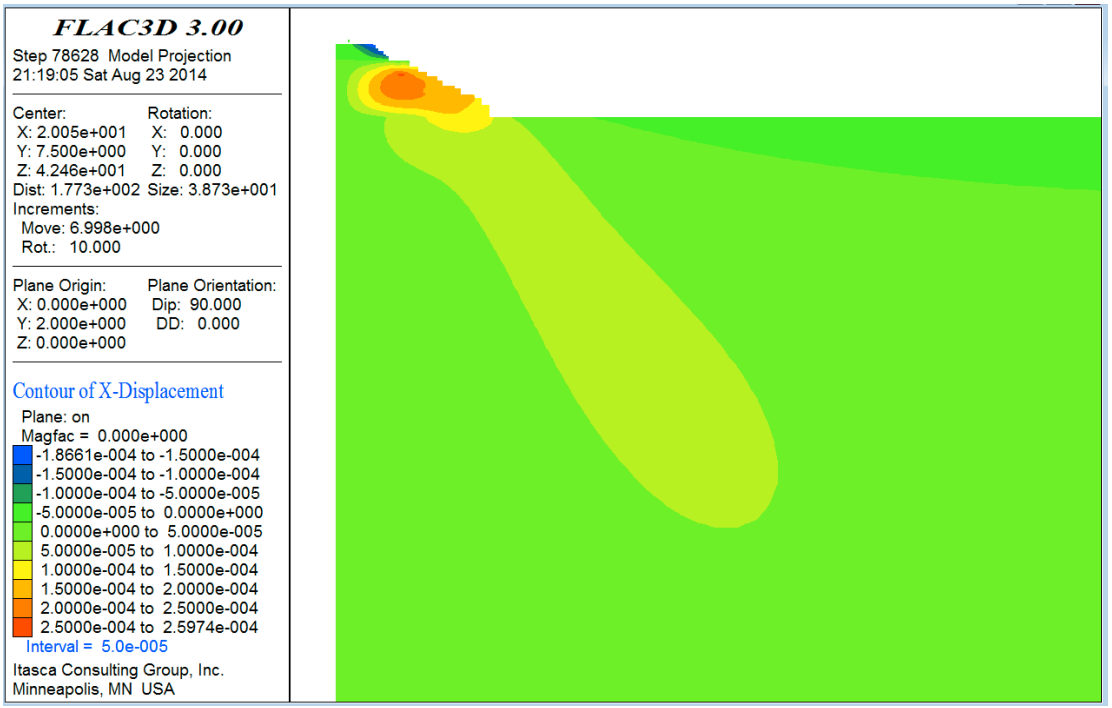

Figure 4.18. Lateral Displacement Contours in X Direction (m)

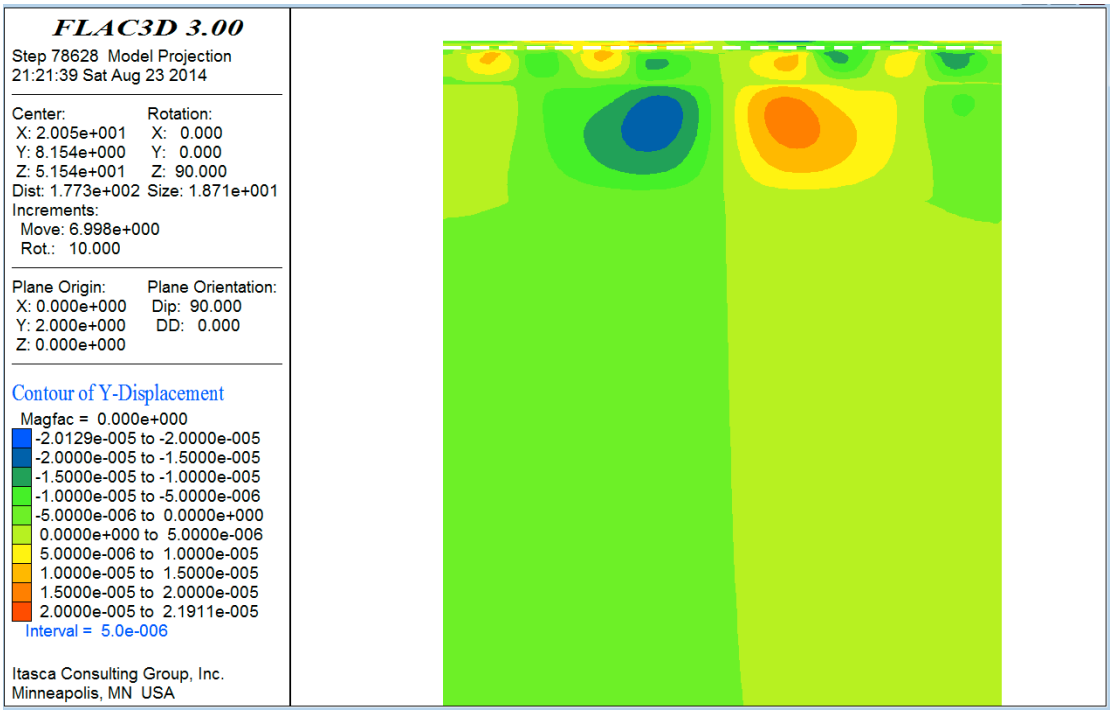

Figure 4.19. Longitudinal Displacement Contours in Y Direction (m)

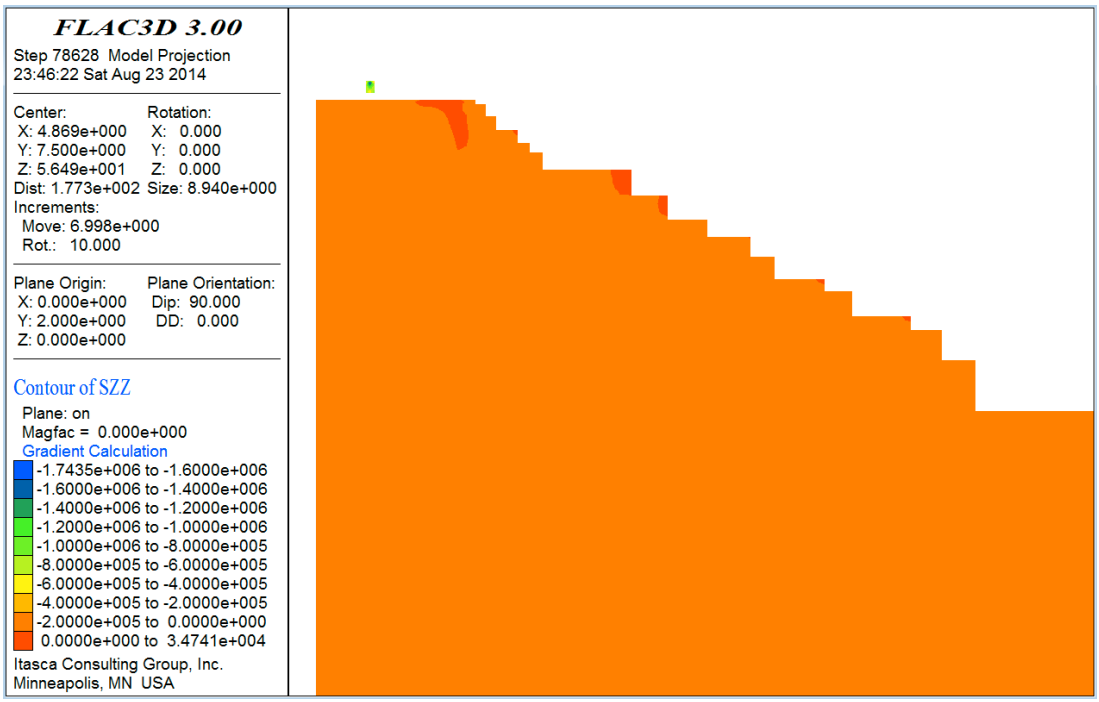

Figure 4.20. Vertical Stress Contours (Pa)

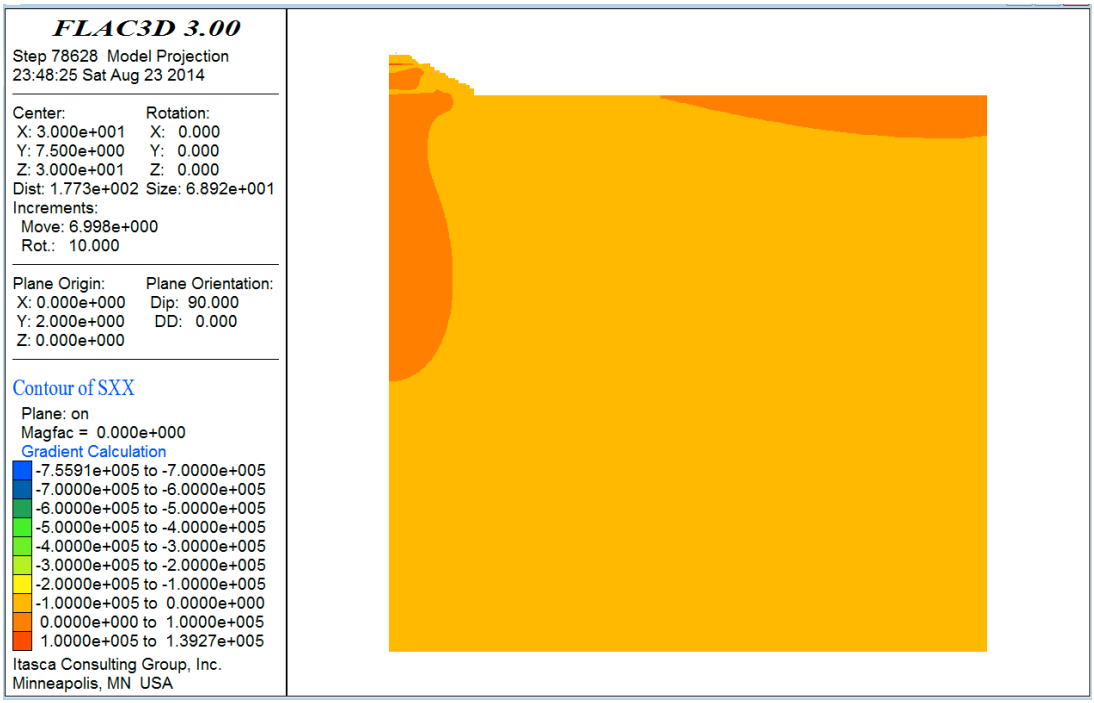

Figure 4.21. Horizontal Stress Contours in Lateral (x) Direction (Pa)

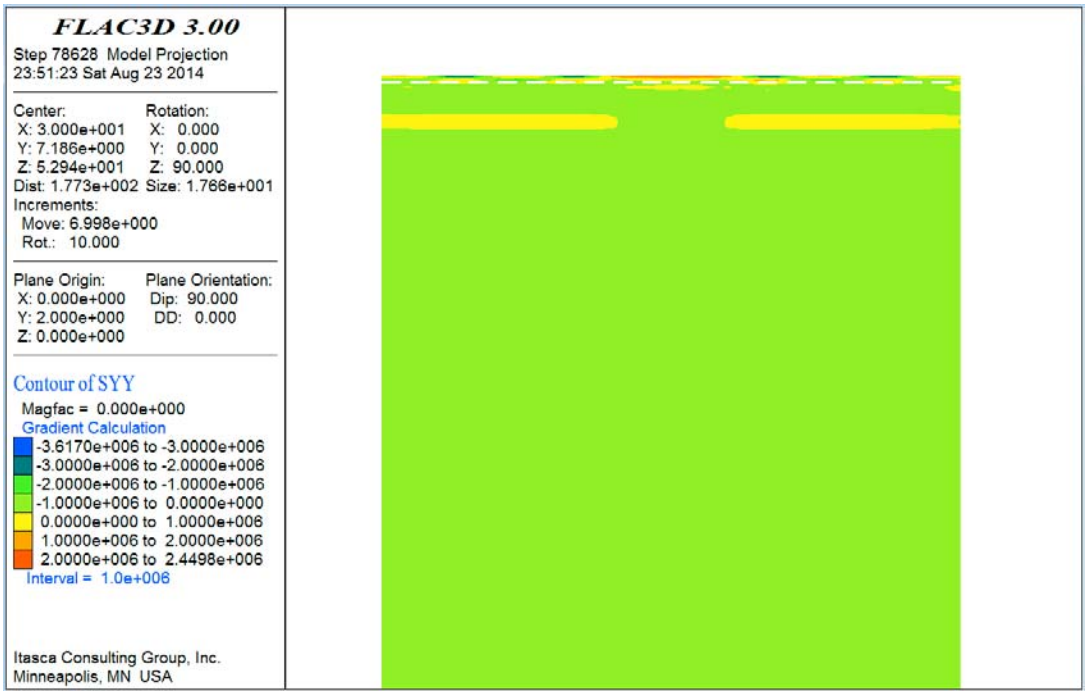

Figure 4.22. Horizontal Stress Contours in Longitudinal (y) Direction (Pa)

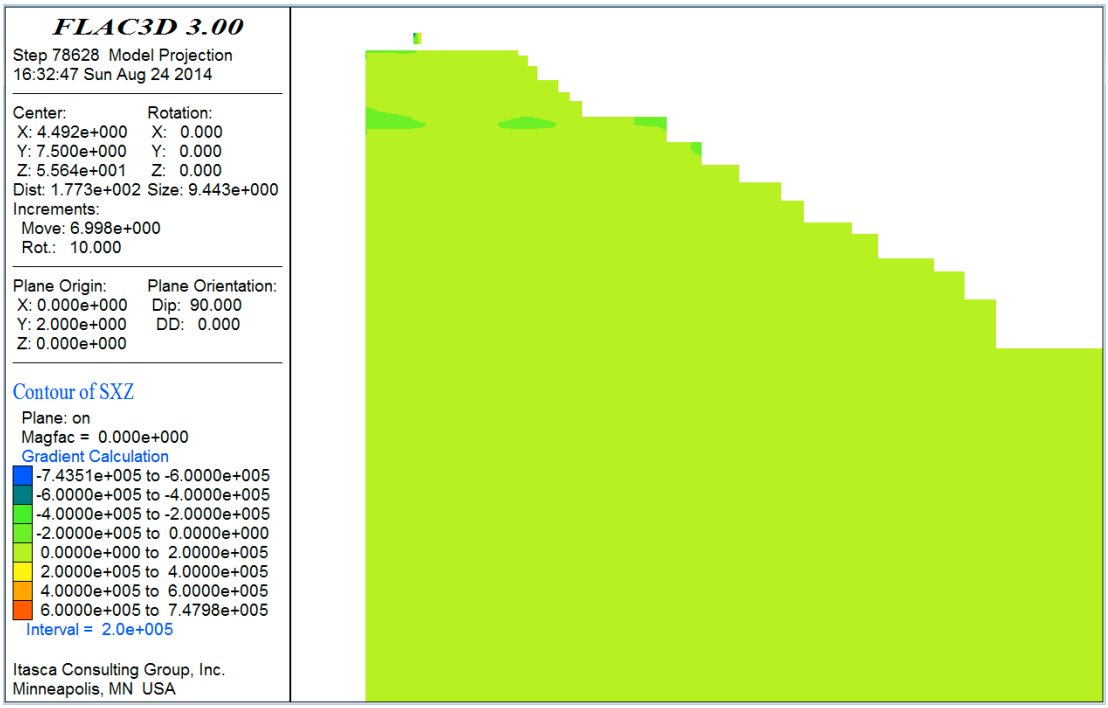

Figure 4.23. Cross-section View of Shear Stress Contours (Pa)

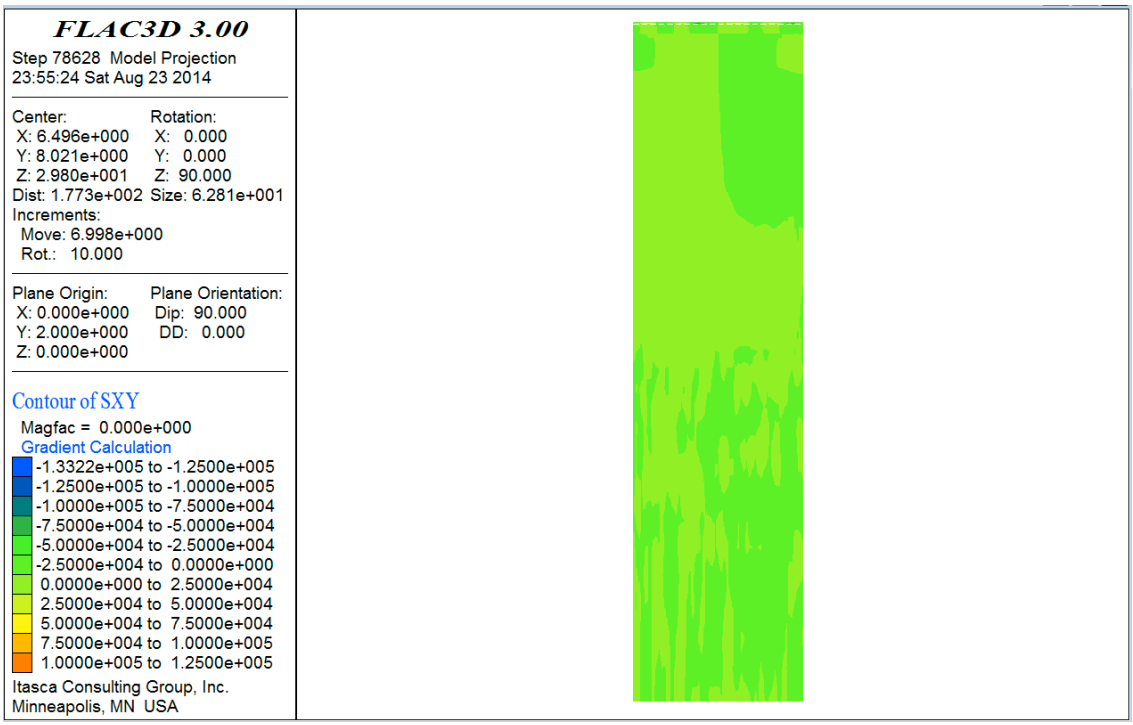

Figure 4.24. Profile View of Shear Stress Contours (Pa)

COMPARISON AND VERIFICATION

Vertical deflections were measured by Frydenlund et al. (1987) on bolts found in the concrete slab which was constructed atop the EPS-blocks. The field measurements ranged from 2 to 3 mm on the west rail. This half of the railway embankment system was modeled by FLAC3D. The model produced vertical deflections ranging from 1.8 to 2.3 mm. This range of results appears to be a reasonable estimate of the lower range of the field measurements. In addition, further calibration of the model is not recommended given the uncertainties in the embankment and foundation material properties which were not reported by Frydenlund et al., (1987), but were estimated by this study. Therefore, it is concluded that FDM, as implemented in FLAC, can satisfactory estimate the vertical displacement of rails systems constructed atop EPS-supported embankments when subjected to a static (i.e., stopped) train loading.

RAIL SYSTEM SUPPORTED BY EPS EMBANKMENT IN DRAPER, UTAH

Problem Statement

The modeling approach developed in the previous sections will now be implemented to estimate the vertical deflections of an EPS geofoam embankment constructed along the UTA FrontRunner South commuter rail

line alignment. Field deflection measurements of this geofoam embankment are included in Chapter 5. Because the estimates contained in this section were performed before the FrontRunner field measurements were available, they constitute a prior prediction. Table 4.3 shows the material properties including LDS (load distribution slab), EPS, etc. EPS properties are determined from ASTM D 6817. Young's modulus of ballast is for Iteration 1.

Table 4.3. Material Properties and Geometry Used in FDM Analysis

Description	E / MPa	v	Geometry
Rail	210000	0.3	78 mm wide, 153 mm deep
Sleeper (3D/2D)	31000/11600	0.3	242 mm wide, 200 mm deep
Ballast	310	0.3	308.8 mm thick
Sub-ballast	130	0.49	203.2 mm thick
Structural Fill	400	0.3	914.4 mm thick
LDS	30000	0.18	203.2 mm thick
EPS 39	10.3	0.103	top layer
EPS 29	7.5	0.103	second to fifth layer
EPS 22	5	0.103	sixth to bottom layer
Foundation Soil	174	0.4	20 m thick

The UTA Frontrunner South alignment extends from Salt Lake City to Provo, Utah. The particular EPS fill selected for the modeling is shown in Figures. 4.25 and 4.26. These show the cross-section of the EPS-supported embankment at Corner Canyon (Parsons et al., 2009) that will be studied using FDM as implemented in FLAC3D. This EPS embankment was constructed over an extension of a concrete drainage culvert so as to not induce damaging settlement to the culvert and the adjacent Union Pacific Rail Line. The loading conditions for the FLAC analyses are shown in Figure 4.27 for a typical Frontrunner Commuter train.

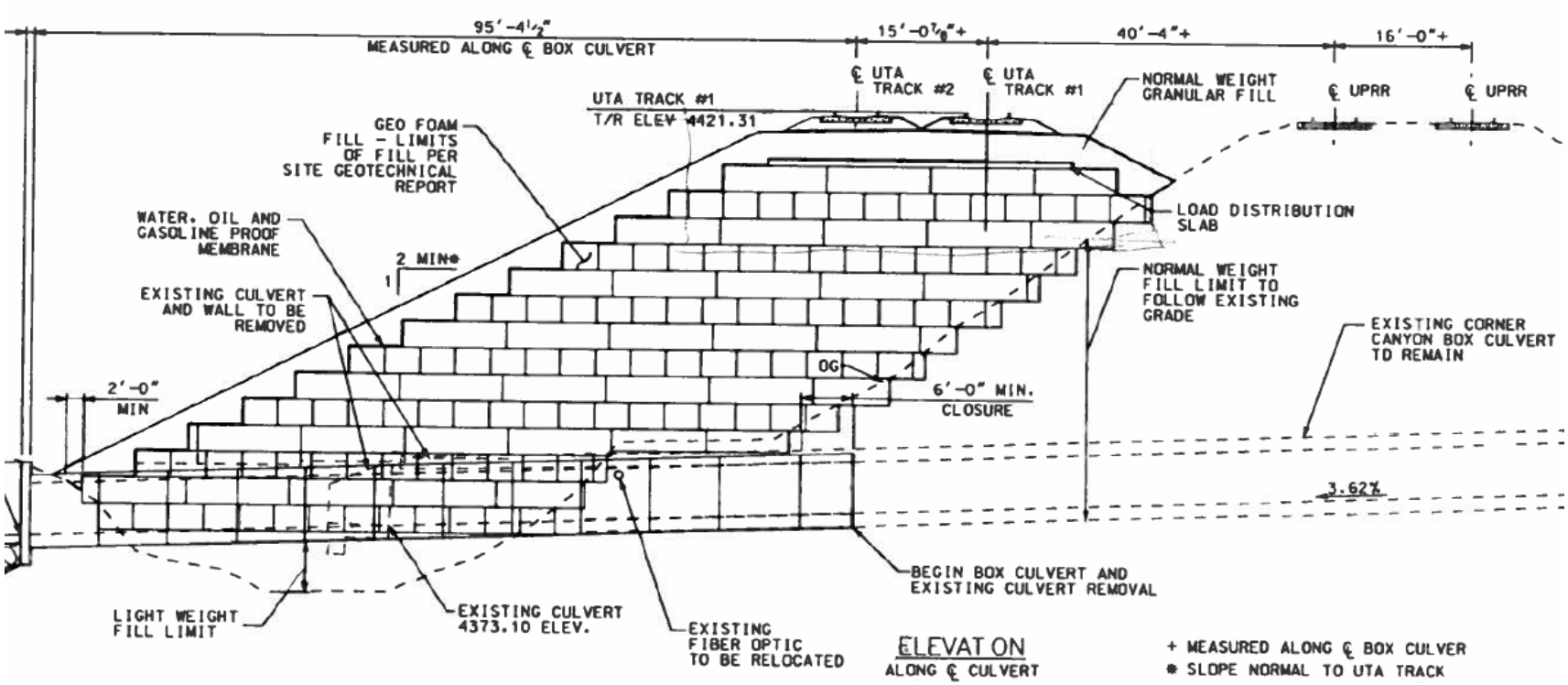

Figure 4.25. Cross-section of the EPS-supported Embankment at Corner Canyon

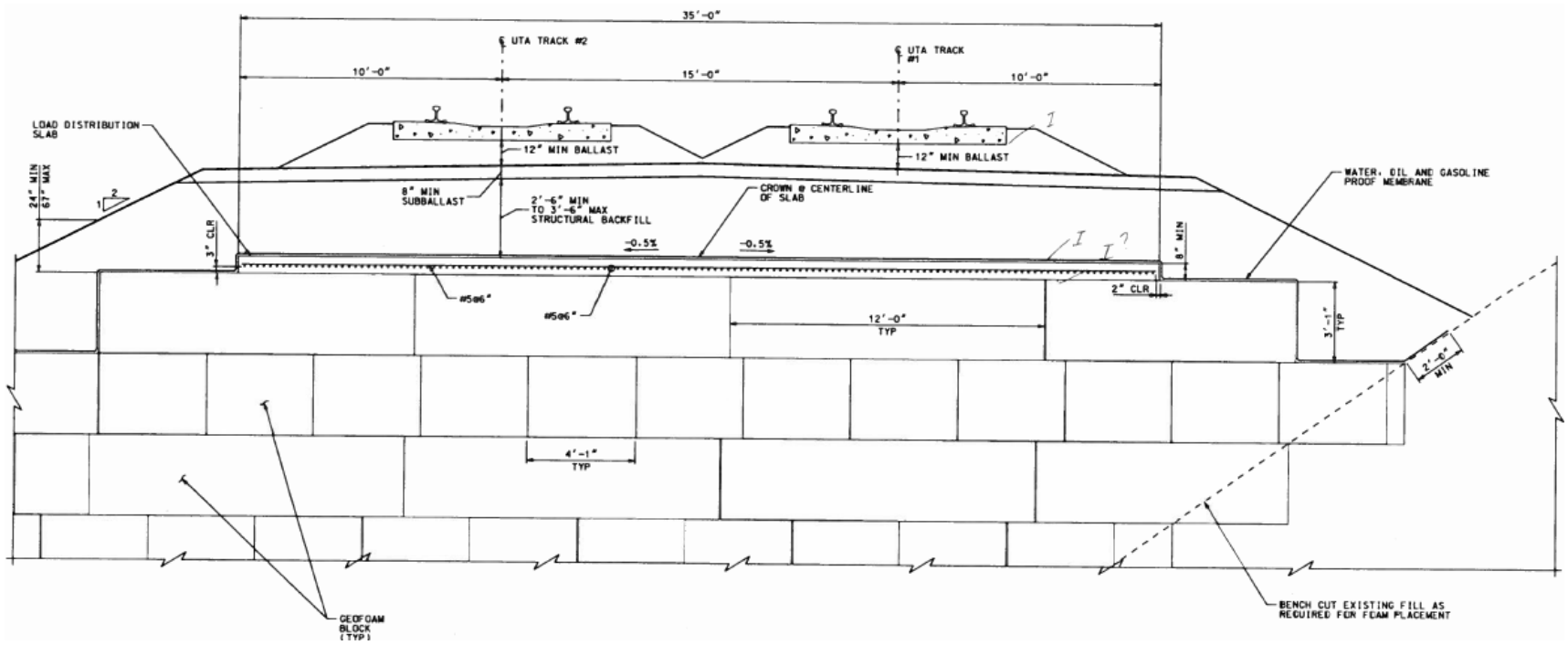

Figure 4.26. EPS Cross-section of the EPS-supported Embankment at Corner Canyon

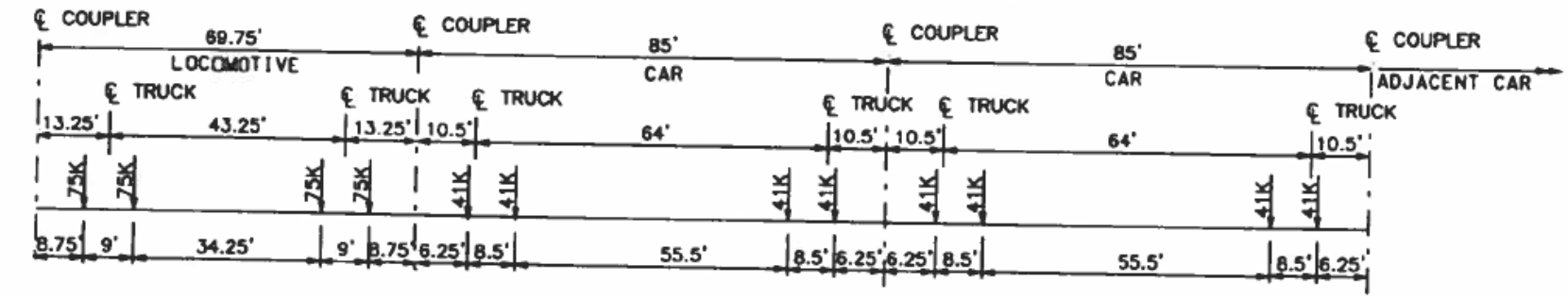

Figure 4.27. Typical Load Conditions for UTA Commuter Rail Train

2D Model Preparatory Study

As previously discussed in the models developed for railway systems supported by both regular earthen embankment (Powrie et al., 2007) and EPS embankment (Frydenlund et al., 1987), the coarse mesh, intermediate mesh and fine mesh spacing resulted in almost the same estimate of vertical displacement of the concrete sleeper. Thus, mesh density is not a major concern in the modeling process if only vertical displacements are to be predicted. However, a fine mesh was used in both the 2D and 3D modeling of the UTA FrontRunner embankment system.

As shown in Figure 4.25, the UTA FrontRunner embankment system is not plane-symmetrical. Simply modeling half of the system will result in incorrect results. However, a full 3D model of the embankment system requires significant amount of computational time and memory and, thus, is not preferable. As a result, a series of 2D models were developed to investigate simplification methods and evaluate the magnitude of the potential differences caused by the simplifications.

Firstly, a 2D model of the full embankment system was developed (Figure 4.28 and Figure 4.29). As was done in modeling the regular earthen embankment (Powrie et al., 2007) and the EPS embankment in Norway (Frydenlund et al., 1987**)**, the boundaries on two sides and the bottom were restrained in both the horizontal and vertical directions. A load of 41 kips (182,337 N) per axial for a car is applied on the outer track. In FLAC, since there are two rails with two nodes for each rail top, a vertical force of 45584 N was applied on each node. Figures. 4.25 and 4.26 show the geometry used in the FLAC model. See Table 4.3 for details about the material properties and geometry used. Note that Imperial units have been converted to SI units in this table. The length of the sleeper is 2.525 m.

Secondly, the 2D model was cut vertically at the center of the left (i.e., western) outer track (Figures. 4.30 and 4.31), similar to what would be done if this represented an axis of symmetry. Thus, in this simplified model, the right boundary was fixed only in horizontal direction and the left and bottom boundaries were fixed in both directions.

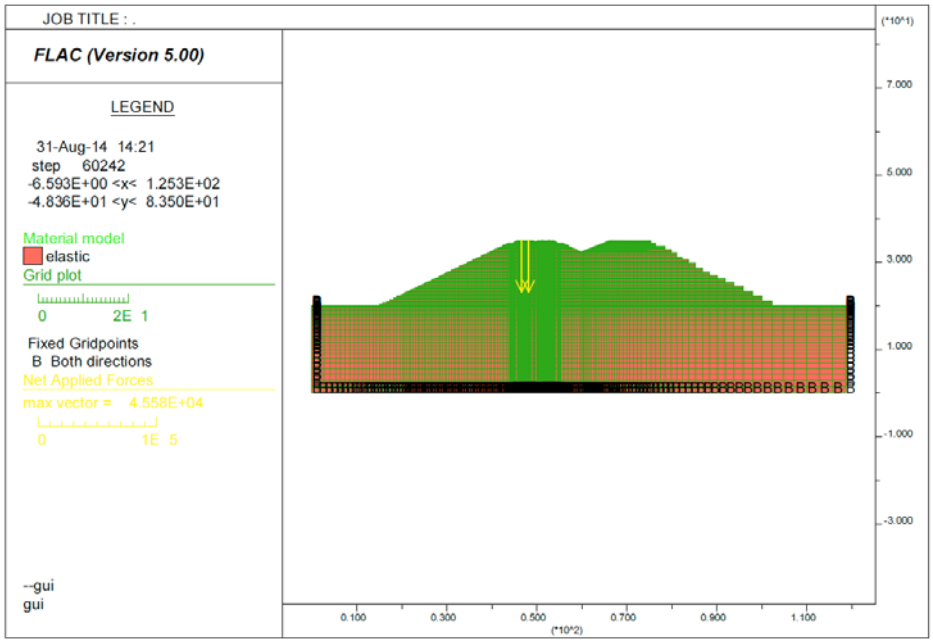

Figure 4.28. Mesh of 2D Model of the Full FrontRunner Embankment System (m)

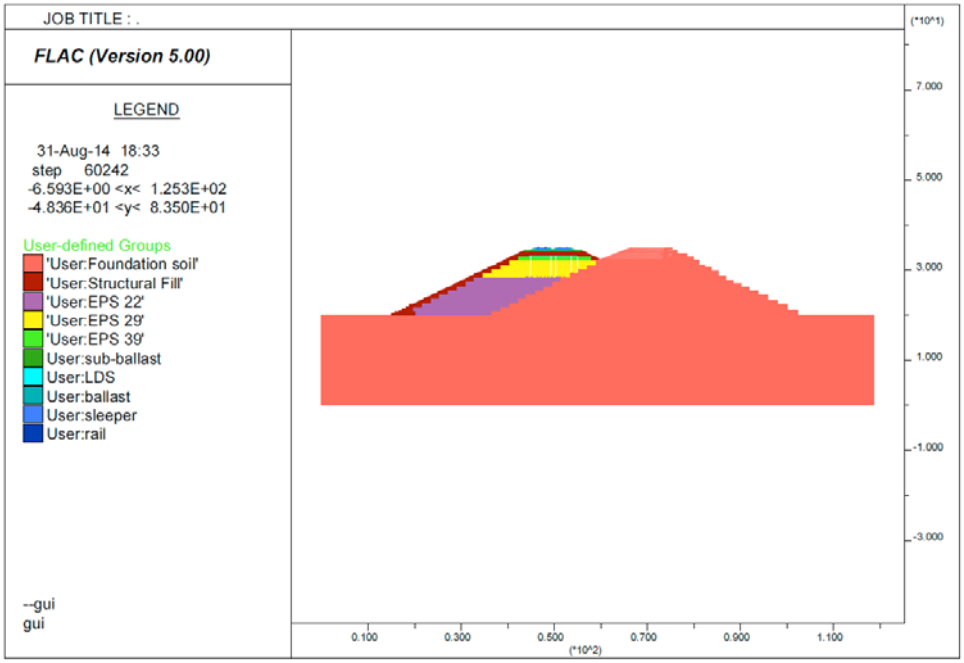

Figure 4.29. Properties of 2D Model of the Full FrontRunner Embankment System (m)

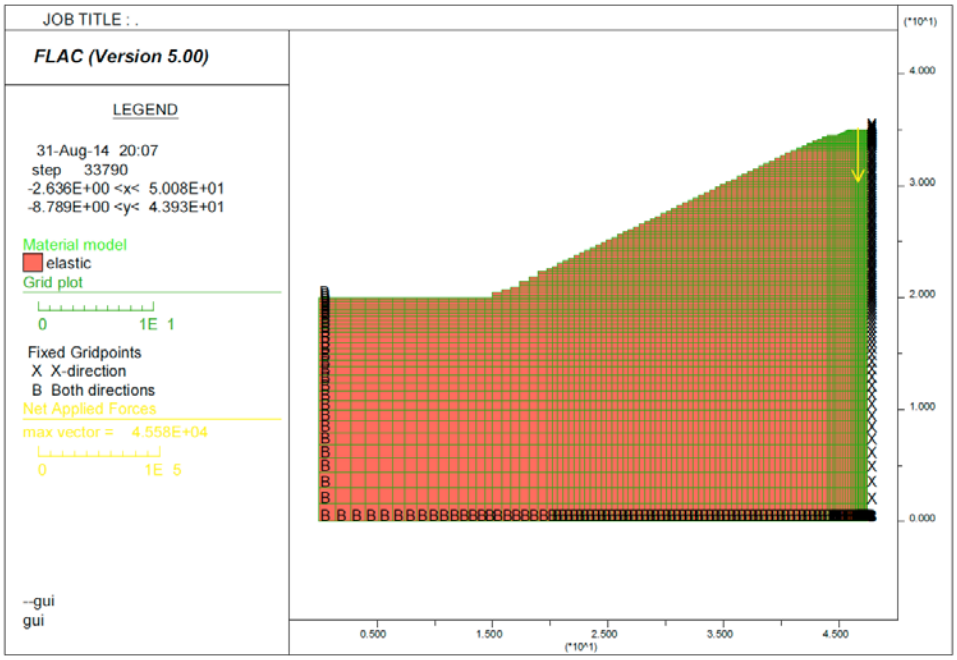

Figure 4.30. Mesh of 2D Model of Initial Simplified FrontRunner Embankment (m)

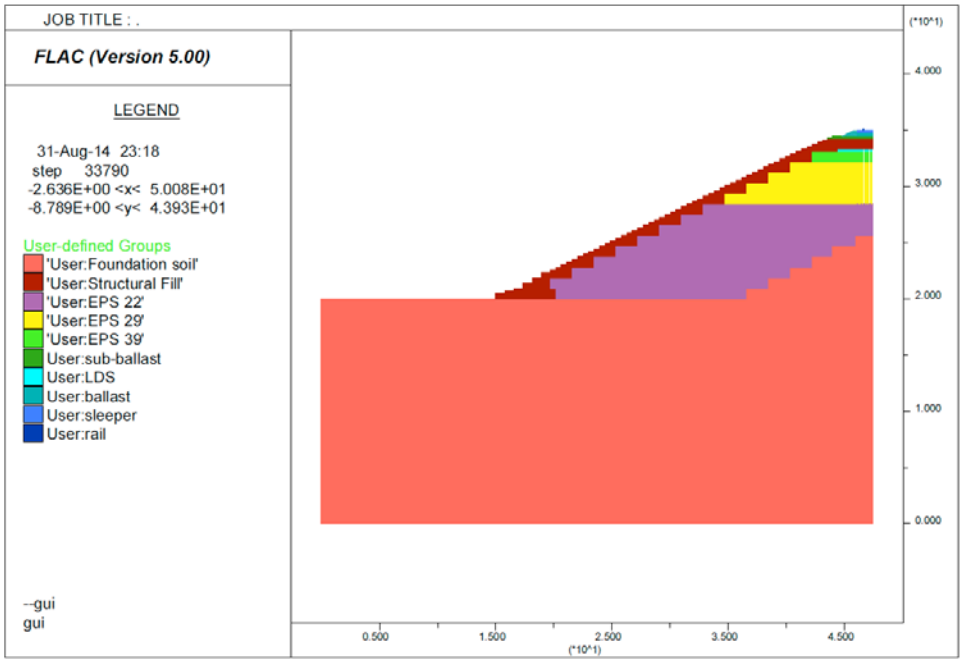

Figure 4.31. Properties of 2D Model of Initial Simplified FrontRunner Embankment (m)

Because the development of a subsequent 3D model was planned, efforts were taken to simplify the 2D cross-section as much as possible. As discussed in modeling the EPS supported embankment system in

Norway, much of the vertical deformation occurred within the EPS part of the embankment due to its relatively low stiffness. The corresponding vertical deformation occurring in the foundation soil was reasonably small. However, a comparison of the two EPS supported embankment systems shows that the EPS portion in the FrontRunner system is much thicker than that of the Norwegian system. Because of this increased thickness, the percentage of the total deformation occurring in the EPS is expected to be higher than the Norwegian case, and the deformation in the foundation soil is expected to be correspondingly less.

A series of 2D models with different dimensions for the foundation soils were developed to investigate the effects of the mesh size and boundaries on the estimated vertical displacement of the rails. Included in these cases were foundation soil dimensions (depth by extended width) of 20 m by 15 m, 10 m by 8 m, 5 m by 3 m and 0 m by 0 m. Except for the above differences in foundation soil dimension, all other parameters remain the same in these exploratory models. The vertical displacement results for the rails are plotted in Figure 4.32. It is obvious from these exploratory models, which produced almost the same vertical displacement result, that most of the vertical displacement is attributed to the EPS portion of the embankment and not to the foundation soil.

Thus, the simplest model (i.e., depth by extended width: 0 m by 0 m) was used in the subsequent 2D model. The results of this 2D model (Figures. 4.33 and 4.34) were compared with the model of the full embankment model (Figures. 4.28 and 4.29) under the same conditions (loading, material properties, etc.). The error introduced by the simplifications used in the modeling as represented by Figures. 4.33 and 4.34 produced an over-estimation of the vertical displacement of about 11%. Thus, using this simplified method produces a slightly conservative by reasonable result when compared with the full model.

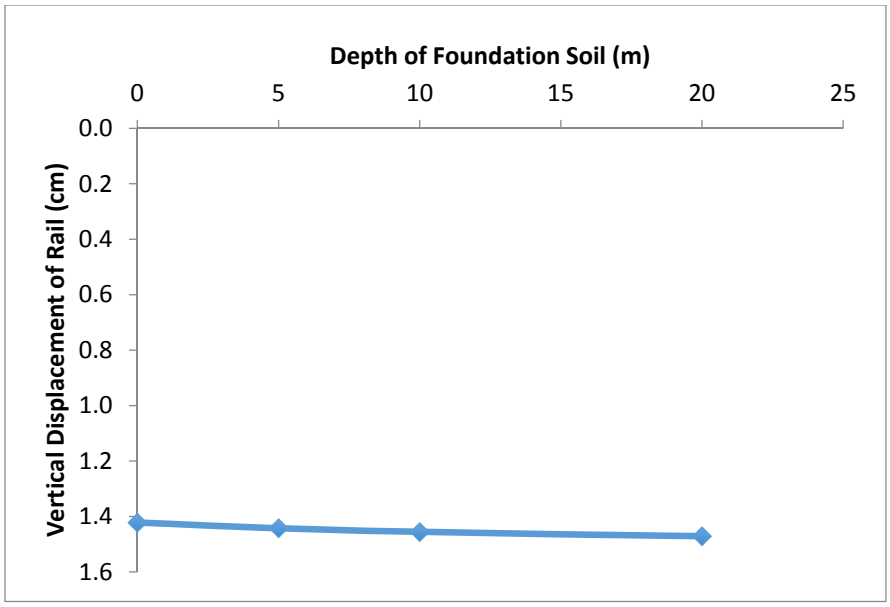

Figure 4.32. Boundary Effect of the Foundation Soils

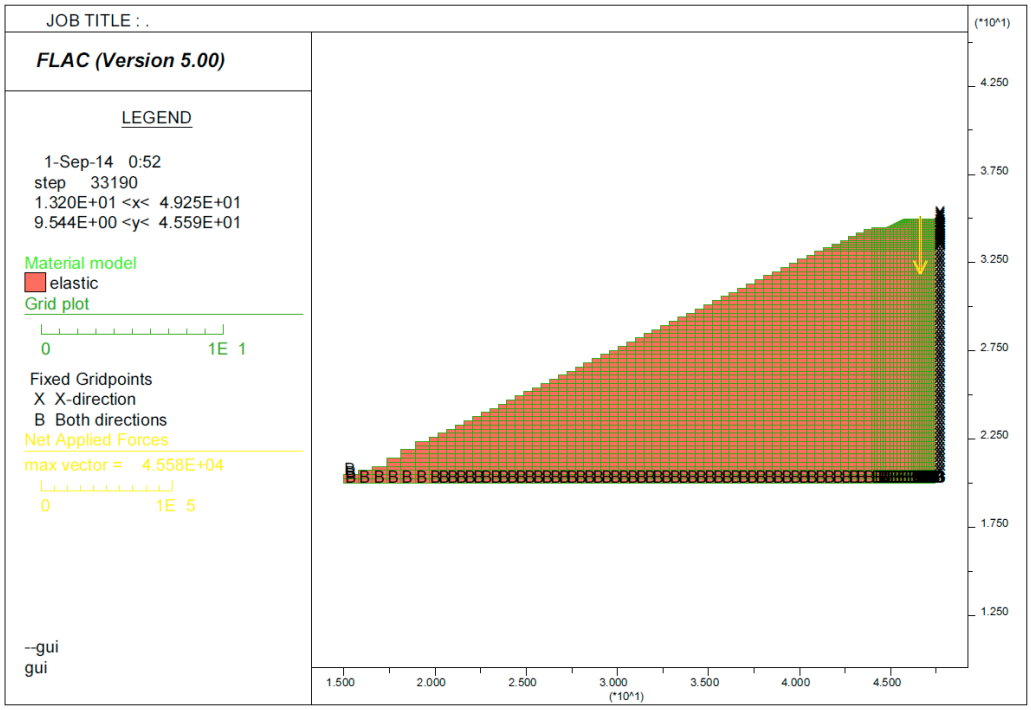

Figure 4.33. Mesh of 2D Model of Final Simplified FrontRunner Embankment (m)

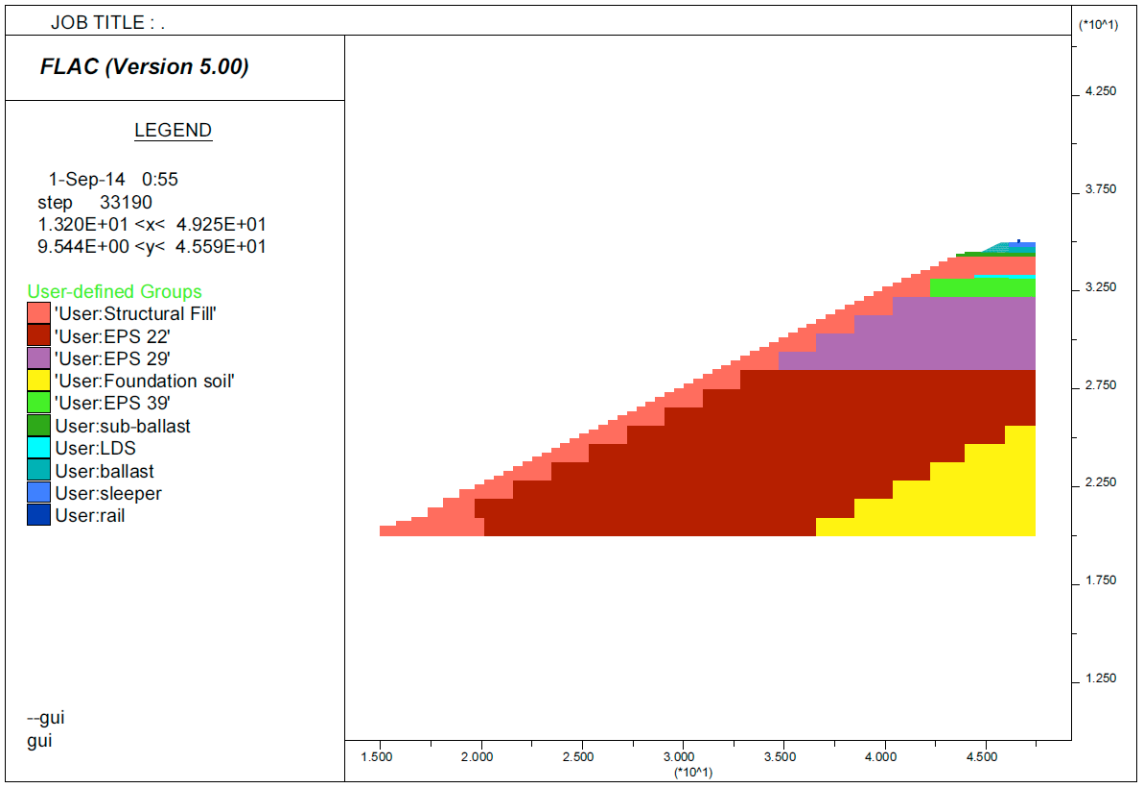

Figure 4.34. Properties of 2D Model of Final Simplified FrontRunner Embankment (m)

3D Solution (FDM)

Based on the ballast tests discussed in Chapter 3, it was found that the ballast system had a different Young's modulus according to the strain level used in the tests. To incorporate this in the FLAC model, an iterative process was used. First, the value of Young's modulus obtained from the literature was used in FLAC model (Iteration 1). After the FLAC model had solved for this condition, the strain of the ballast layer was obtained from the output. The strain was then used to calculate the Young's modulus of ballast based on the correlation developed from the ballast test in Chapter 3. This new Young's modulus was used again in FLAC model (Iteration 2). This process was repeated until the Young's modulus calculated from the strain output is approximately same as the Young's modulus input and vertical displacement of the rails are approximately the same as the previous iteration.

Figure 4.35 and Figure 4.36 show the mesh of the 3D model.

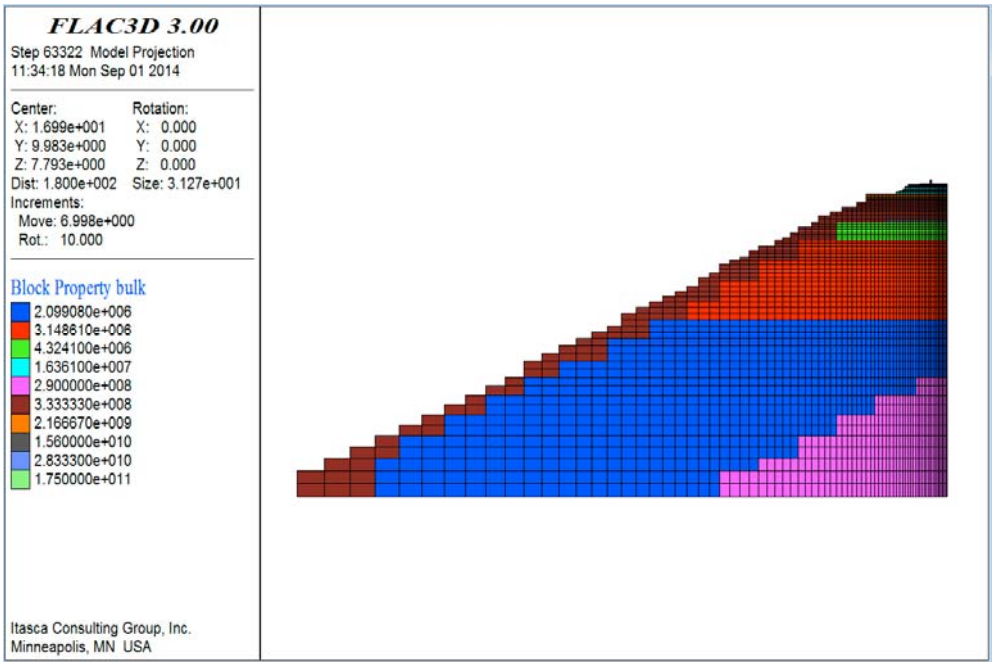

Figure 4.35. Cross-Section View of Model Mesh

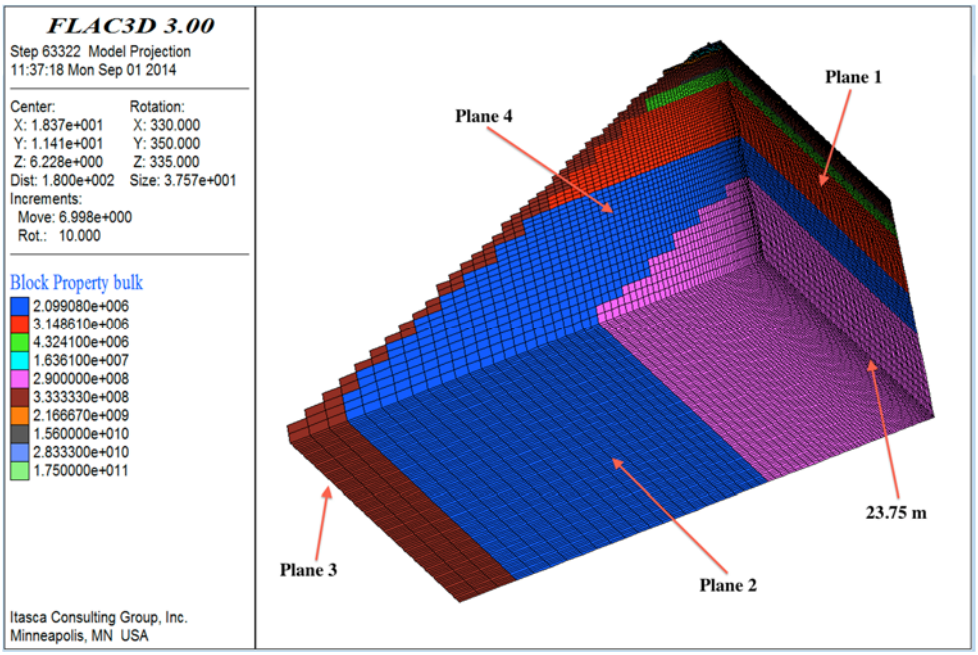

Figure 4.36. 3D View of Model Mesh

The length of the mesh in the longitudinal (y) direction was taken as that of half of the locomotive and half of the car (Figure 4.37 and Figure 4.38) as done by Powrie et al. (2007). Smaller elements were used near the rail where the changes of stresses and strains were expected to be the greatest. The bottom and far-

lateral boundaries (Plane 2 and 3 in Figure 4.36) were prevented from movement in all three directions. The longitudinal boundaries (Plane 4 in Figure 4.36) were fixed in the x direction only. The center plane (Plane 1 in Figure 4.36) was fixed in the y direction only.

The most critical loading conditions are illustrated in Figure 4.38. The properties of each material are shown in Table 4.3. Values of the shear modulus (G) and bulk modulus (K) for the FLAC3D model were calculated from elastic theory based on values of E and v. See Figures. 4.35 and 4.36 for plots of the properties used in the model.

The FLAC3D model produced a maximum vertical rail displacement of 6.1 mm, which occurred directly under the wheels of the locomotive. The vertical displacement contours for this case are shown in Figures. 4.39 and 4.40. The pattern of these contours indicates the load distribution slab (LDS) is effective in distributing the stress of the rail system due to the large bulk and shear moduli used for this slab. In addition, the contours also show that approximately 80% of the vertical deformation occurs in the EPS. Of the remaining components, approximately 15% of the vertical deformation occurs in the support system above LDS (i.e., rail, sleeper, ballast, sub-ballast and structural fill) and approximately 5% of the vertical deformation occurs in the foundation soil. Thus, it is concluded that the vertical displacement of an EPS supported embankment system is mainly controlled by the properties and behavior the EPS for relatively high embankments, such as that modeled herein.

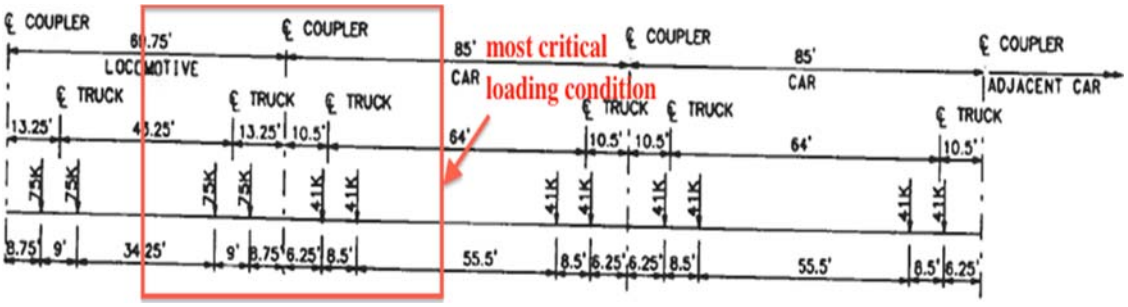

Figure 4.37. Most Critical Loading Condition

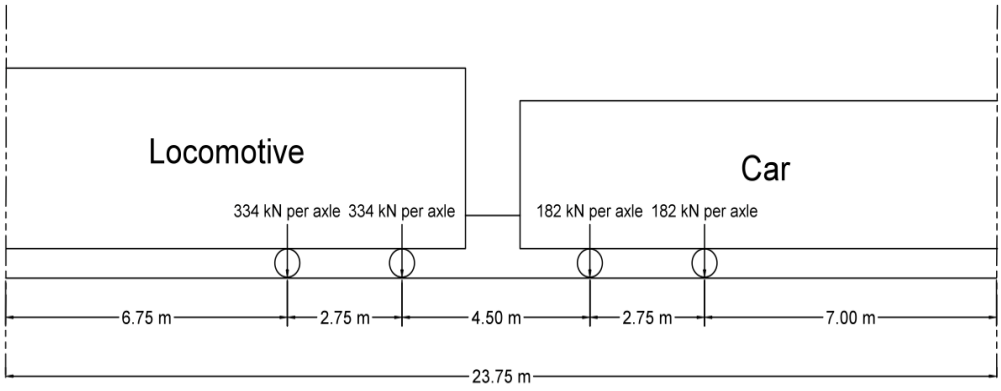

Figure 4.38. Loading Condition Used in 3D Model

Figures. 4.41 and 4.42 show the lateral (x direction) and longitudinal (y direction) displacement of the railway embankment model. The model has a maximum lateral displacement of 0.7 mm and a maximum longitudinal displacement of 0.03 mm, both of which are relatively insignificant compared with the magnitude of the vertical displacement. Figure 4.43 shows the vertical stress contours of the railway embankment model. Figure 4.44 shows the horizontal stress contours of the railway embankment model in the lateral (x) direction.

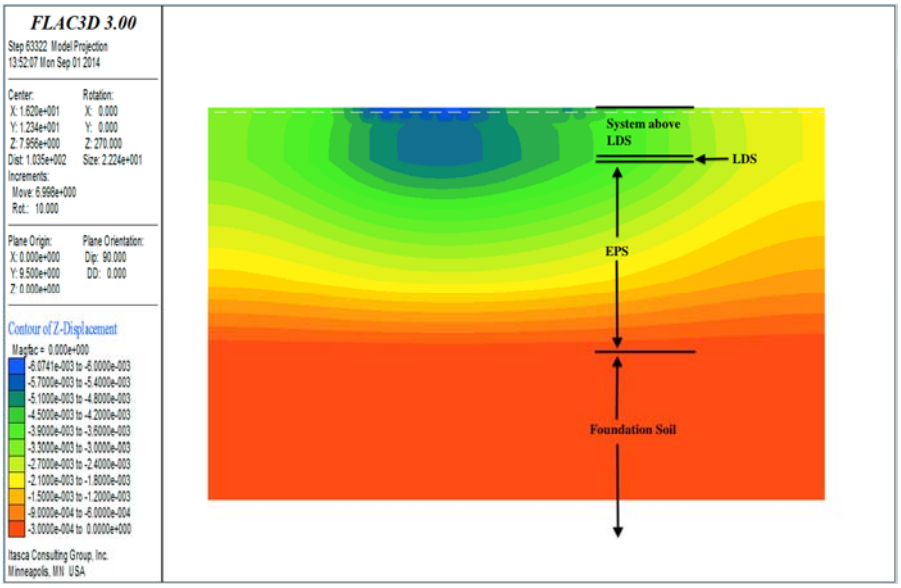

Figure 4.39. Profile View of Vertical Displacement Contours (m)

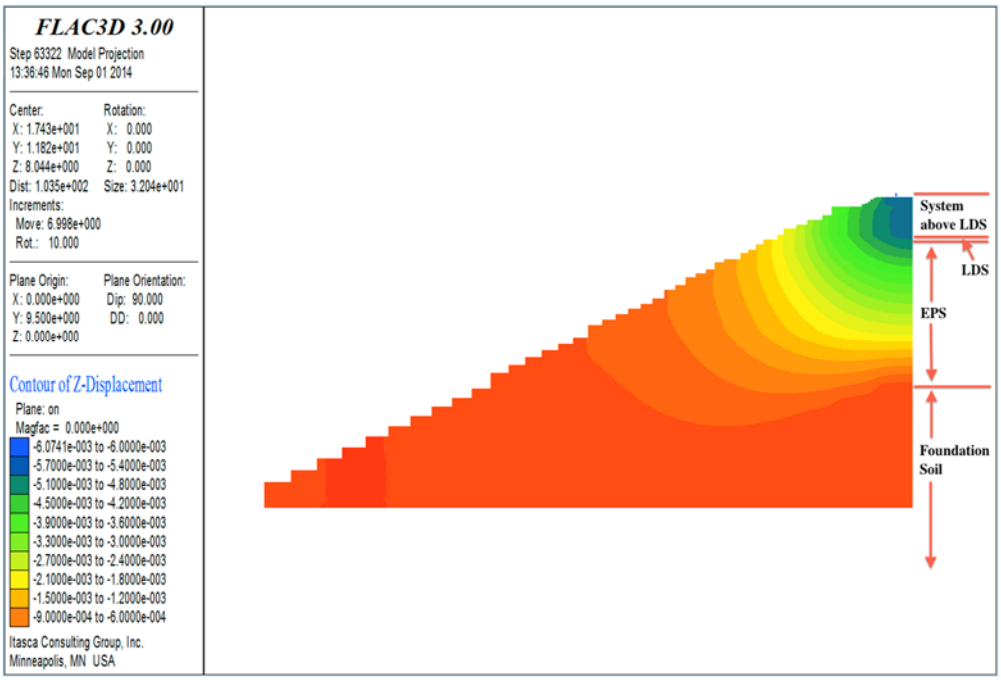

Figure 4.40. Cross-section View of Vertical Displacement Contours (m)

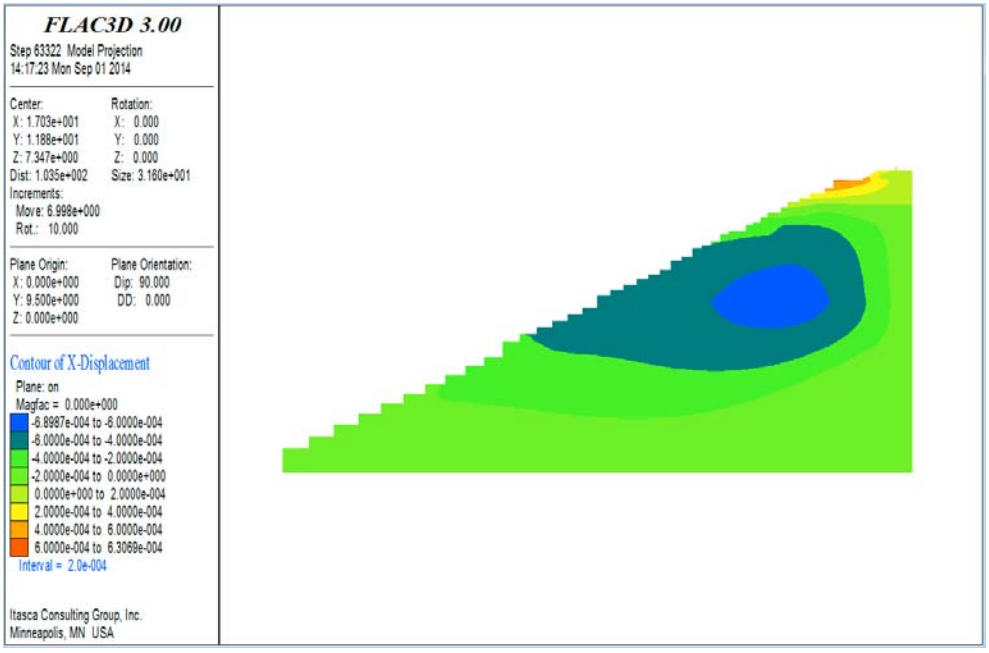

Figure 4.41. Lateral Displacement Contours (m)

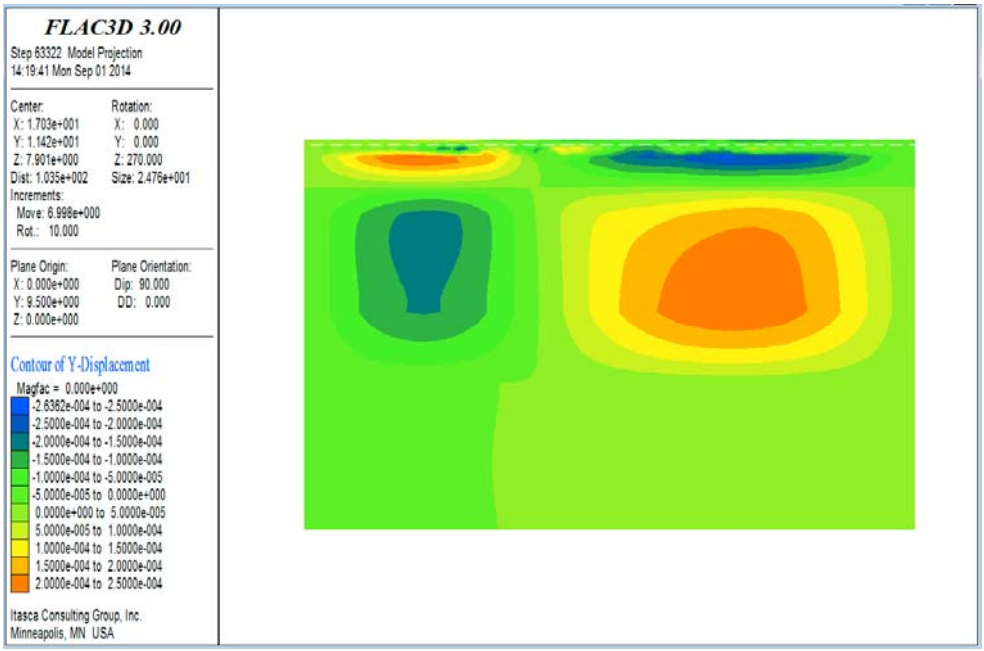

Figure 4.42. Longitudinal Displacement Contours (m)

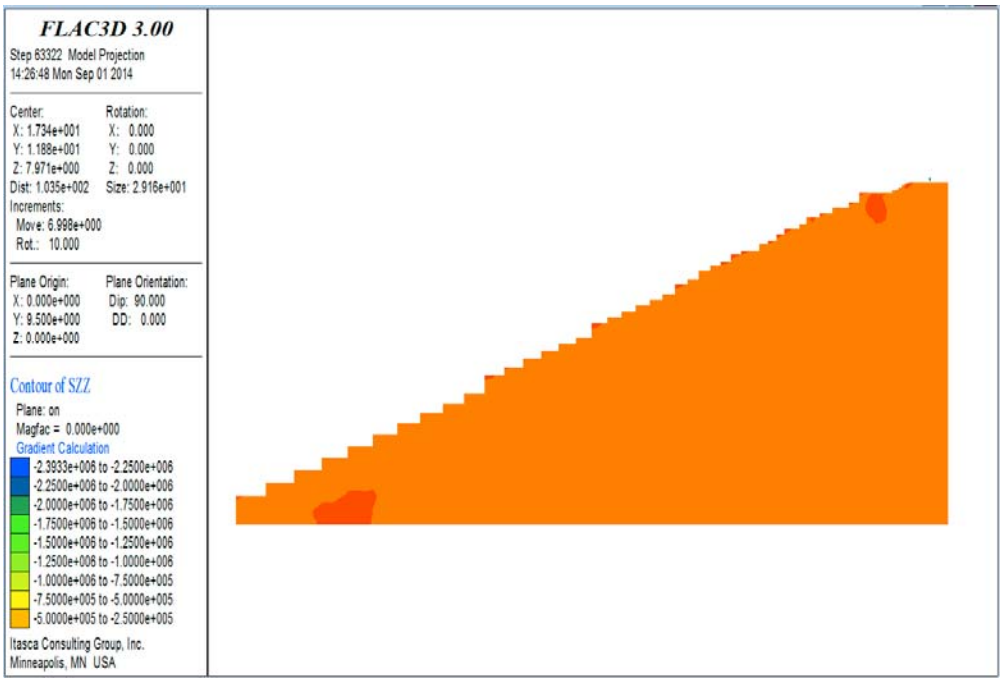

Figure 4.43. Vertical Stress Contours (Pa)

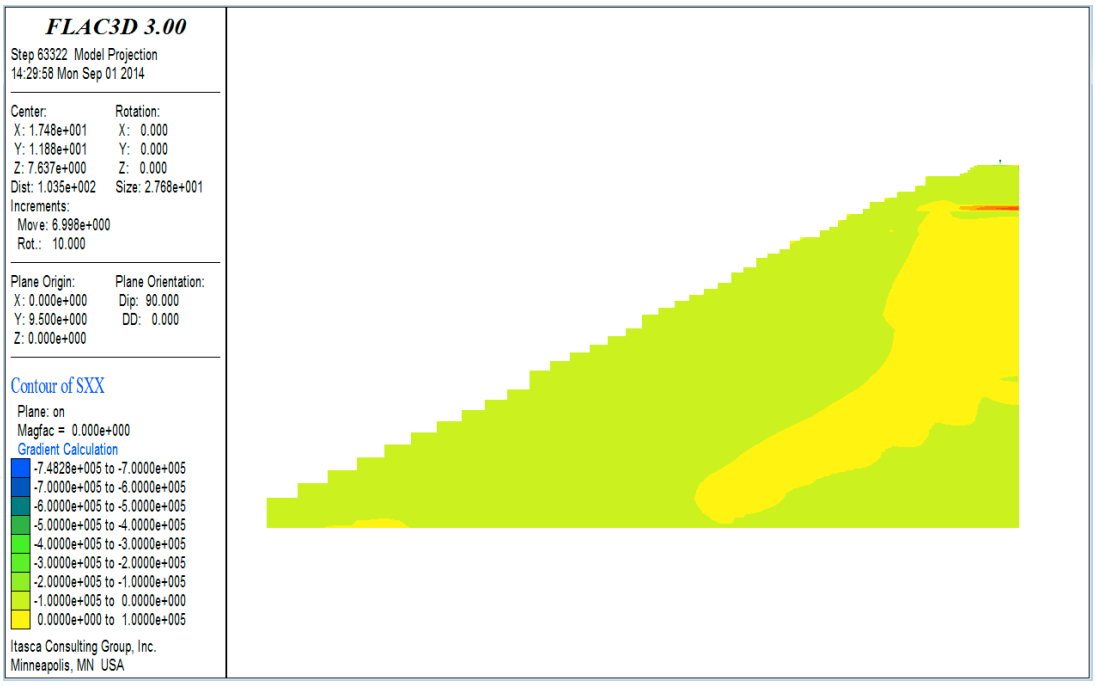

Figure 4.44. Horizontal Stress Contours in Lateral (x) Direction (Pa)

Figure 4.45 show the horizontal stress contours of the railway embankment model in the longitudinal (y) direction.

Figures. 4.46 and 4.47 show the shear stress contours of the railway embankment model. According to these plots, one can observe that the normal stress and shear stress within the model are distributed relatively uniformly by the rail-sleeper-ballast (sub-ballast)-structural fill-LDS system. This is due to the high bulk and shear moduli of these materials.

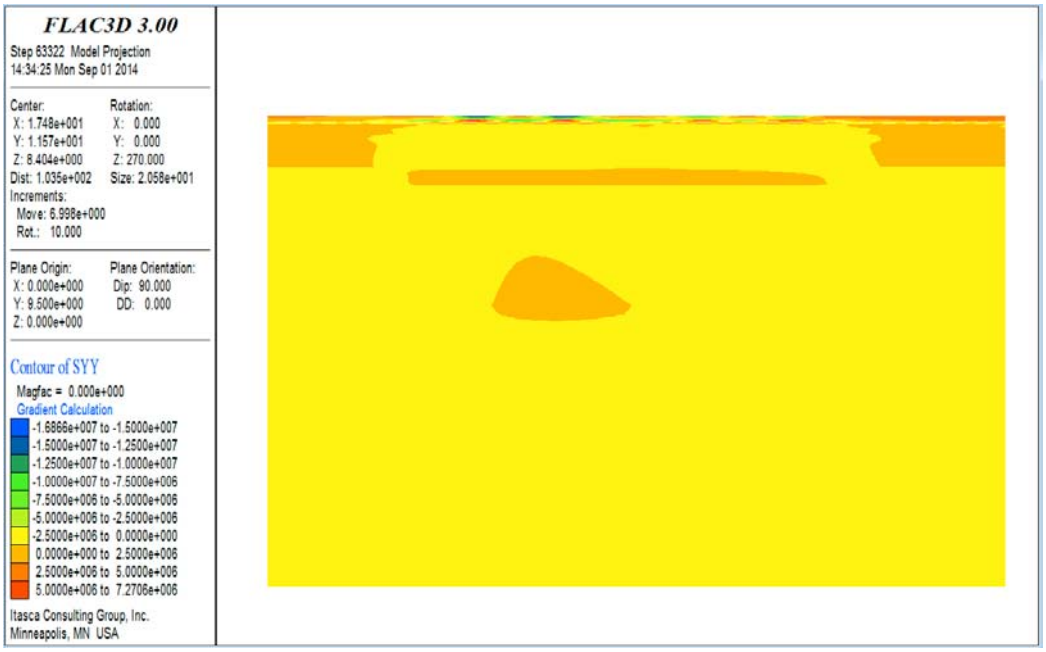

Figure 4.45. Horizontal Stress Contours in Longitudinal (y) Direction (Pa)

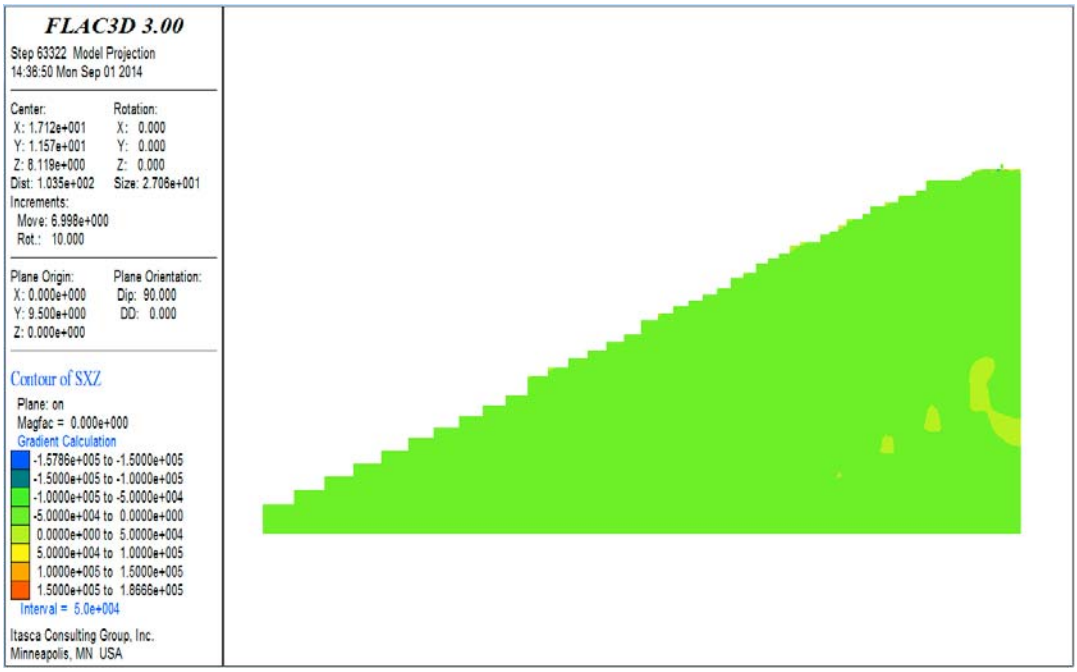

Figure 4.46. Cross-section View of Shear Stress Contours (Pa)

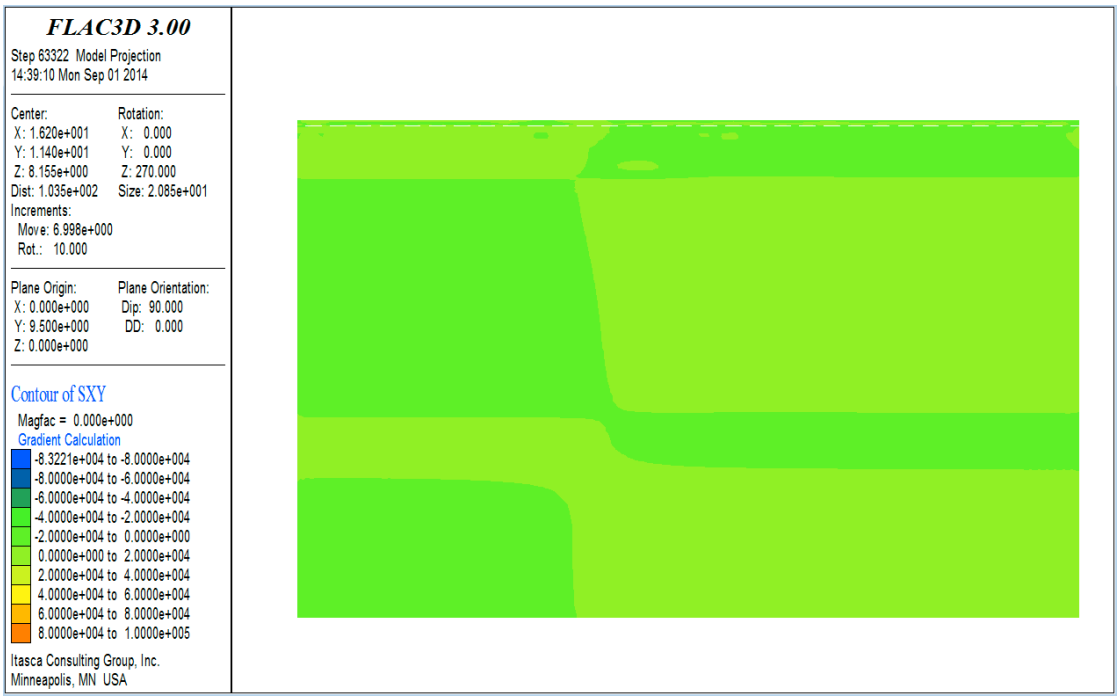

Figure 4.47. Profile View of Shear Stress Contours (Pa)

Summary and Discussion

The development of the FLAC modeling approach was based on simplifications, and their potential ramifications were explored and quantified using a 2D model, as discussed previously. When evaluated as a 2D model, the simplifications produced a slightly conservative estimate, i.e., slightly overestimated the total vertical displacement of the system, when compared with a more extensive 2D model that incorporated the complete geometry of the system.

When the simplified system was modeled using a 3D geometry, the maximum vertical rail displacement was estimated to be 6.1 mm for the most critical (i.e., highest) loading condition, which occurs directly under the wheels of the locomotive. In addition, based on the developed contours of displacement and stress, it is obvious that the load distribution slab (LDS) effectively distributes the vertical stresses of the system due to the large bulk and shear moduli of this concrete slab. It was also found that approximately 80% of the vertical deformation occurs within the EPS. This is due to the much lower bulk and shear moduli of EPS when compared with other materials and components of the system (i.e., rail, sleeper, ballast, structural fill, foundation soil, etc.). It was estimated that approximately 15% of the vertical deformation of the system occurs above the LDS (i.e., rail, sleeper, ballast, sub-ballast and structural fill) and approximately 5% of the vertical deformation occurs in the foundation soil. Therefore, the vertical displacement behavior

of an EPS supported embankment system is mainly controlled by the properties and behavior the EPS for relatively large embankments, such as that modeled herein.

In addition, it was estimated that the system has a maximum lateral displacement of 0.7 mm and a maximum longitudinal displacement of 0.03 mm, both of which are relatively insignificant compared with the magnitude of the vertical displacement. The normal stress and shear stress within the system are distributed relatively uniformly by the rail-sleeper-ballast (sub-ballast)-structural fill-LDS system. This is due to the high bulk and shear moduli of these materials.

SUMMARY AND CONCLUSIONS

This research developed a numerical method to evaluate the vertical displacement of rail systems constructed atop EPS geofoam embankments. To achieve this purpose, a complex 2D FLAC modeling approach was developed to analyze the sleeper deflection for multilayered railway embankment system supported by regular earthen embankment. The result from this initial effort was checked with FEM analysis conducted by other researchers on the same system. The percentage difference of the estimated sleeper deflection was within 8%, which validated the FLAC model in relation the FEM modeling approach used in the literature (Powrie et al., 2007).

Additionally, a more complex FLAC3D model was developed to analyze the vertical displacement of an EPS-supported multilayered railway embankment system constructed in Norway. A series of 2D models were first developed to identify the appropriate mesh size and level of discretization required to reasonably estimate the total surface displacement from the train loading. This exploratory modeling was initially performed because 2D models required significantly less computational time and computer memory. This study suggested that fine, intermediate and coarse meshes produced nearly the same vertical displacement of the sleeper and that a mesh size of 60 m × 60 m (width × depth) was sufficient to produce stable results. A finely graded, non-uniform mesh with a domain size of 60 m × 60 m (width × depth) was thus used in the 3D modeling.

For the 3D modeling of the Norwegian case, the maximum vertical rail displacement calculated by FLAC3D was 2.3 mm which occurred directly under the wheels. In addition, FLAC3D indicated that the concrete slab had a vertical displacement ranging from 1.8 mm to 2.3 mm. The vertical displacement of the railway embankment system compressed much more uniformly in the longitudinal (y) direction than in the lateral (x) direction. In addition, even though the thickness of the EPS layer was only approximately 5% of the full depth of the embankment model, approximately 60% of the vertical compression occurred in the EPS. This is due to the fact that the EPS has a much lower bulk and shear moduli than other materials (i.e.,

rail, sleeper, natural ground, etc.). The system had a maximum predicted lateral displacement of 0.2 mm, and a maximum predicted longitudinal displacement of 0.02 mm. Both of which are relatively insignificant compared with the magnitude of the predicted vertical displacement. The normal and shear stresses within the system are distributed relatively uniformly by the rail-sleeper-ballast-concrete slab system. This is due to the high stiffness (i.e., high bulk and shear moduli) of these materials in relation to the underlying EPS and soil materials.

To confirm the above modeling results, surveyed vertical deflections were used as reported by Frydenlund et al. (1987). These measurements were made on bolts found in the concrete slab constructed atop the EPS-blocks. The field measurements ranged from 2 to 3 mm on the west rail. This half of the railway embankment system was modeled by FLAC3D. The model produced vertical deflections ranging from 1.8 to 2.3 mm. This range of results was deemed to be a reasonable estimate of the lower range of the field measurements. Therefore, it was concluded that FDM, as implemented in FLAC, can satisfactory estimate the static vertical displacement of rails systems constructed atop EPS-supported embankments when subjected to a static (i.e., stopped) train loading.

Finally, a more complex FLAC3D model was developed to analyze the vertical displacement of the EPS-supported UTA FrontRunner embankment system in Corner Canyon, Draper, Utah. In the models developed for railway systems supported by both regular earthen embankment (Powrie et al., 2007) and EPS embankment (Frydenlund et al., 1987), the coarse mesh, intermediate mesh and fine mesh spacing resulted in almost the same estimate of vertical displacement of the concrete sleeper. Thus, it was concluded that mesh density is not a major factor in the modeling process if only vertical displacements are to be predicted. However, a fine mesh was used in both the 2D and 3D modeling of the UTA FrontRunner embankment system.

This system is not plane-symmetrical. It was found that simply modeling half of the system would not result in correct results. However, a full 3D model of the embankment system require significant amount of computational time and memory thus is not preferable. As a result, a series of 2D models were developed to investigate simplification methods and evaluate the magnitude of the potential differences caused by the simplifications. Firstly, a 2D model of the full embankment system was developed. Secondly, the 2D model was cut vertically at the center of the left (i.e., western) outer track, similar to what would be done if this represented an axis of symmetry. Thirdly, a series of 2D models with different dimensions for the foundation soils were developed to investigate the effects of the mesh size and boundaries on the estimated vertical displacement of the rails. Included in these cases were foundation soil dimensions (depth by extended width) of 20 m by 15 m, 10 m by 8 m, 5 m by 3 m and 0 m by 0 m, which produced almost the

same vertical displacement result. Finally, the results of the simplest model (i.e., depth by extended width: 0 m by 0 m) were compared with the model of the full embankment model under the same conditions (loading, material properties, etc.). The error introduced by the simplifications used in the modeling produced an over-estimation of the vertical displacement of about 11%. Using this simplified method produced a slightly conservative but reasonable result when compared with the full model. Thus, this simplest 2D model was used as a representative cross-section of the 3D model.

The FLAC3D model produced a maximum vertical rail displacement of 6.1 mm which occurred directly under the wheels of the locomotive. The pattern of the vertical displacement contours indicated the load distribution slab (LDS) is effective in distributing the stress of the rail system due to the large bulk and shear moduli used for this slab. In addition, the contours also showed that approximately 80% of the vertical deformation occurred in the EPS. Of the remaining components, approximately 15% of the vertical deformation occurred in the support system above LDS (i.e., rail, sleeper, ballast, sub-ballast and structural fill), and approximately 5% of the vertical deformation occurred in the foundation soil. Thus, it was concluded that the vertical displacement of an EPS supported embankment system is mainly controlled by the properties and behavior the EPS for relatively high embankments, such as that modeled herein.

The model had a maximum lateral displacement of 0.7 mm and a maximum longitudinal displacement of 0.03 mm, both of which are relatively insignificant compared with the magnitude of the vertical displacement. The normal stress and shear stress within the model were distributed relatively uniformly by the rail-sleeper-ballast (sub-ballast)-structural fill-LDS system. This was due to the high bulk and shear moduli of these materials.

The project team performed field deflection measurements of the section of the FrontRunner commuter rail system that includes an EPS geofoam embankment after the FLAC3D model was developed. Because the FLAC3D estimates of vertical displacement contained in this chapter were performed before the FrontRunner field measurements were obtained, the FLAC3D results constitute a prior prediction of the deflection behavior of the EPS geofoam embankment system. However, the vertical displacement results obtained from the FLAC3D model will be compared with displacements measured in the field in Chapter 5.

REFERENCES

Aabøe, R., and Frydenlund, T. E., (2011). "40 years of experience with the use of EPS geofoam blocks in road construction", *EPS 2011*, Lillestrom, Norway.

Alfhein, S., Flaate, K., Refsdal, G., Rygg, N., and Aarhus, K., (2011). "The first EPS geoblock road embankment – 1972", NRRL, Norwegian Public Roads Administration, Road Authority of Akershus County, Norwegian Public Roads Administration.

American Railway Engineering and Maintenance-of-Way Association, (2007). "Economics of railway engineering and operations - construction and maintenance operations", *Manual for Railway Engineering*, Volume 4, Chapter 16, Part 10.11.

Arellano, D., and Bartlett, S. F., (2012). "Evaluation of geofoam for support of freight rail tracks", Proposal of National Center for Freight and Infrastructure Research and Education (CFIRE)**,** University of Memphis**,** Herff College of Engineering.

Arellano, D., Stark, T. D., Horvath, J. S., and Leshchinsky, D., (2011). "Guidelines for geofoam applications in slope stability projects", final report prepared for National Cooperative Highway Research Program (NCHRP24-11), Transportation Research Board of the National Academies.

ASTM D6817/D6817M-13a (2013), Standard specification for rigid cellular polystyrene geofoam, *American Society for Testing and Materials* (*ASTM) International*, West Conshohocken, PA.

Bartlett, S.F. and Farnsworth, C.B. (2004). "Monitoring and modeling of innovative foundation treatment and embankment construction used on the I-15 reconstruction project, project management plan and instrument installation report," *Utah Department of Transportation (UDOT)* research report No. UT-04.19, University of Utah, Department of Civil and Environmental Engineering, 202.

Bartlett, S. F., Lawton, E. C., Farnsworth, C. B. and Newman, M. P, (2012), "Design and evaluation of expanded polystyrene geofoam embankments for the I-15 reconstruction project, Salt Lake City, Utah", report prepared for *Utah Department of Transportation Research Division.* University of Utah, Department of Civil and Environmental Engineering

Duskov, M., (1997), "EPS as a light-weight sub-base material in pavement structures," Thesis, Delft University of Technology, Delft, Netherlands, 91-95.

European Manufacturers of EPS (EUMEPS) (2011), "EPS white book, EUMEPS background information on standardisation of EPS", Version 31/03/11, Belgium.

Esveld, C., (2001). "Modern railway track," 2nd Ed., MRT-Productions*,* Zaltbommel, The Netherlands.

Esveld, C., Markine, V. and Duškov, M., (2001). "Feasibility of EPS as a lightweight sub-base material in railway track structures," *Proceedings of the third international conference on EPS Geofoam,* Salt Lake City, Utah, 10-12 December, 1-10.

Farnsworth C. F., Bartlett S. F., Negussey, D. and Stuedlein A. (2008). "Construction and post-construction settlement performance of innovative embankment systems, I-15 reconstruction project, Salt Lake City, Utah," *Journal of Geotechnical and Geoenvironmental Engineering*, 134, 289-301.

Frydenlund, T. E., Myhre, O., Refsdal, G., Aaboe, R., 1987. "Plastic foam in road embankments," Norwegian Road Research Laboratory, Norwegian Edition 61 (in English).

Grabe, P. J., (2002). "Resilient and permanent deformation of railway foundations under principal stress rotation," PhD Dissertation, University of Southampton, UK.

Helwany, S., (2007). "Applied soil mechanics with ABAQUS applications," John Wiley & Sons, Inc., Hoboken, New Jersey.

International Union of Railways (1994). "UCI Code 719R: Earthworks and trackbed layers for railway lines," Paris, France.

Itasca Consulting Group, Inc. (1993-2002). "Fast Lagrangian Analysis of Continua in Three Dimensions, Version 3.00-261." Minneapolis, Minnesota.

Itasca Consulting Group, Inc. (2005). "FLAC: Fast Lagrangian Analysis of Continua: Structural Elements, Version 5." Minneapolis, Minnesota.

Kaynia, A. M., Madshus, C., and Zackrisson, P (2000). "Ground vibration from high-speed trains: prediction and countermeasure," *J. Geotech. Geoenviron. Eng*, 126(6), 531-537.

Miki, G. (1996). "Ten year history of EPS method in Japan and its future challenges," *Proceeding of International Symposium on EPS Construction Method*, Tokyo, 29-30 October, 394-411.

Negussey, D. and Stuedlein, A. (2003). "Geofoam fill performance monitoring." *Utah Department of Transportaion Research Division* Report No. UT-03.17.

O'Riordan, N. and Phear, A. (2001). "Design and construction of ballasted track formation and subgrade for high speed lines," *Proceedings of the International Conference of Hail way Engineering*, London, 30 April-1 May

Powrie, W., Yang, L. A., and Clayton, C. R. I. (2007). "Stress changes in the ground below ballasted railway track during train passage," *Proceedings of the Institution of Mechanical Engineers, Part F, Journal of rail and rapid transit*, March, 221(2), 247-262.

Riad, H. L., Ricci, A. L., Osborn, P. W., D'Angelo, D. A. and Horvath, J. S. (2004). "Design of lightweight fills for road embankments on Boston's central artery/tunnel project," *Proceedings: Fifth international conference on case histories in geotechnical engineering*, New York, NY, 13-17 April.

Snow, R., Webb J., Sander M., (2010). "Light rail on geofoam West Valley UTA TRAX project", *2010 AREMA Conference and Exposition*, Orlando, Florida.

Stark, T. D., Arellano, D., Horvath, J. S., and Leshchinsky, D., (2004). "Geofoam applications in the design and construction of highway embankments", Report prepared for National Cooperative Highway Research Program (NCHRP Web Document 65, Project 24-11), Transportation Research Board of the National Academies.

Stark, T. D., Arellano, D., Horvath, J. S., and Leshchinsky, D., (2004), "Guideline and recommended standard for geofoam applications in highway embankments", Report prepared for National Cooperative Highway Research Program (NCHRP 529), Transportation Research Board of the National Academies.

The Permanent Way Institution (1993). "British railway track-design, construction and maintenance," 6th edition (Ed. G. H. Cope), Echo Press, Loughborough, Leicester, UK.

United States Department of Transportation - Federal Highway Administration (2011), "Expanded Polystyrene (EPS) Geofoam." <http://www.fhwa.dot.gov/research/deployment/geofoam.cfm> (5 April, 2014)

United States Department of Transportation - Federal Highway Administration (2013), "Case in point: the Woodrow Wilson Bridge." <http://www.fhwa.dot.gov/bridge/abc/epscasestudy.cfm> (5 April, 2014)

Parsons et al. (2009). "Corner canyon box culvert, Structure 27", Provo to Salt Lake Frontrunner UTA project RAI1008, construction contract UT07-004GL, July 25.

Zakeri, J. A., and Sadeghi, J. (2007). "Field investigation on load distribution and deflections of railway track sleepers," *Journal of Mechanical Science and Technology*, 21(12), 1948-1956.

CHAPTER 5: DYNAMIC DEFLECTION MONITORING OF EPS EMBANKMENT TO SUPPORT RAILWAY SYSTEM

INTRODUCTION

In the United States, EPS geofoam was recently incorporated in portions of the commuter and light rail systems in Salt Lake City, Utah by the Utah Transit Authority (UTA). The FrontRunner commuter rail south line extends from Salt Lake City to Provo, Utah. Along this line at Corner Canyon in Draper City, EPS has been used in the embankment in order to minimize the stress over a reinforced concrete box culvert. This location has both EPS geofoam and adjacent earthen embankment. Similarly, the light rail line (Green Line) extends from West Valley Central to Salt Lake City International Airport. In this line, EPS has been used in the embankment near Roper Yard, which is operated by the Union Pacific Railroad. These two sites were selected to monitor the dynamic deflections of EPS geofoam embankments.

The main objectives of the field deflection study were to: (1) develop an optical technique to measure the dynamic vertical deflection, (2) evaluate the performance of the developed optical technique, (3) measure the vertical deflection during passage of trains using accelerometers and (4) compare the results of vertical deflection of EPS embankment with that of the earthen embankment.

FIELD DESCRIPTION

The FrontRunner commuter rail system in the Corner Canyon area in Draper City, Utah has rail embankment constructed of both EPS geofoam and conventional fill materials. The site is shown in Figure 5.1. This system consists of (from top to bottom): steel rail, ballast, sub-ballast, concrete reinforcing slab, EPS geofoam and sand. The slope of the embankment is 2H:1V. The cross-section of an embankment is shown in Figure 5.2. Similarly, a photo of the EPS embankment used to support light rail along Green Line near Roper Yard is shown in Figure 5.3.

Figure 5.1. Embankment with EPS geofoam and conventional fill materials in Draper city of Utah along FrontRunner line

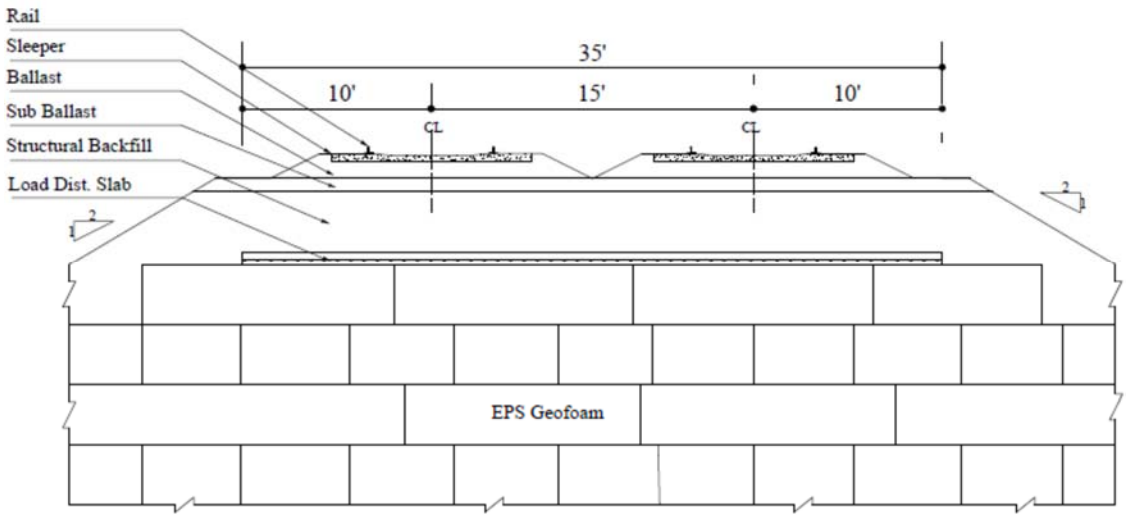

Figure 5.2. Cross-section of an EPS geofoam embankment at corner canyon of Draper city of Utah

Figure 5.3. EPS embankment to support light rail along Green Line near Roper Yard of Utah

EQUIPMENT AND METHODS

Dynamic Deflection Monitoring

In the study, an optical target technique was developed for measuring the dynamic deflection of the rail, but this technique was not deployed in the field due to poor weather conditions (high winds). However, the optical technique is still described initially in this chapter. In order to measure dynamic vertical deflection in field setting, accelerometers were glued on sleepers. The data obtained from the accelerometers were converted into displacement time history and the amount of vertical deflection was determined by using the commercially available software SeismoSignal. After the description of the optical technique, the accelerometer procedure for measuring deflections is described in detail.

Development of Optical Technique

In this method, a paper target (Figure 5.4) was developed and used for laboratory testing of the system and optical interpretation. The target was attached on a wooden frame and kept on the MTS machine as shown.

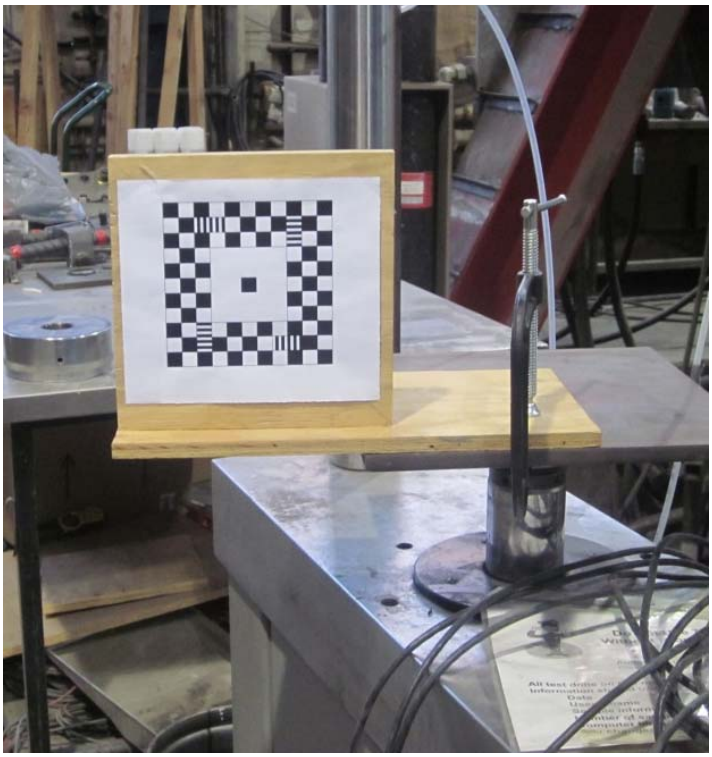

Figure 5.4. Target set-up on MTS machine

The MTS machine has an actuator that can be controlled to produce a systematic and controlled vertical displacement. A LVDT was used to measure the linear displacement versus time. A loading protocol was set up in the MTS machine for cyclic loading of a frequency 0.5 Hz and peak to peak amplitude of 7 mm. The protocol was written to yield time and displacement as output.

Bowness et al. (2007) considered the minimum distance between target and camera to be 10 m in order to minimize the effects of train vibration on the camera. This recommendation was used for this study, where video was recorded by setting a Go-Pro™ camera and telescope at a 10 m distance from the target as shown in Figure 5.5. The Go-Pro™ camera was able to take pictures and videos at a rate of 120 frames per second, and had a Wi-Fi system which could be connected to other electronic devices to display the target. The target was made with black and white squares in order to make analysis easier. After recording the video, an image processing technique was employed to find the vertical deflection.

Figure 5.5. Camera-telescope set up for video recording

In the method, the video recordings were converted into several still frames. The first frame was taken as the base image. The center of the target was determined in terms of pixel number for each frame. The displaced position of center of the target in the vertical direction was determined in terms of pixels and was converted into linear distance.

For the analysis, an algorithm was developed in MATLAB. The algorithm is given in Appendix E. In this process, all images were uploaded initially. The central black square box of the target was chosen as the region of interest. The region was selected to make sure that the total displacement of the square still remains within the peripheral white region. A matrix was created with zeros in all rows and columns. The region of interest was then replaced by the matrix with zero values. Therefore, this region became completely different from the peripheral zones. A histogram was made for the linearly spaced vectors, which were prepared from a one-dimensional (1D) matrix. The 1D matrix was obtained from the rows and columns of the selected region. The threshold value of the pixels in the region was then determined. Values smaller than threshold were made zero. Similarly, values greater than threshold were set equal to one.

The total number of rows where the values were non zero represented the length of the square. Thus, the total number of pixels along the length of one small square was determined. The identity of the center region was then determined in terms of its pixel number. The pixel numbers for the center region of subsequent images were determined in similar manner. Once the minimum pixel numbers were determined, then each pixel number was subtracted from this. (The pixel numbers represented the distance in terms of the number of pixels from the minimum value.) A linear scale was used to measure the side of the big square. The total

number of pixels at one side of the big square were also calculated. A conversion factor was determined for converting pixels into corresponding linear displacement. The time was calculated by dividing the frames to the number of frames in one second. For example, if there were 200 frames in 10 seconds then the 20 frames were obtained in 1 second. From this, a plot was made between displacement and time. The total displacement was then determined from the plot. The displacement versus time from both optical techniques and data extracted from MTS machine was plotted on the same graph for comparison (Figure 5.6).

After laboratory verification, a similar instrument was developed for field implementation. At the Corner Canyon embankment site, there is no level ground around for a distance of 10 m from the target on the rail to where the embankment slope begins. The embankment slopes away from the rail on a 2H:1V side slope.

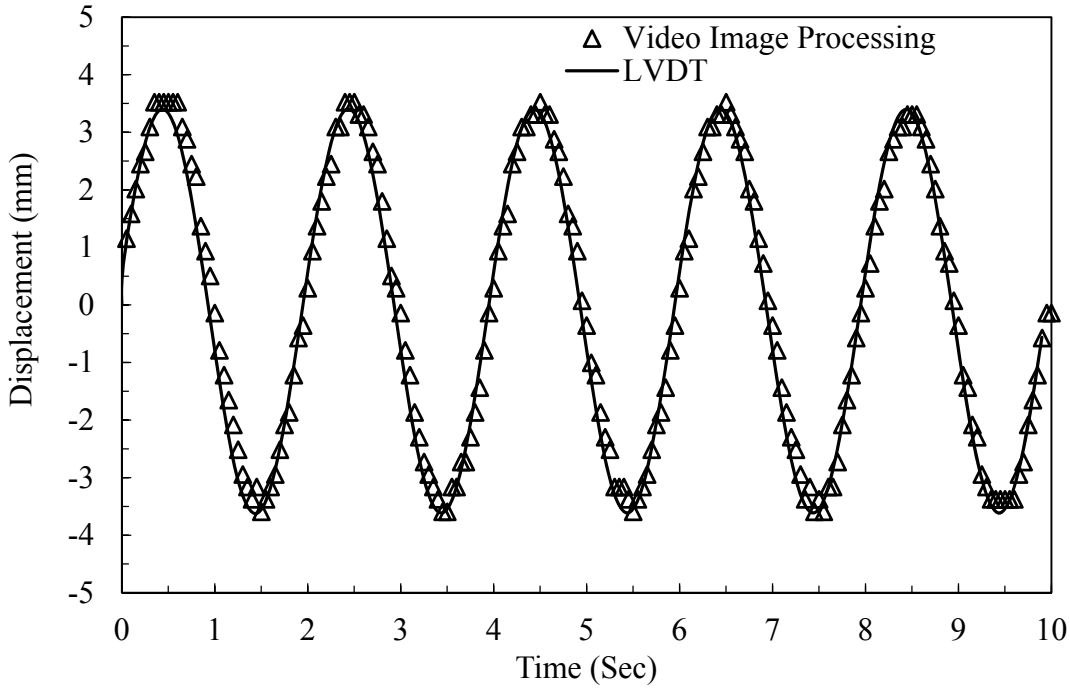

Figure 5.6. Comparison of displacement obtained from image processing in optical technique and LVDT measurement in MTS machine

Therefore in order to measure the deflection on sloped ground, a modification of the set-up was introduced. A telescoping rod was fixed on a survey tripod, and the telescope with a Go-Pro™ camera was mounted at the top of the rod. The rod and camera attached was able to rotate (Figure 5.7). The target could be seen using a Wi-Fi device such as smart phone or tablet using the Wi-Fi system of the Go-Pro™ camera. Unfortunately, however, this technique proved to be very sensitive to vibration for wind and other ambient sources.

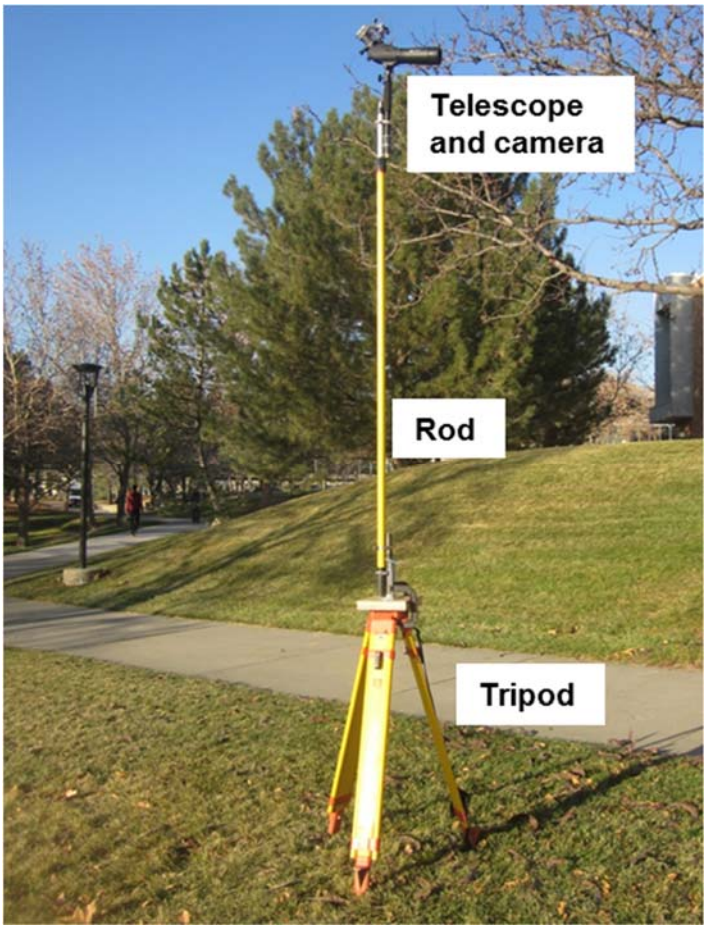

Figure 5.7. Optical technique instrument set up for field measurement of vertical deflection

Accelerometers for Dynamic Deflection Monitoring

Five accelerometers of model 4630A-005 manufactured by Measurement Specialties Inc., California (Figure 5.8) were used in the sites for deflection monitoring. The triaxial accelerometers were cubical in shape with dimension of 25.4 mm. The dynamic range of the accelerometers was $\pm 5g$ with an operating temperature of -55^0 C to 125^0 C (Measurement-Specialities, 2015). Data from the accelerometers were collected at a sampling interval of 1×10^{-3} sec (1000 Hz). The accelerometers were glued on the concrete tie (i.e., sleeper) to measure the deflection. Figure 5.9 shows the orientation of the accelerometer on the sleeper. As shown in Figure 5.9, the Z axis was oriented along the vertical direction, the Y axis was parallel to the rail and the X axis was perpendicular to the rail. The spacing between the accelerometers were installed using the live load configuration provided by American Railway Engineering and Maintenance-of-Way Association (AREMA) manual (AREMA, 2007) for the train locomotive (Figure 5.10).

Figure 5.8. Model 4630A accelerometer

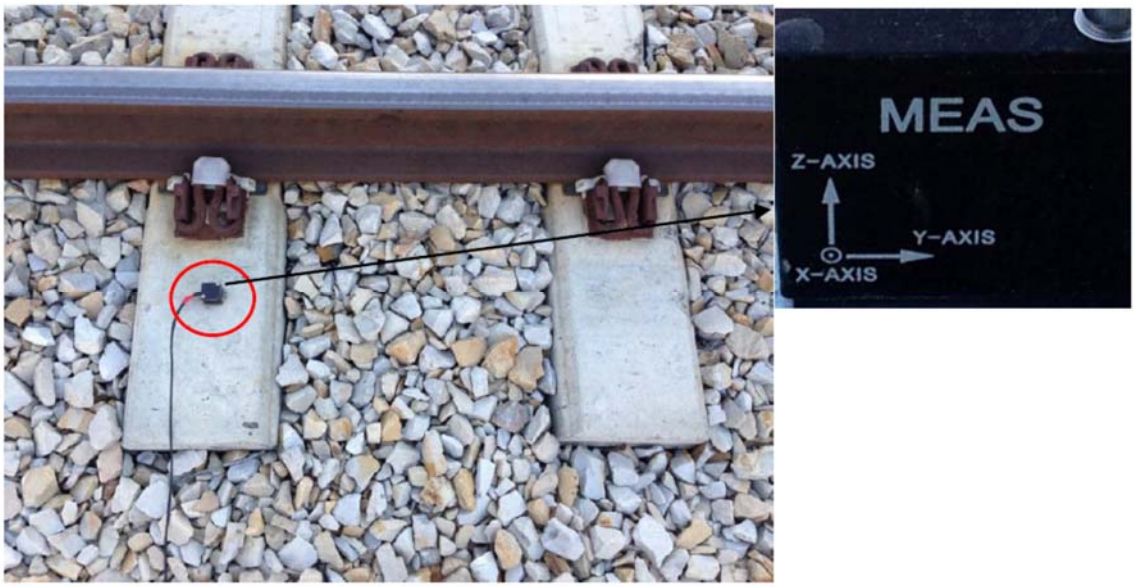

Figure 5.9. Accelerometer glued on sleeper with its orientation

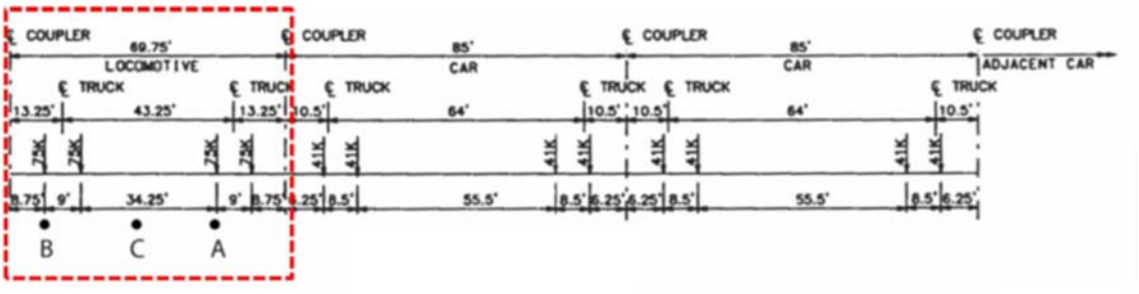

Figure 5.10. Axial load configurations for locomotive and cars with position of accelerometers at A, B and C (AREMA, 2007) for FrontRunner

In Figure 5.10, the letters A, B and C denote the position of the accelerometers. The maximum axle load exerted by a locomotive is 75 K (kips). The configuration of accelerometers was chosen in such a way that the maximum load could be recorded by the sensors. Similarly, Figure 5.11 shows the positioning of accelerometers at A, B and C in the sleepers along the light rail line. A similar orientation and positioning was used for the light rail measurements.

Figure 5.11. Accelerometers positions at A, B and C along light rail line

The FrontRunner train had three double decker passenger cars, one single decker car and a locomotive as shown in Figure 5.12 (locomotive is shown at far left of photo). The train is southbound in this case and is enroute to Provo, Utah. The light train had two cars as shown in Figure 5.13.

Two accelerometers were glued at positions A and B where the maximum axle load would be exerted on the sleeper. A third accelerometer was glued at position C which lied in between A and B. The

accelerometers were then connected to the data logger to extract data. The data logger to be used in the instrumentation was CR9000X is shown in Figure 5.14. The basic CR9000X system consists of CR9011 power supply module, a CR9032 CPU module and CR9052DC Anti-Alias Filter Module with DC Excitation. The filter module connector has a number of channels. Each input channel consists of both regulated constant voltage excitation (VEX) and regulated constant current excitation (IEX) channels.

Figure 5.12. Front runner heading towards south on the route with three double deck cars, one single deck car and a locomotive

Figure 5.13. Light rail heading towards the West Valley Central with two passenger cars

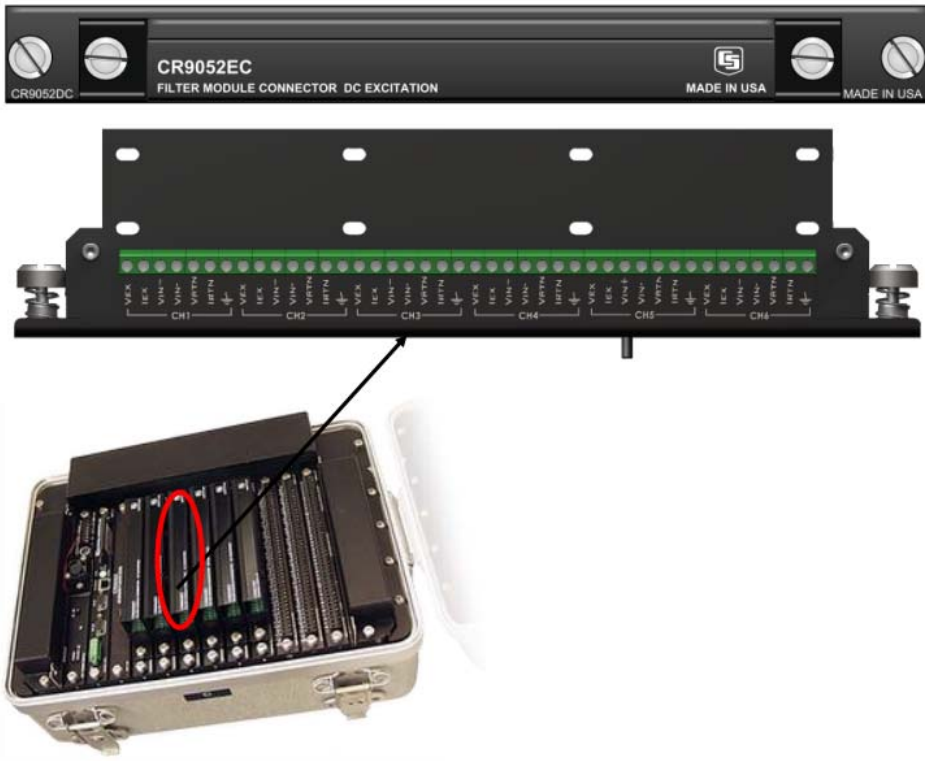

Figure 5.14. CR9000X measurement and control system with CR9052DC Anti-Alias filter modulus and DC excitation

There are five ports for excitation with high voltage input, low voltage input, return and ground. Each accelerometer has five colored wires namely: red, green, white, black and silver and were connected to the five ports on data loggers: excitation (VEX or IEX), high side of the differential voltage input (VIN+), low side of the differential voltage input (VIN-), return (VRTN or IRTN) and ground, respectively.

The Real-time Data Acquisition, RTDAQ™ (RTDAQ, 2011) software was used for the collection of data and was connected to the USB serial port. In RTDAQ, there are three tabs for operation: clock/program, monitor data and collect data. The recorded time in the data logger and personal computer (PC) was synchronized by using the update and check button. The monitor data tab is important for the collection of data. It consists of a ports and flags window. In this window, the flag should be turned on during collection of data. The green light on flag denotes the flag is turned on. Once the train approached the embankment, the flag was turned on. Shortly after the train passed through the embankment array, this flag was turned off.

The data between time of flag being turned on and being turned off was recorded. The collection data tab was used for data collection. In this tab, there are three collection options: collect mode, file mode and file format. All the data options were used in the collect mode. In the file mode and file format, append to end of file and ASCII table data were selected. The start collection tab was used for the collection of data.

After data collection, the next step consisted of the analysis of the field accelerometer data. This was done using the commercially available software SeismoSignal™ (SeismoSoft, 2015). This software has filtering and baseline correction routines which can be used to convert the input acceleration time history to velocity and displacement time histories.

The collected data was impacted by high frequency noise (i.e., vibration) which created spurious baseline errors. Therefore, the baseline correction and frequency filtering features of this software were employed to re-baseline the measurements and to remove unwanted high frequency signal. The available baseline corrections methods were: constant, linear, quadratic and cubic. For this study, the linear baseline correction function was chosen because it provided the most reasonable adjustment to the trend in the data. After completing the base line correction, Fourier and power spectra were plotted for each of the train events. The Fourier amplitude spectrum shows the distribution of amplitude of motion with frequency and the power spectrum reveals the power spectral density with respect to frequency. The frequency band for filtering was determined based on plots of the Fourier and power spectrum (Figures 5.15, 5.16 and 5.17). These plots suggest that much of the signal above about 70 Hz is high frequency noise from vibration, which is not of interest for estimating the deflection of the rail from the moving train.

In addition, the SeismoSignal™ software has four types of filter configurations: lowpass, highpass, bandpass and bandstop. For the creation of the filter configurations, three filter types are available: Butterworth, Chebyshev and Bessel filters. In this study, a Butterworth filter type was used which featured a flat response in the pass band. The Bandpass filtering configuration was applied in the study which allows signals to pass through the given frequency range. The lower frequency in the Bandpass was chosen to be large (10 seconds) based on the time required during the passage of the train and the high frequency was selected based on the frequency and power spectrum plots (Figures 5.15, 5.16 and 5.17). The baseline corrected and filtered time series provides records of the acceleration, velocity and displacement time history of the rail ties. The vertical displacement of the tie was used to estimate the vertical deflection of the rail because there little opportunity for relative vertical movement between the rail and the rail ties.

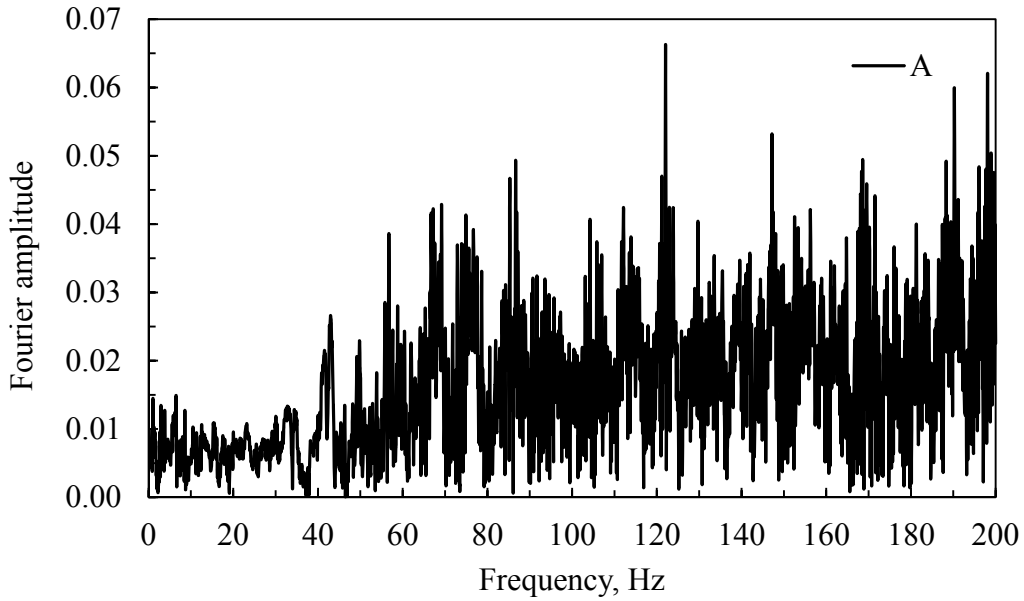

(a)

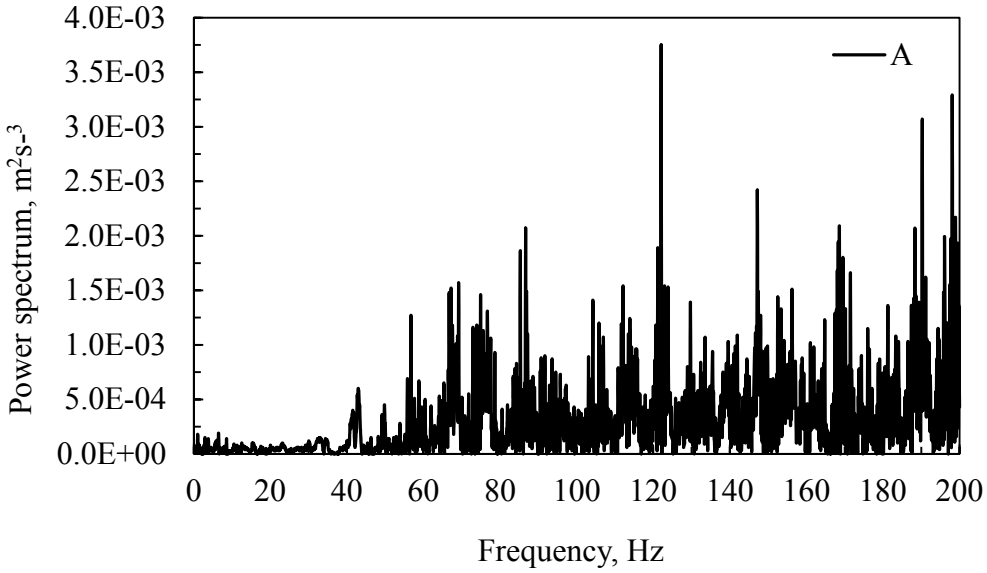

(b)

Figure 5.15. The record of accelerometer at position A along commuter rail line

(a) Fourier amplitude and (b) Power spectrum

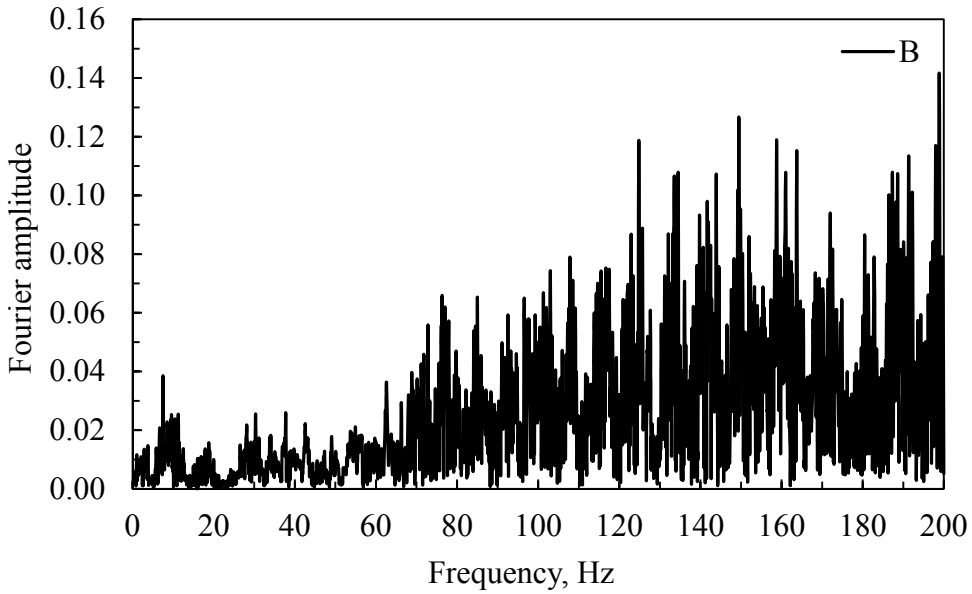

(a)

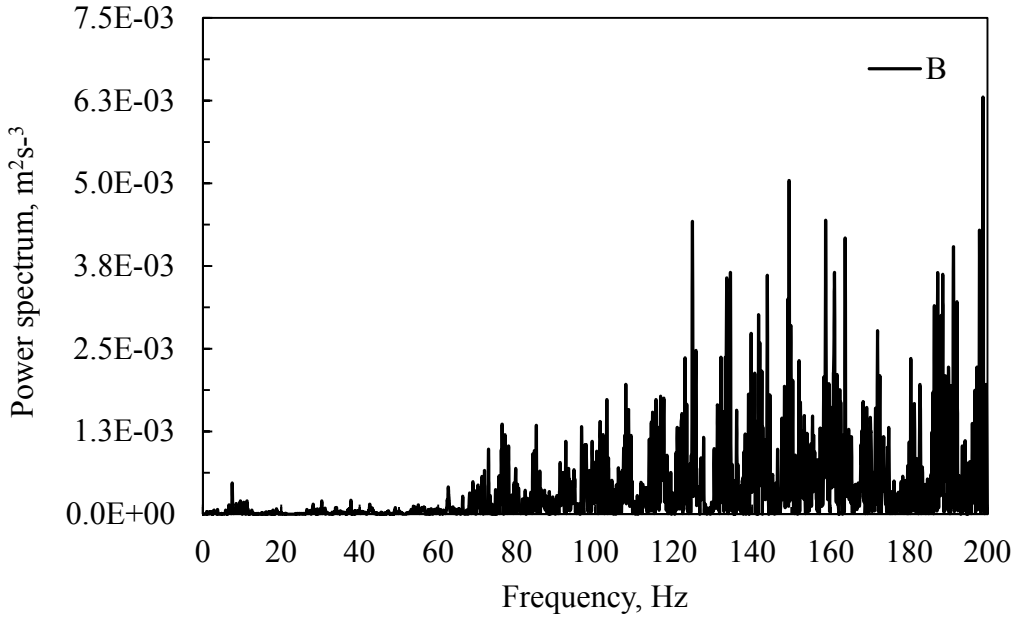

(b)

Figure 5.16. The record of accelerometer at position B along commuter rail line

(a) Fourier amplitude and (b) Power spectrum

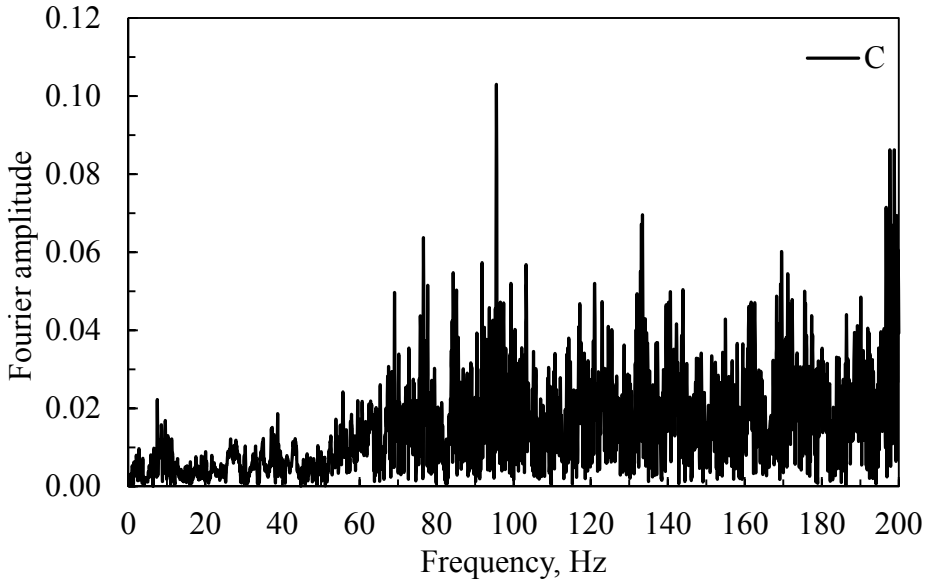

(a)

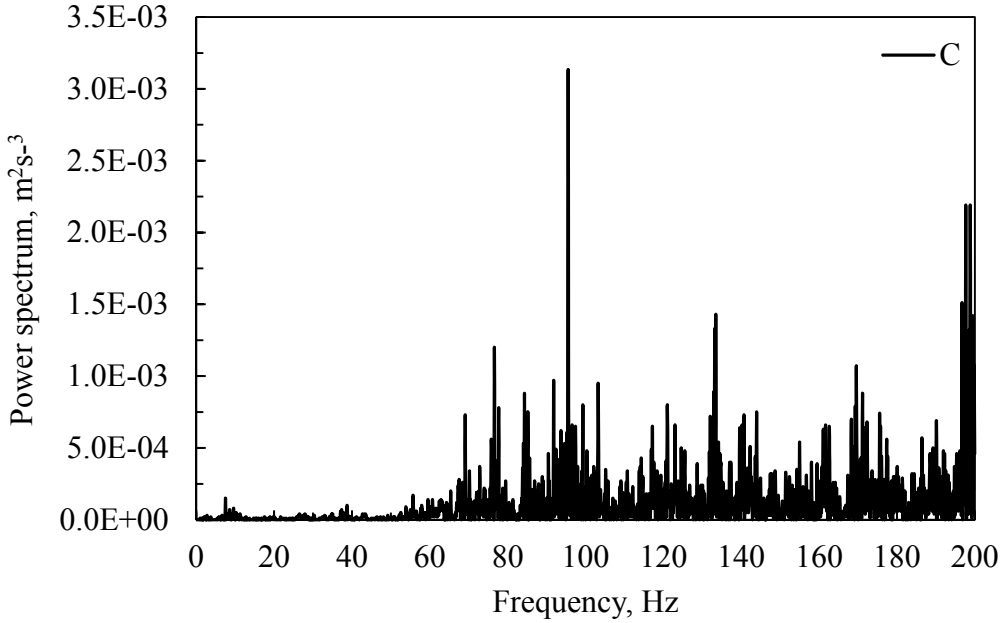

(b)

Figure 5.17. The record of accelerometer at position C along commuter rail line

(a) Fourier amplitude and (b) Power spectrum

RESULTS FROM FIELD MEASUREMENTS

Optical Technique

The results from the test of the laboratory optical technique matched well with the MTS results. This proved that the optical technique, as developed, was able to give reliable results in controlled conditions. However, subsequently this technique was not deployed in the field due to field geometrical constraints and weather conditions. The technique so developed for the field did not perform to its fullest capacity because the study site was windy during the field testing. In addition, it was not possible to gain additional access to the site at a later date when more favorable weather conditions might have prevailed due to the time limits placed on the deflection monitoring by the UTA track access permit. Therefore, the technique was not used for field measurements at the Corner Canyon site.

Nonetheless, the developed technique and algorithm may be useful for future projects or for laboratory measurements for cases where the ambient conditions are more favorable. In short, the optical technique presents a very low cost alternative when compared with the expense required to deploy an accelerometer array and its corresponding high-speed data acquisition system; hence because of this, the optical technique merits further consideration and development.

Accelerometer Array

The orientation of the accelerometers and their locations are shown in Figures 5.9 and 5.11. The possible influence that filtering might have on the vertical displacement results was studied by using various values for the upper frequency of the band pass filter. The estimated displacement time history corresponding to an upper band pass frequency of 30, 60 and 90 Hz are shown in Figure 5.18. This parametric change revealed that the selected displacement record was not significantly altered by the selection of the high frequency for the band pass filter.

The displacement results from the accelerometers positioned at points A, B and C in the EPS embankments along the commuter rail line and light rail lines are described separately in the following sections.

Commuter Rail Line

The Fourier amplitude and power spectra of the recorded data from accelerometers positioned at A, B and C were analyzed in order to finalize the filtering process and to select the upper frequency in the band pass filtering. The Fourier amplitude and power spectrum of A, B and C positions are shown in Figures 5.15, 5.16 and 5.17, respectively.

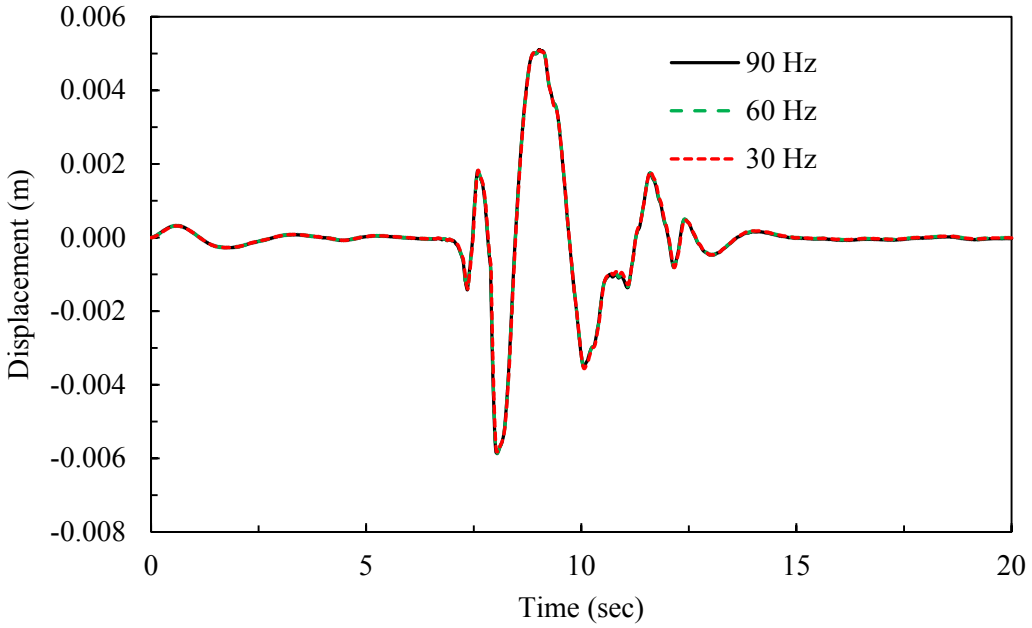

Figure 5.18. Vertical displacement record using different levels for the upper frequency in the Bandpass filter

Based on these plots, it was concluded that the average value of frequency beyond which significant noise started was about 70 Hz and the lowest level of frequency to be considered was 0.1 Hz.

The train bound to Salt Lake City from Provo will be referred to as the north bound (NB) train, and that bound from Salt Lake to Provo will be referred to as the south bound (SB) train hereafter. The train shown in Figure 5.10 was a SB train. In the study, three NB trains named 1, 2 and 3 were monitored for estimating the vertical deflection of rail atop EPS embankment. Three NB trains were named 4, 5 and 6 were monitored for the determination of vertical deflection of rail atop earthen embankment. The accelerometers were placed on the sleepers adjacent to the NB train track; whereas the SB train track was located 1.5 m distance from the position of the accelerometers. The NB trains were used for measuring vertical deflection because the vertical stress on embankments was assumed to be higher under the NB train track due to the placement of the accelerometers directly on this track. However, one NB and one SB train were monitored to compare the results in terms of the vertical deflections.

The input acceleration and the vertical displacement of three trains on EPS embankment are shown in Figures 5.19, 5.20 and 5.21. Figure 5.19 reveals the input acceleration and the vertical displacement

measured by the accelerometer at position A due to trains 1, 2 and 3. In Figure 5.19, a somewhat higher peak displacement occurred at the beginning of the record when the train had just entered over the EPS embankment at about 8 seconds of elapsed time. The maximum displacement for this spike was found to be 6 mm. However, a typical average displacement of about 2 mm was observed for many of the deflection events (Figure 5.20 and 5.21).

The FLAC3D numerical model studies that are presented in Chapter 4 of the EPS geofoam embankment along the FrontRunner commuter rail system produced a maximum rail displacement of 6.1 mm. This estimated displacement is in agreement with the maximum field measured displacement obtained from accelerometers of 6 mm and less than the overall average field measured displacement of 2 mm. Therefore, the FLAC3D model described in Chapter 4 can be used to perform further numerical studies to evaluate displacements of freight rail systems supported by EPS embankments.

Figure 5.20 shows the input acceleration and vertical displacement of the EPS embankment recorded at position B for trains 1, 2 and 3. The third train produced acceleration spike once it had left the EPS portion of the embankment. The maximum and average displacement were found to be around 4 mm and 2 mm, respectively.

Figure 5.21 shows the input acceleration and vertical displacement of EPS embankment measured by an accelerometer at position C for trains 1, 2 and 3. Figure 5.21 shows the maximum and maximum average vertical displacement of EPS were around 4 mm and 2 mm, respectively. The second train produced a spike at the end when it crossed the embankment. The combined accelerometer records for positions A, B and C for trains 1, 2 and 3 are shown in Figure 5.22. These records show that the maximum and average vertical displacement were around 6 mm and 2 mm, respectively. These vertical displacement results are similar to those measured on sleepers for an earthen embankment railway track using geophones by Bowness et al. (2007). These authors report a maximum and average displacement of around 6 mm and 3.5 mm.

For one event, two trains (NB direction and SB direction) passed over the EPS embankment array within short time span. The displacement was monitored for this event. In this analysis, the record of NB train and SB train was denoted by AN and AS for the accelerometer position at location A. Similar notations were used for accelerometers positioned at B and C. The input acceleration of both trains while passing the array is shown in Figure 5.23. The analysis was done separately for each of accelerometers and trains. Comparative plots of the input acceleration and vertical displacements of the EPS embankment recorded by accelerometers A, B and C are shown in Figures 5.24, 5.25 and 5.26, respectively.

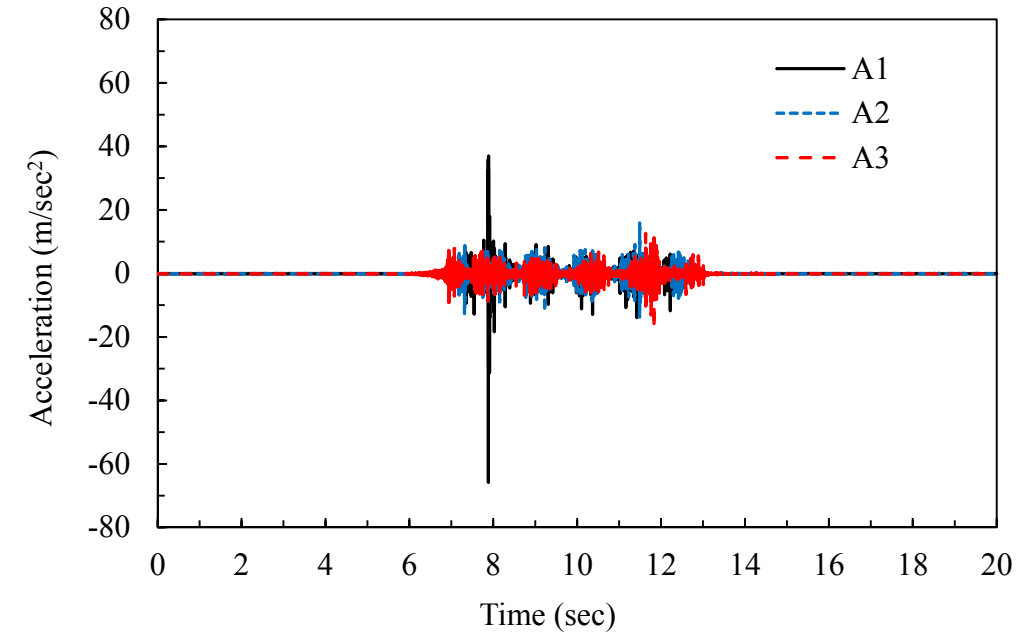

(a)

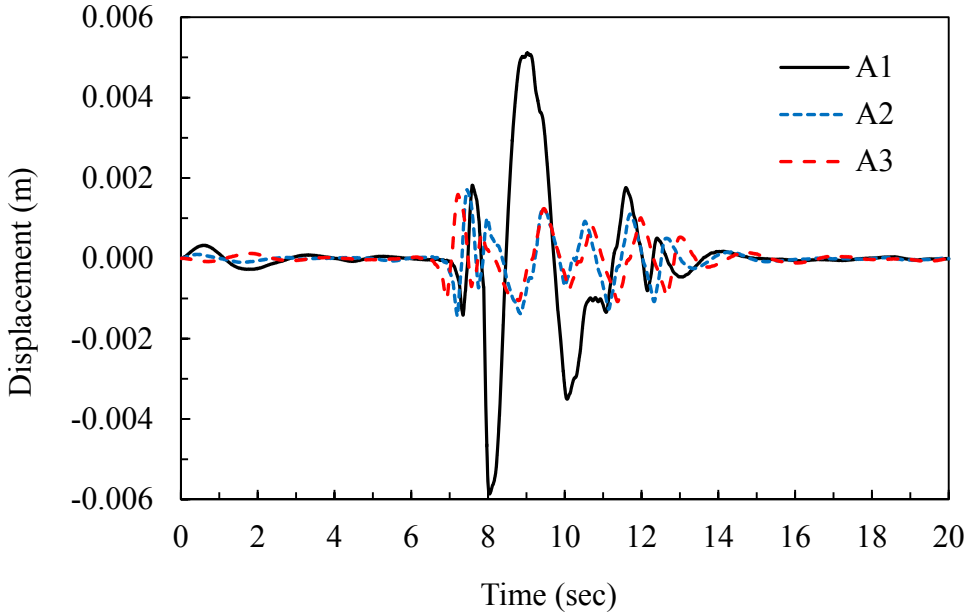

(b)

Figure 5.19. The record of accelerometer position at A of EPS embankment along commuter rail line (a) Input acceleration and (b) Vertical displacement

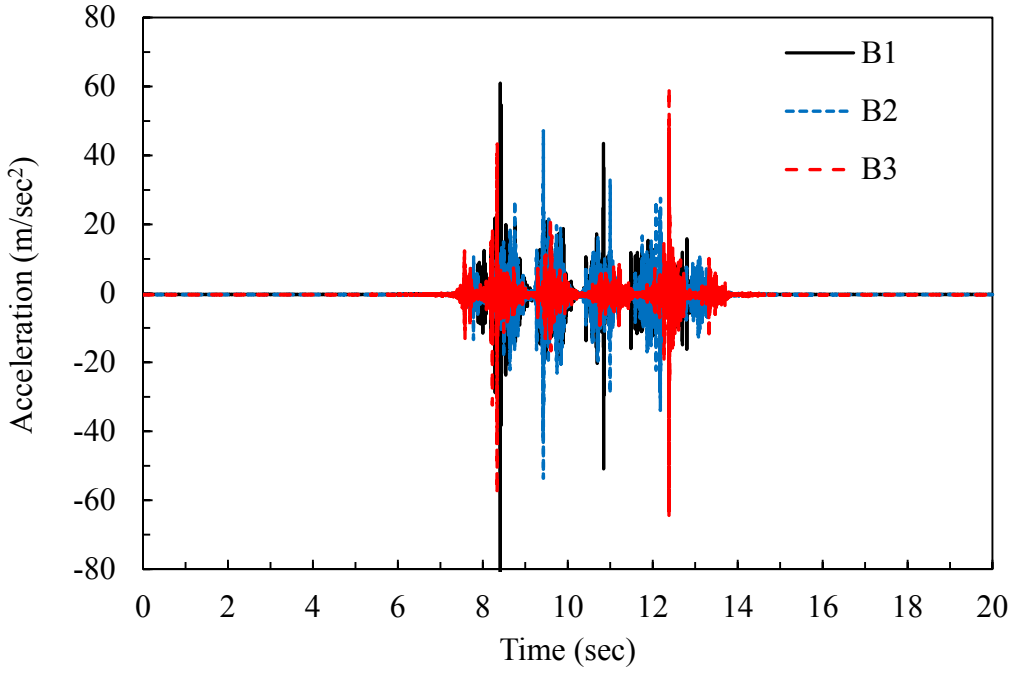

(a)

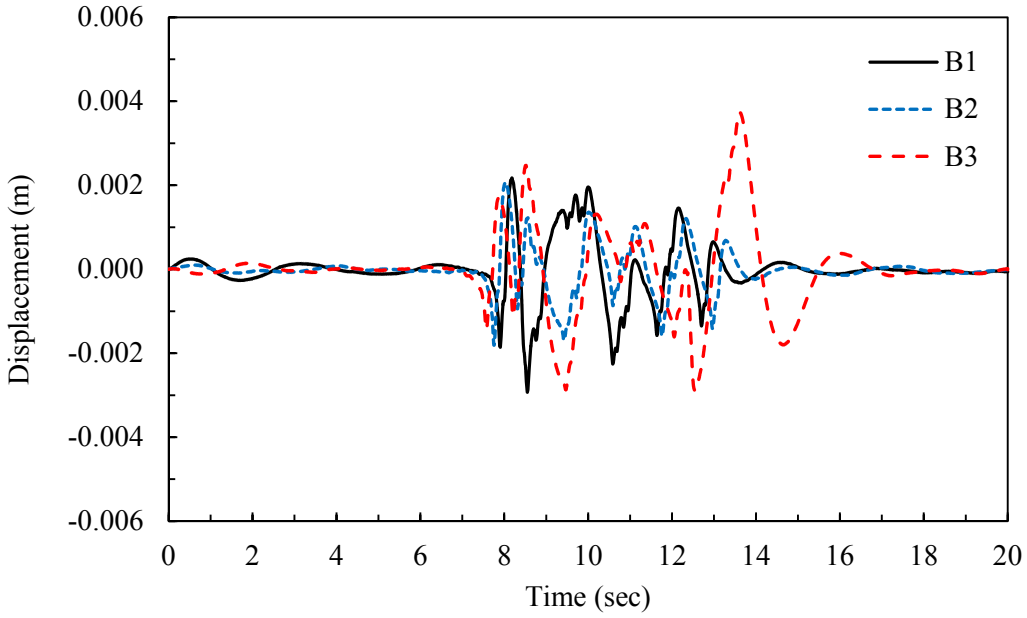

(b)

Figure 5.20. The record of accelerometer position at B of EPS embankment along commuter rail line (a) Input acceleration and (b) Vertical displacement

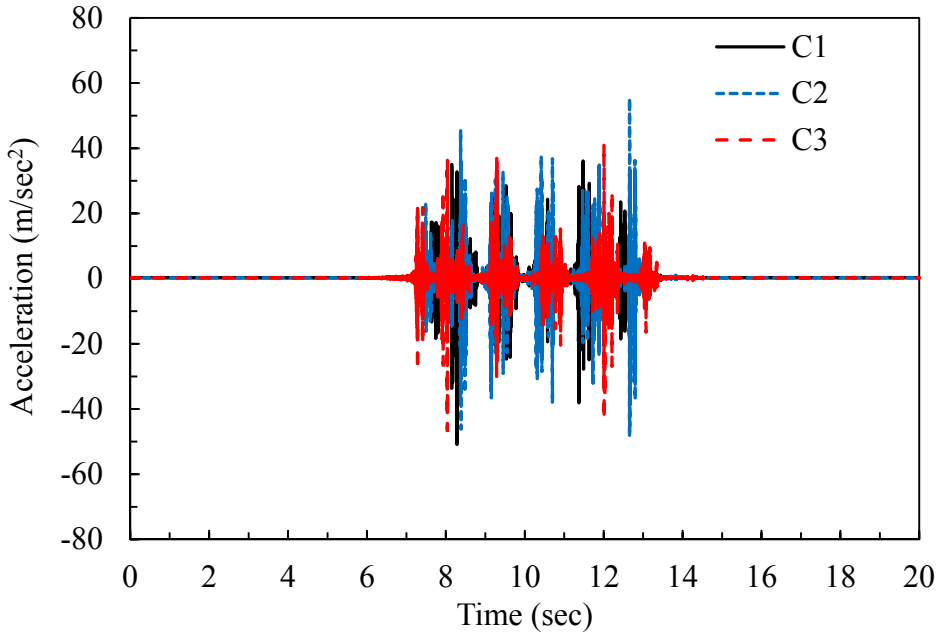

(a)

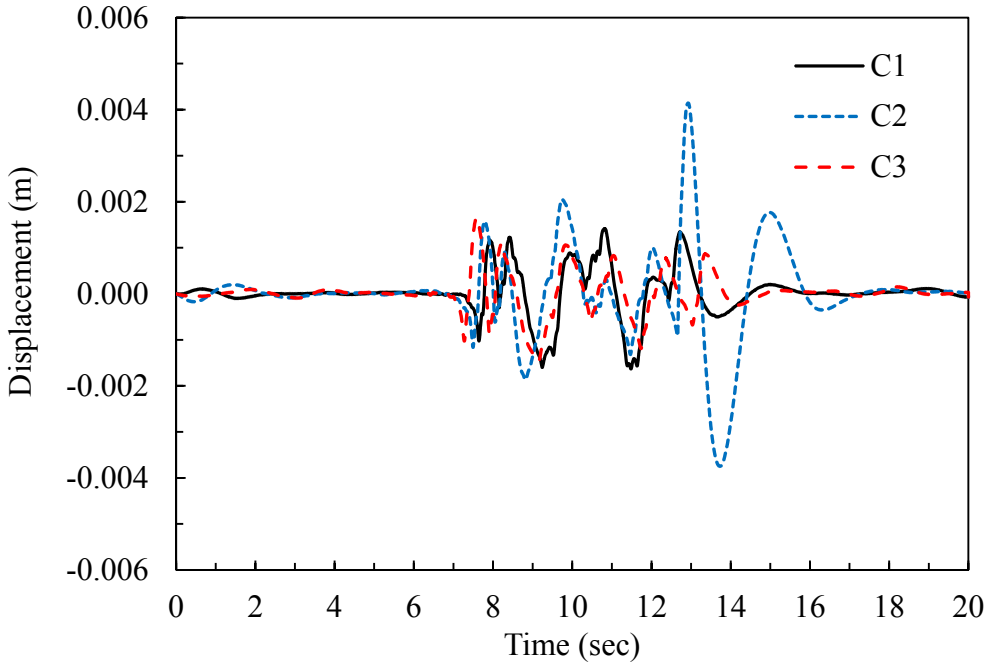

(b)

Figure 5.21. The record of accelerometer position at C of EPS embankment along commuter rail line (a) Input acceleration and (b) Vertical displacement

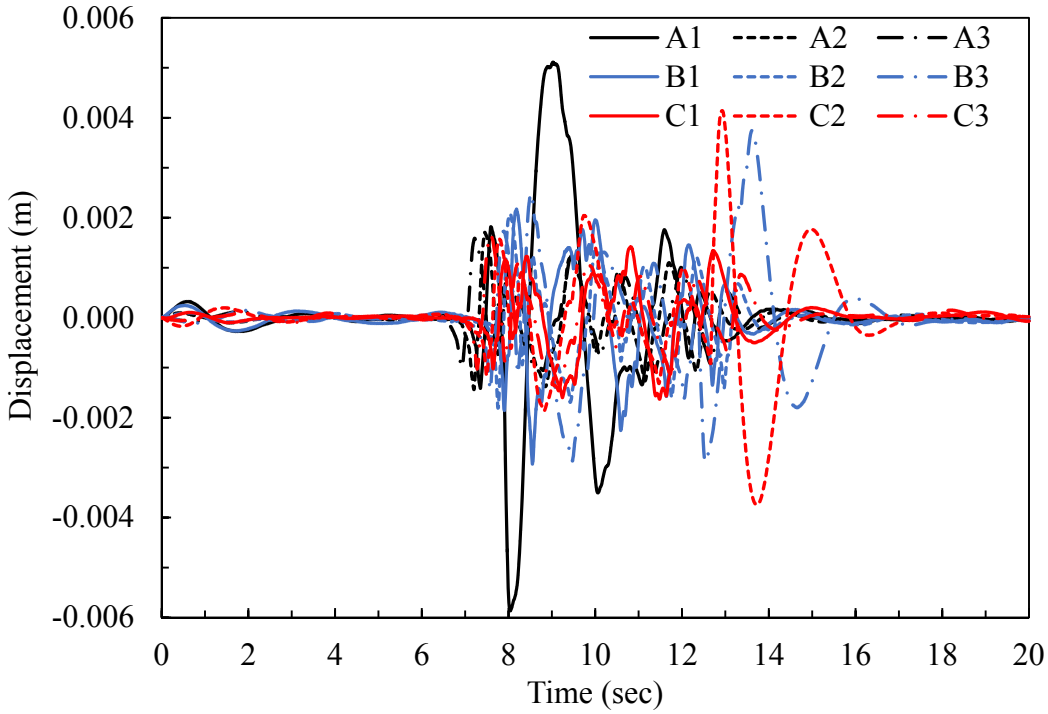

Figure 5.22. Vertical displacement recorded by accelerometers at positions A, B and C for trains 1, 2 and 3 in the EPS embankment along commuter rail line

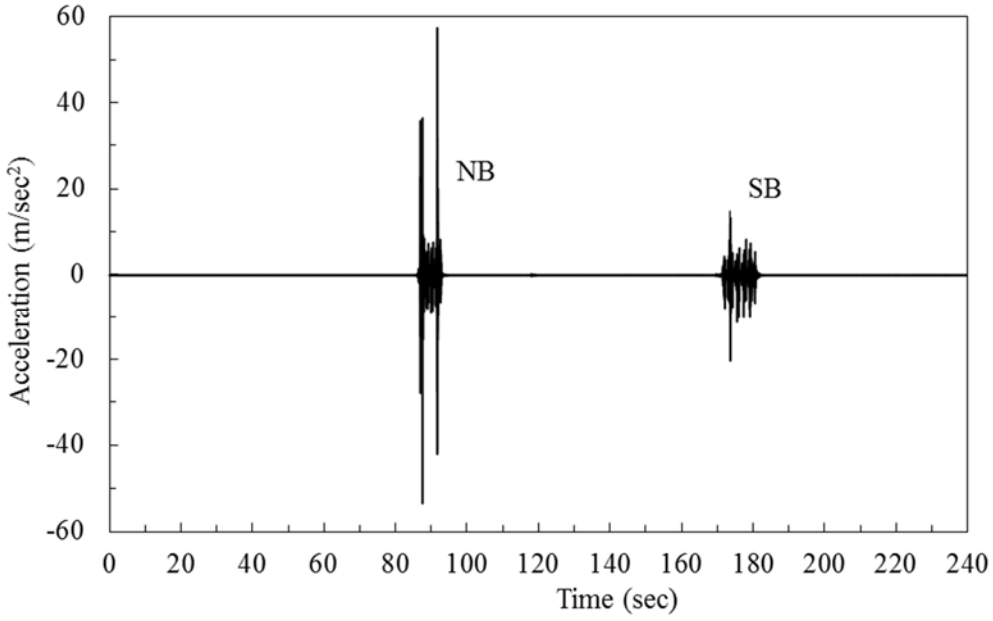

Figure 5.23. The input acceleration of NB and SB train while crossing the EPS embankment along commuter rail line

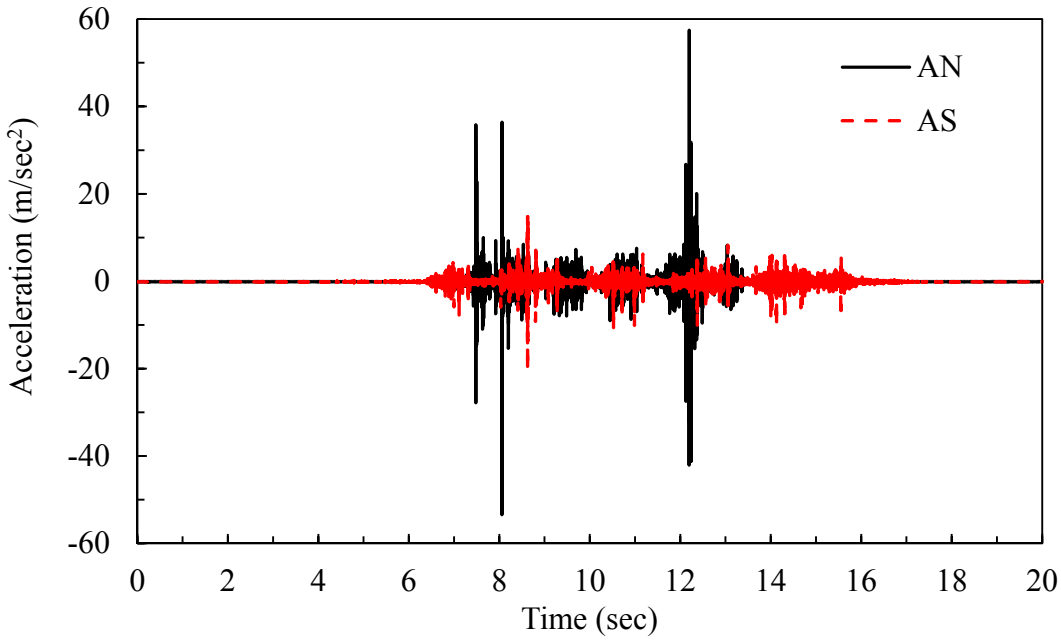

(a)

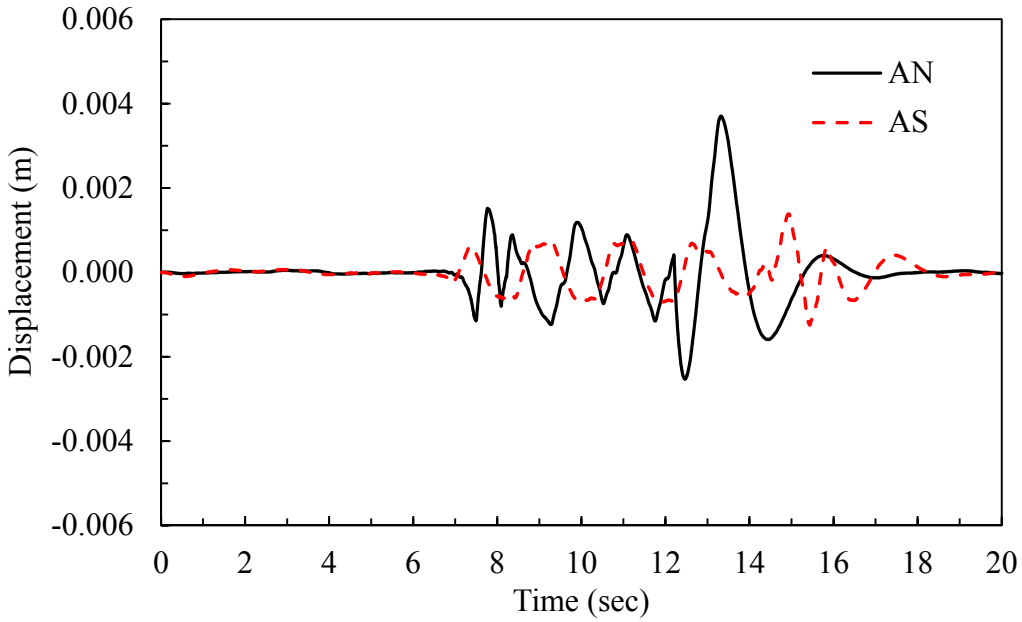

(b)

Figure 5.24. The comparative plot of record on EPS embankment by accelerometer at position A (a) Input acceleration and (b) Vertical displacement

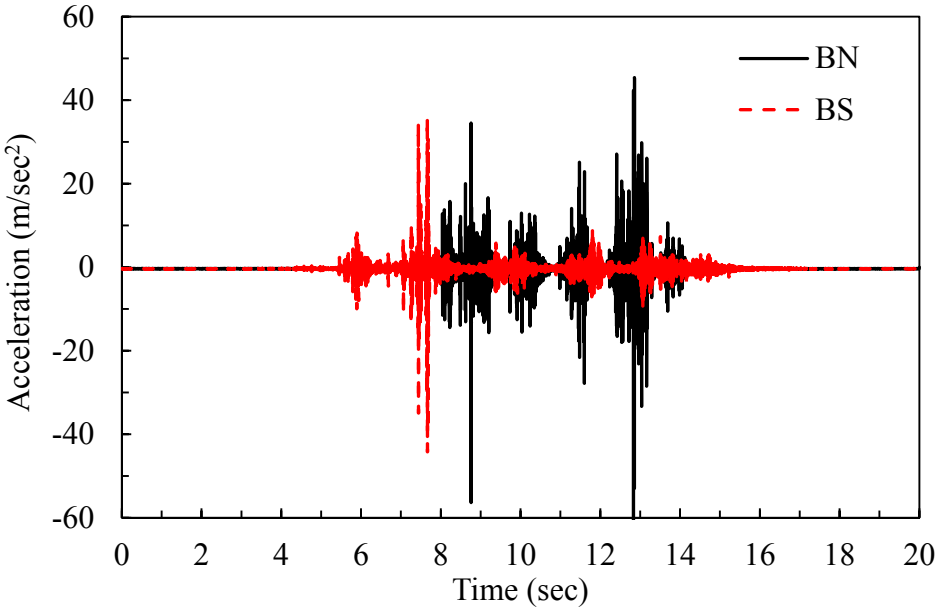

(a)

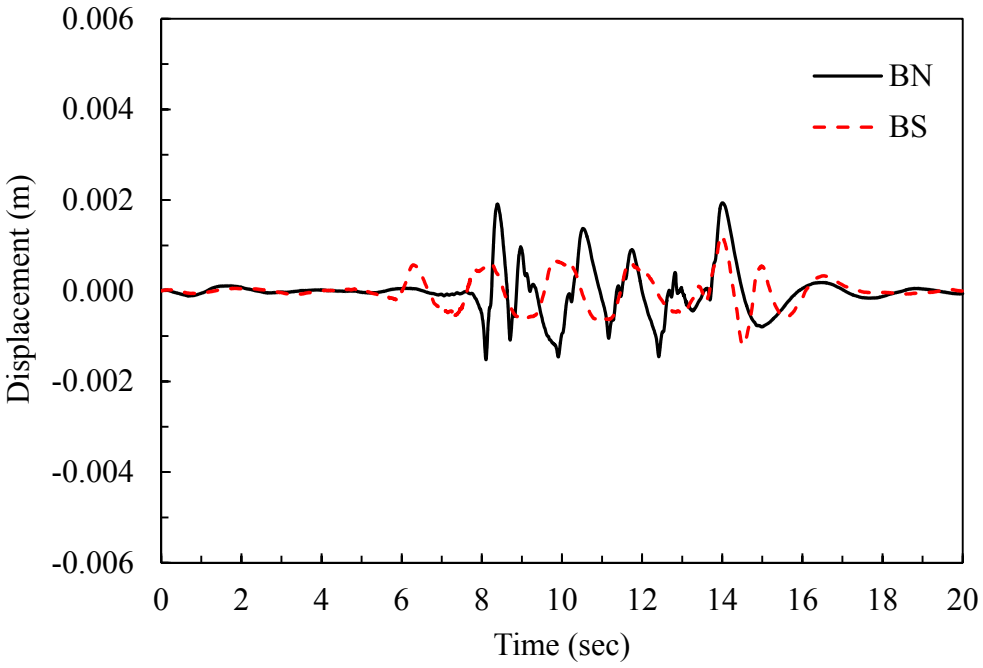

(b)

Figure 5.25. The comparative plot of record on EPS embankment by accelerometer at position B (a) Input acceleration and (b) Vertical displacement

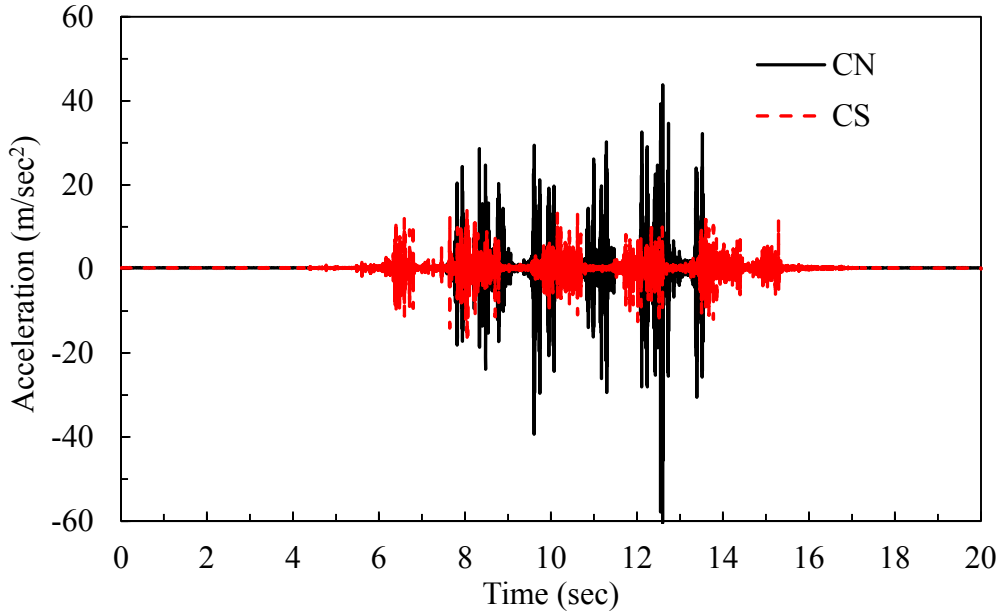

(a)

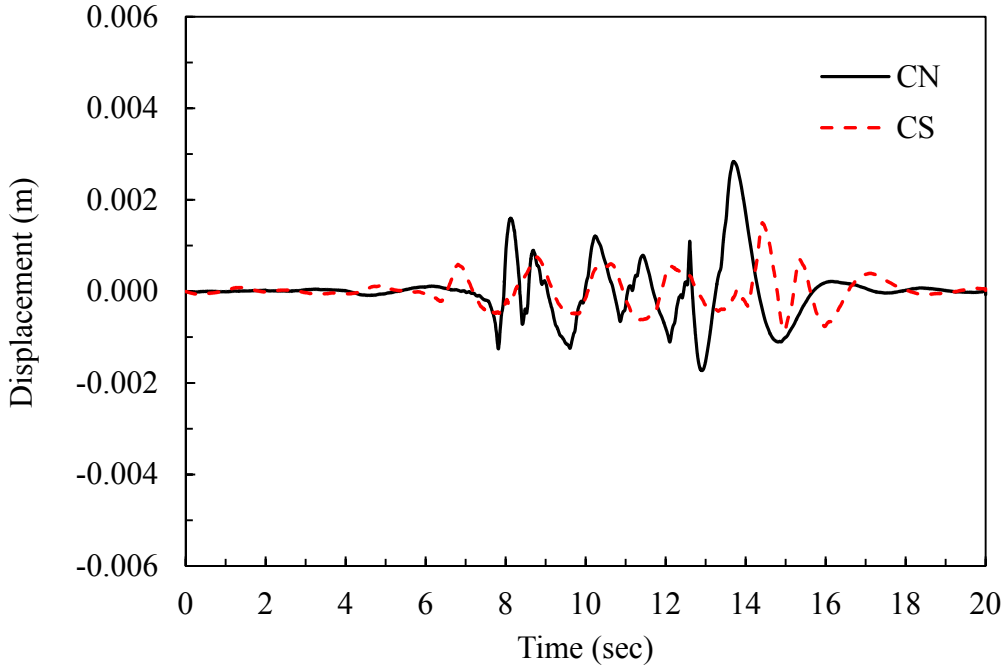

(b)

Figure 5.26. The comparative plot of record on EPS embankment by accelerometer at position C (a) Input acceleration and (b) Vertical displacement

These figures show that the maximum and average vertical displacements for the NB train were about 4 mm and 1.5 mm, respectively; whereas about 1 mm and 0.75 mm was recorded for the SB train, respectively. The lower values for the SB train was due to its greater distance from the position of the accelerometer array placed on the NB rail.

The input acceleration and vertical displacements for three train events named as 4, 5 and 6 on the adjacent earthen embankments are shown in Figures 5.27, 5.28 and 5.29, respectively. Figure 5.27 shows the maximum displacement occurred when the train 4 just entered this portion of the embankment. There was an initial displacement spike at the beginning of this passing, followed by lower displacements a few seconds afterward. The maximum and maximum average displacements were about 12 mm and 3 mm, respectively for the earthen embankment.

Figure 5.28 shows the maximum displacement occurred when trains 5 and 6 just arrived on the earthen portion of the embankment. The maximum and average displacements were around 13 mm and 5 mm, respectively.

A high displacement event occurred when train 6 entered onto the earthen embankment. Figure 5.29 shows a maximum and average displacement of around 22 mm and 5 mm, respectively. The combined displacement results for records at positions A, B and C for trains 4, 5 and 6 are shown in Figure 5.30. This combined plot shows a maximum vertical displacement and maximum average vertical displacement of about 22 mm and 7.5 mm, respectively. These results are higher than those reported by Bowness et al. (2007) for earthen embankment. The difference in results might be due to differences in the embankment materials, construction, geometry, train loads, and from experimental error.

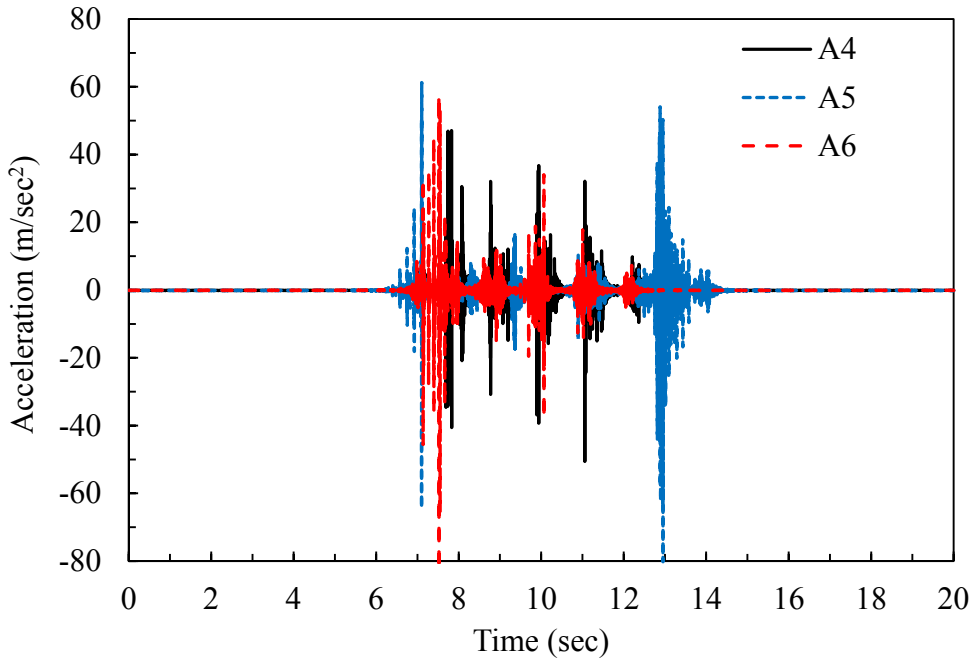

(a)

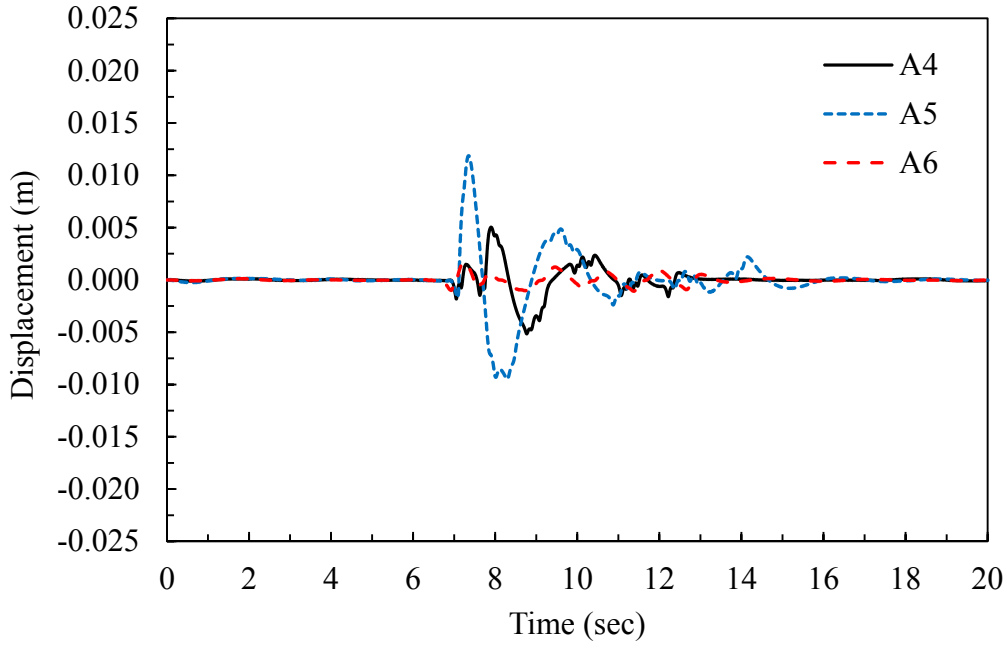

(b)

Figure 5.27. The record of accelerometer position at A of earthen embankment along commuter rail line (a) Input acceleration and (b) Vertical displacement

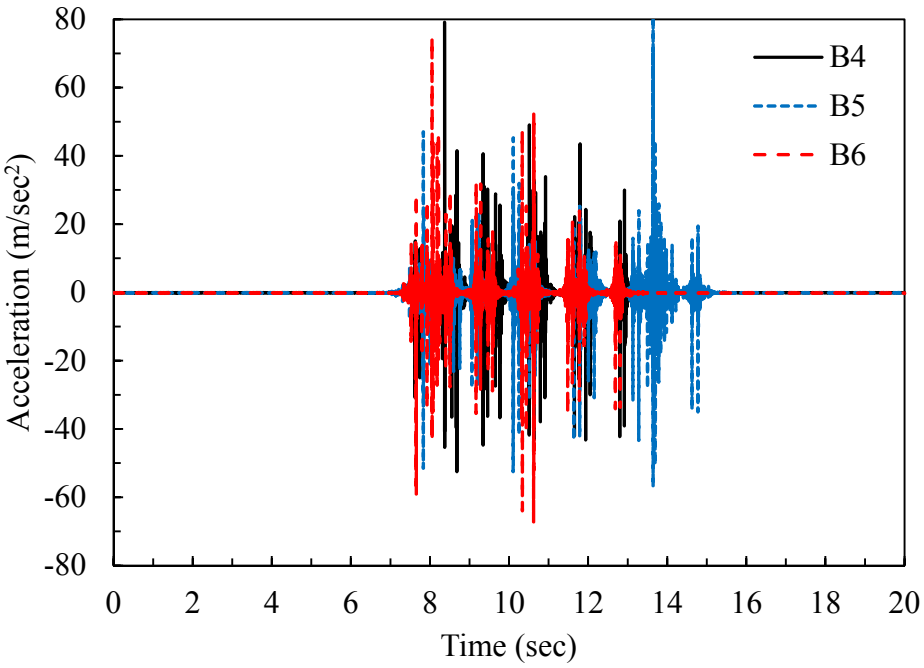

(a)

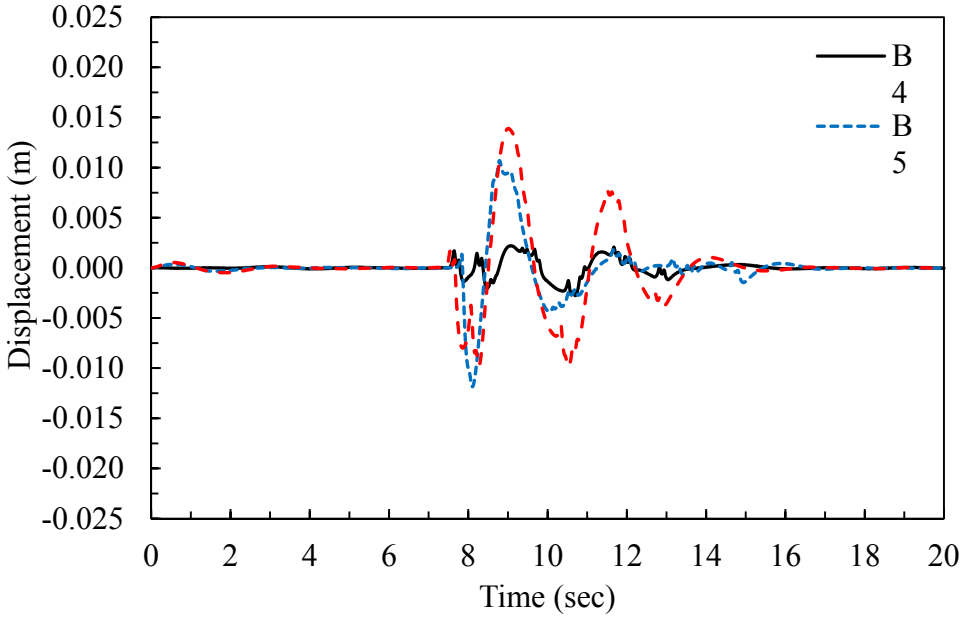

(b)

Figure 5.28. The record of accelerometer position at B of earthen embankment along commuter rail line (a) Input acceleration and (b) Vertical displacement

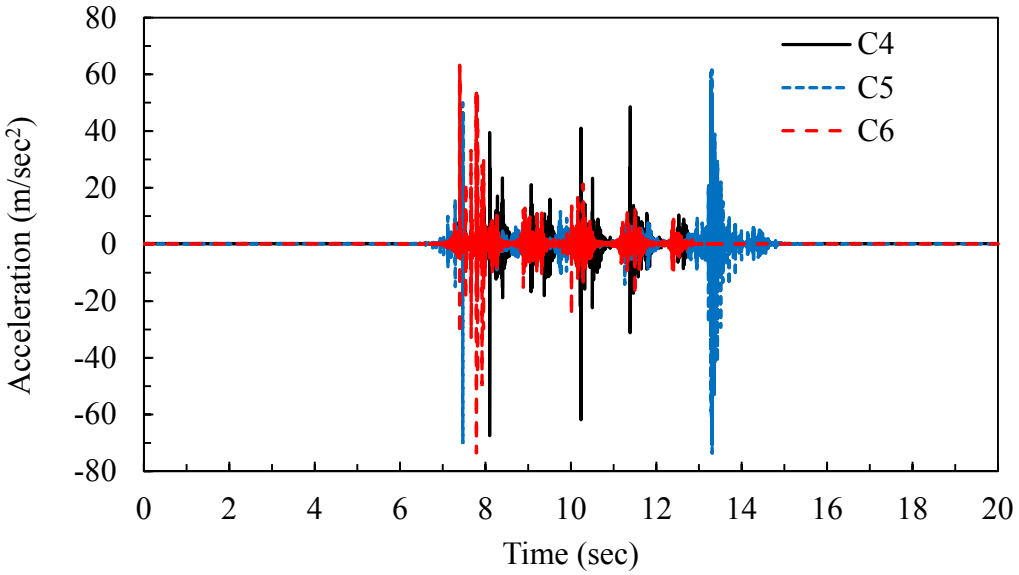

(a)

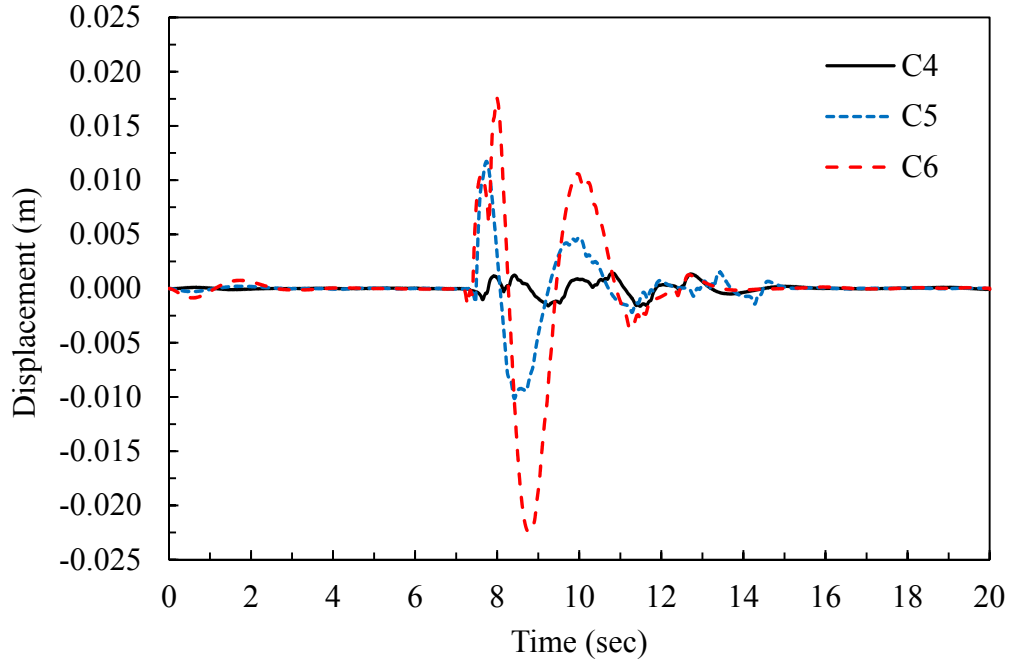

(b)

Figure 5.29. The record of accelerometer position at C of earthen embankment along commuter rail line (a) Input acceleration and (b) Vertical displacement

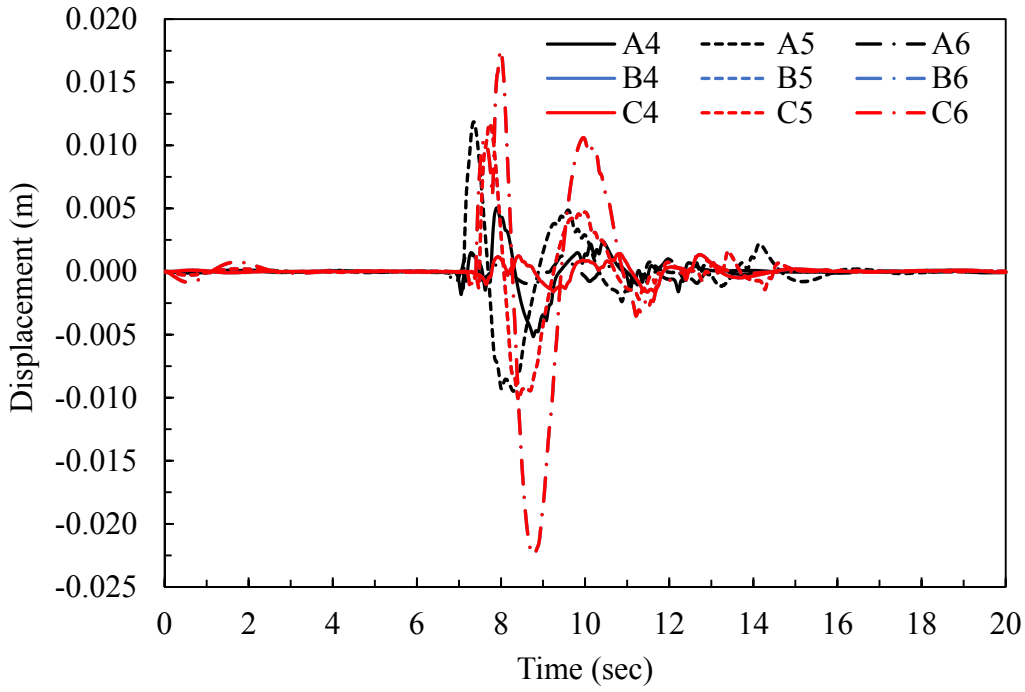

Figure 5.30. Vertical displacement recorded by accelerometers at positions A, B and C for trains 4, 5 and 6 in the earthen embankment along commuter rail line

In summary, the maximum and average vertical displacements for the earthen embankment were found to be higher than those of the EPS embankment. This could be due to the fact that the soil in earthen embankment could have lateral compression due to combined dead and live loads. However, in case of EPS embankment due to inherent properties of EPS material the lateral compression is less likely to occur. Therefore the minimum vertical displacement might occur in EPS embankment. The measurements suggest that EPS embankment, as constructed at this site, is performing as well as, or slightly better that the earthen embankment in terms of rail deflections.

Light Rail Line Array

The Fourier amplitude and power spectrum for the A, B and C positions are shown in Figures 5.31, 5.32 and 5.33, respectively, for the UTA light rail system (i.e., TRAX). The average frequency beyond which significant noise started was about 80 Hz for both Fourier amplitude and power spectrum. Thus, the highest frequency considered in the data interpretation was 80 Hz. The time taken for trains to pass the sensors was less than 10 sec and the lowest level of frequency to be considered was 0.1 Hz.

The westbound (WB) train bound to West Valley Central Station from Salt Lake City International Airport was monitored for this study. The train from the West Valley Central Station to Airport will be referred to as the east bound (EB) train hereafter. The train shown in Figure 5.13 is the WB train. In this study, five WB trains named as 1, 2, 3, 4 and 5 were monitored for the determination of the vertical deflection of concrete rail sleepers constructed atop a large EPS embankment. The WB train were selected for the monitoring and the accelerometers were placed on the sleepers for the WB rail. At this location, the EB track was about 1.5 m distance from the position of the accelerometers on the WB rail.

The acceleration time histories and the vertical displacement of five trains traveling on the EPS embankment are shown in Figures 5.34, 5.35 and 5.36. Figure 5.34 shows the input acceleration and the vertical displacements estimated by the accelerometer at position A due to trains 1, 2 3, 4 and 5. The process of converting the acceleration time history to displacement was the same as that used for the FrontRunner system, discussed previously, except the upper frequency for the band pass filter was set to 80 Hz.

In Figure 5.34, the maximum displacement was estimated to be about 0.6 mm. Figure 5.35 shows the input acceleration and vertical displacement of the EPS embankment recorded for the position of accelerometer at B for trains 1, 2, 3, 4 and 5. The maximum displacement was about 0.5 mm. Figure 5.36 shows the input acceleration and vertical displacement of the EPS embankment measured by accelerometer at position C for trains 1, 2, 3, 4 and 5. Figure 5.34 shows the maximum vertical displacement of EPS was about 0.7 mm.

The records on accelerometers at positions A, B and C for trains 1, 2, 3, 4 and 5 show the average vertical displacements were about 0.6 mm. This value is approximately 4 times smaller than the maximum average vertical displacements that occurred in EPS embankment along the FrontRunner commuter rail line. This is due to the small dead and live load in case of light rail line.

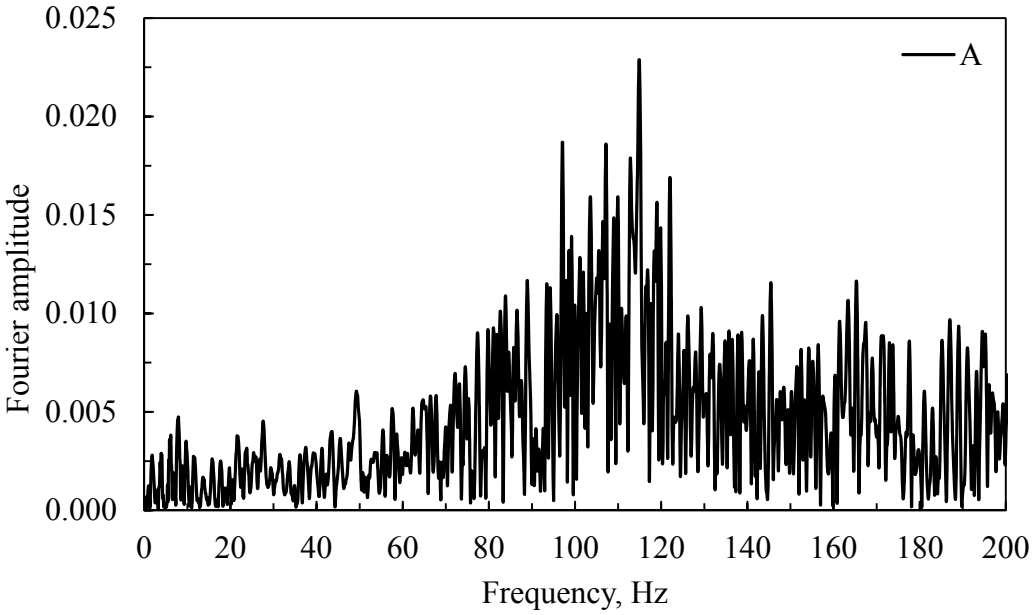

(a)

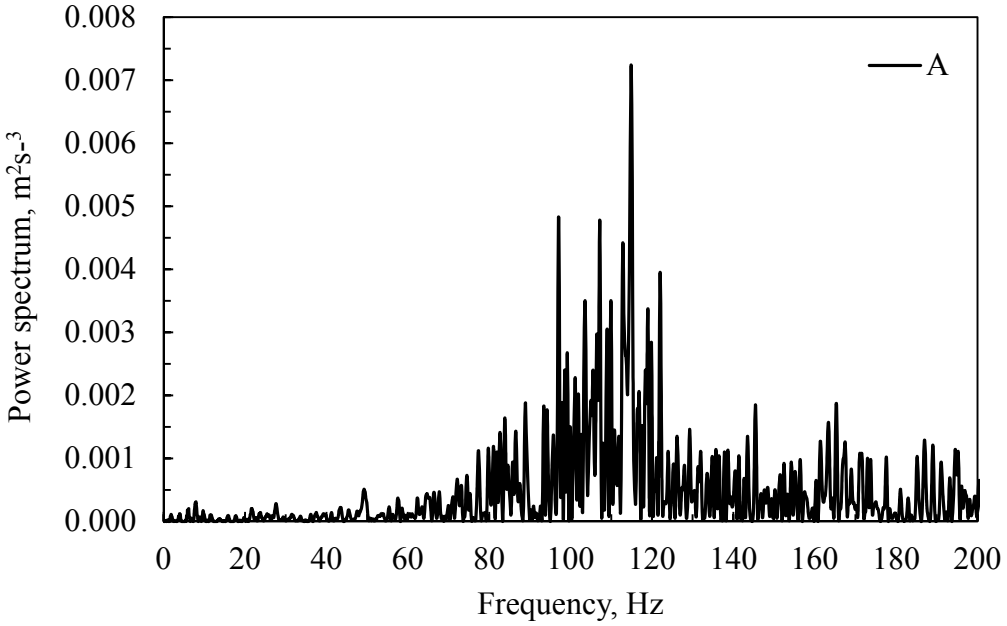

(b)

Figure 5.31. The record of accelerometer at position A along light rail line (a) Fourier amplitude and (b) Power spectrum

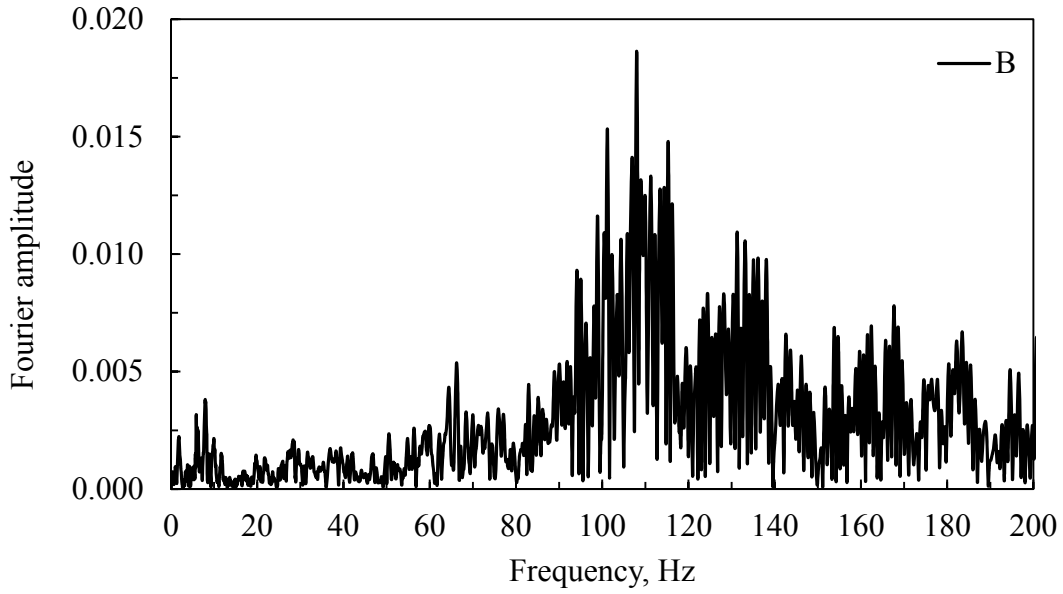

(a)

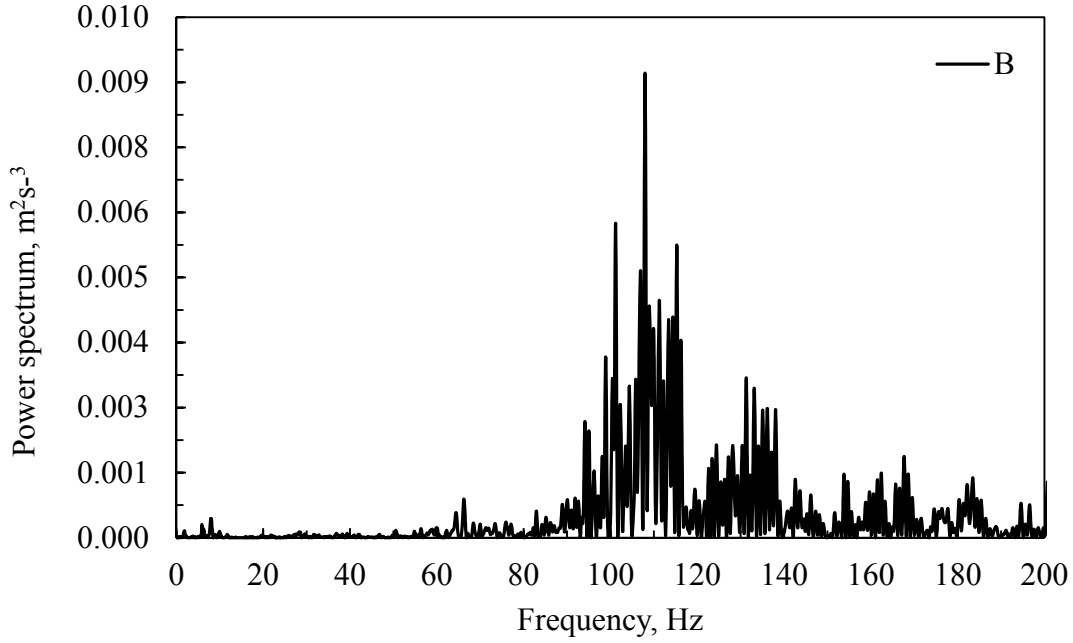

(b)

Figure 5.32. The record of accelerometer at position B along light rail line (a) Fourier amplitude and (b) Power spectrum

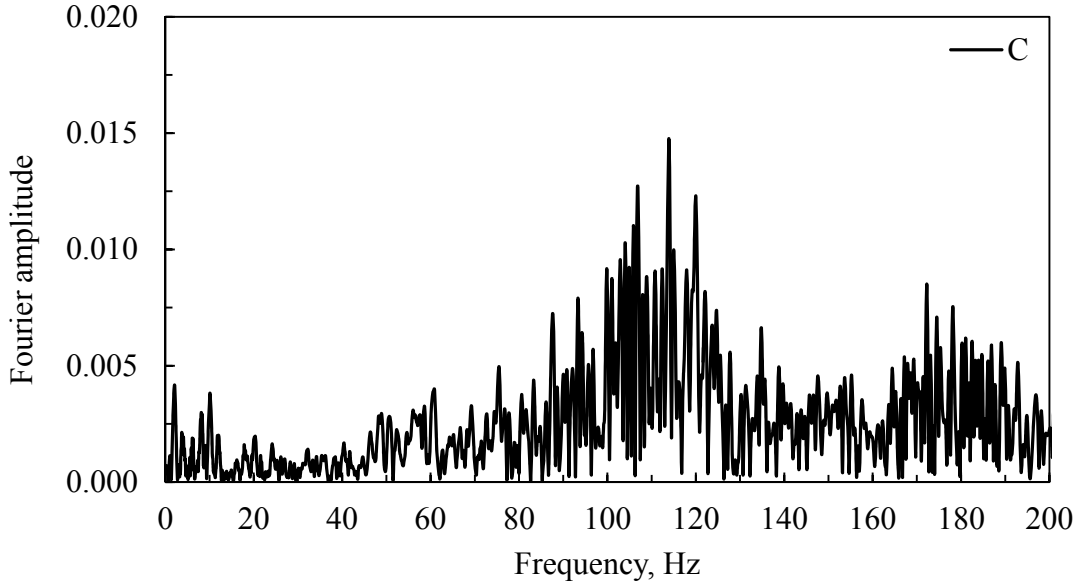

(a)

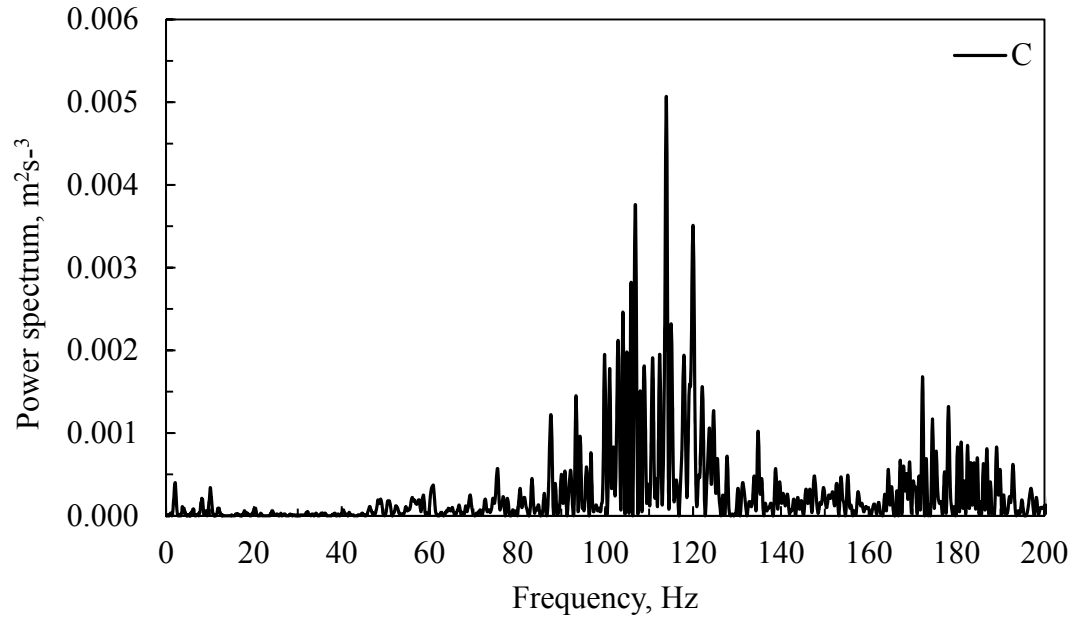

(b)

Figure 5.33. The record of accelerometer at position C along light rail line

(a) Fourier amplitude and (b) Power spectrum

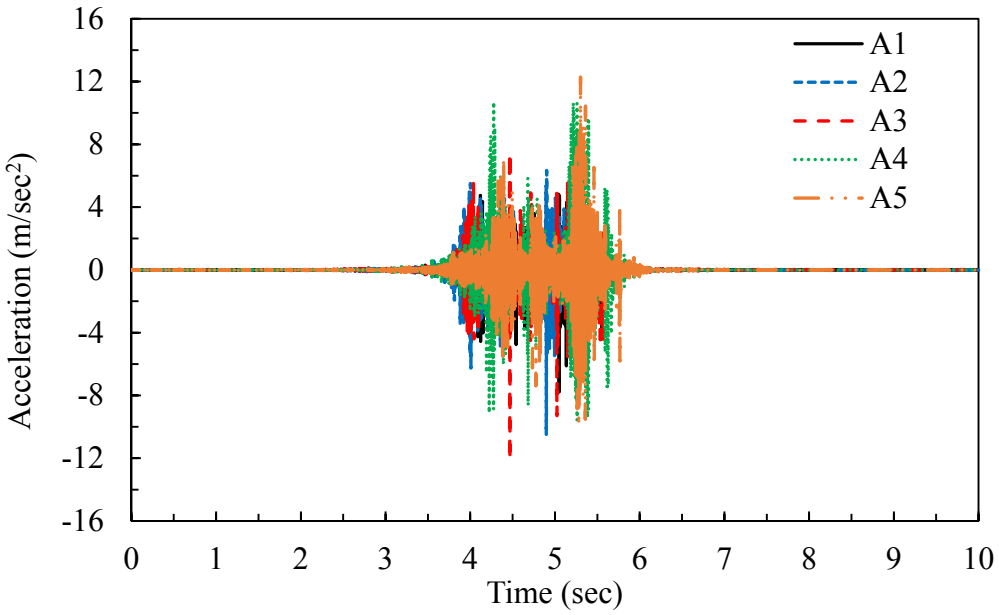

(a)

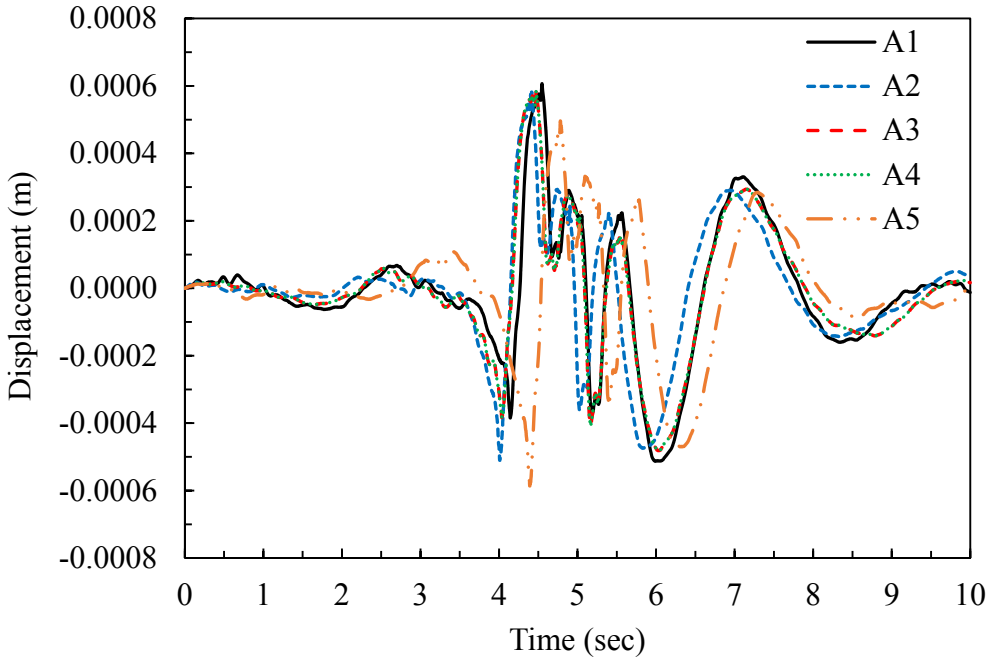

(b)

Figure 5.34. The record of accelerometer position at A of EPS embankment along light rail line (a) Input acceleration and (b) Vertical displacement

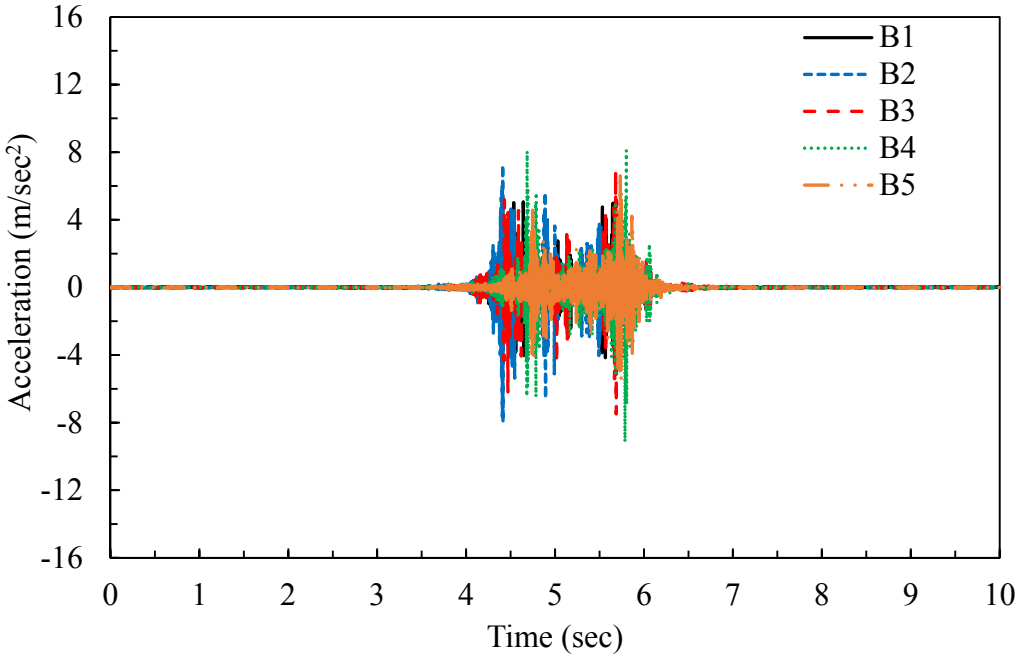

(a)

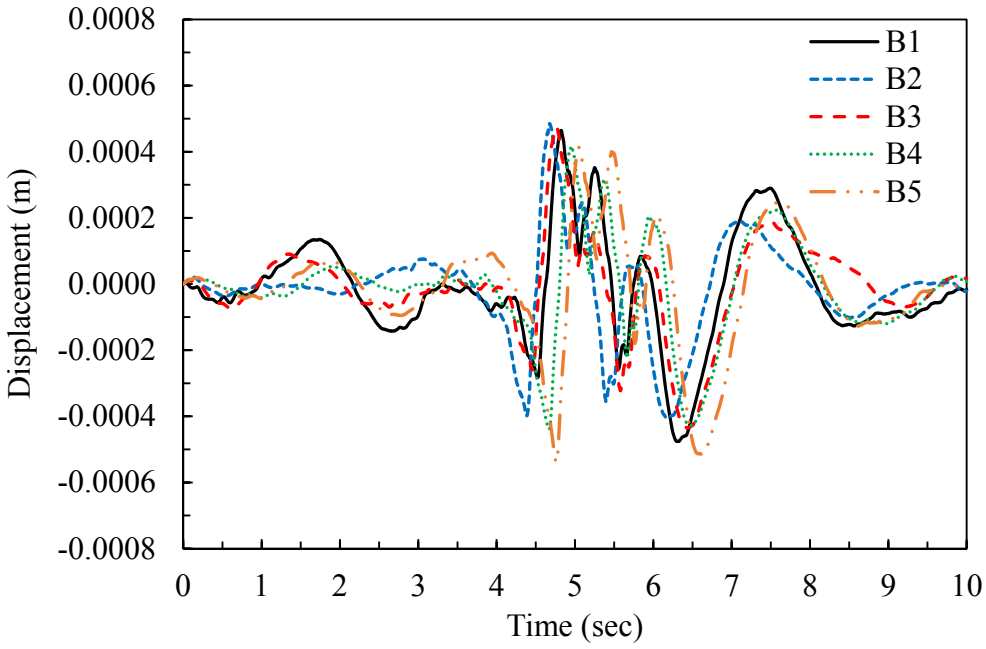

(b)

Figure 5.35. The record of accelerometer position at B of EPS embankment along light rail line (a) Input acceleration and (b) Vertical displacement

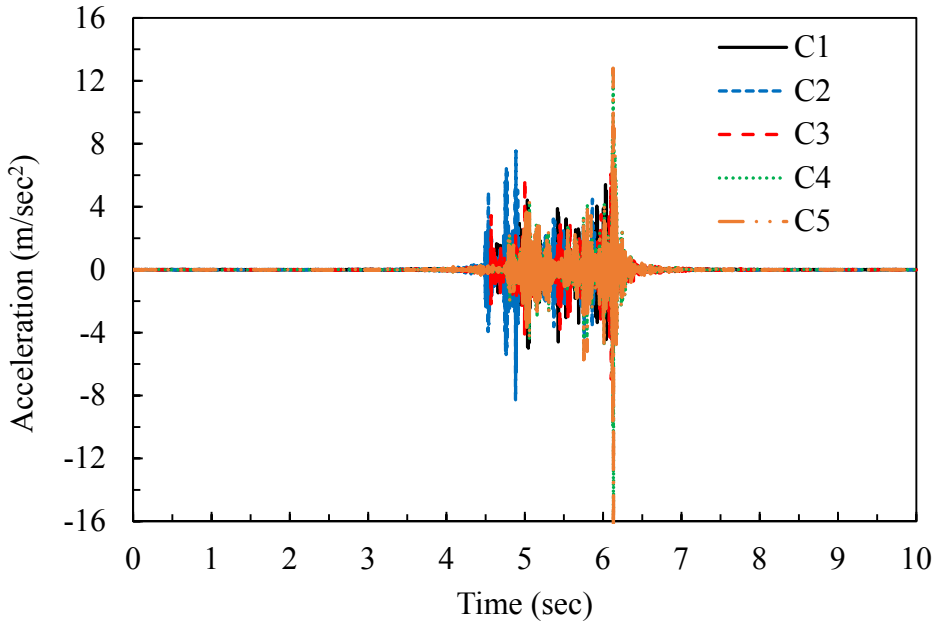

(a)

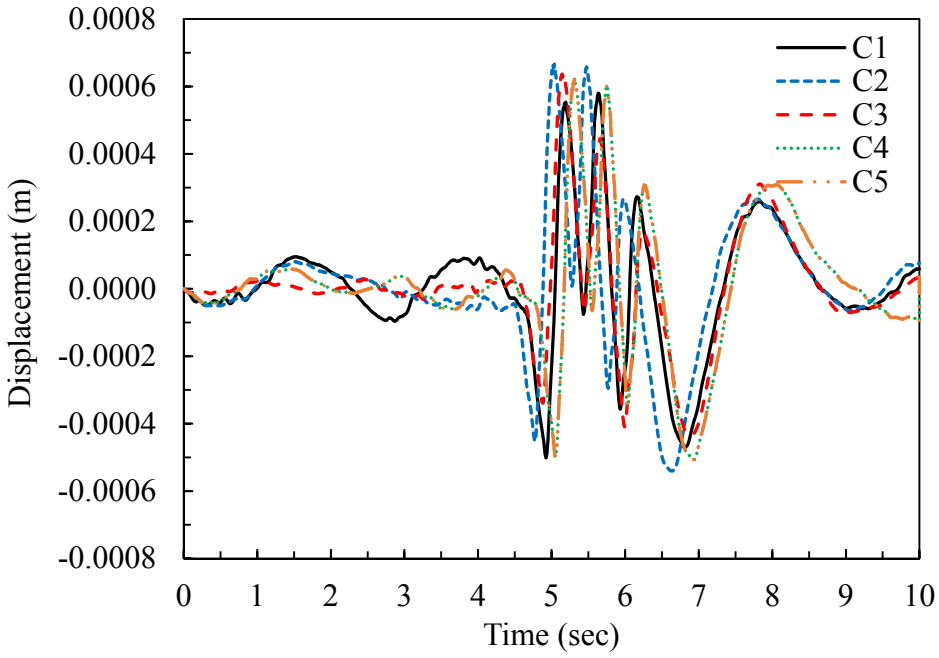

(b)

Figure 5.36. The record of accelerometer position at C of EPS embankment along light rail line (a) Input acceleration and (b) Vertical displacement

CONCLUSIONS

The FrontRunner commuter rail south line extends from Salt Lake City to Provo, Utah. UTA used EPS in the embankments along this line at Corner Canyon in Draper, Utah in order to minimize the vertical stress and subsequent consolidation settlement of the foundation soils underlying a concrete box culvert. This site was selected in this study to monitor the dynamic rail deflection because the site has both EPS geofoam and earthen embankments. Similarly, the light rail green line at River Trail was selected to monitor dynamic deflection. Accelerometer arrays were deployed to measure the acceleration time histories of several trains passing through this area. Subsequently, these time histories were baseline corrected and filtered to produce estimates of the displacement time history.

In addition, a low cost optical technique for vertical deflection measurement was developed. The method was used to measure the deflection in the laboratory and the deflection was compared with LVDT results. The percentage difference of results from these two methods was around 2 percent. However, this method had some limitations in the field. Wind, elevation of site and vibration from trains were major constraints for obtaining accurate results; hence the optical technique was not successfully used to obtain field estimates of deflection of the FrontRunner commuter rail. However, this method may still prove to be applicable for laboratory use, or for situations where the conditions for field deployment are more favorable.

Results from the accelerometer array show the maximum and average displacements for the sleepers positioned on the EPS embankment was about 6 mm and 2 mm, respectively for the FrontRunner system. The same system constructed on earthen embankment underwent a maximum and average displacement of 22 mm and 7.5 mm, respectively. Therefore, the average displacement occurring on the EPS embankment was about 25 percent of that incurred by the earthen embankment.

The FLAC3D numerical model studies that are presented in Chapter 4 of the EPS geofoam embankment along the FrontRunner commuter rail system produced a maximum rail displacement of 6.1 mm. This estimated displacement is in agreement with the maximum field measured displacement obtained from accelerometers of 6 mm and less than the overall average field measured displacement of 2 mm. Therefore, the FLAC3D model described in Chapter 4 can be used to perform further numerical studies to evaluate displacements of freight rail systems supported by EPS embankments.

The average value of the vertical displacements occurring atop the EPS embankment for the light rail (i.e., TRAX) line were about 0.6 mm. This average value is almost four times smaller than the average displacement value measured for the FrontRunner system. This suggests that deflections of rail systems on

EPS embankments is relatively small and therefore has a similar or better performance than that of earthen embankments. Larger amount of deflection in case of earthen embankment could have been because of lateral compression of soil due to combined dead and live loads whereas in case of EPS embankment, lateral compression is less likely to occur due to the inherent property of EPS material.

REFERENCES

AREMA (2007). "Manual for Railway Engineering." American Railway Engineering and Maintenance-of Way Association, Lanham, Maryland, USA.

Bowness, D., Lock, A., Powrie, W., Priest, J., and Richards, D. "Monitoring the dynamic displacements of railway track." *Proc., Institution of Mechanical Engineers, Part F: Journal of Rail and Rapid Transit*, 13-22.

Chebli, H., Clouteau, D., and Schmitt, L. (2008). "Dynamic response of high-speed ballasted railway tracks: 3D periodic model and in situ measurements." *Soil Dynamics and Earthquake Engineering*, 28(2), 118-131.

Frydenlund, T. E., Myhre, O., Refsdal, G., and Aaboe, R. (1987). "Plastic foam in road embankments."Norwegian Road Research Laboratory, Norwegian Edition 61 (in English).

Ho, S., Tsang, W., Lee, K., Lee, K., Lai, W., Tam, H., and Ho, T. "Monitoring of the vertical movements of rail sleepers with the passage of trains." *Proc., Institution of Engineering and Technology International Conference on Railway Condition Monitoring, 2006*, IEEE, 108-114.

Ling, X.-Z., Chen, S.-J., Zhu, Z.-Y., Zhang, F., Wang, L.-N., and Zou, Z.-Y. (2010). "Field monitoring on the train-induced vibration response of track structure in the Beiluhe permafrost region along Qinghai–Tibet railway in China." *Cold Regions Science and Technology*, 60(1), 75-83.

Lu, S. (2008). "Real-time vertical track deflection measurement system." Ph.D. thesis, University of Nebraska, Lincoln, Nebraska, USA.

Madshus, C., and Kaynia, A. (2000). "High-speed railway lines on soft ground: dynamic behaviour at critical train speed." *Journal of Sound and Vibration*, 231(3), 689-701.

Measurement-Specialities (2015). "Model 4630 Accelerometer." <http//www.meas-spec.com/downloads/4630.pdf>. (March 4, 2015).

O'Brien, A. (2001). "Design and construction of the UK's first polysterene embankment for railway use." *Proc., 3rd International EPS Geofoam Conference,* Salt Lake City, Utah, USA.

Pinto, N., Ribeiro, C., Mendes, J., and Calçada, R. (2009). "An optical system for monitoring the vertical displacements of the track in high speed railways." *Proc., 3rd International Integrity Reliability and Failure,* Portugal, 1-9.

Priest, J., and Powrie, W. (2009). "Determination of dynamic track modulus from measurement of track velocity during train passage." *Journal of geotechnical and geoenvironmental engineering*, 135(11), 1732-1740.

Psimoulis, P. A., and Stiros, S. C. (2013). "Measuring deflections of a short-span railway bridge using a robotic total station." *Journal of Bridge Engineering*, 18(2), 182-185.

RTDAQ (2011). "Campbell Scintific, Inc.", Logan, Utah.

SeismoSoft (2015). "SeismoSignal 5.1.0." <http//www.seismosoft.com/en/Download.aspx>. (February 17, 2015).

CHAPTER 6: CONCLUSIONS AND RECOMMENDATIONS

INTRODUCTION

The objectives of this project are (1) to develop preliminary design guidelines for the use of geofoam to support freight rail tracks and (2) to develop a design of a full-scale test embankment for freight rail. The research approach consisted of laboratory static and cyclic tests on railway ballast (Phase I), evaluation and numerical modeling of deflections and vertical displacements of rail systems supported by EPS embankments (Phase II), and field dynamic deflection monitoring of EPS embankments along the UTA Front Runner South commuter rail line and the West Valley TRAX light rail extension line (Phase III). Key conclusions from each of these three research phases are provided followed by a discussion of the two project objectives.

LABORATORY STATIC AND CYCLIC TESTS ON RAILWAY BALLAST (PHASE I)

Monotonic and cyclic triaxial tests at low amplitude and cyclic tests in a large chamber at low and high amplitudes were conducted in the laboratory to determine the Young's modulus of elasticity and resilient modulus of ballast material that has been used over an EPS geofoam embankment in a section of the FrontRunner commuter rail system in Corner Canyon in Draper City, Utah. The Young's modulus of elasticity and resilient modulus of the ballast material obtained from the laboratory tests were used in the numerical modeling study of Phase II.

The monotonic triaxial test results revealed that the Young's modulus of elasticity of the ballast material was 52,000 kPa at very low confining pressures. The average resilient modulus at low amplitude (5 mm) was found to be 14,000 kPa based on cyclic triaxial tests. The resilient modulus obtained from the cyclic triaxial test was approximately 25 percent less than the large chamber test value. The lower resilient modulus obtained from the triaxial test can be partially attributed to the lower density of the ballast material obtained in the triaxial test, the need to assume a Poisson's ratio to obtain the resilient modulus based on the large chamber test results while an estimate of Poisson's ratio was not needed to obtain the resilient modulus from triaxial test results, the difference in boundary conditions, i.e., flexible in the cyclic triaxial test and constrained in the large chamber test, between the two tests, and the variance in particle diameters in the ballast samples tested between the triaxial test, which had to be crushed into particle sizes smaller than 25.4 mm per the ASTM test procedure, and the full-size ballast used in the large chamber test.

Additional studies are needed to verify the differences between the two test procedures. Although the triaxial test is typically regarded as a more precise test, large chamber test results could be used to determine the resilient modulus of granular material for preliminary design.

The resilient modulus was almost double when the amplitude was increased by 6 times based on large chamber tests. The increase in resilient modulus with amplitude can be caused by the increase in density that occurs in the ballast sample with increase in amplitude.

EVALUATION AND NUMERICAL MODELING OF DEFLECTIONS AND VERTICAL DISPLACEMENTS OF RAIL SYSTEMS SUPPORTED BY EPS EMBANKMENTS (PHASE II)

A numerical method to evaluate the rail deflections for systems constructed atop EPS embankments was developed. A FLAC3D model was developed to analyze the vertical displacement of an EPS-supported multilayered railway embankment system constructed in Norway. The model produced vertical deflections ranging from 1.8 to 2.3 mm. The field measurements ranged from 2 to 3 mm. The range of deflection results obtained with the model was deemed to be a reasonable estimate of the lower range of the field measurements. Therefore, it was concluded that FDM, as implemented in FLAC, can satisfactory estimate the static vertical displacement of rails systems constructed atop EPS-supported embankments when subjected to a static (i.e., stopped) train loading.

An additional FLAC3D model was developed to analyze the vertical displacement of the EPS-supported UTA FrontRunner embankment system in Corner Canyon, Draper, Utah. The FLAC3D model produced a maximum rail displacement of 6.1 mm. This estimated displacement is in agreement with the maximum field measured displacement obtained from accelerometers in Phase III of the project of 6 mm and less than the overall average field measured displacement of 2 mm. Therefore, the FLAC3D model can satisfactory estimate the dynamic vertical displacement of rails systems constructed atop EPS-supported embankments when subjected to a dynamic (i.e., moving) train loading. Additionally, the FLAC3D model can be used to perform further numerical studies to evaluate displacements of commuter rail systems supported by EPS embankments.

Although loads from commuter rail systems such as the UTA FrontRunner modeled in the FLAC3D model are typically less than freight rail loads, the field instrumentation data collected as part of this study suggests that the FLAC3D model can be used to perform further numerical studies to evaluate displacements of freight rail systems supported by EPS embankments and can be used to develop preliminary designs of EPS embankments that support freight rail loads.

FIELD DYNAMIC DEFLECTION MONITORING OF EPS EMBANKMENTS ALONG THE UTA FRONT RUNNER SOUTH COMMUTER RAIL LINE AND THE WEST VALLEY TRAX LIGHT RAIL EXTENSION LINE (PHASE III)

The FrontRunner commuter rail south line extends from Salt Lake City to Provo, Utah. UTA used EPS in the embankments along this line at Corner Canyon in Draper, Utah in order to minimize vertical stress and subsequent consolidation settlement of the foundation soils underlying a concrete box culvert. This site was selected in this study to monitor the dynamic rail deflection because the site has both EPS geofoam and earthen embankments. Similarly, the light rail green line at River Trail was selected to monitor dynamic deflection. Accelerometer arrays were deployed to measure the acceleration time histories of several trains passing through these areas. Subsequently, these time histories were baseline corrected and filtered to produce estimates of the displacement time history.

Results from the accelerometer arrays showed the maximum and average displacements for the rail ties positioned on the EPS embankment were about 6 mm and 2 mm, respectively, for the FrontRunner system. The same system constructed on earthen embankment underwent maximum and average displacements of 22 mm and 7.5 mm, respectively. Therefore, the average displacements occurring on the EPS embankment were about 25 percent of that incurred by the earthen embankment. This suggests that adequately designed EPS embankments can yield deflections of rail systems on EPS embankments that are relatively small and, therefore, can have a similar or better performance than that of earthen embankments.

The average value of vertical displacements occurring atop the EPS embankment for the light rail (i.e., TRAX) line were about 0.6 mm. This average value is almost four times smaller than the average displacement value measured for the Front Runner system because loadings from light rail systems are less than commuter rail systems.

A low cost optical technique for direct vertical deflection measurement of rails was developed. The method was used to measure the deflection in the laboratory and the deflection was compared with LVDT results. The percentage difference of results from these two methods was around 2 percent. However, this method had some limitations in the field. Wind, elevation of site and vibration from trains were major constraints for obtaining accurate results; hence the optical technique was not successfully used to obtain field estimates of deflection of the FrontRunner commuter rail. However, this method may still prove to be applicable for laboratory use, or for situations where the conditions for field deployment are more favorable.

PROJECT OBJECTIVES

The objectives of the project were (1) to develop preliminary design guidelines for the use of geofoam to support freight rail tracks and (2) to develop a design of a full-scale test embankment for freight rail. A summary of each of these project objectives is subsequently provided.

The current successful performance of over 129,000 m^3 (168,000 yd^3) of EPS-block geofoam along the TRAX light rail and 10,900 m^3 (14,300 yd^3) of geofoam along the Front Runner South commuter line suggests that these geofoam configurations can serve as the basis for preliminary design of other proposed rail systems supported on geofoam. The experience with design of EPS roadway embankments also suggests that the selection of a suitable type of EPS to support rail loads be based on selection of an EPS type that has an elastic limit stress that exceeds the anticipated stresses within the geofoam from any applied loads. General guidance for the use of EPS-block geofoam in stand-alone roadway embankments and roadway bridge approaches is included in the following two National Cooperative Highway Research Program (NCHRP) documents: NCHRP Report 529 (Stark et al., 2004a) and NCHRP Web Document 65 (Stark et al., 2005b). General guidance for geofoam embankments incorporated in slopes is included in NCHRP Project 24-11(02) report (Arellano et al., 2011).

Although the field monitoring program was limited to commuter and light rail loads, the field instrumentation data collected as part of this study suggests that the FLAC3D model developed as part of this project can be used to perform further numerical studies to evaluate displacements of freight rail systems supported by EPS embankments. The results of the numerical studies can be used to develop preliminary designs of EPS embankments that support freight rail loads for the purpose of developing a design of a full-scale test embankment. The full-scale test embankment can be monitored with accelerometers to measure deflections under freight car loadings and the field deflection results can be used to develop a design procedure for EPS-block geofoam embankments to support freight rail loads. The selection of a specific site for the full-scale embankment study is required before the design of a full-scale test embankment for support of freight rail can be accomplished because site-specific information such as the properties of the EPS embankment foundation materials are needed. The results of the field instrumentation data collected as part of a full-scale freight railroad embankment study can then be used to develop design procedures for the use of EPS-block geofoam in freight railroad embankments.

SUMMARY

Although loads from light and commuter rail systems are typically less than freight rail loads, the field instrumentation data collected of the light and commuter rail EPS embankment sections as part of this study can be used to develop preliminary designs of freight rail. Additionally, the field data can also be used to improve current light and commuter rail designs. The availability of actual performance data will also make the use of geofoam more attractive to light and commuter rail agencies throughout the U.S. because it will remove current uncertainties and misconceptions that exist regarding the use of geofoam to support rail loads. In summary, data from the field instrumentation collected as part of this study and the numerical evaluations performed as part of this study will contribute to wider understanding and application of geofoam in light and commuter rail projects, as well as provide a pathway for wider acceptance of the technology for freight rail applications.

REFERENCES

Stark, T.D., Arellano, D., Horvath, J.S., and Leshchinsky, D. (2004). "NCHRP Report 529: Guideline and Recommended Standard for Geofoam Applications in Highway Embankments," Transportation Research Board, Washington, D.C., 71 pp. Available at http://trb.org/publications/nchrp/nchrp_rpt_529.pdf .

Stark, T.D., Arellano, D., Horvath, J.S., and Leshchinsky, D. (2004). "NCHRP Web Document 65 (Project 24-11): Geofoam Applications in the Design and Construction of Highway Embankments," Transportation Research Board, Washington, D.C., 792 pp. Available at http://trb.org/publications/nchrp/nchrp_w65.pdf .

Arellano, D., Stark, T.D., Horvath, J.S., Leshchinsky, D. (2011). "Guidelines for Geofoam Applications in Slope Stability Projects." NCHRP Project 24-11(02) Final Report, Transportation Research Board, Washington, D.C., 602 pp. Available at http://onlinepubs.trb.org/onlinepubs/nchrp/docs/NCHRP24-11(02)_FR.pdf .

APPENDIX A

COMPARISON OF POINT LOAD ON HOMOGENEOUS ELASTIC HALF-SPACE USING ELASTIC THEORY AND FINITE DIFFERENCE METHOD (FDM)

A.1 Problem Statement

A vertical point load of 10 kN is applied at the surface of a semi-infinite soil mass as indicated in Figure A.1. Assume that the soil is linear elastic with E = 1E7 kPa and v = 0.3.

The point load is applied on semi-infinite homogeneous, linearly elastic, and isotropic half-space.

A.2 Solution

A.2.1 Elastic Theory Solution (Boussinesq, 1883)

For the case of a vertical point load P applied at the origin of the coordinate system (Figure A.1), the vertical stress increase at any point (*x, y, z*) within the semi-infinite soil mass is given by

$$\Delta\sigma = \frac{3P}{2\pi}\frac{z^3}{(x^2+y^2+z^2)^{\frac{5}{2}}} \qquad \textbf{(A.1)}$$

where P is the intensity of the point load given in force units and *x, y*, and *z* are the coordinates of the point at which the increase of vertical stress is calculated.

To calculate the increase in vertical stress directly under the applied load for z = 0 to 1 m, we substitute x = 0 and y = 0 into Equation (A.1). To calculate the increase in vertical stress directly at x = 0.1 m for z = 0 to 1 m, we substitute x = 0.1 and y = 0 into Equation (A.1). Using this equation, we can calculate the increase in vertical stress as a function of *z*. The results are plotted in Figure A.2.

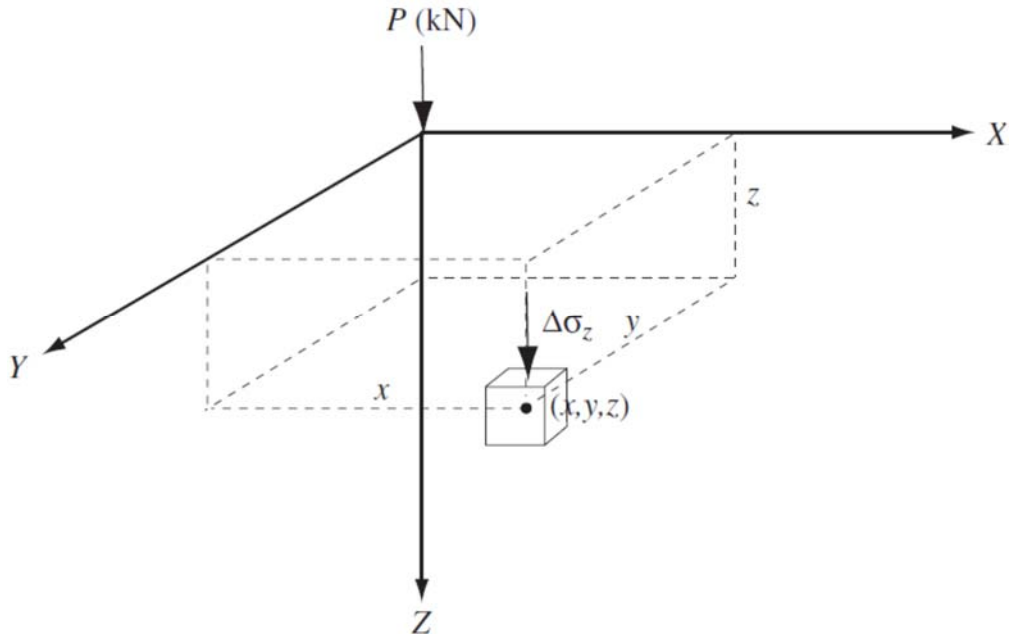

Figure A.1 Vertical Stresses Caused by a Point Load

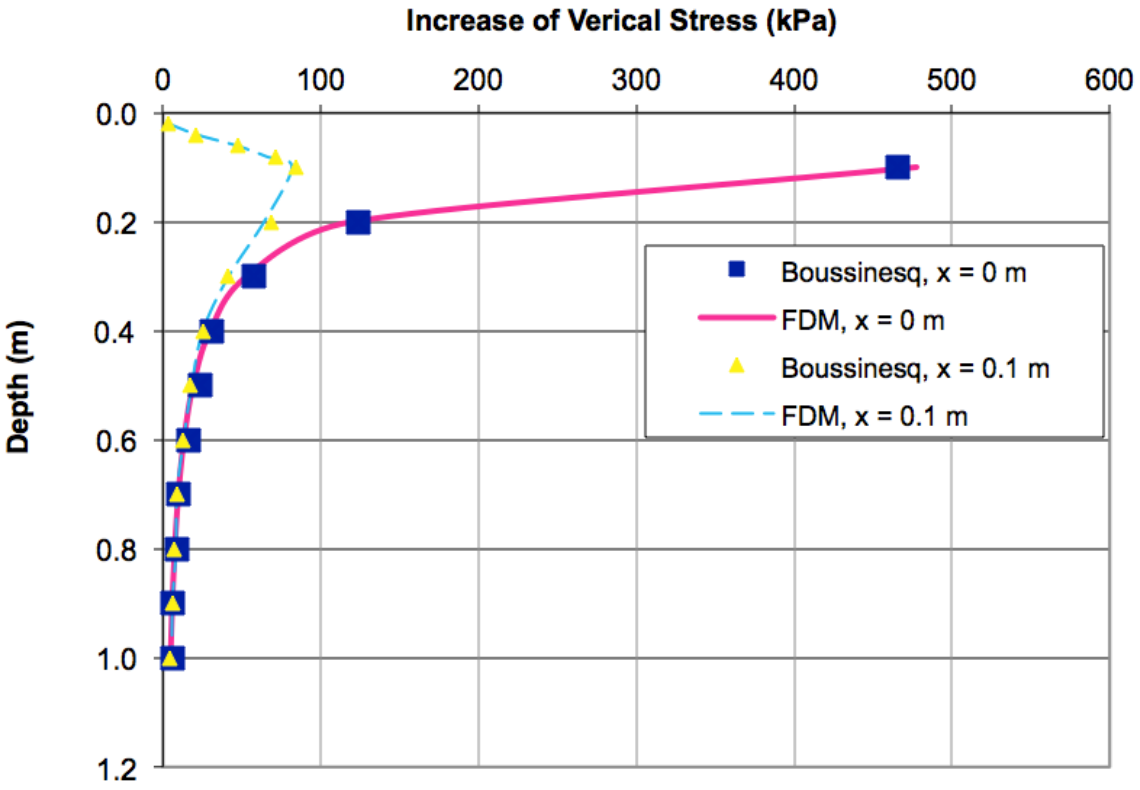

Figure A.2 Comparison of Increase of Vertical Stress Caused by Point Load

A.2.2 FDM Solution (FLAC)

For simplicity, the semi-infinite soil mass is assumed to be a cylinder 1 m in radius and 2 m in height, as shown in Figure A.3. The reason of using a cylindrical shape in this simulation is to take advantage of axisymmetry, in which we can utilize axisymmetric two-dimensional analysis instead of three-dimensional analysis. The mesh is made finer in the zone around the point load where stress concentration is expected.

Assume the soil at the bottom of the model cannot move in both direction, Thus fix in both x and y direction in the model (z direction in reality) at bottom. Assume the soil on the side of the model can only move in vertical direction but cannot move in horizontal direction, thus fix only in the x direction on side.

Treat point load 10 kN as equivalent stress over a small circular area with radius

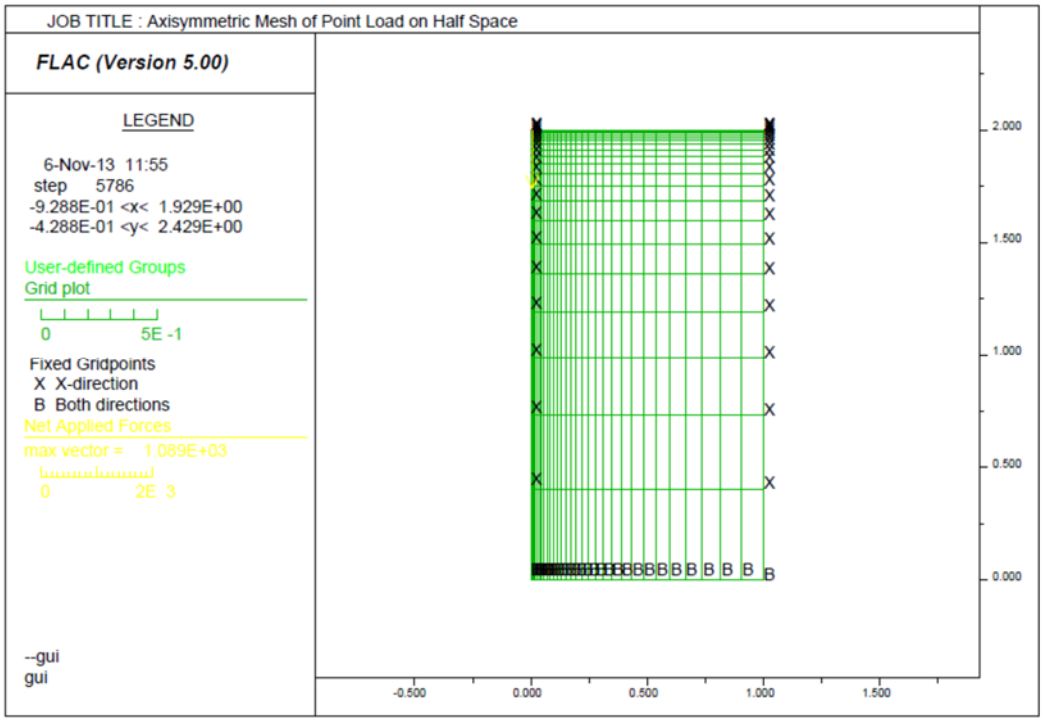

Figure A.3 Axisymmetric Mesh of Point Load on Half Space

6E-3 m, which is the first mesh from center. The soil is assumed to be linear elastic with E = 1E7 kPa and v = 0.3, based on which shear modulus (G) and bulk modulus can be calculated: G = 3.85E9 and K = 8.33E9. Also assume soil has a dry density of 2000 kg/m^3.

The results are also shown in Figure A.2.

A.3 Comparison, Conclusion and Discussion

Figure A.2 shows excellent agreement between the stresses calculated using the Boussinesq and FDM solutions.

A.4 FLAC Codes

```
config axisymmetry
grid 30,20
model elastic
;
;model geometry, a cylinder 2 m in height, 1 meter in radius; “ratio” defines distribution of mesh
gen 0,0 0,2 1,2 1,0 ratio (1.1,0.8)
;
;model properties, assume the soil is linear elastic with E=1E7 kPa and v=0.3, the following
properties are calculated:
prop density=2000.0 bulk=8.33333E9 shear=3.84615E9
;
;boundary conditions
fix  x y j 1; fix in both x and y direction at bottom
fix  x i 31; fix only in the x direction on side
;
;loading condition, treat point load 10 kN as stress over a small circular area with radius 6E-3 m,
which is the first mesh from center
apply syy -8.8419416E7 from 1,21 to 2,21
;
solve
```

APPENDIX B

COMPARISON OF LINE LOAD ON HOMOGENEOUS ELASTIC HALF-SPACE USING FINITE ELEMENT METHOD (FEM) AND ELASTIC THEORY

B.1 Problem Statement

A vertical line load of 10 kN/m is applied at the surface of a semi-infinite soil mass as indicated in Figure B.1. Assume that the soil is linear elastic with E = 1E7 kPa and $\nu = 0.3$.

The line load is applied on semi-infinite homogeneous, linearly elastic, and isotropic half-space.

B.2 Solution

B.2.1 Elastic Theory Solution

Due to the nature of line load (Helwany, 2007), the resulting stresses in the x–z plane are independent of y (i.e., we will get the same stresses in any x–z plane as we travel along the y-axis). This type of loading–geometry is termed plane strain. The vertical stress increase at any point (x, z) is given as

$$\Delta\sigma = \frac{2qz^3}{\pi(x^2 + z^2)^2} \tag{B.1}$$

where q is the line load (force/unit length) and x and z are the coordinates at which the stress increase is calculated.

To calculate the increase in vertical stress directly under the applied load for z = 0 to 0.3 m, we substitute $x = 0$ into (B.1). Using this equation, we can calculate the increase in vertical stress as a function of z. The results are plotted in Figure B.2.

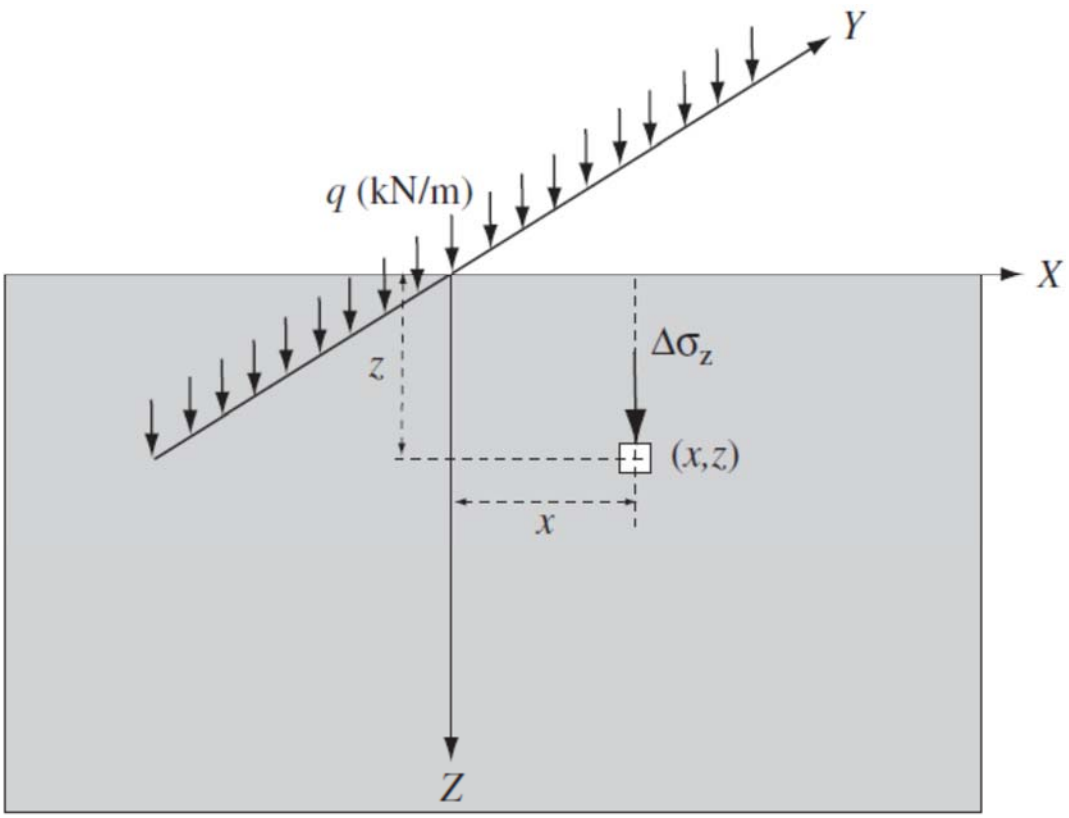

Figure B.1 Stresses Caused by a Line Load

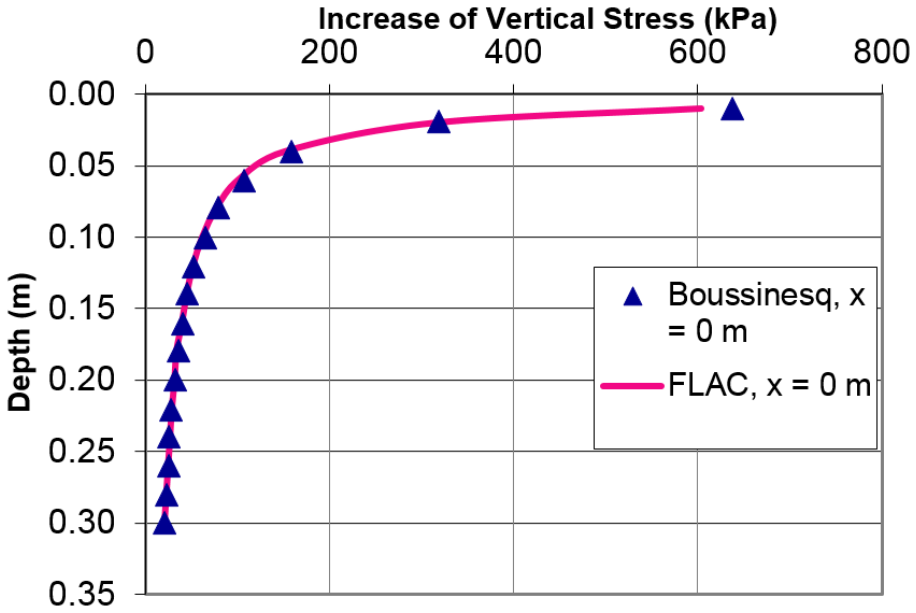

Figure B.2 Comparison of Increase of Vertical Stress Caused by Line Load

B.2.2 FDM Solution (FLAC).

A plane strain condition is assumed in which the semi-infinite soil mass is represented by a 1 m × 2 m (x–z) plane as shown in Figure B.3. The two-dimensional plane strain mesh used has 30 elements in the x-direction and 20 elements in the z-direction. The mesh is made finer in the zone around the point load where stress concentration is expected. Assume the soil at the bottom of the model cannot move in both direction, Thus fix in both x and y direction in the model (z direction in reality) at bottom. Assume the soil on the side of the model can only move in vertical direction but cannot move in horizontal direction, thus fix only in the x direction on side.

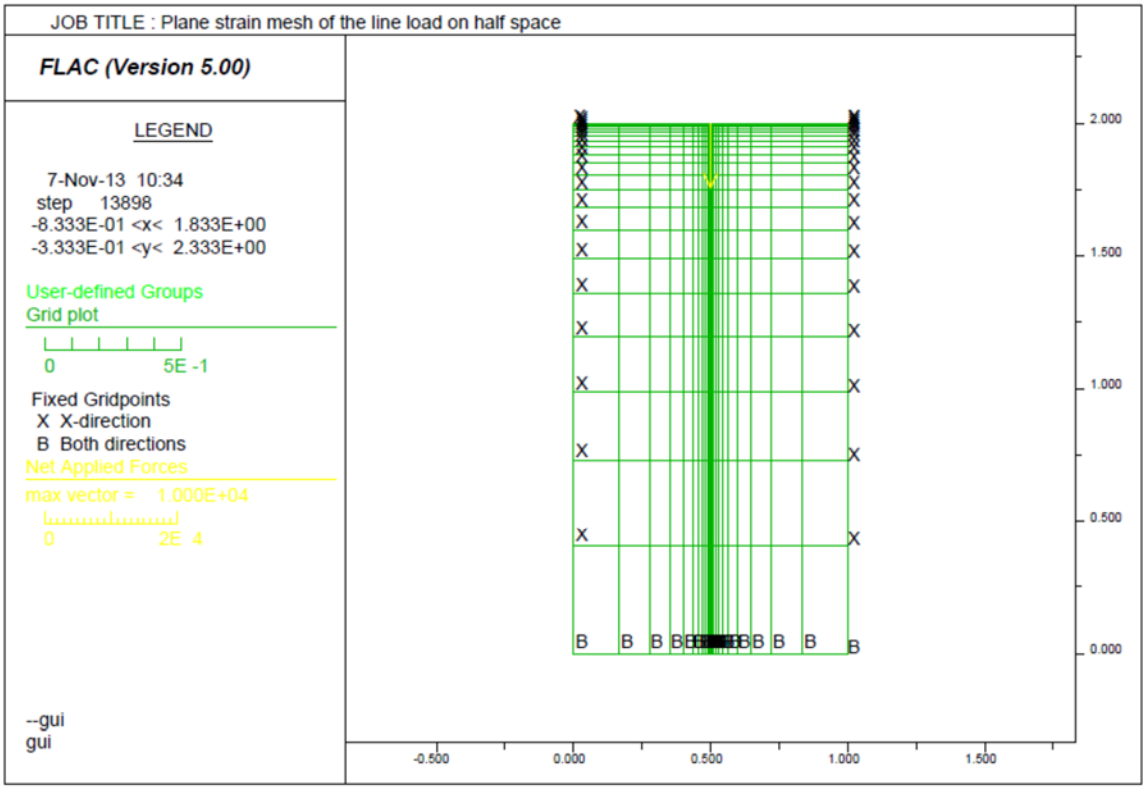

Figure B.3 Plane Strain Mesh of the Line Load on Half Space

Apply a line load of 10 kN/m. In the model, use a force of 10 kN because of the plain

strain assumption.

The soil is assumed to be linear elastic with E = 1E7 kPa and v = 0.3, based on which shear modulus (G) and bulk modulus (K) can be calculated: G = 3.85E9 and K = 8.33E9. Also assume soil has a dry density of 2000 kg/m^3.

The results are also shown in Figure B.2.

B.3 Comparison, Conclusion and Discussion

Figure B.2 shows excellent agreement between the stresses calculated using the analytical solution using Equation (B.1) and FDM solutions.

B.4 FLAC Codes

```
config
grid 30,20
model elastic
;
;model geometry, 1 m × 2 m (x–z) plane; "ratio" defines distribution of mesh
gen 0,0 0,2 0.5,2 0.5,0 ratio (0.667,0.8) i=1,16 j=1,21 ;left half
gen 0.5,0 0.5,2 1,2 1,0 ratio (1.5,0.8) i=16,31 j=1,21 ;right half
;
;model properties, assume the soil is linear elastic with E=1E7 kPa and v=0.3, the following
properties are calculated:
prop density=2000.0 bulk=8.33333E9 shear=3.84615E9
;
;boundary conditions
fix  x y j 1 ;fix in both x and y direction at bottom
fix  x i 31 ;fix only in x direction on side
fix  x i 1 ;fix only in x direction on side
;
;loading condition:Apply a line load of 10 kN/m. In the model, use a force of 10 kN because of
the plain strain assumption.
apply yforce -10000.0 from 16,21 to 16,21
;
solve
```

APPENDIX C

COMPARISON OF CIRCULAR LOAD ON LAYERED SOIL SYSTEM USING FINITE ELEMENT METHOD (FEM) AND FINITE DIFFERENCE METHOD (FDM)

C.1 Problem Statement

Consider a system with four layers of varying stiffness and thickness as shown in Figure C.1. A pressure of 10 kPa is uniformly distributed on a circular area with $R = 0.5$ m.

The soil is homogenous within each layer.

C.2 Solution

C.2.1 FEM Solution

A FEM analysis was conducted by Helwany (2007) on the same problem. Results are plotted in Figure C.2 along with the Boussinesq solution for one layer soil system assuming that the soil is linear elastic with E = 1E7 kPa and $v = 0.3$.

C.2.2 FDM Solution (FLAC)

Assume that the semi-infinite soil mass is a cylinder 50 m in radius and 50 m in height. The 10 kPa pressure is applied at the top surface on a circular area with 0.5 m radius. The purpose of the analysis is to calculate the increase in vertical stress within the stratified soil mass due to the application of a uniformly distributed load on a circular area. The two-dimensional axisymmetric mesh used has 30 elements in the x-direction and 30 elements in the y-direction (z direction in reality), as shown in Figure C.3. The mesh includes four layers with the elastic moduli shown in Figure C.1. The mesh is made finer in the zone around the pressurized circle, where stress concentration is expected. The increase in vertical stress under the center of the pressurized circle is plotted as a function of depth as shown in Figure C.2.

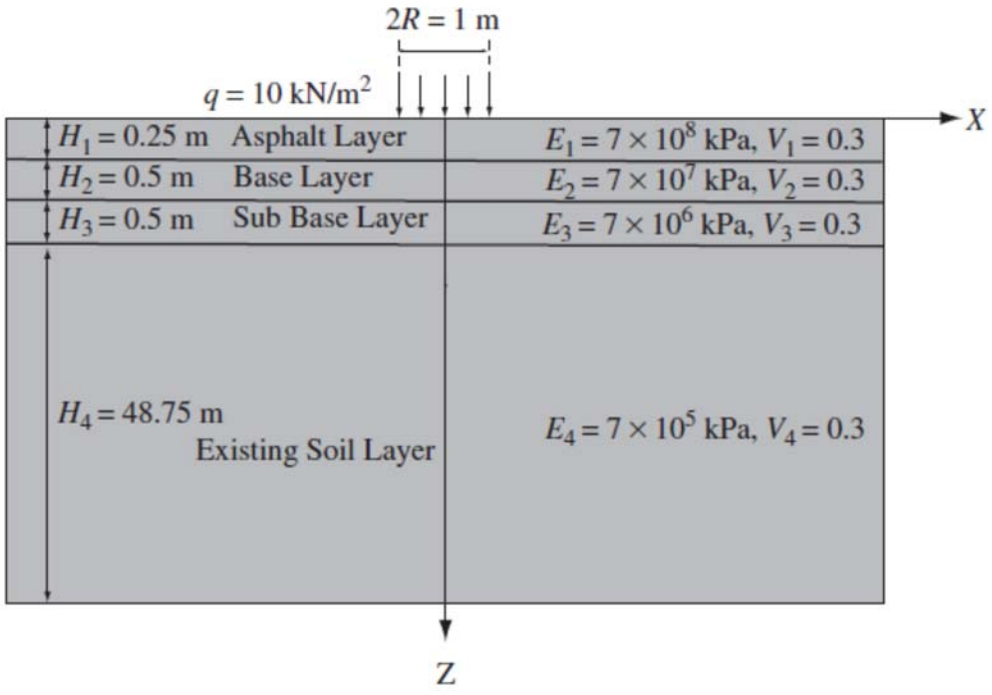

Figure C.1 Stress increase in a layered soil system with a uniformly loaded circular area

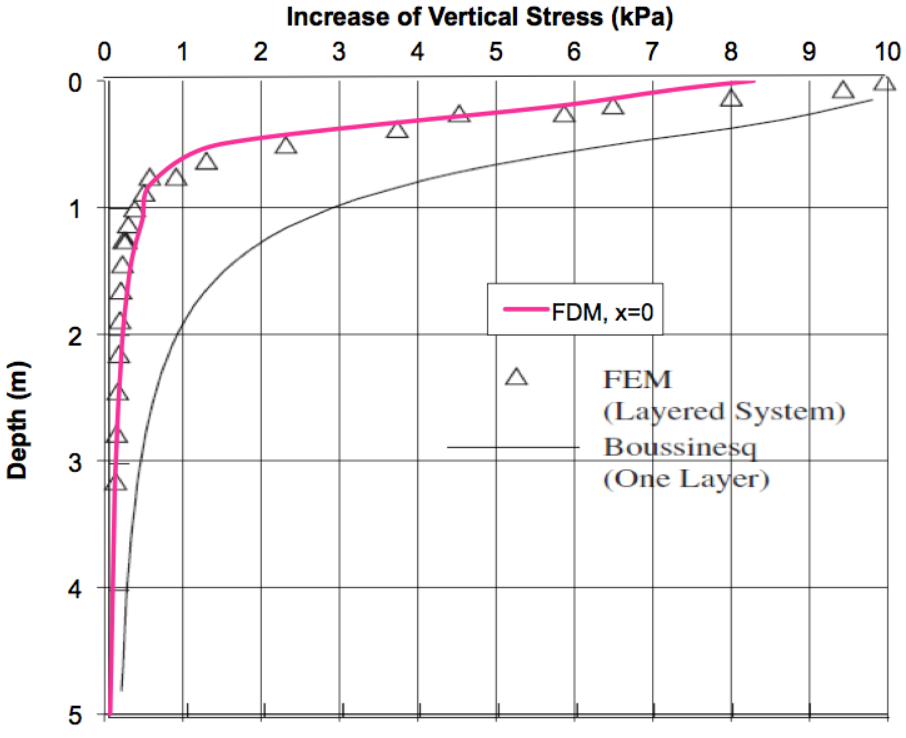

Figure C.2 Comparison of Increase of Vertical Stress Caused by Circular Load

Assume the soil at the bottom of the model cannot move in both direction, Thus fix in both x and y direction in the model (z direction in reality) at bottom. Assume the soil on the side of the model can only move in vertical direction but cannot move in horizontal direction, thus fix only in the x direction on side.

The 10 kPa pressure is applied at the top surface on a circular area with 0.5 m radius. The properties of each layer are shown in Figure C.1. Shear modulus (G) and bulk modulus (K) can be calculated based on E and v. Also assume soil has a dry density of 2000 kg/m^3

The results are also shown in Figure C.2.

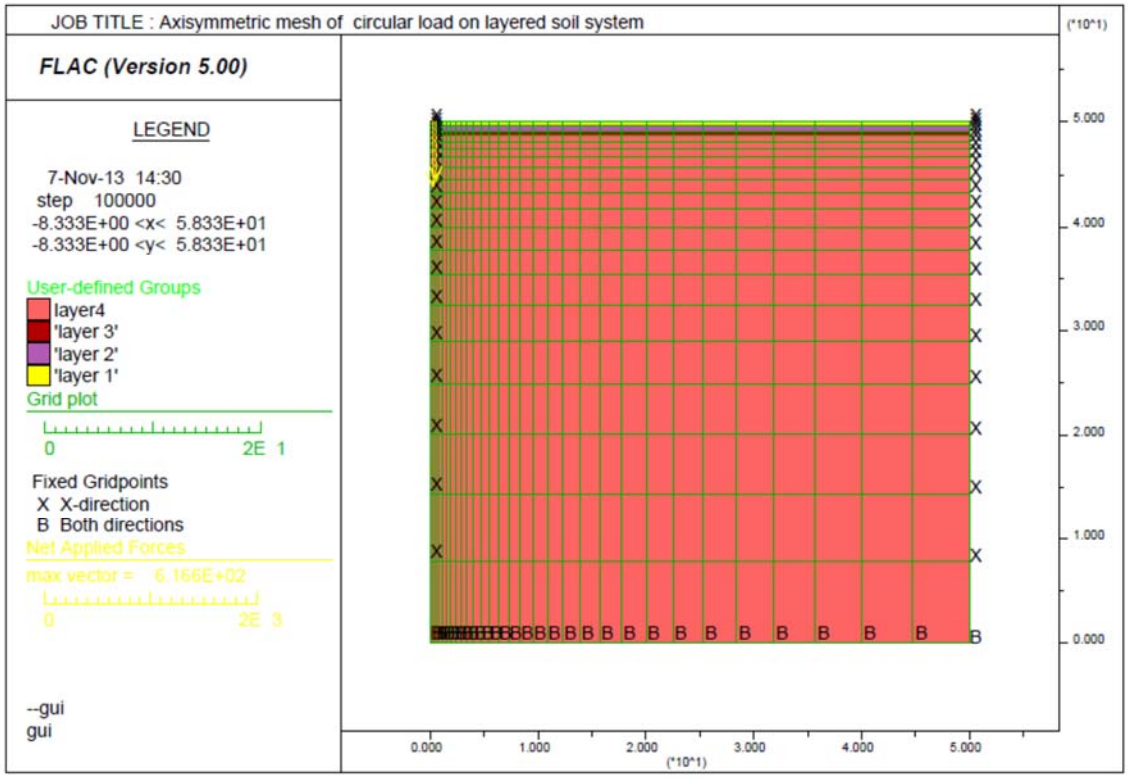

Figure C.3 Axisymmetric Mesh of Circular Load on Layered Soil System

C.3 Comparison, Conclusion and Discussion

Figure C.2 shows excellent agreement between the FEM and FDM solutions.

C.4 FLAC Codes

```
config axisymmetry
grid 30,20
model elastic
;
;model geometry, a cylinder 50 m in height, 50 m in radius
;"ratio" defines distribution of mesh
;the horizontal mesh is adjusted so that the first two meshes have a width of 0.5 m
gen 0,0 0,50 50,50 50,0 ratio (1.113,0.85)
;
; boundary condition,
fix  x y j 1; fix in both x and y direction at bottom
fix  x i 31; fix only in the x direction on side
;
;loading condition, The 10 kPa pressure is applied at the top surface on a circular area with 0.5 m
radius.
apply syy -10000.0 from 1,21 to 3,21
;
;model properties
group 'layer 1' j 20
model elastic group 'layer 1'
prop density=2000.0 bulk=5.83333E11 shear=2.69231E11 group 'layer 1'
group 'layer 2' j 19
model mohr group 'layer 2'
prop density=2000.0 bulk=5.83333E10 shear=2.69231E10 group 'layer 2'
group 'layer 3' j 18
model elastic group 'layer 3'
prop density=2000.0 bulk=5.83333E9 shear=2.69231E9 group 'layer 3'
group 'layer4' j 1 17
model elastic group 'layer4'
prop density=2000.0 bulk=5.83333E8 shear=2.69231E8 group 'layer4'
;
solve
```

APPENDIX D

FLAC CODE OF FDM MODEL FOR RAIL SYSTEMS

SUPPORTED BY REGULAR EARTH

EMBANKMENT DUE TO

TRAIN LOAD

```
config
grid 45,48
gen (0.0,0.0) (0.0,60.0) (0.661,60.0) (0.661,0.0) ratio 0.9,0.87 i 1 6 j 1 36
gen (0.0,60.0) (0.0,60.5) (0.661,60.5) (0.661,60.0) ratio 0.9,0.90000004 i 1 6 j 36 40
gen (0.0,60.5) (0.0,60.7) (0.661,60.7) (0.661,60.5) ratio 0.9,0.8999999 i 1 6 j 40 42
gen (0.0,60.7) (0.0,61.0) (0.661,61.0) (0.661,60.7) ratio 0.9,0.9 i 1 6 j 42 45
gen (0.0,61.0) (0.0,61.2) (0.661,61.2) (0.661,61.0) ratio 0.9,0.8999999 i 1 6 j 45 47
gen (0.0,61.2) (0.0,61.353) (0.661,61.353) (0.661,61.2) ratio 0.9,1.0 i 1 6 j 47 49
gen (0.661,0.0) (0.661,60.0) (0.739,60.0) (0.739,0.0) ratio 1.0,0.87 i 6 7 j 1 36
gen (0.661,60.0) (0.661,60.5) (0.739,60.5) (0.739,60.0) ratio 1.0,0.90000004 i 6 7 j 36 40
gen (0.661,60.5) (0.661,60.7) (0.739,60.7) (0.739,60.5) ratio 1.0,0.8999999 i 6 7 j 40 42
gen (0.661,60.7) (0.661,61.0) (0.739,61.0) (0.739,60.7) ratio 1.0,0.9 i 6 7 j 42 45
gen (0.661,61.0) (0.661,61.2) (0.739,61.2) (0.739,61.0) ratio 1.0,0.8999999 i 6 7 j 45 47
gen (0.661,61.2) (0.661,61.353) (0.739,61.353) (0.739,61.2) i 6 7 j 47 49
gen (0.739,0.0) (0.739,60.0) (1.21,60.0) (1.21,0.0) ratio 1.1,0.87 i 7 11 j 1 36
gen (0.739,60.0) (0.739,60.5) (1.21,60.5) (1.21,60.0) ratio 1.1,0.90000004 i 7 11 j 36 40
gen (0.739,60.5) (0.739,60.7) (1.21,60.7) (1.21,60.5) ratio 1.1,0.8999999 i 7 11 j 40 42
gen (0.739,60.7) (0.739,61.0) (1.21,61.0) (1.21,60.7) ratio 1.1,0.9 i 7 11 j 42 45
gen (0.739,61.0) (0.739,61.2) (1.21,61.2) (1.21,61.0) ratio 1.1,0.8999999 i 7 11 j 45 47
gen (0.739,61.2) (0.739,61.353) (1.21,61.353) (1.21,61.2) ratio 1.1,1.0 i 7 11 j 47 49
gen (1.21,0.0) (1.21,60.0) (2.21,60.0) (2.21,0.0) ratio 1.1,0.87 i 11 18 j 1 36
gen (1.21,60.0) (1.21,60.5) (2.21,60.5) (2.21,60.0) ratio 1.1,0.90000004 i 11 18 j 36 40
gen (1.21,60.5) (1.21,60.7) (2.21,60.7) (2.21,60.5) ratio 1.1,0.8999999 i 11 18 j 40 42
gen (1.21,60.7) (1.21,61.0) (2.21,61.0) (2.21,60.7) ratio 1.1,0.9 i 11 18 j 42 45
gen (1.21,61.0) (1.21,61.2) (2.21,61.2) (2.21,61.0) ratio 1.1,0.8999999 i 11 18 j 45 47
gen (1.21,61.2) (1.21,61.353) (2.21,61.353) (2.21,61.2) ratio 1.1,1.0 i 11 18 j 47 49
gen (2.21,0.0) (2.21,60.0) (3.717,60.0) (3.717,0.0) ratio 1.1,0.87 i 18 26 j 1 36
gen (2.21,60.0) (2.21,60.5) (3.717,60.5) (3.717,60.0) ratio 1.1,0.90000004 i 18 26 j 36 40
gen (2.21,60.5) (2.21,60.7) (3.717,60.7) (3.717,60.5) ratio 1.1,0.8999999 i 18 26 j 40 42
gen (2.21,60.7) (2.21,61.0) (3.717,61.0) (3.717,60.7) ratio 1.1,0.9 i 18 26 j 42 45
gen (2.21,61.0) (2.21,61.2) (3.717,61.2) (3.717,61.0) ratio 1.1,0.8999999 i 18 26 j 45 47
gen (2.21,61.2) (2.21,61.353) (3.717,61.353) (3.717,61.2) ratio 1.1,1.0 i 18 26 j 47 49
gen (3.717,0.0) (3.717,60.0) (60.0,60.0) (60.0,0.0) ratio 1.3,0.87 i 26 46 j 1 36
gen (3.717,60.0) (3.717,60.5) (60.0,60.5) (60.0,60.0) ratio 1.3,0.90000004 i 26 46 j 36 40
gen (3.717,60.5) (3.717,60.7) (60.0,60.7) (60.0,60.5) ratio 1.3,0.8999999 i 26 46 j 40 42
gen (3.717,60.7) (3.717,61.0) (60.0,61.0) (60.0,60.7) ratio 1.3,0.9 i 26 46 j 42 45
gen (3.717,61.0) (3.717,61.2) (60.0,61.2) (60.0,61.0) ratio 1.3,0.8999999 i 26 46 j 45 47
gen (3.717,61.2) (3.717,61.353) (60.0,61.353) (60.0,61.2) ratio 1.3,1.0 i 26 46 j 47 49
model elastic i=1,45 j=1,48
model null i 1 5 j 47 48
group 'null' i 1 5 j 47 48
group delete 'null'
model null i 7 30 j 47 48
group 'null' i 7 30 j 47 48
group delete 'null'
model null i 31 36 j 47 48
group 'null' i 31 36 j 47 48
group delete 'null'
model null i 37 40 j 47 48
group 'null' i 37 40 j 47 48
group delete 'null'
```

```
model null i 41 43 j 47 48
group 'null' i 41 43 j 47 48
group delete 'null'
model null i 44 45 j 47 48
group 'null' i 44 45 j 47 48
group delete 'null'
model null i 18 26 j 42 46
group 'null' i 18 26 j 42 46
group delete 'null'
model null i 27 j 42 45
group 'null' i 27 j 42 45
group delete 'null'
model null i 27 35 j 45 46
group 'null' i 27 35 j 45 46
group delete 'null'
model null i 28 35 j 42 44
group 'null' i 28 35 j 42 44
group delete 'null'
model null i 36 42 j 42 46
group 'null' i 36 42 j 42 46
group delete 'null'
model null i 43 45 j 42 46
group 'null' i 43 45 j 42 46
group delete 'null'
model null i 26 35 j 36 41
group 'null' i 26 35 j 36 41
group delete 'null'
model null i 36 39 j 36 41
group 'null' i 36 39 j 36 41
group delete 'null'
model null i 40 44 j 36 41
group 'null' i 40 44 j 36 41
group delete 'null'
model null i 45 j 36 41
group 'null' i 45 j 36 41
group delete 'null'
gen 1.21,60.7 1.21,61.2 1.41,61.3 2.21,60.7 ratio 1.1,0.9626995 i 11 18 j 42 47
gen 2.21,60.0 2.21,60.7 2.667,60.7 3.717,60.0 ratio 1.1,0.91918045 i 18 26 j 36 42
group 'User:rail' i 6 j 47 48
model elastic group 'User:rail'
prop density=7842.0 bulk=1.75E11 shear=8.07692E10 group 'User:rail'
group 'User:sleeper' i 1 10 j 45 46
model elastic group 'User:sleeper'
prop density=2398.0 bulk=1.08333E10 shear=5E9 group 'User:sleeper'
group 'User:ballast' i 1 17 j 42 44
model elastic group 'User:ballast'
prop density=1698.0 bulk=2.58333E8 shear=1.19231E8 group 'User:ballast'
group 'User:ballast' i 11 17 j 45 46
model elastic group 'User:ballast'
prop density=1698.0 bulk=2.58333E8 shear=1.19231E8 group 'User:ballast'
group 'User:sub-ballast' i 1 25 j 40 41
```

```
model elastic group 'User:sub-ballast'
prop density=2298.0 bulk=2.16666E9 shear=4.36242E7 group 'User:sub-ballast'
group 'User:prepared subgrade' i 1 25 j 36 39
model elastic group 'User:prepared subgrade'
prop density=1998.0 bulk=1.66667E9 shear=3.3557E7 group 'User:prepared subgrade'
group 'User:natural ground' i 1 38 j 17 35
model elastic group 'User:natural ground'
prop density=1998.0 bulk=5.00001E8 shear=1.00671E7 group 'User:natural ground'
group 'User:natural ground' i 39 44 j 11 35
model elastic group 'User:natural ground'
prop density=1998.0 bulk=5.00001E8 shear=1.00671E7 group 'User:natural ground'
group 'User:natural ground' i 45 j 15 35
model elastic group 'User:natural ground'
prop density=1998.0 bulk=5.00001E8 shear=1.00671E7 group 'User:natural ground'
group 'User:natural ground' i 1 38 j 4 16
model elastic group 'User:natural ground'
prop density=1998.0 bulk=5.00001E8 shear=1.00671E7 group 'User:natural ground'
group 'User:natural ground' i 1 38 j 1 3
model elastic group 'User:natural ground'
prop density=1998.0 bulk=5.00001E8 shear=1.00671E7 group 'User:natural ground'
group 'User:natural ground' i 39 45 j 1 10
model elastic group 'User:natural ground'
prop density=1998.0 bulk=5.00001E8 shear=1.00671E7 group 'User:natural ground'
group 'User:natural ground' i 45 j 11 14
model elastic group 'User:natural ground'
prop density=1998.0 bulk=5.00001E8 shear=1.00671E7 group 'User:natural ground'
fix x y j 1
fix x i 1
fix x y i 46
set gravity=9.81
solve
ini xdis 0 ydis 0
ini xvel 0 yvel 0
history 999 unbalanced
apply yforce -62500.0 from 6,49 to 6,49
apply yforce -62500.0 from 7,49 to 7,49
solve
```

APPENDIX E

FLAC CODE OF FDM MODEL FOR VERTICAL DISPLACEMENT OF A RAILWAY SYSTEM SUPPORTED BY EPS EMBANKMENT IN NORWAY DUE TO TRAIN LOAD

E.1 2D Model

The codes presented here are for the model with intermediate mesh. Both the depth and width of the foundation soil are 60 m.

```
config
grid 68,63
gen (0.0,0.0) (0.0,56.187) (0.661,56.187) (0.661,0.0) ratio 1.0,0.95 i 1 5 j 1 41
gen (0.0,56.187) (0.0,56.337) (0.661,56.337) (0.661,56.187) i 1 5 j 41 42
gen (0.0,56.337) (0.0,56.937) (0.661,56.937) (0.661,56.337) i 1 5 j 42 45
gen (0.0,56.937) (0.0,57.537) (0.661,57.537) (0.661,56.937) i 1 5 j 45 48
gen (0.0,57.537) (0.0,58.137) (0.661,58.137) (0.661,57.537) i 1 5 j 48 51
gen (0.0,58.137) (0.0,58.737) (0.661,58.737) (0.661,58.137) i 1 5 j 51 54
gen (0.0,58.737) (0.0,58.887) (0.661,58.887) (0.661,58.737) i 1 5 j 54 55
gen (0.0,58.887) (0.0,59.647) (0.661,59.647) (0.661,58.887) i 1 5 j 55 60
gen (0.0,59.647) (0.0,59.847) (0.661,59.847) (0.661,59.647) i 1 5 j 60 62
gen (0.0,59.847) (0.0,60.0) (0.661,60.0) (0.661,59.847) i 1 5 j 62 64
gen (0.661,0.0) (0.661,56.187) (0.739,56.187) (0.739,0.0) ratio 1.0,0.95 i 5 6 j 1 41
gen (0.661,56.187) (0.661,56.337) (0.739,56.337) (0.739,56.187) i 5 6 j 41 42
gen (0.661,56.337) (0.661,56.937) (0.739,56.937) (0.739,56.337) i 5 6 j 42 45
gen (0.661,56.937) (0.661,57.537) (0.739,57.537) (0.739,56.937) i 5 6 j 45 48
gen (0.661,57.537) (0.661,58.137) (0.739,58.137) (0.739,57.537) i 5 6 j 48 51
gen (0.661,58.137) (0.661,58.737) (0.739,58.737) (0.739,58.137) i 5 6 j 51 54
gen (0.661,58.737) (0.661,58.887) (0.739,58.887) (0.739,58.737) i 5 6 j 54 55
gen (0.661,58.887) (0.661,59.647) (0.739,59.647) (0.739,58.887) i 5 6 j 55 60
gen (0.661,59.647) (0.661,59.847) (0.739,59.847) (0.739,59.647) i 5 6 j 60 62
gen (0.661,59.847) (0.661,60.0) (0.739,60.0) (0.739,59.847) i 5 6 j 62 64
gen (0.739,0.0) (0.739,56.187) (1.21,56.187) (1.21,0.0) ratio 1.0,0.95 i 6 9 j 1 41
gen (0.739,56.187) (0.739,56.337) (1.21,56.337) (1.21,56.187) i 6 9 j 41 42
gen (0.739,56.337) (0.739,56.937) (1.21,56.937) (1.21,56.337) i 6 9 j 42 45
gen (0.739,56.937) (0.739,57.537) (1.21,57.537) (1.21,56.937) i 6 9 j 45 48
gen (0.739,57.537) (0.739,58.137) (1.21,58.137) (1.21,57.537) i 6 9 j 48 51
gen (0.739,58.137) (0.739,58.737) (1.21,58.737) (1.21,58.137) i 6 9 j 51 54
gen (0.739,58.737) (0.739,58.887) (1.21,58.887) (1.21,58.737) i 6 9 j 54 55
gen (0.739,58.887) (0.739,59.647) (1.21,59.647) (1.21,58.887) i 6 9 j 55 60
gen (0.739,59.647) (0.739,59.847) (1.21,59.847) (1.21,59.647) i 6 9 j 60 62
gen (0.739,59.847) (0.739,60.0) (1.21,60.0) (1.21,59.847) i 6 9 j 62 64
gen (1.21,0.0) (1.21,56.187) (1.88,56.187) (1.88,0.0) ratio 1.0,0.95 i 9 13 j 1 41
gen (1.21,56.187) (1.21,56.337) (1.88,56.337) (1.88,56.187) i 9 13 j 41 42
gen (1.21,56.337) (1.21,56.937) (1.88,56.937) (1.88,56.337) i 9 13 j 42 45
gen (1.21,56.937) (1.21,57.537) (1.88,57.537) (1.88,56.937) i 9 13 j 45 48
gen (1.21,57.537) (1.21,58.137) (1.88,58.137) (1.88,57.537) i 9 13 j 48 51
gen (1.21,58.137) (1.21,58.737) (1.88,58.737) (1.88,58.137) i 9 13 j 51 54
gen (1.21,58.737) (1.21,58.887) (1.88,58.887) (1.88,58.737) i 9 13 j 54 55
gen (1.21,58.887) (1.21,59.647) (1.88,59.647) (1.88,58.887) i 9 13 j 55 60
gen (1.21,59.647) (1.21,59.847) (1.88,59.847) (1.88,59.647) i 9 13 j 60 62
gen (1.21,59.847) (1.21,60.0) (1.88,60.0) (1.88,59.847) i 9 13 j 62 64
gen (1.88,0.0) (1.88,56.187) (2.88,56.187) (2.88,0.0) ratio 1.0,0.95 i 13 18 j 1 41
gen (1.88,56.187) (1.88,56.337) (2.88,56.337) (2.88,56.187) i 13 18 j 41 42
```

gen (1.88,56.337) (1.88,56.937) (2.88,56.937) (2.88,56.337) i 13 18 j 42 45
gen (1.88,56.937) (1.88,57.537) (2.88,57.537) (2.88,56.937) i 13 18 j 45 48
gen (1.88,57.537) (1.88,58.137) (2.88,58.137) (2.88,57.537) i 13 18 j 48 51
gen (1.88,58.137) (1.88,58.737) (2.88,58.737) (2.88,58.137) i 13 18 j 51 54
gen (1.88,58.737) (1.88,58.887) (2.88,58.887) (2.88,58.737) i 13 18 j 54 55
gen (1.88,58.887) (1.88,59.647) (2.88,59.647) (2.88,58.887) i 13 18 j 55 60
gen (1.88,59.647) (1.88,59.847) (2.88,59.847) (2.88,59.647) i 13 18 j 60 62
gen (1.88,59.847) (1.88,60.0) (2.88,60.0) (2.88,59.847) i 13 18 j 62 64
gen (2.88,0.0) (2.88,56.187) (3.5,56.187) (3.5,0.0) ratio 1.0,0.95 i 18 22 j 1 41
gen (2.88,56.187) (2.88,56.337) (3.5,56.337) (3.5,56.187) i 18 22 j 41 42
gen (2.88,56.337) (2.88,56.937) (3.5,56.937) (3.5,56.337) i 18 22 j 42 45
gen (2.88,56.937) (2.88,57.537) (3.5,57.537) (3.5,56.937) i 18 22 j 45 48
gen (2.88,57.537) (2.88,58.137) (3.5,58.137) (3.5,57.537) i 18 22 j 48 51
gen (2.88,58.137) (2.88,58.737) (3.5,58.737) (3.5,58.137) i 18 22 j 51 54
gen (2.88,58.737) (2.88,58.887) (3.5,58.887) (3.5,58.737) i 18 22 j 54 55
gen (2.88,58.887) (2.88,59.647) (3.5,59.647) (3.5,58.887) i 18 22 j 55 60
gen (2.88,59.647) (2.88,59.847) (3.5,59.847) (3.5,59.647) i 18 22 j 60 62
gen (2.88,59.847) (2.88,60.0) (3.5,60.0) (3.5,59.847) i 18 22 j 62 64
gen (3.5,0.0) (3.5,56.187) (4.0,56.187) (4.0,0.0) ratio 1.0,0.95 i 22 25 j 1 41
gen (3.5,56.187) (3.5,56.337) (4.0,56.337) (4.0,56.187) i 22 25 j 41 42
gen (3.5,56.337) (3.5,56.937) (4.0,56.937) (4.0,56.337) i 22 25 j 42 45
gen (3.5,56.937) (3.5,57.537) (4.0,57.537) (4.0,56.937) i 22 25 j 45 48
gen (3.5,57.537) (3.5,58.137) (4.0,58.137) (4.0,57.537) i 22 25 j 48 51
gen (3.5,58.137) (3.5,58.737) (4.0,58.737) (4.0,58.137) i 22 25 j 51 54
gen (3.5,58.737) (3.5,58.887) (4.0,58.887) (4.0,58.737) i 22 25 j 54 55
gen (3.5,58.887) (3.5,59.647) (4.0,59.647) (4.0,58.887) i 22 25 j 55 60
gen (3.5,59.647) (3.5,59.847) (4.0,59.847) (4.0,59.647) i 22 25 j 60 62
gen (3.5,59.847) (3.5,60.0) (4.0,60.0) (4.0,59.847) i 22 25 j 62 64
gen (4.0,0.0) (4.0,56.187) (4.5,56.187) (4.5,0.0) ratio 1.0,0.95 i 25 27 j 1 41
gen (4.0,56.187) (4.0,56.337) (4.5,56.337) (4.5,56.187) i 25 27 j 41 42
gen (4.0,56.337) (4.0,56.937) (4.5,56.937) (4.5,56.337) i 25 27 j 42 45
gen (4.0,56.937) (4.0,57.537) (4.5,57.537) (4.5,56.937) i 25 27 j 45 48
gen (4.0,57.537) (4.0,58.137) (4.5,58.137) (4.5,57.537) i 25 27 j 48 51
gen (4.0,58.137) (4.0,58.737) (4.5,58.737) (4.5,58.137) i 25 27 j 51 54
gen (4.0,58.737) (4.0,58.887) (4.5,58.887) (4.5,58.737) i 25 27 j 54 55
gen (4.0,58.887) (4.0,59.647) (4.5,59.647) (4.5,58.887) i 25 27 j 55 60
gen (4.0,59.647) (4.0,59.847) (4.5,59.847) (4.5,59.647) i 25 27 j 60 62
gen (4.0,59.847) (4.0,60.0) (4.5,60.0) (4.5,59.847) i 25 27 j 62 64
gen (4.5,0.0) (4.5,56.187) (5.0,56.187) (5.0,0.0) ratio 1.0,0.95 i 27 29 j 1 41
gen (4.5,56.187) (4.5,56.337) (5.0,56.337) (5.0,56.187) i 27 29 j 41 42
gen (4.5,56.337) (4.5,56.937) (5.0,56.937) (5.0,56.337) i 27 29 j 42 45
gen (4.5,56.937) (4.5,57.537) (5.0,57.537) (5.0,56.937) i 27 29 j 45 48
gen (4.5,57.537) (4.5,58.137) (5.0,58.137) (5.0,57.537) i 27 29 j 48 51
gen (4.5,58.137) (4.5,58.737) (5.0,58.737) (5.0,58.137) i 27 29 j 51 54
gen (4.5,58.737) (4.5,58.887) (5.0,58.887) (5.0,58.737) i 27 29 j 54 55
gen (4.5,58.887) (4.5,59.647) (5.0,59.647) (5.0,58.887) i 27 29 j 55 60
gen (4.5,59.647) (4.5,59.847) (5.0,59.847) (5.0,59.647) i 27 29 j 60 62
gen (4.5,59.847) (4.5,60.0) (5.0,60.0) (5.0,59.847) i 27 29 j 62 64
gen (5.0,0.0) (5.0,56.187) (8.3,56.187) (8.3,0.0) ratio 1.0,0.95 i 29 38 j 1 41
gen (5.0,56.187) (5.0,56.337) (8.3,56.337) (8.3,56.187) i 29 38 j 41 42
gen (5.0,56.337) (5.0,56.937) (8.3,56.937) (8.3,56.337) i 29 38 j 42 45

```
gen (5.0,56.937) (5.0,57.537) (8.3,57.537) (8.3,56.937) i 29 38 j 45 48
gen (5.0,57.537) (5.0,58.137) (8.3,58.137) (8.3,57.537) i 29 38 j 48 51
gen (5.0,58.137) (5.0,58.737) (8.3,58.737) (8.3,58.137) i 29 38 j 51 54
gen (5.0,58.737) (5.0,58.887) (8.3,58.887) (8.3,58.737) i 29 38 j 54 55
gen (5.0,58.887) (5.0,59.647) (8.3,59.647) (8.3,58.887) i 29 38 j 55 60
gen (5.0,59.647) (5.0,59.847) (8.3,59.847) (8.3,59.647) i 29 38 j 60 62
gen (5.0,59.847) (5.0,60.0) (8.3,60.0) (8.3,59.847) i 29 38 j 62 64
gen (8.3,0.0) (8.3,56.187) (8.6,56.187) (8.6,0.0) ratio 1.0,0.95 i 38 39 j 1 41
gen (8.3,56.187) (8.3,56.337) (8.6,56.337) (8.6,56.187) i 38 39 j 41 42
gen (8.3,56.337) (8.3,56.937) (8.6,56.937) (8.6,56.337) i 38 39 j 42 45
gen (8.3,56.937) (8.3,57.537) (8.6,57.537) (8.6,56.937) i 38 39 j 45 48
gen (8.3,57.537) (8.3,58.137) (8.6,58.137) (8.6,57.537) i 38 39 j 48 51
gen (8.3,58.137) (8.3,58.737) (8.6,58.737) (8.6,58.137) i 38 39 j 51 54
gen (8.3,58.737) (8.3,58.887) (8.6,58.887) (8.6,58.737) i 38 39 j 54 55
gen (8.3,58.887) (8.3,59.647) (8.6,59.647) (8.6,58.887) i 38 39 j 55 60
gen (8.3,59.647) (8.3,59.847) (8.6,59.847) (8.6,59.647) i 38 39 j 60 62
gen (8.3,59.847) (8.3,60.0) (8.6,60.0) (8.6,59.847) i 38 39 j 62 64
gen (8.6,0.0) (8.6,56.187) (60.0,56.187) (60.0,0.0) ratio 1.05,0.95 i 39 69 j 1 41
gen (8.6,56.187) (8.6,56.337) (60.0,56.337) (60.0,56.187) ratio 1.05,1.0 i 39 69 j 41 42
gen (8.6,56.337) (8.6,56.937) (60.0,56.937) (60.0,56.337) ratio 1.05,1.0 i 39 69 j 42 45
gen (8.6,56.937) (8.6,57.537) (60.0,57.537) (60.0,56.937) ratio 1.05,1.0 i 39 69 j 45 48
gen (8.6,57.537) (8.6,58.137) (60.0,58.137) (60.0,57.537) ratio 1.05,1.0 i 39 69 j 48 51
gen (8.6,58.137) (8.6,58.737) (60.0,58.737) (60.0,58.137) ratio 1.05,1.0 i 39 69 j 51 54
gen (8.6,58.737) (8.6,58.887) (60.0,58.887) (60.0,58.737) ratio 1.05,1.0 i 39 69 j 54 55
gen (8.6,58.887) (8.6,59.647) (60.0,59.647) (60.0,58.887) ratio 1.05,1.0 i 39 69 j 55 60
gen (8.6,59.647) (8.6,59.847) (60.0,59.847) (60.0,59.647) ratio 1.05,1.0 i 39 69 j 60 62
gen (8.6,59.847) (8.6,60.0) (60.0,60.0) (60.0,59.847) ratio 1.05,1.0 i 39 69 j 62 64
model elastic i=1,68 j=1,63
model null i 39 49 j 41 63
group 'null' i 39 49 j 41 63
group delete 'null'
model null i 50 59 j 41 63
group 'null' i 50 59 j 41 63
group delete 'null'
model null i 60 66 j 41 63
group 'null' i 60 66 j 41 63
group delete 'null'
model null i 67 68 j 41 63
group 'null' i 67 68 j 41 63
group delete 'null'
model null i 18 34 j 55 63
group 'null' i 18 34 j 55 63
group delete 'null'
model null i 35 38 j 55 63
group 'null' i 35 38 j 55 63
group delete 'null'
model null i 22 29 j 54
group 'null' i 22 29 j 54
group delete 'null'
model null i 30 37 j 54
group 'null' i 30 37 j 54
```

```
group delete 'null'
model null i 38 j 54
group 'null' i 38 j 54
group delete 'null'
model null i 6 17 j 62 63
group 'null' i 6 17 j 62 63
group delete 'null'
model null i 1 4 j 62 63
group 'null' i 1 4 j 62 63
group delete 'null'
model null i 38 j 42 53
group 'null' i 38 j 42 53
group delete 'null'
model null i 37 j 43 53
group 'null' i 37 j 43 53
group delete 'null'
model null i 36 j 44 53
group 'null' i 36 j 44 53
group delete 'null'
model null i 35 j 45 53
group 'null' i 35 j 45 53
group delete 'null'
model null i 34 j 46 53
group 'null' i 34 j 46 53
group delete 'null'
model null i 33 j 47 53
group 'null' i 33 j 47 53
group delete 'null'
model null i 32 j 48 53
group 'null' i 32 j 48 53
group delete 'null'
model null i 31 j 49 53
group 'null' i 31 j 49 53
group delete 'null'
model null i 30 j 50 53
group 'null' i 30 j 50 53
group delete 'null'
model null i 29 j 51 53
group 'null' i 29 j 51 53
group delete 'null'
model null i 28 j 52 53
group 'null' i 28 j 52 53
group delete 'null'
model null i 27 j 53
group 'null' i 27 j 53
group delete 'null'
model null i 26 j 53
group 'null' i 26 j 53
group delete 'null'
model null i 24 25 j 53
group 'null' i 24 25 j 53
```

```
group delete 'null'
model null i 26 27 j 52
group 'null' i 26 27 j 52
group delete 'null'
model null i 28 j 51
group 'null' i 28 j 51
group delete 'null'
gen 1.3775,58.887 1.3775,59.847 1.88,59.847 2.88,58.887 ratio 1.0330254,0.96044856 i 10 18 j
55 62
group 'User:rail' i 5 j 62 63
model elastic group 'User:rail'
prop density=7820.0 bulk=1.75E11 shear=8.08E10 group 'User:rail'
group 'User:sleeper' i 1 8 j 60 61
model elastic group 'User:sleeper'
prop density=2398.0 bulk=1.08330E10 shear=5E9 group 'User:sleeper'
group 'User:ballast' i 1 17 j 55 59
model elastic group 'User:ballast'
prop density=2300.0 bulk=2.5833E8 shear=1.1923E8 group 'User:ballast'
group 'User:ballast' i 9 17 j 60 61
model elastic group 'User:ballast'
prop density=2300.0 bulk=2.5833E8 shear=1.1923E8 group 'User:ballast'
group 'User:reinforced concrete slab' i 1 21 j 54
model elastic group 'User:reinforced concrete slab'
prop density=2400.0 bulk=2.22222E10 shear=1.6667E10 group 'User:reinforced concrete slab'
group 'User:EPS29' i 1 21 j 51 53
model elastic group 'User:EPS29'
prop density=30.0 bulk=3.1486E6 shear=3.3998E6 group 'User:EPS29'
group 'User:EPS29' i 1 24 j 48 50
model elastic group 'User:EPS29'
prop density=30.0 bulk=3.1486E6 shear=3.3998E6 group 'User:EPS29'
group 'User:EPS29' i 1 26 j 45 47
model elastic group 'User:EPS29'
prop density=30.0 bulk=3.1486E6 shear=3.3998E6 group 'User:EPS29'
group 'User:EPS29' i 1 28 j 42 44
model elastic group 'User:EPS29'
prop density=30.0 bulk=3.1486E6 shear=3.3998E6 group 'User:EPS29'
group 'User:drainage(gravel/sand)' i 1 38 j 41
model elastic group 'User:drainage(gravel/sand)'
prop density=2000.0 bulk=2.5E8 shear=1.15E8 group 'User:drainage(gravel/sand)'
group 'User:fill' notnull i 22 27 j 51 53
model elastic notnull group 'User:fill'
prop density=2000.0 bulk=2.5E8 shear=1.15E8 notnull group 'User:fill'
group 'User:fill' notnull i 25 31 j 48 50
model elastic notnull group 'User:fill'
prop density=2000.0 bulk=2.5E8 shear=1.15E8 notnull group 'User:fill'
group 'User:fill' notnull i 27 34 j 45 47
model elastic notnull group 'User:fill'
prop density=2000.0 bulk=2.5E8 shear=1.15E8 notnull group 'User:fill'
group 'User:fill' notnull i 29 37 j 42 44
model elastic notnull group 'User:fill'
prop density=2000.0 bulk=2.5E8 shear=1.15E8 notnull group 'User:fill'
```

```
group 'User:fill' j 37 40
model elastic group 'User:fill'
prop density=2000.0 bulk=2.5E8 shear=1.15E8 group 'User:fill'
group 'User:sand' j 16 36
model elastic group 'User:sand'
prop density=2000.0 bulk=8.3333E7 shear=3.8462E7 group 'User:sand'
group 'User:sand' j 1 15
model elastic group 'User:sand'
prop density=2000.0 bulk=8.3333E7 shear=3.8462E7 group 'User:sand'
fix  x y j 1
fix  x y i 69 j 1 41
fix  x i 1 j 1 62
apply yforce -19375.0 from 5,64 to 5,64
apply yforce -19375.0 from 6,64 to 6,64
solve
```

E.2 3D Model

```
;set mechanical ratio 1e-4
gen zone brick size 100 60 100 p0 0,0,0 p1 60,0,0 p2 0,15,0 p3 0,0,60 ratio 1.05 1.0 0.95;
model elas
;
model null range x 0 0.661 z 59.847 60 ; inside of rail
model null range x 0.739 60 z 59.847 60 ; outside of rail
model null range x 1.2 60 z 59.747 59.847 ; outside of upper  sleeper
model null range x 2.05 60 z 59.687 59.847 ; slope outside of ballast 1
model null range x 2.21 60 z 59.527 59.687 ; slope outside of ballast 2
model null range x 2.38 60 z 59.367 59.527 ; slope outside of ballast 3
model null range x 2.55 60 z 59.207 59.367 ; slope outside of ballast 4
model null range x 2.71 60 z 59.047 59.207 ; slope outside of ballast 5
model null range x 2.88 60 z 58.887 59.047 ; slope outside of ballast 6
model null range x 4.01 60 z 58.737 58.887 ; slope outside of load distribution slab
model null range x 4.01 60 z 58.482 58.737 ; slope outside of EPs 1
model null range x 4.52 60 z 58.227 58.482 ; slope outside of EPs 2
model null range x 5.03 60 z 57.972 58.227 ; slope outside of EPs 3
model null range x 5.54 60 z 57.717 57.972 ; slope outside of EPs 4
model null range x 6.05 60 z 57.462 57.717 ; slope outside of EPs 5
model null range x 6.56 60 z 57.207 57.462 ; slope outside of EPs 6
model null range x 7.07 60 z 56.952 57.207 ; slope outside of EPs 7
model null range x 7.58 60 z 56.697 56.952 ; slope outside of EPs 8
model null range x 8.09 60 z 56.442 56.697 ; slope outside of EPs 9
model null range x 8.60 60 z 55.737 56.442 ; slope outside of EPs 10
model null range y 0.249 0.751 z 59.747 59.847 ; gap under rail between sleepers
model null range y 0.999 1.501 z 59.747 59.847 ; gap under rail between sleepers
model null range y 1.749 2.251 z 59.747 59.847 ; gap under rail between sleepers
model null range y 2.499 3.001 z 59.747 59.847 ; gap under rail between sleepers
model null range y 3.249 3.751 z 59.747 59.847 ; gap under rail between sleepers
model null range y 3.999 4.501 z 59.747 59.847 ; gap under rail between sleepers
model null range y 4.749 5.251 z 59.747 59.847 ; gap under rail between sleepers
```

```
model null range y 5.499 6.001 z 59.747 59.847 ; gap under rail between sleepers
model null range y 6.249 6.751 z 59.747 59.847 ; gap under rail between sleepers
model null range y 6.999 7.501 z 59.747 59.847 ; gap under rail between sleepers
model null range y 7.749 8.251 z 59.747 59.847 ; gap under rail between sleepers
model null range y 8.499 9.001 z 59.747 59.847 ; gap under rail between sleepers
model null range y 9.249 9.751 z 59.747 59.847 ; gap under rail between sleepers
model null range y 9.999 10.501 z 59.747 59.847 ; gap under rail between sleepers
model null range y 10.749 11.251 z 59.747 59.847 ; gap under rail between sleepers
model null range y 11.499 12.001 z 59.747 59.847 ; gap under rail between sleepers
model null range y 12.249 12.751 z 59.747 59.847 ; gap under rail between sleepers
model null range y 12.999 13.501 z 59.747 59.847 ; gap under rail between sleepers
model null range y 13.749 14.251 z 59.747 59.847 ; gap under rail between sleepers
model null range y 14.499 15.001 z 59.747 59.847 ; gap under rail between sleepers
;
prop bulk 175000e6 shear 80769e6 range z 59.847 60; rail steel
prop bulk 258e6 shear 118e6 range x 0 60 z 0 59.647; ballast under sleeper
prop bulk 258e6 shear 118e6 range x 0 60 z 59.647 59.747; ballast between sleeper
;prop bulk 10833e6 shear 5000e6 range x 0 1.21 z 59.647 59.847 ; sleeper concrete continuous
prop bulk 28333e6 shear 13077e6 range x 0 1.21 y -0.001 0.251 z 59.647 59.847 ; sleeper
concrete 1
prop bulk 28333e6 shear 13077e6 range x 0 1.21 y 0.749 1.001 z 59.647 59.847 ; sleeper concrete
2
prop bulk 28333e6 shear 13077e6 range x 0 1.21 y 1.499 1.751 z 59.647 59.847 ; sleeper concrete
3
prop bulk 28333e6 shear 13077e6 range x 0 1.21 y 2.249 2.501 z 59.647 59.847 ; sleeper concrete
4
prop bulk 28333e6 shear 13077e6 range x 0 1.21 y 2.999 3.251 z 59.647 59.847 ; sleeper concrete
5
prop bulk 28333e6 shear 13077e6 range x 0 1.21 y 3.749 4.001 z 59.647 59.847 ; sleeper concrete
6
prop bulk 28333e6 shear 13077e6 range x 0 1.21 y 4.499 4.751 z 59.647 59.847 ; sleeper concrete
7
prop bulk 28333e6 shear 13077e6 range x 0 1.21 y 5.249 5.501 z 59.647 59.847 ; sleeper concrete
8
prop bulk 28333e6 shear 13077e6 range x 0 1.21 y 5.999 6.251 z 59.647 59.847 ; sleeper concrete
9
prop bulk 28333e6 shear 13077e6 range x 0 1.21 y 6.749 7.001 z 59.647 59.847 ; sleeper concrete
10
prop bulk 28333e6 shear 13077e6 range x 0 1.21 y 7.449 7.751 z 59.647 59.847 ; sleeper concrete
11
prop bulk 28333e6 shear 13077e6 range x 0 1.21 y 8.249 8.501 z 59.647 59.847 ; sleeper concrete
12
prop bulk 28333e6 shear 13077e6 range x 0 1.21 y 8.999 9.251 z 59.647 59.847 ; sleeper concrete
13
prop bulk 28333e6 shear 13077e6 range x 0 1.21 y 9.749 10.001 z 59.647 59.847 ; sleeper
concrete 14
prop bulk 28333e6 shear 13077e6 range x 0 1.21 y 10.499 10.751 z 59.647 59.847 ; sleeper
concrete 15
prop bulk 28333e6 shear 13077e6 range x 0 1.21 y 11.249 11.501 z 59.647 59.847 ; sleeper
concrete 16
prop bulk 28333e6 shear 13077e6 range x 0 1.21 y 11.999 12.251 z 59.647 59.847 ; sleeper
```

```
concrete 17
prop bulk 28333e6 shear 13077e6 range x 0 1.21 y 12.749 13.001 z 59.647 59.847 ; sleeper
concrete 18
prop bulk 28333e6 shear 13077e6 range x 0 1.21 y 13.499 13.751 z 59.647 59.847 ; sleeper
concrete 19
prop bulk 28333e6 shear 13077e6 range x 0 1.21 y 14.249 14.501 z 59.647 59.847 ; sleeper
concrete 20
prop bulk 258e6 shear 119e6 range x 1.21 1.88  z 59.647 59.747 ; ballast outside of sleeper
prop bulk 28333e6 shear 13077e6 range x 0 4.01 z 58.737 58.887; load distribution slab
prop bulk 250e6 shear 115e6 range z 55.737 58.737 ; fill in shoulder of slope EPS
prop bulk 3.15e6 shear 3.4e6 range x 0 3.5 z 58.137 58.737 ; EPs 29
prop bulk 3.15e6 shear 3.4e6 range x 0 4.0 z 57.537 58.137 ; EPs 29
prop bulk 3.15e6 shear 3.4e6 range x 0 4.5 z 56.937 57.537 ; EPs 29
prop bulk 3.15e6 shear 3.4e6 range x 0 5.0 z 56.337 56.937 ; EPs 29
prop bulk 3.15e6 shear 3.4e6 range x 0 5.5 z 55.737 56.337 ; EPs 29
prop bulk 83e6 shear 38e6 range z 0 55.737; foundation soil
;
;boundary conditions
;
fix x y z range z -.01 .01 ; fixes base
fix x y z range x 59.99 60.01 ; fixes right boundary
fix y range y -0.01 0.01 ; fixes front face in y direction (axis of symmetry)
fix y range y 14.99 15.01 ; fixes back face in y direction (axis of symmetry)
fix x range x -0.01 0.01; fixes left boundary in x direction (axis of symmetry)
;
apply zforce -77.5e3 range z 59.99 60.01 x 0.701 0.703 y 1.999 2.001 ; axle load 1
apply zforce -77.5e3 range z 59.99 60.01 x 0.701 0.703 y 4.999 5.001 ; axle load 2
apply zforce -77.5e3 range z 59.99 60.01 x 0.701 0.703 y 9.999 10.001; axle load 3
apply zforce -77.5e3 range z 59.99 60.01 x 0.701 0.703 y 12.999 13.001; axle load 4
;
hist unbal
;step 40000
Solve
;
plot create PROPV ; shows properties in X section
plot set color On
plot set caption On
plot set caption left
plot set caption size 26
plot set title On
plot set title top
plot set foreground black
plot set background white
plot set window position (0.00,0.00) size(1.00,0.89)
plot set plane normal (0.000,1.000,0.000)
plot set plane origin (30.0000e+000,7.500e+000,30.0000e+000)
plot set mode model
plot set center (30.0000e+000,6.000e+000,30.0000e+000)
plot set rotation (0.00, 0.00, 0.00)
plot set distance 180
plot set angle 22
```

```
plot set magnification  1.0e+000
plot add block prop bulk
plot add contour zdisp
;
save Norway-EPS.sav
```

APPENDIX F

FLAC CODE OF FDM MODEL FOR VERTICAL DISPLACEMENT OF UTA FRONTRUNNER RAILWAY SYSTEM SUPPORTED BY EPS EMBANKMENT IN CORNER CANYON DUE TO TRAIN LOAD

F.1 2D Model

The codes presented here are for the model with 0 m depth and extended width of the foundation soil.

```
config
grid 216,106
;generate raw mesh
gen (0.0,0.0) (0.0,20.0) (15.0,20.0) (15.0,0.0) ratio 0.95,0.93 i 1 16 j 1 31
gen (0.0,20.0) (0.0,33.1572) (15.0,33.1572) (15.0,20.0) ratio 0.95,1.0 i 1 16 j 31 87
gen (0.0,33.1572) (0.0,33.3604) (15.0,33.3604) (15.0,33.1572) ratio 0.95,1.0 i 1 16 j 87 89
gen (0.0,33.3604) (0.0,34.2748) (15.0,34.2748) (15.0,33.3604) ratio 0.95,1.0 i 1 16 j 89 98
gen (0.0,34.2748) (0.0,34.478) (15.0,34.478) (15.0,34.2748) ratio 0.95,1.0 i 1 16 j 98 100
gen (0.0,34.478) (0.0,34.7828) (15.0,34.7828) (15.0,34.478) ratio 0.95,1.0 i 1 16 j 100 103
gen (0.0,34.7828) (0.0,34.9828) (15.0,34.9828) (15.0,34.7828) ratio 0.95,1.0 i 1 16 j 103 105
gen (0.0,34.9828) (0.0,35.1358) (15.0,35.1358) (15.0,34.9828) ratio 0.95,1.0 i 1 16 j 105 107
gen (15.0,0.0) (15.0,20.0) (19.699,20.0) (19.699,0.0) ratio 1.0,0.93 i 16 22 j 1 31
gen (15.0,20.0) (15.0,33.1572) (19.699,33.1572) (19.699,20.0) i 16 22 j 31 87
gen (15.0,33.1572) (15.0,33.3604) (19.699,33.3604) (19.699,33.1572) i 16 22 j 87 89
gen (15.0,33.3604) (15.0,34.2748) (19.699,34.2748) (19.699,33.3604) i 16 22 j 89 98
gen (15.0,34.2748) (15.0,34.478) (19.699,34.478) (19.699,34.2748) i 16 22 j 98 100
gen (15.0,34.478) (15.0,34.7828) (19.699,34.7828) (19.699,34.478) i 16 22 j 100 103
gen (15.0,34.7828) (15.0,34.9828) (19.699,34.9828) (19.699,34.7828) i 16 22 j 103 105
gen (15.0,34.9828) (15.0,35.1358) (19.699,35.1358) (19.699,34.9828) i 16 22 j 105 107
gen (19.699,0.0) (19.699,20.0) (42.2542,20.0) (42.2542,0.0) ratio 1.0,0.93 i 22 70 j 1 31
gen (19.699,20.0) (19.699,33.1572) (42.2542,33.1572) (42.2542,20.0) i 22 70 j 31 87
gen (19.699,33.1572) (19.699,33.3604) (42.2542,33.3604) (42.2542,33.1572) i 22 70 j 87 89
gen (19.699,33.3604) (19.699,34.2748) (42.2542,34.2748) (42.2542,33.3604) i 22 70 j 89 98
gen (19.699,34.2748) (19.699,34.478) (42.2542,34.478) (42.2542,34.2748) i 22 70 j 98 100
gen (19.699,34.478) (19.699,34.7828) (42.2542,34.7828) (42.2542,34.478) i 22 70 j 100 103
gen (19.699,34.7828) (19.699,34.9828) (42.2542,34.9828) (42.2542,34.7828) i 22 70 j 103 105
gen (19.699,34.9828) (19.699,35.1358) (42.2542,35.1358) (42.2542,34.9828) i 22 70 j 105 107
gen (42.2542,0.0) (42.2542,20.0) (43.956,20.0) (43.956,0.0) ratio 1.0,0.93 i 70 74 j 1 31
gen (42.2542,20.0) (42.2542,33.1572) (43.956,33.1572) (43.956,20.0) i 70 74 j 31 87
gen (42.2542,33.1572) (42.2542,33.3604) (43.956,33.3604) (43.956,33.1572) i 70 74 j 87 89
gen (42.2542,33.3604) (42.2542,34.2748) (43.956,34.2748) (43.956,33.3604) i 70 74 j 89 98
gen (42.2542,34.2748) (42.2542,34.478) (43.956,34.478) (43.956,34.2748) i 70 74 j 98 100
gen (42.2542,34.478) (42.2542,34.7828) (43.956,34.7828) (43.956,34.478) i 70 74 j 100 103
gen (42.2542,34.7828) (42.2542,34.9828) (43.956,34.9828) (43.956,34.7828) i 70 74 j 103 105
gen (42.2542,34.9828) (42.2542,35.1358) (43.956,35.1358) (43.956,34.9828) i 70 74 j 105 107
gen (43.956,0.0) (43.956,20.0) (44.7369,20.0) (44.7369,0.0) ratio 1.0,0.93 i 74 79 j 1 31
gen (43.956,20.0) (43.956,33.1572) (44.7369,33.1572) (44.7369,20.0) i 74 79 j 31 87
gen (43.956,33.1572) (43.956,33.3604) (44.7369,33.3604) (44.7369,33.1572) i 74 79 j 87 89
gen (43.956,33.3604) (43.956,34.2748) (44.7369,34.2748) (44.7369,33.3604) i 74 79 j 89 98
gen (43.956,34.2748) (43.956,34.478) (44.7369,34.478) (44.7369,34.2748) i 74 79 j 98 100
gen (43.956,34.478) (43.956,34.7828) (44.7369,34.7828) (44.7369,34.478) i 74 79 j 100 103
gen (43.956,34.7828) (43.956,34.9828) (44.7369,34.9828) (44.7369,34.7828) i 74 79 j 103 105
gen (43.956,34.9828) (43.956,35.1358) (44.7369,35.1358) (44.7369,34.9828) i 74 79 j 105 107
gen (44.7369,0.0) (44.7369,20.0) (45.7465,20.0) (45.7465,0.0) ratio 1.0,0.93 i 79 84 j 1 31
```

gen (44.7369,20.0) (44.7369,33.1572) (45.7465,33.1572) (45.7465,20.0) i 79 84 j 31 87
gen (44.7369,33.1572) (44.7369,33.3604) (45.7465,33.3604) (45.7465,33.1572) i 79 84 j 87 89
gen (44.7369,33.3604) (44.7369,34.2748) (45.7465,34.2748) (45.7465,33.3604) i 79 84 j 89 98
gen (44.7369,34.2748) (44.7369,34.478) (45.7465,34.478) (45.7465,34.2748) i 79 84 j 98 100
gen (44.7369,34.478) (44.7369,34.7828) (45.7465,34.7828) (45.7465,34.478) i 79 84 j 100 103
gen (44.7369,34.7828) (44.7369,34.9828) (45.7465,34.9828) (45.7465,34.7828) i 79 84 j 103 105
gen (44.7369,34.9828) (44.7369,35.1358) (45.7465,35.1358) (45.7465,34.9828) i 79 84 j 105 107
gen (45.7465,0.0) (45.7465,20.0) (46.13695,20.0) (46.13695,0.0) ratio 1.0,0.93 i 84 86 j 1 31
gen (45.7465,20.0) (45.7465,33.1572) (46.13695,33.1572) (46.13695,20.0) i 84 86 j 31 87
gen (45.7465,33.1572) (45.7465,33.3604) (46.13695,33.3604) (46.13695,33.1572) i 84 86 j 87 89
gen (45.7465,33.3604) (45.7465,34.2748) (46.13695,34.2748) (46.13695,33.3604) i 84 86 j 89 98
gen (45.7465,34.2748) (45.7465,34.478) (46.13695,34.478) (46.13695,34.2748) i 84 86 j 98 100
gen (45.7465,34.478) (45.7465,34.7828) (46.13695,34.7828) (46.13695,34.478) i 84 86 j 100 103
gen (45.7465,34.7828) (45.7465,34.9828) (46.13695,34.9828) (46.13695,34.7828) i 84 86 j 103
105
gen (45.7465,34.9828) (45.7465,35.1358) (46.13695,35.1358) (46.13695,34.9828) i 84 86 j 105
107
gen (46.13695,0.0) (46.13695,20.0) (46.58645,20.0) (46.58645,0.0) ratio 1.0,0.93 i 86 90 j 1 31
gen (46.13695,20.0) (46.13695,33.1572) (46.58645,33.1572) (46.58645,20.0) i 86 90 j 31 87
gen (46.13695,33.1572) (46.13695,33.3604) (46.58645,33.3604) (46.58645,33.1572) i 86 90 j 87
89
gen (46.13695,33.3604) (46.13695,34.2748) (46.58645,34.2748) (46.58645,33.3604) i 86 90 j 89
98
gen (46.13695,34.2748) (46.13695,34.478) (46.58645,34.478) (46.58645,34.2748) i 86 90 j 98
100
gen (46.13695,34.478) (46.13695,34.7828) (46.58645,34.7828) (46.58645,34.478) i 86 90 j 100
103
gen (46.13695,34.7828) (46.13695,34.9828) (46.58645,34.9828) (46.58645,34.7828) i 86 90 j
103 105
gen (46.13695,34.9828) (46.13695,35.1358) (46.58645,35.1358) (46.58645,34.9828) i 86 90 j
105 107
gen (46.58645,0.0) (46.58645,20.0) (46.66445,20.0) (46.66445,0.0) ratio 1.0,0.93 i 90 91 j 1 31
gen (46.58645,20.0) (46.58645,33.1572) (46.66445,33.1572) (46.66445,20.0) i 90 91 j 31 87
gen (46.58645,33.1572) (46.58645,33.3604) (46.66445,33.3604) (46.66445,33.1572) i 90 91 j 87
89
gen (46.58645,33.3604) (46.58645,34.2748) (46.66445,34.2748) (46.66445,33.3604) i 90 91 j 89
98
gen (46.58645,34.2748) (46.58645,34.478) (46.66445,34.478) (46.66445,34.2748) i 90 91 j 98
100
gen (46.58645,34.478) (46.58645,34.7828) (46.66445,34.7828) (46.66445,34.478) i 90 91 j 100
103
gen (46.58645,34.7828) (46.58645,34.9828) (46.66445,34.9828) (46.66445,34.7828) i 90 91 j
103 105
gen (46.58645,34.9828) (46.58645,35.1358) (46.66445,35.1358) (46.66445,34.9828) i 90 91 j
105 107
gen (46.66445,0.0) (46.66445,20.0) (48.12445,20.0) (48.12445,0.0) ratio 1.0,0.93 i 91 106 j 1 31
gen (46.66445,20.0) (46.66445,33.1572) (48.12445,33.1572) (48.12445,20.0) i 91 106 j 31 87
gen (46.66445,33.1572) (46.66445,33.3604) (48.12445,33.3604) (48.12445,33.1572) i 91 106 j
87 89
gen (46.66445,33.3604) (46.66445,34.2748) (48.12445,34.2748) (48.12445,33.3604) i 91 106 j
89 98

gen (46.66445,34.2748) (46.66445,34.478) (48.12445,34.478) (48.12445,34.2748) i 91 106 j 98 100
gen (46.66445,34.478) (46.66445,34.7828) (48.12445,34.7828) (48.12445,34.478) i 91 106 j 100 103
gen (46.66445,34.7828) (46.66445,34.9828) (48.12445,34.9828) (48.12445,34.7828) i 91 106 j 103 105
gen (46.66445,34.9828) (46.66445,35.1358) (48.12445,35.1358) (48.12445,34.9828) i 91 106 j 105 107
gen (48.12445,0.0) (48.12445,20.0) (48.20245,20.0) (48.20245,0.0) ratio 1.0,0.93 i 106 107 j 1 31
gen (48.12445,20.0) (48.12445,33.1572) (48.20245,33.1572) (48.20245,20.0) i 106 107 j 31 87
gen (48.12445,33.1572) (48.12445,33.3604) (48.20245,33.3604) (48.20245,33.1572) i 106 107 j 87 89
gen (48.12445,33.3604) (48.12445,34.2748) (48.20245,34.2748) (48.20245,33.3604) i 106 107 j 89 98
gen (48.12445,34.2748) (48.12445,34.478) (48.20245,34.478) (48.20245,34.2748) i 106 107 j 98 100
gen (48.12445,34.478) (48.12445,34.7828) (48.20245,34.7828) (48.20245,34.478) i 106 107 j 100 103
gen (48.12445,34.7828) (48.12445,34.9828) (48.20245,34.9828) (48.20245,34.7828) i 106 107 j 103 105
gen (48.12445,34.9828) (48.12445,35.1358) (48.20245,35.1358) (48.20245,34.9828) i 106 107 j 105 107
gen (48.20245,0.0) (48.20245,20.0) (48.65795,20.0) (48.65795,0.0) ratio 1.0,0.93 i 107 111 j 1 31
gen (48.20245,20.0) (48.20245,33.1572) (48.65795,33.1572) (48.65795,20.0) i 107 111 j 31 87
gen (48.20245,33.1572) (48.20245,33.3604) (48.65795,33.3604) (48.65795,33.1572) i 107 111 j 87 89
gen (48.20245,33.3604) (48.20245,34.2748) (48.65795,34.2748) (48.65795,33.3604) i 107 111 j 89 98
gen (48.20245,34.2748) (48.20245,34.478) (48.65795,34.478) (48.65795,34.2748) i 107 111 j 98 100
gen (48.20245,34.478) (48.20245,34.7828) (48.65795,34.7828) (48.65795,34.478) i 107 111 j 100 103
gen (48.20245,34.7828) (48.20245,34.9828) (48.65795,34.9828) (48.65795,34.7828) i 107 111 j 103 105
gen (48.20245,34.9828) (48.20245,35.1358) (48.65795,35.1358) (48.65795,34.9828) i 107 111 j 105 107
gen (48.65795,0.0) (48.65795,20.0) (49.0424,20.0) (49.0424,0.0) ratio 1.0,0.93 i 111 113 j 1 31
gen (48.65795,20.0) (48.65795,33.1572) (49.0424,33.1572) (49.0424,20.0) i 111 113 j 31 87
gen (48.65795,33.1572) (48.65795,33.3604) (49.0424,33.3604) (49.0424,33.1572) i 111 113 j 87 89
gen (48.65795,33.3604) (48.65795,34.2748) (49.0424,34.2748) (49.0424,33.3604) i 111 113 j 89 98
gen (48.65795,34.2748) (48.65795,34.478) (49.0424,34.478) (49.0424,34.2748) i 111 113 j 98 100
gen (48.65795,34.478) (48.65795,34.7828) (49.0424,34.7828) (49.0424,34.478) i 111 113 j 100 103
gen (48.65795,34.7828) (48.65795,34.9828) (49.0424,34.9828) (49.0424,34.7828) i 111 113 j 103 105
gen (48.65795,34.9828) (48.65795,35.1358) (49.0424,35.1358) (49.0424,34.9828) i 111 113 j 105 107
gen (49.0424,0.0) (49.0424,20.0) (50.3185,20.0) (50.3185,0.0) ratio 1.0,0.93 i 113 119 j 1 31

gen (49.0424,20.0) (49.0424,33.1572) (50.3185,33.1572) (50.3185,20.0) i 113 119 j 31 87
gen (49.0424,33.1572) (49.0424,33.3604) (50.3185,33.3604) (50.3185,33.1572) i 113 119 j 87 89
gen (49.0424,33.3604) (49.0424,34.2748) (50.3185,34.2748) (50.3185,33.3604) i 113 119 j 89 98
gen (49.0424,34.2748) (49.0424,34.478) (50.3185,34.478) (50.3185,34.2748) i 113 119 j 98 100
gen (49.0424,34.478) (49.0424,34.7828) (50.3185,34.7828) (50.3185,34.478) i 113 119 j 100 103
gen (49.0424,34.7828) (49.0424,34.9828) (50.3185,34.9828) (50.3185,34.7828) i 113 119 j 103
105
gen (49.0424,34.9828) (49.0424,35.1358) (50.3185,35.1358) (50.3185,34.9828) i 113 119 j 105
107
gen (50.3185,0.0) (50.3185,20.0) (50.70895,20.0) (50.70895,0.0) ratio 1.0,0.93 i 119 121 j 1 31
gen (50.3185,20.0) (50.3185,33.1572) (50.70895,33.1572) (50.70895,20.0) i 119 121 j 31 87
gen (50.3185,33.1572) (50.3185,33.3604) (50.70895,33.3604) (50.70895,33.1572) i 119 121 j 87
89
gen (50.3185,33.3604) (50.3185,34.2748) (50.70895,34.2748) (50.70895,33.3604) i 119 121 j 89
98
gen (50.3185,34.2748) (50.3185,34.478) (50.70895,34.478) (50.70895,34.2748) i 119 121 j 98
100
gen (50.3185,34.478) (50.3185,34.7828) (50.70895,34.7828) (50.70895,34.478) i 119 121 j 100
103
gen (50.3185,34.7828) (50.3185,34.9828) (50.70895,34.9828) (50.70895,34.7828) i 119 121 j
103 105
gen (50.3185,34.9828) (50.3185,35.1358) (50.70895,35.1358) (50.70895,34.9828) i 119 121 j
105 107
gen (50.70895,0.0) (50.70895,20.0) (51.15845,20.0) (51.15845,0.0) ratio 1.0,0.93 i 121 125 j 1 31
gen (50.70895,20.0) (50.70895,33.1572) (51.15845,33.1572) (51.15845,20.0) i 121 125 j 31 87
gen (50.70895,33.1572) (50.70895,33.3604) (51.15845,33.3604) (51.15845,33.1572) i 121 125 j
87 89
gen (50.70895,33.3604) (50.70895,34.2748) (51.15845,34.2748) (51.15845,33.3604) i 121 125 j
89 98
gen (50.70895,34.2748) (50.70895,34.478) (51.15845,34.478) (51.15845,34.2748) i 121 125 j 98
100
gen (50.70895,34.478) (50.70895,34.7828) (51.15845,34.7828) (51.15845,34.478) i 121 125 j
100 103
gen (50.70895,34.7828) (50.70895,34.9828) (51.15845,34.9828) (51.15845,34.7828) i 121 125 j
103 105
gen (50.70895,34.9828) (50.70895,35.1358) (51.15845,35.1358) (51.15845,34.9828) i 121 125 j
105 107
gen (51.15845,0.0) (51.15845,20.0) (51.23645,20.0) (51.23645,0.0) ratio 1.0,0.93 i 125 126 j 1 31
gen (51.15845,20.0) (51.15845,33.1572) (51.23645,33.1572) (51.23645,20.0) i 125 126 j 31 87
gen (51.15845,33.1572) (51.15845,33.3604) (51.23645,33.3604) (51.23645,33.1572) i 125 126 j
87 89
gen (51.15845,33.3604) (51.15845,34.2748) (51.23645,34.2748) (51.23645,33.3604) i 125 126 j
89 98
gen (51.15845,34.2748) (51.15845,34.478) (51.23645,34.478) (51.23645,34.2748) i 125 126 j 98
100
gen (51.15845,34.478) (51.15845,34.7828) (51.23645,34.7828) (51.23645,34.478) i 125 126 j
100 103
gen (51.15845,34.7828) (51.15845,34.9828) (51.23645,34.9828) (51.23645,34.7828) i 125 126 j
103 105
gen (51.15845,34.9828) (51.15845,35.1358) (51.23645,35.1358) (51.23645,34.9828) i 125 126 j
105 107

gen (51.23645,0.0) (51.23645,20.0) (52.69645,20.0) (52.69645,0.0) ratio 1.0,0.93 i 126 141 j 1 31
gen (51.23645,20.0) (51.23645,33.1572) (52.69645,33.1572) (52.69645,20.0) i 126 141 j 31 87
gen (51.23645,33.1572) (51.23645,33.3604) (52.69645,33.3604) (52.69645,33.1572) i 126 141 j 87 89
gen (51.23645,33.3604) (51.23645,34.2748) (52.69645,34.2748) (52.69645,33.3604) i 126 141 j 89 98
gen (51.23645,34.2748) (51.23645,34.478) (52.69645,34.478) (52.69645,34.2748) i 126 141 j 98 100
gen (51.23645,34.478) (51.23645,34.7828) (52.69645,34.7828) (52.69645,34.478) i 126 141 j 100 103
gen (51.23645,34.7828) (51.23645,34.9828) (52.69645,34.9828) (52.69645,34.7828) i 126 141 j 103 105
gen (51.23645,34.9828) (51.23645,35.1358) (52.69645,35.1358) (52.69645,34.9828) i 126 141 j 105 107
gen (52.69645,0.0) (52.69645,20.0) (52.77445,20.0) (52.77445,0.0) ratio 1.0,0.93 i 141 142 j 1 31
gen (52.69645,20.0) (52.69645,33.1572) (52.77445,33.1572) (52.77445,20.0) i 141 142 j 31 87
gen (52.69645,33.1572) (52.69645,33.3604) (52.77445,33.3604) (52.77445,33.1572) i 141 142 j 87 89
gen (52.69645,33.3604) (52.69645,34.2748) (52.77445,34.2748) (52.77445,33.3604) i 141 142 j 89 98
gen (52.69645,34.2748) (52.69645,34.478) (52.77445,34.478) (52.77445,34.2748) i 141 142 j 98 100
gen (52.69645,34.478) (52.69645,34.7828) (52.77445,34.7828) (52.77445,34.478) i 141 142 j 100 103
gen (52.69645,34.7828) (52.69645,34.9828) (52.77445,34.9828) (52.77445,34.7828) i 141 142 j 103 105
gen (52.69645,34.9828) (52.69645,35.1358) (52.77445,35.1358) (52.77445,34.9828) i 141 142 j 105 107
gen (52.77445,0.0) (52.77445,20.0) (53.22395,20.0) (53.22395,0.0) ratio 1.0,0.93 i 142 146 j 1 31
gen (52.77445,20.0) (52.77445,33.1572) (53.22395,33.1572) (53.22395,20.0) i 142 146 j 31 87
gen (52.77445,33.1572) (52.77445,33.3604) (53.22395,33.3604) (53.22395,33.1572) i 142 146 j 87 89
gen (52.77445,33.3604) (52.77445,34.2748) (53.22395,34.2748) (53.22395,33.3604) i 142 146 j 89 98
gen (52.77445,34.2748) (52.77445,34.478) (53.22395,34.478) (53.22395,34.2748) i 142 146 j 98 100
gen (52.77445,34.478) (52.77445,34.7828) (53.22395,34.7828) (53.22395,34.478) i 142 146 j 100 103
gen (52.77445,34.7828) (52.77445,34.9828) (53.22395,34.9828) (53.22395,34.7828) i 142 146 j 103 105
gen (52.77445,34.9828) (52.77445,35.1358) (53.22395,35.1358) (53.22395,34.9828) i 142 146 j 105 107
gen (53.22395,0.0) (53.22395,20.0) (53.6144,20.0) (53.6144,0.0) ratio 1.0,0.93 i 146 148 j 1 31
gen (53.22395,20.0) (53.22395,33.1572) (53.6144,33.1572) (53.6144,20.0) i 146 148 j 31 87
gen (53.22395,33.1572) (53.22395,33.3604) (53.6144,33.3604) (53.6144,33.1572) i 146 148 j 87 89
gen (53.22395,33.3604) (53.22395,34.2748) (53.6144,34.2748) (53.6144,33.3604) i 146 148 j 89 98
gen (53.22395,34.2748) (53.22395,34.478) (53.6144,34.478) (53.6144,34.2748) i 146 148 j 98 100
gen (53.22395,34.478) (53.22395,34.7828) (53.6144,34.7828) (53.6144,34.478) i 146 148 j 100

103
gen (53.22395,34.7828) (53.22395,34.9828) (53.6144,34.9828) (53.6144,34.7828) i 146 148 j 103 105
gen (53.22395,34.9828) (53.22395,35.1358) (53.6144,35.1358) (53.6144,34.9828) i 146 148 j 105 107
gen (53.6144,0.0) (53.6144,20.0) (55.4049,20.0) (55.4049,0.0) ratio 1.0,0.93 i 148 157 j 1 31
gen (53.6144,20.0) (53.6144,33.1572) (55.4049,33.1572) (55.4049,20.0) i 148 157 j 31 87
gen (53.6144,33.1572) (53.6144,33.3604) (55.4049,33.3604) (55.4049,33.1572) i 148 157 j 87 89
gen (53.6144,33.3604) (53.6144,34.2748) (55.4049,34.2748) (55.4049,33.3604) i 148 157 j 89 98
gen (53.6144,34.2748) (53.6144,34.478) (55.4049,34.478) (55.4049,34.2748) i 148 157 j 98 100
gen (53.6144,34.478) (53.6144,34.7828) (55.4049,34.7828) (55.4049,34.478) i 148 157 j 100 103
gen (53.6144,34.7828) (53.6144,34.9828) (55.4049,34.9828) (55.4049,34.7828) i 148 157 j 103 105
gen (53.6144,34.9828) (53.6144,35.1358) (55.4049,35.1358) (55.4049,34.9828) i 148 157 j 105 107
gen (55.4049,0.0) (55.4049,20.0) (57.1067,20.0) (57.1067,0.0) ratio 1.0,0.93 i 157 161 j 1 31
gen (55.4049,20.0) (55.4049,33.1572) (57.1067,33.1572) (57.1067,20.0) i 157 161 j 31 87
gen (55.4049,33.1572) (55.4049,33.3604) (57.1067,33.3604) (57.1067,33.1572) i 157 161 j 87 89
gen (55.4049,33.3604) (55.4049,34.2748) (57.1067,34.2748) (57.1067,33.3604) i 157 161 j 89 98
gen (55.4049,34.2748) (55.4049,34.478) (57.1067,34.478) (57.1067,34.2748) i 157 161 j 98 100
gen (55.4049,34.478) (55.4049,34.7828) (57.1067,34.7828) (57.1067,34.478) i 157 161 j 100 103
gen (55.4049,34.7828) (55.4049,34.9828) (57.1067,34.9828) (57.1067,34.7828) i 157 161 j 103 105
gen (55.4049,34.9828) (55.4049,35.1358) (57.1067,35.1358) (57.1067,34.9828) i 157 161 j 105 107
gen (57.1067,0.0) (57.1067,20.0) (59.9261,20.0) (59.9261,0.0) ratio 1.0,0.93 i 161 167 j 1 31
gen (57.1067,20.0) (57.1067,33.1572) (59.9261,33.1572) (59.9261,20.0) i 161 167 j 31 87
gen (57.1067,33.1572) (57.1067,33.3604) (59.9261,33.3604) (59.9261,33.1572) i 161 167 j 87 89
gen (57.1067,33.3604) (57.1067,34.2748) (59.9261,34.2748) (59.9261,33.3604) i 161 167 j 89 98
gen (57.1067,34.2748) (57.1067,34.478) (59.9261,34.478) (59.9261,34.2748) i 161 167 j 98 100
gen (57.1067,34.478) (57.1067,34.7828) (59.9261,34.7828) (59.9261,34.478) i 161 167 j 100 103
gen (57.1067,34.7828) (57.1067,34.9828) (59.9261,34.9828) (59.9261,34.7828) i 161 167 j 103 105
gen (57.1067,34.9828) (57.1067,35.1358) (59.9261,35.1358) (59.9261,34.9828) i 161 167 j 105 107
gen (59.9261,0.0) (59.9261,20.0) (118.6713,20.0) (118.6713,0.0) ratio 1.05,0.93 i 167 217 j 1 31
gen (59.9261,20.0) (59.9261,33.1572) (118.6713,33.1572) (118.6713,20.0) ratio 1.05,1.0 i 167 217 j 31 87
gen (59.9261,33.1572) (59.9261,33.3604) (118.6713,33.3604) (118.6713,33.1572) ratio 1.05,1.0 i 167 217 j 87 89
gen (59.9261,33.3604) (59.9261,34.2748) (118.6713,34.2748) (118.6713,33.3604) ratio 1.05,1.0 i 167 217 j 89 98
gen (59.9261,34.2748) (59.9261,34.478) (118.6713,34.478) (118.6713,34.2748) ratio 1.05,1.0 i 167 217 j 98 100
gen (59.9261,34.478) (59.9261,34.7828) (118.6713,34.7828) (118.6713,34.478) ratio 1.05,1.0 i 167 217 j 100 103
gen (59.9261,34.7828) (59.9261,34.9828) (118.6713,34.9828) (118.6713,34.7828) ratio 1.05,1.0 i 167 217 j 103 105
gen (59.9261,34.9828) (59.9261,35.1358) (118.6713,35.1358) (118.6713,34.9828) ratio 1.05,1.0 i 167 217 j 105 107
model elastic i=1,216 j=1,106

```
;delete excessive grids
model null i 1 18 j 105 106
group 'null' i 1 18 j 105 106
group delete 'null'
model null i 19 49 j 105 106
group 'null' i 19 49 j 105 106
group delete 'null'
model null i 50 85 j 105 106
group 'null' i 50 85 j 105 106
group delete 'null'
model null i 86 89 j 105 106
group 'null' i 86 89 j 105 106
group delete 'null'
model null i 91 105 j 105 106
group 'null' i 91 105 j 105 106
group delete 'null'
model null i 107 121 j 105 106
group 'null' i 107 121 j 105 106
group delete 'null'
model null i 122 124 j 105 106
group 'null' i 122 124 j 105 106
group delete 'null'
model null i 126 140 j 105 106
group 'null' i 126 140 j 105 106
group delete 'null'
model null i 142 156 j 105 106
group 'null' i 142 156 j 105 106
group delete 'null'
model null i 157 178 j 105 106
group 'null' i 157 178 j 105 106
group delete 'null'
model null i 179 192 j 105 106
group 'null' i 179 192 j 105 106
group delete 'null'
model null i 193 205 j 105 106
group 'null' i 193 205 j 105 106
group delete 'null'
model null i 207 j 105
group 'null' i 207 j 105
group delete 'null'
model null i 206 215 j 105 106
group 'null' i 206 215 j 105 106
group delete 'null'
model null i 216 j 105 106
group 'null' i 216 j 105 106
group delete 'null'
model null i 73 78 j 103 104
group 'null' i 73 78 j 103 104
group delete 'null'
model null i 54 72 j 103 104
group 'null' i 54 72 j 103 104
```

```
group delete 'null'
model null i 24 53 j 103 104
group 'null' i 24 53 j 103 104
group delete 'null'
model null i 1 23 j 103 104
group 'null' i 1 23 j 103 104
group delete 'null'
model null i 71 78 j 100 102
group 'null' i 71 78 j 100 102
group delete 'null'
model null i 37 70 j 100 102
group 'null' i 37 70 j 100 102
group delete 'null'
model null i 9 36 j 100 102
group 'null' i 9 36 j 100 102
group delete 'null'
model null i 1 8 j 100 102
group 'null' i 1 8 j 100 102
group delete 'null'
model null i 155 160 j 100 104
group 'null' i 155 160 j 100 104
group delete 'null'
model null i 153 154 j 100 104
group 'null' i 153 154 j 100 104
group delete 'null'
model null i 161 166 j 100 104
group 'null' i 161 166 j 100 104
group delete 'null'
model null i 64 j 87 99
group 'null' i 64 j 87 99
group delete 'null'
model null i 65 j 87 99
group 'null' i 65 j 87 99
group delete 'null'
model null i 17 63 j 87 99
group 'null' i 17 63 j 87 99
group delete 'null'
model null i 1 16 j 87 99
group 'null' i 1 16 j 87 99
group delete 'null'
model null i 58 61 j 83 86
group 'null' i 58 61 j 83 86
group delete 'null'
model null i 54 57 j 79 82
group 'null' i 54 57 j 79 82
group delete 'null'
model null i 51 57 j 79 86
group 'null' i 51 57 j 79 86
group delete 'null'
model null i 51 53 j 75 78
group 'null' i 51 53 j 75 78
```

```
group delete 'null'
model null i 35 50 j 75 86
group 'null' i 35 50 j 75 86
group delete 'null'
model null i 44 49 j 71 74
group 'null' i 44 49 j 71 74
group delete 'null'
model null i 36 45 j 67 70
group 'null' i 36 45 j 67 70
group delete 'null'
model null i 34 41 j 63 66
group 'null' i 34 41 j 63 66
group delete 'null'
model null i 30 37 j 59 62
group 'null' i 30 37 j 59 62
group delete 'null'
model null i 26 33 j 55 58
group 'null' i 26 33 j 55 58
group delete 'null'
model null i 25 29 j 51 54
group 'null' i 25 29 j 51 54
group delete 'null'
model null i 35 43 j 71 74
group 'null' i 35 43 j 71 74
group delete 'null'
model null i 25 35 j 63 70
group 'null' i 25 35 j 63 70
group delete 'null'
model null i 19 34 j 60 86
group 'null' i 19 34 j 60 86
group delete 'null'
model null i 19 29 j 51 59
group 'null' i 19 29 j 51 59
group delete 'null'
model null i 22 25 j 47 50
group 'null' i 22 25 j 47 50
group delete 'null'
model null i 18 21 j 43 46
group 'null' i 18 21 j 43 46
group delete 'null'
model null i 18 21 j 47 50
group 'null' i 18 21 j 47 50
group delete 'null'
model null i 13 17 j 39 42
group 'null' i 13 17 j 39 42
group delete 'null'
model null i 6 17 j 43 86
group 'null' i 6 17 j 43 86
group delete 'null'
model null i 18 j 51 86
group 'null' i 18 j 51 86
```

```
group delete 'null'
model null i 9 13 j 35 38
group 'null' i 9 13 j 35 38
group delete 'null'
model null i 7 9 j 31 34
group 'null' i 7 9 j 31 34
group delete 'null'
model null i 6 12 j 35 42
group 'null' i 6 12 j 35 42
group delete 'null'
model null i 6 j 31 34
group 'null' i 6 j 31 34
group delete 'null'
model null i 1 5 j 31 86
group 'null' i 1 5 j 31 86
;alter shape
gen 44.7369,34.478 45.7465,34.9828 46.13695,34.9828 46.13695,34.478 ratio
0.9963045,0.9960688 i 79 86 j 100 105
model null i 66 67 j 87
group 'null' i 66 67 j 87
group delete 'null'
model null i 66 67 j 88
group 'null' i 66 67 j 88
group delete 'null'
model null i 66 68 j 89 90
group 'null' i 66 68 j 89 90
group delete 'null'
model null i 66 69 j 91 92
group 'null' i 66 69 j 91 92
group delete 'null'
model null i 66 70 j 93 94
group 'null' i 66 70 j 93 94
group delete 'null'
model null i 66 71 j 95 96
group 'null' i 66 71 j 95 96
group delete 'null'
model null i 66 72 j 97 98
group 'null' i 66 72 j 97 98
group delete 'null'
model null i 66 73 j 99
group 'null' i 66 73 j 99
group delete 'null'
model null i 62 66 j 86
group 'null' i 62 66 j 86
group delete 'null'
model null i 62 65 j 85
group 'null' i 62 65 j 85
group delete 'null'
model null i 62 64 j 84
group 'null' i 62 64 j 84
group delete 'null'
```

```
model null i 62 63 j 83
group 'null' i 62 63 j 83
group delete 'null'
model null i 58 62 j 82
group 'null' i 58 62 j 82
group delete 'null'
model null i 58 61 j 81
group 'null' i 58 61 j 81
group delete 'null'
model null i 58 60 j 80
group 'null' i 58 60 j 80
group delete 'null'
model null i 58 59 j 79
group 'null' i 58 59 j 79
group delete 'null'
model null i 54 58 j 78
group 'null' i 54 58 j 78
group delete 'null'
model null i 54 57 j 77
group 'null' i 54 57 j 77
group delete 'null'
model null i 54 56 j 76
group 'null' i 54 56 j 76
group delete 'null'
model null i 54 55 j 75
group 'null' i 54 55 j 75
group delete 'null'
model null i 50 54 j 74
group 'null' i 50 54 j 74
group delete 'null'
model null i 50 53 j 73
group 'null' i 50 53 j 73
group delete 'null'
model null i 50 52 j 72
group 'null' i 50 52 j 72
group delete 'null'
model null i 50 51 j 71
group 'null' i 50 51 j 71
group delete 'null'
model null i 46 50 j 70
group 'null' i 46 50 j 70
group delete 'null'
model null i 46 49 j 69
group 'null' i 46 49 j 69
group delete 'null'
model null i 46 48 j 68
group 'null' i 46 48 j 68
group delete 'null'
model null i 46 47 j 67
group 'null' i 46 47 j 67
group delete 'null'
```

```
model null i 42 46 j 66
group 'null' i 42 46 j 66
group delete 'null'
model null i 42 45 j 65
group 'null' i 42 45 j 65
group delete 'null'
model null i 42 44 j 64
group 'null' i 42 44 j 64
group delete 'null'
model null i 42 43 j 63
group 'null' i 42 43 j 63
group delete 'null'
model null i 38 42 j 62
group 'null' i 38 42 j 62
group delete 'null'
model null i 38 41 j 61
group 'null' i 38 41 j 61
group delete 'null'
model null i 40 j 60
group 'null' i 40 j 60
group delete 'null'
model null i 38 39 j 60
group 'null' i 38 39 j 60
group delete 'null'
model null i 38 39 j 59
group 'null' i 38 39 j 59
group delete 'null'
model null i 34 38 j 58
group 'null' i 34 38 j 58
group delete 'null'
model null i 34 37 j 57
group 'null' i 34 37 j 57
group delete 'null'
model null i 34 36 j 56
group 'null' i 34 36 j 56
group delete 'null'
model null i 34 35 j 55
group 'null' i 34 35 j 55
group delete 'null'
model null i 30 34 j 54
group 'null' i 30 34 j 54
group delete 'null'
model null i 30 33 j 53
group 'null' i 30 33 j 53
group delete 'null'
model null i 30 32 j 52
group 'null' i 30 32 j 52
group delete 'null'
model null i 30 31 j 51
group 'null' i 30 31 j 51
group delete 'null'
```

```
model null i 26 30 j 50
group 'null' i 26 30 j 50
group delete 'null'
model null i 26 29 j 49
group 'null' i 26 29 j 49
group delete 'null'
model null i 26 28 j 48
group 'null' i 26 28 j 48
group delete 'null'
model null i 26 27 j 47
group 'null' i 26 27 j 47
group delete 'null'
model null i 22 26 j 46
group 'null' i 22 26 j 46
group delete 'null'
model null i 22 25 j 45
group 'null' i 22 25 j 45
group delete 'null'
model null i 22 24 j 44
group 'null' i 22 24 j 44
group delete 'null'
model null i 22 23 j 43
group 'null' i 22 23 j 43
group delete 'null'
model null i 18 22 j 42
group 'null' i 18 22 j 42
group delete 'null'
model null i 18 21 j 41
group 'null' i 18 21 j 41
group delete 'null'
model null i 10 15 j 31
group 'null' i 10 15 j 31
group delete 'null'
model null i 10 15 j 32 34
group 'null' i 10 15 j 32 34
group delete 'null'
model null i 16 j 33 34
group 'null' i 16 j 33 34
group delete 'null'
model null i 14 17 j 35 36
group 'null' i 14 17 j 35 36
group delete 'null'
model null i 14 18 j 37 38
group 'null' i 14 18 j 37 38
group delete 'null'
model null i 18 19 j 39 40
group 'null' i 18 19 j 39 40
group delete 'null'
model null i 20 j 40
group 'null' i 20 j 40
group delete 'null'
```

model null i 20 j 39
group 'null' i 20 j 39
group delete 'null'
model null i 19 j 37 38
group 'null' i 19 j 37 38
group delete 'null'
model null i 18 j 35 36
group 'null' i 18 j 35 36
group delete 'null'
model null i 17 j 34
group 'null' i 17 j 34
group delete 'null'
gen 49.0424,34.478 49.0424,34.9828 49.68045,34.663776 49.68045,34.478 ratio
0.999973,0.9960688 i 113 116 j 100 105
gen 49.68045,34.478 49.68045,34.663776 50.3185,34.9828 50.3185,34.478 ratio
0.9960738,0.99554783 i 116 119 j 100 105
gen 53.22395,34.478 53.22395,34.9828 53.6144,34.9828 54.609123,34.478 ratio
1.0041904,0.9960688 i 146 153 j 100 105
model null i 163 165 j 87
group 'null' i 163 165 j 87
group delete 'null'
model null i 163 165 j 88
group 'null' i 163 165 j 88
group delete 'null'
model null i 162 165 j 89 90
group 'null' i 162 165 j 89 90
group delete 'null'
model null i 161 164 j 91 92
group 'null' i 161 164 j 91 92
group delete 'null'
model null i 160 164 j 93 94
group 'null' i 160 164 j 93 94
group delete 'null'
model null i 159 164 j 95 96
group 'null' i 159 164 j 95 96
group delete 'null'
model null i 158 164 j 97 98
group 'null' i 158 164 j 97 98
group delete 'null'
model null i 157 j 99
group 'null' i 157 j 99
group delete 'null'
model null i 158 166 j 98 99
group 'null' i 158 166 j 98 99
group delete 'null'
model null i 165 166 j 87 97
group 'null' i 165 166 j 87 97
group delete 'null'
model null i 166 j 84
group 'null' i 166 j 84
group delete 'null'

```
model null i 165 166 j 85 86
group 'null' i 165 166 j 85 86
group delete 'null'
model null i 164 j 86
group 'null' i 164 j 86
group delete 'null'
; last step to finish grid generation
gen 59.9261,32.45235 66.2378,34.9828 74.26906,34.9828 74.26906,32.45235 ratio
1.05,0.9671929 i 167 193 j 84 105
model null i 211 216 j 31 104
group 'null' i 211 216 j 31 104
group delete 'null'
model null i 194 210 j 99 104
group 'null' i 194 210 j 99 104
group delete 'null'
model null i 195 210 j 92 98
group 'null' i 195 210 j 92 98
group delete 'null'
model null i 197 210 j 86 91
group 'null' i 197 210 j 86 91
group delete 'null'
model null i 198 210 j 83 85
group 'null' i 198 210 j 83 85
group delete 'null'
model null i 199 210 j 79 82
group 'null' i 199 210 j 79 82
group delete 'null'
model null i 200 210 j 76 78
group 'null' i 200 210 j 76 78
group delete 'null'
model null i 201 210 j 73 75
group 'null' i 201 210 j 73 75
group delete 'null'
model null i 202 210 j 68 72
group 'null' i 202 210 j 68 72
group delete 'null'
model null i 203 210 j 64 67
group 'null' i 203 210 j 64 67
group delete 'null'
model null i 204 210 j 61 63
group 'null' i 204 210 j 61 63
group delete 'null'
model null i 205 210 j 58 60
group 'null' i 205 210 j 58 60
group delete 'null'
model null i 206 210 j 54 57
group 'null' i 206 210 j 54 57
group delete 'null'
model null i 207 210 j 50 53
group 'null' i 207 210 j 50 53
group delete 'null'
```

```
model null i 208 210 j 45 49
group 'null' i 208 210 j 45 49
group delete 'null'
model null i 209 210 j 41 44
group 'null' i 209 210 j 41 44
group delete 'null'
model null i 210 j 36 40
group 'null' i 210 j 36 40
group delete 'null'
;assign properties
group 'User:rail' i 90 j 105 106
model elastic group 'User:rail'
prop density=7842.0 bulk=1.75E11 shear=8.07692E10 group 'User:rail'
group 'User:rail' i 106 j 105 106
model elastic group 'User:rail'
prop density=7842.0 bulk=1.75E11 shear=8.07692E10 group 'User:rail'
group 'User:rail' i 125 j 105 106
model elastic group 'User:rail'
prop density=7842.0 bulk=1.75E11 shear=8.07692E10 group 'User:rail'
group 'User:rail' i 141 j 105 106
model elastic group 'User:rail'
prop density=7842.0 bulk=1.75E11 shear=8.07692E10 group 'User:rail'
group 'User:sleeper' i 86 110 j 103 104
model elastic group 'User:sleeper'
prop density=2398.0 bulk=9.6667E9 shear=4.4615E9 group 'User:sleeper'
group 'User:sleeper' i 121 145 j 103 104
model elastic group 'User:sleeper'
prop density=2398.0 bulk=9.6667E9 shear=4.4615E9 group 'User:sleeper'
group 'User:ballast' i 79 115 j 100 102
model elastic group 'User:ballast'
prop density=2002 bulk=1.3750E8 shear=6.3462E7 group 'User:ballast'
group 'User:ballast' i 79 85 j 103 104
model elastic group 'User:ballast'
prop density=2002 bulk=1.3750E8 shear=6.3462E7 group 'User:ballast'
group 'User:ballast' i 111 115 j 103 104
model elastic group 'User:ballast'
prop density=2002 bulk=1.3750E8 shear=6.3462E7 group 'User:ballast'
group 'User:ballast' i 116 120 j 100 104
model elastic group 'User:ballast'
prop density=2002 bulk=1.3750E8 shear=6.3462E7 group 'User:ballast'
group 'User:ballast' i 121 145 j 100 102
model elastic group 'User:ballast'
prop density=2002 bulk=1.3750E8 shear=6.3462E7 group 'User:ballast'
group 'User:ballast' i 146 152 j 100 104
model elastic group 'User:ballast'
prop density=2002 bulk=1.3750E8 shear=6.3462E7 group 'User:ballast'
group 'User:sub-ballast' notnull i 74 157 j 98 99
model elastic notnull group 'User:sub-ballast'
prop density=2002 bulk=2.16667E9 shear=4.36242E7 notnull group 'User:sub-ballast'
group 'User:sub-ballast' i 73 j 98
model elastic group 'User:sub-ballast'
```

prop density=2002 bulk=2.16667E9 shear=4.36242E7 group 'User:sub-ballast'
group 'User:Structural Fill' notnull i 69 157 j 89 97
model elastic notnull group 'User:Structural Fill'
prop density=1922.2 bulk=3.33333E8 shear=1.53846E8 notnull group 'User:Structural Fill'
group 'User:Structural Fill' notnull i 158 161 j 89 96
model elastic notnull group 'User:Structural Fill'
prop density=1922.2 bulk=3.33333E8 shear=1.53846E8 notnull group 'User:Structural Fill'
group 'User:Structural Fill' i 68 76 j 87 88
model elastic group 'User:Structural Fill'
prop density=1922.2 bulk=3.33333E8 shear=1.53846E8 group 'User:Structural Fill'
group 'User:Structural Fill' i 155 162 j 87 88
model elastic group 'User:Structural Fill'
prop density=1922.2 bulk=3.33333E8 shear=1.53846E8 group 'User:Structural Fill'
group 'User:Structural Fill' notnull i 163 165 j 84 86
model elastic notnull group 'User:Structural Fill'
prop density=1922.2 bulk=3.33333E8 shear=1.53846E8 notnull group 'User:Structural Fill'
group 'User:Structural Fill' i 163 164 j 83
model elastic group 'User:Structural Fill'
prop density=1922.2 bulk=3.33333E8 shear=1.53846E8 group 'User:Structural Fill'
group 'User:Structural Fill' notnull i 64 69 j 83 86
model elastic notnull group 'User:Structural Fill'
prop density=1922.2 bulk=3.33333E8 shear=1.53846E8 notnull group 'User:Structural Fill'
group 'User:Structural Fill' notnull i 60 65 j 79 82
model elastic notnull group 'User:Structural Fill'
prop density=1922.2 bulk=3.33333E8 shear=1.53846E8 notnull group 'User:Structural Fill'
group 'User:Structural Fill' notnull i 56 61 j 75 78
model elastic notnull group 'User:Structural Fill'
prop density=1922.2 bulk=3.33333E8 shear=1.53846E8 notnull group 'User:Structural Fill'
group 'User:Structural Fill' notnull i 52 57 j 71 74
model elastic notnull group 'User:Structural Fill'
prop density=1922.2 bulk=3.33333E8 shear=1.53846E8 notnull group 'User:Structural Fill'
group 'User:Structural Fill' notnull i 48 53 j 67 70
model elastic notnull group 'User:Structural Fill'
prop density=1922.2 bulk=3.33333E8 shear=1.53846E8 notnull group 'User:Structural Fill'
group 'User:Structural Fill' notnull i 44 49 j 63 66
model elastic notnull group 'User:Structural Fill'
prop density=1922.2 bulk=3.33333E8 shear=1.53846E8 notnull group 'User:Structural Fill'
group 'User:Structural Fill' notnull i 40 45 j 59 62
model elastic notnull group 'User:Structural Fill'
prop density=1922.2 bulk=3.33333E8 shear=1.53846E8 notnull group 'User:Structural Fill'
group 'User:Structural Fill' notnull i 36 41 j 55 58
model elastic notnull group 'User:Structural Fill'
prop density=1922.2 bulk=3.33333E8 shear=1.53846E8 notnull group 'User:Structural Fill'
group 'User:Structural Fill' notnull i 32 37 j 51 54
model elastic notnull group 'User:Structural Fill'
prop density=1922.2 bulk=3.33333E8 shear=1.53846E8 notnull group 'User:Structural Fill'
group 'User:Structural Fill' notnull i 28 33 j 47 50
model elastic notnull group 'User:Structural Fill'
prop density=1922.2 bulk=3.33333E8 shear=1.53846E8 notnull group 'User:Structural Fill'
group 'User:Structural Fill' notnull i 24 29 j 43 46
model elastic notnull group 'User:Structural Fill'

```
prop density=1922.2 bulk=3.33333E8 shear=1.53846E8 notnull group 'User:Structural Fill'
group 'User:Structural Fill' notnull i 21 25 j 39 42
model elastic notnull group 'User:Structural Fill'
prop density=1922.2 bulk=3.33333E8 shear=1.53846E8 notnull group 'User:Structural Fill'
group 'User:Structural Fill' notnull i 19 21 j 35 38
model elastic notnull group 'User:Structural Fill'
prop density=1922.2 bulk=3.33333E8 shear=1.53846E8 notnull group 'User:Structural Fill'
group 'User:Structural Fill' notnull i 16 22 j 31 34
model elastic notnull group 'User:Structural Fill'
prop density=1922.2 bulk=3.33333E8 shear=1.53846E8 notnull group 'User:Structural Fill'
group 'User:Foundation soil' i 165 166 j 79 83
model elastic group 'User:Foundation soil'
prop density=1840.0 bulk=2.9E8 shear=6.21429E7 group 'User:Foundation soil'
group 'User:Foundation soil' i 161 166 j 75 78
model elastic group 'User:Foundation soil'
prop density=1840.0 bulk=2.9E8 shear=6.21429E7 group 'User:Foundation soil'
group 'User:Foundation soil' i 157 166 j 71 74
model elastic group 'User:Foundation soil'
prop density=1840.0 bulk=2.9E8 shear=6.21429E7 group 'User:Foundation soil'
group 'User:Foundation soil' i 156 j 71 74
model elastic group 'User:Foundation soil'
prop density=1840.0 bulk=2.9E8 shear=6.21429E7 group 'User:Foundation soil'
group 'User:Foundation soil' i 148 162 j 67 70
model elastic group 'User:Foundation soil'
prop density=1840.0 bulk=2.9E8 shear=6.21429E7 group 'User:Foundation soil'
group 'User:Foundation soil' i 147 j 67 70
model elastic group 'User:Foundation soil'
prop density=1840.0 bulk=2.9E8 shear=6.21429E7 group 'User:Foundation soil'
group 'User:Foundation soil' i 128 164 j 63 66
model elastic group 'User:Foundation soil'
prop density=1840.0 bulk=2.9E8 shear=6.21429E7 group 'User:Foundation soil'
group 'User:Foundation soil' i 116 151 j 59 62
model elastic group 'User:Foundation soil'
prop density=1840.0 bulk=2.9E8 shear=6.21429E7 group 'User:Foundation soil'
group 'User:Foundation soil' i 102 151 j 55 58
model elastic group 'User:Foundation soil'
prop density=1840.0 bulk=2.9E8 shear=6.21429E7 group 'User:Foundation soil'
group 'User:Foundation soil' i 85 118 j 51 54
model elastic group 'User:Foundation soil'
prop density=1840.0 bulk=2.9E8 shear=6.21429E7 group 'User:Foundation soil'
group 'User:Foundation soil' i 74 106 j 47 50
model elastic group 'User:Foundation soil'
prop density=1840.0 bulk=2.9E8 shear=6.21429E7 group 'User:Foundation soil'
group 'User:Foundation soil' i 70 106 j 43 46
model elastic group 'User:Foundation soil'
prop density=1840.0 bulk=2.9E8 shear=6.21429E7 group 'User:Foundation soil'
group 'User:Foundation soil' i 66 73 j 39 42
model elastic group 'User:Foundation soil'
prop density=1840.0 bulk=2.9E8 shear=6.21429E7 group 'User:Foundation soil'
group 'User:Foundation soil' i 62 73 j 35 38
model elastic group 'User:Foundation soil'
```

```
prop density=1840.0 bulk=2.9E8 shear=6.21429E7 group 'User:Foundation soil'
group 'User:Foundation soil' i 58 73 j 31 34
model elastic group 'User:Foundation soil'
prop density=1840.0 bulk=2.9E8 shear=6.21429E7 group 'User:Foundation soil'
group 'User:Foundation soil' i 1 147 j 1 30
model elastic group 'User:Foundation soil'
prop density=1840.0 bulk=2.9E8 shear=6.21429E7 group 'User:Foundation soil'
group 'User:Foundation soil' i 74 160 j 31 42
model elastic group 'User:Foundation soil'
prop density=1840.0 bulk=2.9E8 shear=6.21429E7 group 'User:Foundation soil'
group 'User:Foundation soil' i 107 160 j 43 50
model elastic group 'User:Foundation soil'
prop density=1840.0 bulk=2.9E8 shear=6.21429E7 group 'User:Foundation soil'
group 'User:Foundation soil' i 119 160 j 51 54
model elastic group 'User:Foundation soil'
prop density=1840.0 bulk=2.9E8 shear=6.21429E7 group 'User:Foundation soil'
group 'User:Foundation soil' i 152 160 j 55 62
model elastic group 'User:Foundation soil'
prop density=1840.0 bulk=2.9E8 shear=6.21429E7 group 'User:Foundation soil'
group 'User:Foundation soil' i 148 200 j 1 30
model elastic group 'User:Foundation soil'
prop density=1840.0 bulk=2.9E8 shear=6.21429E7 group 'User:Foundation soil'
group 'User:Foundation soil' i 161 200 j 31 62
model elastic group 'User:Foundation soil'
prop density=1840.0 bulk=2.9E8 shear=6.21429E7 group 'User:Foundation soil'
group 'User:Foundation soil' i 163 200 j 67 70
model elastic group 'User:Foundation soil'
prop density=1840.0 bulk=2.9E8 shear=6.21429E7 group 'User:Foundation soil'
group 'User:Foundation soil' i 165 200 j 63 66
model elastic group 'User:Foundation soil'
prop density=1840.0 bulk=2.9E8 shear=6.21429E7 group 'User:Foundation soil'
group 'User:Foundation soil' i 167 193 j 71 104
model elastic group 'User:Foundation soil'
prop density=1840.0 bulk=2.9E8 shear=6.21429E7 group 'User:Foundation soil'
group 'User:Foundation soil' notnull i 194 201 j 71 98
model elastic notnull group 'User:Foundation soil'
prop density=1840.0 bulk=2.9E8 shear=6.21429E7 notnull group 'User:Foundation soil'
group 'User:Foundation soil' notnull i 201 216 j 1 70
model elastic notnull group 'User:Foundation soil'
prop density=1840.0 bulk=2.9E8 shear=6.21429E7 notnull group 'User:Foundation soil'
group 'User:LDS' i 77 154 j 87 88
model elastic group 'User:LDS'
prop density=2400.0 bulk=1.56E10 shear=1.27E10 group 'User:LDS'
group 'User:EPS 39' i 70 162 j 83 86
model elastic group 'User:EPS 39'
prop density=38.4 bulk=4.3241E6 shear=4.66908E6 group 'User:EPS 39'
group 'User:EPS 29' i 66 164 j 79 82
model elastic group 'User:EPS 29'
prop density=28.8 bulk=3.14861E6 shear=3.39982E6 group 'User:EPS 29'
group 'User:EPS 29' i 62 160 j 75 78
model elastic group 'User:EPS 29'
```

```
prop density=28.8 bulk=3.14861E6 shear=3.39982E6 group 'User:EPS 29'
group 'User:EPS 29' i 58 155 j 71 74
model elastic group 'User:EPS 29'
prop density=28.8 bulk=3.14861E6 shear=3.39982E6 group 'User:EPS 29'
group 'User:EPS 29' i 54 146 j 67 70
model elastic group 'User:EPS 29'
prop density=28.8 bulk=3.14861E6 shear=3.39982E6 group 'User:EPS 29'
group 'User:EPS 22' i 50 127 j 63 66
model elastic group 'User:EPS 22'
prop density=21.6 bulk=2.09908E6 shear=2.26655E6 group 'User:EPS 22'
group 'User:EPS 22' i 46 115 j 59 62
model elastic group 'User:EPS 22'
prop density=21.6 bulk=2.09908E6 shear=2.26655E6 group 'User:EPS 22'
group 'User:EPS 22' i 42 101 j 55 58
model elastic group 'User:EPS 22'
prop density=21.6 bulk=2.09908E6 shear=2.26655E6 group 'User:EPS 22'
group 'User:EPS 22' i 38 84 j 51 54
model elastic group 'User:EPS 22'
prop density=21.6 bulk=2.09908E6 shear=2.26655E6 group 'User:EPS 22'
group 'User:EPS 22' i 34 73 j 47 50
model elastic group 'User:EPS 22'
prop density=21.6 bulk=2.09908E6 shear=2.26655E6 group 'User:EPS 22'
group 'User:EPS 22' i 30 69 j 43 46
model elastic group 'User:EPS 22'
prop density=21.6 bulk=2.09908E6 shear=2.26655E6 group 'User:EPS 22'
group 'User:EPS 22' i 26 65 j 39 42
model elastic group 'User:EPS 22'
prop density=21.6 bulk=2.09908E6 shear=2.26655E6 group 'User:EPS 22'
group 'User:EPS 22' i 22 61 j 35 38
model elastic group 'User:EPS 22'
prop density=21.6 bulk=2.09908E6 shear=2.26655E6 group 'User:EPS 22'
group 'User:EPS 22' i 23 57 j 31 34
model elastic group 'User:EPS 22'
prop density=21.6 bulk=2.09908E6 shear=2.26655E6 group 'User:EPS 22'
model null i 99 j 104
group 'null' i 99 j 104
group delete 'null'
model null i 99 115 j 86 103
group 'null' i 99 115 j 86 103
group delete 'null'
model null i 99 142 j 70 85
group 'null' i 99 142 j 70 85
group delete 'null'
model null i 99 157 j 38 69
group 'null' i 99 157 j 38 69
group delete 'null'
model null i 99 162 j 10 37
group 'null' i 99 162 j 10 37
group delete 'null'
model null i 99 164 j 1 9
group 'null' i 99 164 j 1 9
```

```
group delete 'null'
model null i 165 202 j 1 35
group 'null' i 165 202 j 1 35
group delete 'null'
model null i 163 164 j 10 36
group 'null' i 163 164 j 10 36
group delete 'null'
model null i 100 178 j 70 104
group 'null' i 100 178 j 70 104
group delete 'null'
model null i 106 j 105 106
group 'null' i 106 j 105 106
group delete 'null'
model null i 125 j 105 106
group 'null' i 125 j 105 106
group delete 'null'
model null i 141 j 105 106
group 'null' i 141 j 105 106
group delete 'null'
model null i 158 188 j 36 69
group 'null' i 158 188 j 36 69
group delete 'null'
model null i 179 193 j 70 104
group 'null' i 179 193 j 70 104
group delete 'null'
model null i 189 203 j 36 69
group 'null' i 189 203 j 36 69
group delete 'null'
model null i 194 201 j 70 98
group 'null' i 194 201 j 70 98
group delete 'null'
model null i 204 216 j 1 60
group 'null' i 204 216 j 1 60
group delete 'null'
model null i 203 j 1 35
group 'null' i 203 j 1 35
group delete 'null'
;group 'User:EPS 22' i 85 98 j 51 54
;model elastic group 'User:EPS 22'
;prop density=21.6 bulk=2.09908E6 shear=2.26655E6 group 'User:EPS 22'
;group 'User:EPS 22' i 74 98 j 47 50
;model elastic group 'User:EPS 22'
;prop density=21.6 bulk=2.09908E6 shear=2.26655E6 group 'User:EPS 22'
;group 'User:EPS 22' i 70 98 j 43 46
;model elastic group 'User:EPS 22'
;prop density=21.6 bulk=2.09908E6 shear=2.26655E6 group 'User:EPS 22'
;group 'User:EPS 22' i 66 98 j 39 42
;model elastic group 'User:EPS 22'
;prop density=21.6 bulk=2.09908E6 shear=2.26655E6 group 'User:EPS 22'
;group 'User:EPS 22' i 62 98 j 35 38
;model elastic group 'User:EPS 22'
```

```
;prop density=21.6 bulk=2.09908E6 shear=2.26655E6 group 'User:EPS 22'
;group 'User:EPS 22' i 58 98 j 31 34
;model elastic group 'User:EPS 22'
;prop density=21.6 bulk=2.09908E6 shear=2.26655E6 group 'User:EPS 22'
;group 'User:EPS 22' i 22 j 31 34
;model elastic group 'User:EPS 22'
;prop density=21.6 bulk=2.09908E6 shear=2.26655E6 group 'User:EPS 22'
;boundary conditions
;settlement duing to self weight of the system is already finished
;set gravity=9.81
fix  x y i 1 99 j 1
fix  x y i 1 j 1 31
fix  x i 99 j 1 105
model null i 1 98 j 1 8
group 'null' i 1 98 j 1 8
group delete 'null'
model null i 1 6 j 9 30
group 'null' i 1 6 j 9 30
group delete 'null'
fix  x y i 7 99 j 9
fix  x y i 7 j 9 31
model null i 7 98 j 9 15
group 'null' i 7 98 j 9 15
group delete 'null'
model null i 7 11 j 16 30
group 'null' i 7 11 j 16 30
group delete 'null'
fix  x y i 12 99 j 16
fix  x y i 12 j 16 31
model null i 12 15 j 16 30
group 'null' i 12 15 j 16 30
group delete 'null'
model null j 16 30
group 'null' j 16 30
group delete 'null'
fix  x y i 16 99 j 31
fix  x y i 16 j 31 33
apply yforce -45584 from 90,107 to 90,107
apply yforce -45584 from 91,107 to 91,107
solve
```

F.2 3D Model

The codes presented here are for the model of final iteration.

```
set mechanical ratio 0.5e-5
gen zone brick size 80 95 80 p0 0 0 0 p1 32.39445 0 0 p2 0 23.75 0 p3 0 0 15.1358 ratio 0.96 1.0
0.96;
model elas
```

prop bulk 3.33333e8 shear 1.53846e8 range x 0 32.39445 y 0 23.75 z 0 15.1358; fill in shoulder of slope EPS and under subballast
model null range x 0 31.58645 z 14.9828 15.1358; outside of rail
model null range x 31.66445 32.39445 z 14.9828 15.1358; inside of rail
model null range x 0 31.1365 z 14.9328 14.9828; outside of upper sleeper
model null range y 0.249 0.751 z 14.9328 14.9828 ; gap under rail between sleepers
model null range y 0.999 1.501 z 14.9328 14.9828 ; gap under rail between sleepers
model null range y 1.749 2.251 z 14.9328 14.9828 ; gap under rail between sleepers
model null range y 2.499 3.001 z 14.9328 14.9828 ; gap under rail between sleepers
model null range y 3.249 3.751 z 14.9328 14.9828 ; gap under rail between sleepers
model null range y 3.999 4.501 z 14.9328 14.9828 ; gap under rail between sleepers
model null range y 4.749 5.251 z 14.9328 14.9828 ; gap under rail between sleepers
model null range y 5.499 6.001 z 14.9328 14.9828 ; gap under rail between sleepers
model null range y 6.249 6.751 z 14.9328 14.9828 ; gap under rail between sleepers
model null range y 6.999 7.501 z 14.9328 14.9828 ; gap under rail between sleepers
model null range y 7.749 8.251 z 14.9328 14.9828 ; gap under rail between sleepers
model null range y 8.499 9.001 z 14.9328 14.9828 ; gap under rail between sleepers
model null range y 9.249 9.751 z 14.9328 14.9828 ; gap under rail between sleepers
model null range y 9.999 10.501 z 14.9328 14.9828 ; gap under rail between sleepers
model null range y 10.749 11.251 z 14.9328 14.9828 ; gap under rail between sleepers
model null range y 11.499 12.001 z 14.9328 14.9828 ; gap under rail between sleepers
model null range y 12.249 12.751 z 14.9328 14.9828 ; gap under rail between sleepers
model null range y 12.999 13.501 z 14.9328 14.9828 ; gap under rail between sleepers
model null range y 13.749 14.251 z 14.9328 14.9828 ; gap under rail between sleepers
model null range y 14.499 15.001 z 14.9328 14.9828 ; gap under rail between sleepers
model null range y 15.249 15.751 z 14.9328 14.9828 ; gap under rail between sleepers
model null range y 15.9 16.6 z 14.9328 14.9828 ; gap under rail between sleepers
model null range y 16.7 17.3 z 14.9328 14.9828 ; gap under rail between sleepers
model null range y 17.499 18.001 z 14.9328 14.9828 ; gap under rail between sleepers
model null range y 18.249 18.751 z 14.9328 14.9828 ; gap under rail between sleepers
model null range y 18.999 19.501 z 14.9328 14.9828 ; gap under rail between sleepers
model null range y 19.749 20.251 z 14.9328 14.9828 ; gap under rail between sleepers
model null range y 20.499 21.001 z 14.9328 14.9828 ; gap under rail between sleepers
model null range y 21.249 21.751 z 14.9328 14.9828 ; gap under rail between sleepers
model null range y 21.999 22.501 z 14.9328 14.9828 ; gap under rail between sleepers
model null range y 22.749 23.251 z 14.9328 14.9828 ; gap under rail between sleepers
model null range y 23.499 23.75 z 14.9328 14.9828 ; gap under rail between sleepers
model null range x 0 30.7065 z 14.8987 14.9828 ; outside of ballast 1
model null range x 0 30.5782 z 14.8145 14.8987 ; outside of ballast 2
model null range x 0 30.4100 z 14.7304 14.8145 ; outside of ballast 3
model null range x 0 30.2417 z 14.6463 14.7304 ; outside of ballast 4
model null range x 0 30.0734 z 14.5621 14.6463 ; outside of ballast 5
model null range x 0 29.9052 z 14.4780 14.5621 ; outside of ballast 6

model null range x 0 28.5496 z 14.2748 14.478; outside of subballast
model null range x 0 28.5496 z 14.0518 14.2748; outside of structual fill 1
model null range x 0 28.0077 z 13.8289 14.0518; outside of structual fill 2
model null range x 0 27.4658 z 13.6059 13.8289; outside of structual fill 3
model null range x 0 26.9238 z 13.3830 13.6059; outside of structual fill 4
model null range x 0 26.3819 z 13.1600 13.3830; outside of structual fill 5
model null range x 0 25.8400 z 12.9250 13.1600 ; out side of EPS 1

model null range x 0 25.3786 z 12.6900 12.9250 ; out side of EPS 2
model null range x 0 24.9171 z 12.4550 12.6900 ; out side of EPS 3
model null range x 0 24.4557 z 12.2200 12.4550 ; out side of EPS 4
model null range x 0 23.9943 z 11.9850 12.2200 ; out side of EPS 5
model null range x 0 23.5329 z 11.7500 11.9850 ; out side of EPS 6
model null range x 0 23.0714 z 11.5150 11.7500 ; out side of EPS 7
model null range x 0 22.6100 z 11.2800 11.5150 ; out side of EPS 8
model null range x 0 22.1486 z 11.0450 11.2800 ; out side of EPS 9
model null range x 0 21.6871 z 10.8100 11.0450 ; out side of EPS 10
model null range x 0 21.2257 z 10.5750 10.8100 ; out side of EPS 11
model null range x 0 20.7643 z 10.3400 10.5750 ; out side of EPS 12
model null range x 0 20.3029 z 10.1050 10.3400 ; out side of EPS 13
model null range x 0 19.8414 z 9.8700 10.1050 ; out side of EPS 14
model null range x 0 19.3800 z 9.6350 9.8700 ; out side of EPS 15
model null range x 0 18.9186 z 9.4000 9.6350 ; out side of EPS 16
model null range x 0 18.4571 z 9.1650 9.4000 ; out side of EPS 17
model null range x 0 17.9957 z 8.9300 9.1650 ; out side of EPS 18
model null range x 0 17.5343 z 8.6950 8.9300 ; out side of EPS 19
model null range x 0 17.0729 z 8.4600 8.6950 ; out side of EPS 20
model null range x 0 16.6114 z 8.2250 8.4600 ; out side of EPS 21
model null range x 0 16.1500 z 7.9900 8.2250 ; out side of EPS 22
model null range x 0 15.6886 z 7.7550 7.9900 ; out side of EPS 23
model null range x 0 15.2271 z 7.5200 7.7550 ; out side of EPS 24
model null range x 0 14.7657 z 7.2850 7.5200 ; out side of EPS 25
model null range x 0 14.3043 z 7.0500 7.2850 ; out side of EPS 26
model null range x 0 13.8429 z 6.8150 7.0500 ; out side of EPS 27
model null range x 0 13.3814 z 6.5800 6.8150 ; out side of EPS 28
model null range x 0 12.9200 z 6.3450 6.5800 ; out side of EPS 29
model null range x 0 12.4586 z 6.1100 6.3450 ; out side of EPS 30
model null range x 0 11.9971 z 5.8750 6.1100 ; out side of EPS 31
model null range x 0 11.5357 z 5.6400 5.8750 ; out side of EPS 32
model null range x 0 11.0743 z 5.4050 5.6400 ; out side of EPS 33
model null range x 0 10.6129 z 5.1700 5.4050 ; out side of EPS 34
model null range x 0 10.1514 z 4.9350 5.1700 ; out side of EPS 35
model null range x 0 9.6900 z 4.7000 4.9350 ; out side of EPS 36
model null range x 0 9.2286 z 4.4650 4.7000 ; out side of EPS 37
model null range x 0 8.7671 z 4.2300 4.4650 ; out side of EPS 38
model null range x 0 8.3057 z 3.9950 4.2300 ; out side of EPS 39
model null range x 0 7.8443 z 3.7600 3.9950 ; out side of EPS 40
model null range x 0 7.3829 z 3.5250 3.7600 ; out side of EPS 41
model null range x 0 6.9214 z 3.2900 3.5250 ; out side of EPS 42
model null range x 0 6.4600 z 3.0550 3.2900 ; out side of EPS 43
model null range x 0 5.9986 z 2.8200 3.0550 ; out side of EPS 44
model null range x 0 5.5371 z 2.5850 2.8200 ; out side of EPS 45
model null range x 0 5.0757 z 2.3500 2.5850 ; out side of EPS 46
model null range x 0 4.6143 z 2.1150 2.3500 ; out side of EPS 47
model null range x 0 4.1529 z 1.8800 2.1150 ; out side of EPS 48
model null range x 0 3.6914 z 1.6450 1.8800 ; out side of EPS 49
model null range x 0 3.2300 z 1.4100 1.6450 ; out side of EPS 50
model null range x 0 2.7686 z 1.1750 1.4100 ; out side of EPS 51
model null range x 0 2.3071 z 0.9400 1.1750 ; out side of EPS 52

model null range x 0 1.8457 z 0.7050 0.9400 ; out side of EPS 53
model null range x 0 1.3843 z 0.4700 0.7050 ; out side of EPS 54
model null range x 0 0.9229 z 0.2350 0.4700 ; out side of EPS 55
model null range x 0 0.4614 z 0.0000 0.2350 ; out side of EPS 56
prop bulk 1.75e11 shear 8.07692e10 range z 14.9828 15.1358; rail steel
prop bulk 1.6361e7 shear 7.5513e6 range z 14.478 14.9328; ballast
prop bulk 28333e6 shear 13077e6 range x 31.1365 32.39445 y -0.001 0.251 z 14.7828 14.9828 ; sleeper concrete 1
prop bulk 28333e6 shear 13077e6 range x 31.1365 32.39445 y 0.749 1.001 z 14.7828 14.9828 ; sleeper concrete 2
prop bulk 28333e6 shear 13077e6 range x 31.1365 32.39445 y 1.499 1.751 z 14.7828 14.9828 ; sleeper concrete 3
prop bulk 28333e6 shear 13077e6 range x 31.1365 32.39445 y 2.249 2.501 z 14.7828 14.9828 ; sleeper concrete 4
prop bulk 28333e6 shear 13077e6 range x 31.1365 32.39445 y 2.999 3.251 z 14.7828 14.9828 ; sleeper concrete 5
prop bulk 28333e6 shear 13077e6 range x 31.1365 32.39445 y 3.749 4.001 z 14.7828 14.9828 ; sleeper concrete 6
prop bulk 28333e6 shear 13077e6 range x 31.1365 32.39445 y 4.499 4.751 z 14.7828 14.9828 ; sleeper concrete 7
prop bulk 28333e6 shear 13077e6 range x 31.1365 32.39445 y 5.249 5.501 z 14.7828 14.9828 ; sleeper concrete 8
prop bulk 28333e6 shear 13077e6 range x 31.1365 32.39445 y 5.999 6.251 z 14.7828 14.9828 ; sleeper concrete 9
prop bulk 28333e6 shear 13077e6 range x 31.1365 32.39445 y 6.749 7.001 z 14.7828 14.9828 ; sleeper concrete 10
prop bulk 28333e6 shear 13077e6 range x 31.1365 32.39445 y 7.449 7.751 z 14.7828 14.9828 ; sleeper concrete 11
prop bulk 28333e6 shear 13077e6 range x 31.1365 32.39445 y 8.249 8.501 z 14.7828 14.9828 ; sleeper concrete 12
prop bulk 28333e6 shear 13077e6 range x 31.1365 32.39445 y 8.999 9.251 z 14.7828 14.9828 ; sleeper concrete 13
prop bulk 28333e6 shear 13077e6 range x 31.1365 32.39445 y 9.749 10.001 z 14.7828 14.9828 ; sleeper concrete 14
prop bulk 28333e6 shear 13077e6 range x 31.1365 32.39445 y 10.499 10.751 z 14.7828 14.9828 ; sleeper concrete 15
prop bulk 28333e6 shear 13077e6 range x 31.1365 32.39445 y 11.249 11.501 z 14.7828 14.9828 ; sleeper concrete 16
prop bulk 28333e6 shear 13077e6 range x 31.1365 32.39445 y 11.999 12.251 z 14.7828 14.9828 ; sleeper concrete 17
prop bulk 28333e6 shear 13077e6 range x 31.1365 32.39445 y 12.749 13.001 z 14.7828 14.9828 ; sleeper concrete 18
prop bulk 28333e6 shear 13077e6 range x 31.1365 32.39445 y 13.499 13.751 z 14.7828 14.9828 ; sleeper concrete 19
prop bulk 28333e6 shear 13077e6 range x 31.1365 32.39445 y 14.249 14.501 z 14.7828 14.9828 ; sleeper concrete 20
prop bulk 28333e6 shear 13077e6 range x 31.1365 32.39445 y 14.999 15.251 z 14.7828 14.9828 ; sleeper concrete 21
prop bulk 28333e6 shear 13077e6 range x 31.1365 32.39445 y 15.749 16.001 z 14.7828 14.9828 ; sleeper concrete 22
prop bulk 28333e6 shear 13077e6 range x 31.1365 32.39445 y 16.4 16.8 z 14.7828 14.9828 ;

```
sleeper concrete 23
prop bulk 28333e6 shear 13077e6 range x 31.1365 32.39445 y 17.2 17.6 z 14.7828 14.9828 ;
sleeper concrete 24
prop bulk 28333e6 shear 13077e6 range x 31.1365 32.39445 y 17.999 18.251 z 14.7828 14.9828
; sleeper concrete 25
prop bulk 28333e6 shear 13077e6 range x 31.1365 32.39445 y 18.749 19.001 z 14.7828 14.9828
; sleeper concrete 26
prop bulk 28333e6 shear 13077e6 range x 31.1365 32.39445 y 19.499 19.751 z 14.7828 14.9828
; sleeper concrete 27
prop bulk 28333e6 shear 13077e6 range x 31.1365 32.39445 y 20.249 20.501 z 14.7828 14.9828
; sleeper concrete 28
prop bulk 28333e6 shear 13077e6 range x 31.1365 32.39445 y 20.999 21.251 z 14.7828 14.9828
; sleeper concrete 29
prop bulk 28333e6 shear 13077e6 range x 31.1365 32.39445 y 21.749 22.001 z 14.7828 14.9828
; sleeper concrete 30
prop bulk 28333e6 shear 13077e6 range x 31.1365 32.39445 y 22.499 22.751 z 14.7828 14.9828
; sleeper concrete 31
prop bulk 28333e6 shear 13077e6 range x 31.1365 32.39445 y 23.249 23.501 z 14.7828 14.9828
; sleeper concrete 32
prop bulk 2.16667e9 shear 4.36242e7 range z 14.2748 14.478; subballast
prop bulk 1.56e10 shear 1.27e10 range x 29.4 32.39445 z 13.1572 13.3604; LDS
prop bulk 4.3241e6 shear 4.66908e6 range x 27.2 32.39445 z 12.2 13.1572; EPS39
prop bulk 3.14861e6 shear 3.39982e6 range x 25.3 32.39445 z 11.3 12.2; EPS29 1
prop bulk 3.14861e6 shear 3.39982e6 range x 23.4 32.39445 z 10.3378 11.3; EPS29 2
prop bulk 3.14861e6 shear 3.39982e6 range x 21.6154 32.39445 z 9.395 10.3378; EPS29 3
prop bulk 3.14861e6 shear 3.39982e6 range x 19.7358 32.39445 z 8.4582 9.395; EPS29 4
prop bulk 2.09908e6 shear 2.26655e6 range x 17.8562 32.39445 z 7.5184 8.4582; EPS22 1
prop bulk 2.09908e6 shear 2.26655e6 range x 15.9766 32.39445 z 6.5786 7.5184; EPS22 2
prop bulk 2.09908e6 shear 2.26655e6 range x 14.097 32.39445 z 5.6388 6.5786; EPS22 3
prop bulk 2.09908e6 shear 2.26655e6 range x 12.2174 30.9 z 4.699 5.6388; EPS22 4
prop bulk 2.09908e6 shear 2.26655e6 range x 10.3378 28.9 z 3.7592 4.699; EPS22 5
prop bulk 2.09908e6 shear 2.26655e6 range x 8.4582 27.1 z 2.8194 3.7592; EPS22 6
prop bulk 2.09908e6 shear 2.26655e6 range x 6.5786 25.3 z 1.8796 2.8194; EPS22 7
prop bulk 2.09908e6 shear 2.26655e6 range x 4.699 23.4 z 0.9398 1.8796; EPS22 8
prop bulk 2.09908e6 shear 2.26655e6 range x 5.1689 21.6154 z 0 0.9398; EPS22 9
prop bulk 2.9e8 shear 6.21429e7 range x 30.9 32.39445 z 4.699 5.6388; Foundation soil 1
prop bulk 2.9e8 shear 6.21429e7 range x 28.9 32.39445 z 3.7592 4.699; Foundation soil 2
prop bulk 2.9e8 shear 6.21429e7 range x 27.1 32.39445 z 2.8194 3.7592; Foundation soil 3
prop bulk 2.9e8 shear 6.21429e7 range x 25.3 32.39445 z 1.8796 2.8194; Foundation soil 4
prop bulk 2.9e8 shear 6.21429e7 range x 23.4 32.39445 z 0.9398 1.8796; Foundation soil 5
prop bulk 2.9e8 shear 6.21429e7 range x 21.6154 32.39445 z 0 0.9398; Foundation soil 6
;
;boundary condisions
fix x y z range z -0.01 0.01; fix base
fix x y z range x -0.01 0.01; fix left boundary
fix y range y -0.01 0.01 ; fixes front face in y direction (axis of symmetry)
fix y range y 23.74 23.76 ; fixes back face in y direction (axis of symmetry)
fix x range x 32.394 32.395; fixes right boundary in x direction (axis of symmetry)
;
apply zforce -83.404e3 range x 31.581 31.583 y 6.74 6.76 z 15.135 15.137 ; axle load 1 left node
apply zforce -83.404e3 range x 31.665 31.667 y 6.74 6.76 z 15.135 15.137 ; axle load 1 right
```

```
node
apply zforce -83.404e3 range x 31.581 31.583 y 9.49 9.51 z 15.135 15.137 ; axle load 2 left node
apply zforce -83.404e3 range x 31.665 31.667 y 9.49 9.51 z 15.135 15.137 ; axle load 2 right
node
apply zforce -45.584e3 range x 31.581 31.583 y 13.99 14.01 z 15.135 15.137 ; axle load 3 left
node
apply zforce -45.584e3 range x 31.665 31.667 y 13.99 14.01 z 15.135 15.137 ; axle load 3 right
node
apply zforce -45.584e3 range x 31.581 31.583 y 16.74 16.76 z 15.135 15.137 ; axle load 4 left
node
apply zforce -45.584e3 range x 31.665 31.667 y 16.74 16.76 z 15.135 15.137 ; axle load 4 right
node
hist n = 5
hist unbal
hist gp zdisp 31.582 9.5 15.136
hist gp zdisp 31.666 9.5 15.136
hist gp zdisp 31.582 6.75 15.136
hist gp zdisp 31.666 6.75 15.136
hist gp zdisp 31.582 14.0 15.136
hist gp zdisp 31.666 14.0 15.136
hist gp zdisp 31.582 16.75 15.136
hist gp zdisp 31.666 16.75 15.136
print hist
;step 10000
Solve
plot create PROPV ; shows properties in X section
plot set color On
plot set caption On
plot set caption left
plot set caption size 26
plot set title On
plot set title top
plot set foreground black
plot set background white
plot set window position (0.00,0.00) size(1.00,0.89)
;plot set plane normal (0.000,1.000,0.000)
;plot set plane origin (15.0000e+000,10.00e+000,7.5000e+000)
plot set mode model
plot set center (15.0000e+000,10.00e+000,7.5000e+000)
plot set rotation (0.00, 0.00, 0.00)
plot set distance 180
plot set angle 22
plot set magnification  1.0e+000
plot add block prop bulk
plot add contour zdisp
save 3DUTA-EPS3.sav
```

APPENDIX F

ALOGORITHM FOR IMAGE PROCESSING IN OPTICAL TECHNIQUE

```
%% Load all data
[filename,pathname]=uigetfile('*.jpg','open image from camera');
n=380; % number of frames
Input=[pathname filename];
for i=1:9
   path=[Input(1:50),num2str(i),'.jpg'];
   temp=imread(path);
   Data(:,:,i)=temp(:,:,1);
end
for i=10:99
   path=[Input(1:49),num2str(i),'.jpg'];
   temp=imread(path);
   Data(:,:,i)=temp(:,:,1);
end
for i=100:n
   path=[Input(1:48),num2str(i),'.jpg'];
   temp=imread(path);
   Data(:,:,i)=temp(:,:,1);
end
%% Finding region of interest
pin=40;% choose frame for reference(base image) at which no disturbance
```

```
figure;image(Data(:,:,pin));
pause;
v=round(axis);
a=double(Data(:,:,pin));
figure;image(a)
b=zeros(size(a,1),size(a,2));
b(v(3):v(4),v(1):v(2))=a(v(3):v(4),v(1):v(2)); temp=a(v(3):v(4),v(1):v(2));
figure;image(b);
temp1=double(temp(1:size(temp,1)*size(temp,2)));
x=linspace(min(temp1),max(temp1),20);
figure;plot(x,hist(temp1,x)); [thx,thy]=ginput(1);
b(b>thx)=0;
figure;image(b);
b(b>0)=1;
clm=sum(b,2);
total_pixels=sum(clm);
test=find(clm>0);
centery=round(test(1)+length(test)/2);
figure;plot(1:size(b,1),clm);
[centery,sizeofROI] = findcenter(Data,v,thx);
n_centery=centery(51:252);
```

```
figure;plot(n_centery)
%% Finding center
function [centery,sizeofROI] = findcenter(Data,v,thx)
for i=1:size(Data,3)
   a=double(Data(:,:,i));
   b=zeros(size(a,1),size(a,2));
   b(v(3):v(4),v(1):v(2))=a(v(3):v(4),v(1):v(2));
   b(b>thx)=0;
   b(b>0)=1;
   sizeofROI(i)=sum(sum(b));
   clm=sum(b,2);
   test=find(clm>0);
   centery(i)=round(test(1)+length(test)/2);
end
figure;plot(centery)
figure;plot(sizeofROI)
end
%% Finding pixel to length
pin = 40;
Test_im=double(Data(:,:,pin));
figure;image(Test_im);
```

```
yvalue = 275;

figure;plot(Test_im(yvalue,:))
```